



In-Situ Analysis of Polymer Film Coats Using
AFM and Thermal Probe Methods

By
David Adam Baker

Thesis submitted for the degree of Doctor of Philosophy

School of Pharmacy
University of East Anglia
Norwich, Norfolk
NR4 7TJ

December 2012

©This copy of the thesis has been supplied on the condition that anyone who consults it is understood to recognise that its copyright rests with the author and that no quotation from the thesis nor any information derived therefrom may be published without the author's prior written consent.

Abstract

The in-situ analysis of pharmaceutical solid dosage forms films is of great interest to pharmaceutical research, especially with the drive towards continuous processing compared to batch processing requiring either in-line or on-line analysis of pharmaceuticals. The size and shape of many solid dosage forms impedes their in-situ analysis, particularly when using thermal analysis techniques such as differential scanning calorimetry (DSC). Thermal probe methods, which combine atomic force microscopy (AFM) with thermal analysis, permits imaging and characterisation of solid dosage forms in-situ. The goal of this thesis is to perform the in-situ analysis of film coated minitables through the use of thermal probe methods.

Minitables, which are small diameter tablets, were coated with Opadry I, Opadry II or Surelease, and blends of Surelease and Opadry I and Surelease and Opadry II. In addition the same systems were prepared as cast free films to ascertain differences resulting from the two methods of producing the films. Distinct morphologies were observed between the film coated minitables and cast free films, particularly for the polymer blends. Thermal analysis by modulated temperature DSC (MTDSC) and localised thermomechanical analysis (L-TMA) of film coated minitables coated with polymer blends indicating miscibility. However the novel technique of heated tip tapping mode was employed, which was able to resolve separate domains of the polymer blends, which appeared as nanophases. Heated tip tapping mode was further employed to determine changes in the surface morphology of film coated minitables which had undergone curing. It was successfully used to observe the further coalescence of Surelease and the alteration in the phase distribution of the polymer blends after film coated minitables had been cured. Polymer films with incorporated pigments were also analysed by thermal probe methods with differences in pigment distribution being observed between film coated minitables and cast free films. Tapping mode AFM was able to determine the location of pigment particles and the novel use of L-TMA performed in tapping mode allowed thermal analysis without changing AFM mode. Overall the use of AFM combined with thermal probes achieved the aim of performing in-situ analysis of polymer film coats; however further research to correlate in-vivo behaviour of film coats would be of value.

Acknowledgements

Firstly thanks must be made to my supervisors', Professor Duncan Craig and Doctor Andrew Round, whose support and guidance over the course of the project was invaluable and much appreciated. Especially to Professor Craig for giving me the opportunity to study for a PhD and for the inspiration provided during my undergraduate studies to enter research.

Thanks must also be made to Ali Rajabi-Siahboomi and Marina Levina from Colorcon for their technical assistance and guidance on the project, and for their kind donations of samples. Hue Vong and Darsha Palmer also from Colorcon and Roshan Shetty of Anasys instruments contributed their excellent technical knowledge with assistance on the materials and techniques used during the study.

All the UEA pharmaceuticals group past and present that have provided help with equipment and samples, and made the PhD experience thoroughly enjoyable, I must thank. Special thanks must be given to Dr Jonathan Moffat for all his help with AFM and FTIR experiments and along with Kate and Ben made the AFM lab a great place to work. Thanks must also be made to Xuan Dai, Jin Meng and Bertrand Leze, who all helped greatly in my training on equipment. Also to Aled Evans whose equal love of late nights and coffee club enabled nights in the lab to be more enjoyable and productive than they could have been.

I must also thank my parents Ann and Colin for their motivation to achieve academic success from school through to university was of great help. A special mention must also be made to my Gramps and Grandma who both passed away during my PhD, but whose help over the past few years at university was invaluable.

Finally to my lovely fiancée Kate, thanks for always being there for me with your love and support throughout, and for your patience whilst completing the dissertation. I couldn't have done all this without you.

David Baker

Table of Contents

Abstract.....	2
Acknowledgements.....	3
Table of Contents	4
Figures and Tables.....	9
1. Introduction.....	21
1.1 Components of the Coating Solution	22
1.1.1 Polymers.....	22
1.1.1.1 Immediate Release Polymers	24
1.1.1.2 Sustained Release Polymers.....	25
1.1.1.3 Enteric Coating Polymers	28
1.1.1.4 Polymer Blends	28
1.2 Solvents	32
1.2.1 Organic Solvents	32
1.2.2 Aqueous Colloidal Dispersions	33
1.3 Additives to Coating Solutions and Dispersions.....	35
1.3.1 Plasticisers.....	35
1.3.2 Other Additives	38
1.3.3 Drugs	38
1.4 Substrates	41
1.4.1 Tablets	41
1.4.2 Pellets	42
1.4.3 Minitablets	43
1.5 Film Coating	43
1.5.1 Film Forming	43
1.5.1.1 Film Forming from Organic Solvents	44
1.5.1.2 Film Forming from Aqueous Dispersions.....	45
1.5.1.3 Minimum Film Forming Temperature	46
1.5.2 Adhesion.....	47
1.5.3 Curing.....	48
1.6 Film Forming Techniques	49
1.6.1 Spray Coating.....	49
1.6.2 Film Casting.....	52
1.6.3 Spin Coating.....	53
1.7 Defects in Film Coats.....	54
1.8 Previous Research	56

1.8.1	Microscopy Techniques.....	56
1.8.1.1	Atomic Force Microscopy.....	56
1.8.2	Spectroscopy Techniques	61
1.8.2.1	Near Infrared	62
1.8.2.2	Raman Spectroscopy.....	64
1.8.2.3	Terahertz Pulsed Imaging.....	65
1.8.2.4	Laser Induced Breakdown Spectroscopy.....	67
1.9	Research Objectives	68
2.	General Methods and Materials	71
2.1	Thermal Analysis of Pharmaceutical Materials	71
2.1.1	Theory of Thermal Analysis.....	72
2.1.2	Differential Scanning Calorimetry	73
2.2	Atomic Force Microscopy.....	79
2.2.1	Tapping Mode AFM.....	82
2.3	Thermal Probe Methods of AFM	88
2.4	Fourier Transform Infrared Spectroscopy.....	94
2.5	Scanning Electron Microscopy	97
2.6	Materials.....	99
2.6.1	Opadry I	99
2.6.1.1	The Glass Transition of HPMC.....	100
2.6.2	Polyethylene Glycol.....	101
2.6.3	Opadry II	102
2.6.3.1	Thermal Transitions of PVA.....	104
2.6.3	Surelease	105
2.6.3.1	Thermal Transitions of Ethylcellulose	106
3.	Characterisation of Materials	108
3.1	Introduction.....	108
3.2	Materials and Methods.....	109
3.2.1	Preparation of Films.....	109
3.2.2	Atomic Force Microscopy and Thermal Probe Methods	110
3.2.3	Modulated Temperature Differential Scanning Calorimetry.....	111
3.2.4	Scanning Electron Microscopy	111
3.2.5	Fourier Transform Infrared Spectroscopy.....	112
3.3	Results.....	112
3.3.1	Cast Films	112
3.3.1.1	AFM Images.....	112
3.3.1.2	Thermal Analysis	113

3.3.1.2.1 Opadry I	113
3.3.1.2.2 Surelease	116
3.3.1.2.3 Opadry II	117
3.3.2 Film Coated Minitablets.....	119
3.3.2.1 AFM Images.....	119
3.3.2.2. Scanning Electron Microscopy Images.....	120
3.3.2.3 Thermal Analysis	121
3.3.2.3.1 Opadry I	122
3.3.2.3.2 Surelease	124
3.3.2.3.3 Opadry II	125
3.3.3 FTIR Spectra	128
3.3.4 Area of Discrimination of Probes.....	130
3.3.5 Effect of Heating Rate of the Softening Point	131
3.4 Discussion	135
3.5 Conclusions	137
4. Analysis of Polymer Blends and Comparison of Film Coated Minitablets to Cast Free Films	138
4.1 Introduction	138
4.2 Research Objectives	139
4.3 Materials and Methods	140
4.3.1 Preparation of Film Coated Minitablets.....	140
4.3.2 Atomic Force Microscopy and Thermal Probe Methods	140
4.3.3 Modulated Temperature DSC.....	142
4.3.4 Scanning Electron Microscope	143
4.3.5 Fourier Transform Infrared Spectroscopy.....	143
4.4 Results	143
4.4.1 Analysis of Individual Coating Systems	144
4.4.2 Analysis of Film Coated Minitablets Coated with Polymer Blends	148
4.4.2.1 SEM	148
4.4.2.2 Surelease and Opadry I Film Coated Minitablets	149
4.4.2.2.1 Modulated Temperature DSC.....	150
4.4.2.2.2 Localised Thermomechanical Analysis.....	153
4.4.2.2.3 Heated Tip Tapping Mode AFM	159
4.4.2.3 Surelease and Opadry II Film Coated Minitablets.....	174
4.4.2.3.1 Modulated Temperature DSC.....	174
4.4.2.3.2 Localised Thermomechanical Analysis.....	176
4.4.2.3.3 Heated Tip Tapping Mode AFM	180

4.4.2.4 FTIR of Film Coated Minitablets.....	183
4.4.3 Analysis of Cast Free Films	185
4.4.3.1 Analysis of Surelease and Opadry I Cast Films.....	185
4.4.3.1.1 Localised Thermomechanical Analysis.....	186
4.4.3.1.2 Modulated Temperature DSC.....	187
4.4.3.1.3 Heated Tip Tapping Mode AFM	190
4.4.3.2 Analysis of Surelease and Opadry II Cast Films.....	193
4.4.3.2.1 Modulated Temperature DSC.....	193
4.4.3.2.2 Localised Thermomechanical Analysis.....	195
4.5 Conclusions.....	198
5. Characterisation of Cured Film Coated Minitablets	200
5.1 Introduction	200
5.2 Research Objectives	201
5.3 Materials and Methods.....	202
5.4 Results.....	202
5.4.1 Analysis of Individual Polymers	202
5.4.2 Surelease	203
5.4.2.1 Heated Tip Tapping Mode AFM	203
5.4.2.2 Contact Mode Images and L-TMA Analysis	206
5.4.3 Surelease and Opadry I 50:50 blend	213
5.4.3.1 Heated Tip Tapping Mode Imaging	213
5.4.3.2 Contact mode images and L-TMA.....	216
5.4.4 Surelease and Opadry II 50:50 Blend	222
5.4.4.1 Heated Tip Tapping Mode.....	222
5.4.4.2 Contact Mode Images and L-TMA	224
5.5 Discussion	230
5.6 Conclusions.....	234
6. Analysis of Pigments Incorporated into Polymer Films	235
6.1 Introduction	235
6.2 Materials and Methods.....	237
6.3 Results.....	239
6.3.1 Iron Oxide	239
6.3.1.2 Modulated Temperature DSC of Iron Oxide Powder.....	239
6.3.1.2 L-TMA of Iron Oxide Powder	240
6.3.2 Cast Films	241
6.3.2.1 Opadry I with 10% w/w Iron Oxide.....	241
6.3.2.1.1 Modulated Temperature DSC.....	241

6.3.2.1.2 Contact Mode AFM and L-TMA	242
6.3.2.1.3 Tapping Mode AFM and L-TMA.....	245
6.3.2.2 Opadry II and 10% w/w Iron Oxide.....	248
6.3.2.2.1 Modulated Temperature DSC.....	248
6.3.2.2.2 Tapping Mode AFM	249
6.3.2.2.3 Contact Mode AFM and L-TMA	250
6.3.2.3 Minitablets	253
6.3.2.3.1 Opadry I and 10% w/w Iron Oxide.....	253
6.3.2.3.2 Opadry II and 10% w/w Iron Oxide.....	254
6.3.3 Use of AFM for the Measurement of Gloss	256
6.4 Discussion	257
6.5 Conclusions	261
7. Conclusions	263
7.1 Final Conclusions.....	263
7.2 Suggestions for Further Work	267
7.2.1 Scanning Thermal Microscopy	267
7.2.2 Dissolution Testing.....	268
7.3 Concluding Remarks	269
References	272

Figures and Tables

Figure 1.1 Showing Theophylline release from Eudragit RS30D and RL30D blends of varying proportions (Reproduced from Amighi and Moës, 1995)	30
Figure 1.2 showing the zeta potentials of zein dispersions from pH 2.5-5 (Reproduced from Guo et al., 2008)	34
Figure 1.3 Showing phase separation occurring with increasing concentration of salicylic acid (SA) in chitosan films (reproduced from Puttipipatkachorn et al., 2001)	40
Figure 1.4 Film forming from aqueous latex particles (reproduced from Chevalier <i>et al.</i> , 1992)	46
Figure 1.5 Caleva Mini Coater Drier 2 (reproduced from Caleva 2013).....	50
Figure 1.6 Spray head from the Caleva Mini Coater Drier 2 (reproduced from Caleva 2013)	51
Figure 1.7 AFM images of Silk Fibroin films either treated with MeOH or untreated. Scale bar length in images A and B is 2.5µm and C and D it is 0.5µm (reproduced from (Hofmann <i>et al.</i> , 2006)	58
Figure 1.8 various thermal conductivity images. Of note is the image in the top right, which is explained in the text. (Reproduced from Royall <i>et al.</i> , 2001a).....	60
Figure 1.9 Near-IR spectra of a cast EC film (dot-dash line), an uncoated tablet core (dotted line) and film coated tablets (solid line) taken at various times during the coating run. Reproduced from (Kirsch and Drennen, 1996).....	62
Fig 1.10 Formation and erosion of the gel layer in a HPMC matrix (bottom), and dissolution of the API. Reproduced from (Avalle <i>et al.</i> , 2011).....	64
Figure 1.11 A typical terahertz waveform. See text for explanation. Reproduced from Zeitler <i>et al</i> 2007a).....	66
Figure 1.12 A spatially resolved 3D image of a tablet coat. Reproduced from Ho <i>et al.</i> , 2008)	66
Figure 2.1 Common transitions on a DSC trace of quench cooled paracetamol (Qi <i>et al.</i> , 2008)	75

Figure 2.2 Common transitions on a MTDSC trace. See text for explanation (reproduced from Royall <i>et al.</i> , 1999a).....	78
Figure 2.3 Schematic of AFM (Price <i>et al.</i> , 1999a).....	80
Figure 2.4 Schematic of laser and photodiode detector (Thornton <i>et al.</i> , 2000).....	82
Figure 2.5 Diagram with frequency plotted on the x axis. The dotted line represents phase angle with respect to frequency, and the solid line represents amplitude of the freely oscillating cantilever (reproduced from Garcia <i>et al.</i> , 2002).....	84
Figure 2.6 A Wollaston wire probe (reproduced from Royall <i>et al.</i> , 2001b)	89
Figure 2.7 SEM image and diagram of the current flow in a nano-TA probe (reproduced from Nelson <i>et al.</i> , 2007).....	92
Figure 2.8 Schematic of the Wheatstone bridge circuit employed in SThM (reproduced from Grosse <i>et al.</i> , 2007)	93
Figure 2.9 Structure of HPMC	99
Figure 2.10 Structure of PEG.....	101
Figure 2.11 Structure of PVA	103
Figure 2.12 Structure of Ethylcellulose	105
Figure 2.13. MTDSC trace showing ethylcellulose transitions. See text for explanation (Reproduced from Lai <i>et al.</i> , 2010).....	106
Table 3.1 Process conditions for film coating *flow rate increased to 30ml/hr after 15 minutes.....	109
Figure 3.1 AFM images of cast polymer films (from left to right) Surelease, Opadry I, Opadry II.....	113
Figure 3.2 MTDSC of Opadry I cast films	114
Figure 3.3 L-TMA results of Opadry I cast films	115
Figure 3.4 MTDSC trace of Surelease cast film	116
Figure 3.6 MTDSC of Opadry II cast films	118
Figure 3.7 L-TMA of Opadry II cast films	119
Figure 3.8 Contact mode AFM images of film coated minitabets (from left to right)	

Surelease, Opadry I, Opadry II	120
Figure 3.9 SEM image of Opadry I film coated minitablet cross section.....	120
Figure 3.10 SEM image of Opadry I film coated minitablet surface.....	121
Figure 3.11 MTDSC of an uncoated powdered minitablet	122
Figure 3.12 MTDSC of Opadry I coated minitablets.....	123
Figure 3.13 L-TMA of Opadry I coated minitablets	123
Figure 3.14 MTDSC of Surelease coated minitablets.....	124
Figure 3.15 L-TMA of Surelease coated minitablets	125
Figure 3.16 MTDSC of Opadry II coated minitablets	126
Figure 3.17 L-TMA of Opadry II coated minitablets with nano-TA probes.....	126
Figure 3.18 AFM image obtained in contact mode of film coated minitablet (left) and corresponding L-TMA result (right)	127
Figure 3.19 FTIR spectra of Surelease coated minitablets	128
Figure 3.20 FTIR spectra of Opadry I coated minitablets	129
Figure 3.21 FTIR spectra of Opadry II coated minitablets	129
Figure 3.22 Topography (left) and phase images (right) of a 5µm area of an Opadry II cast film, before (top) and after (bottom) an L-TMA measurement with 1 representing the L-TMA location.....	130
Figure 3.23 Onset voltages recorded at different heating rates for the calibration samples.....	132
Figure 3.24 Transition temperature of PE calibrated at various heating rates	133
Figure 3.25 Transition temperatures of Surelease cast films with various heating rates	133
Figure 3.26 Comparison of transition temperatures observed for PE and Surelease at various heating rates.....	134
Table 4.1 Process conditions for film coating *flow rate increased to 30ml/hr after 15 minutes	140
Figure 4.1 Heated Tip Tapping Mode images of a 50-50 blend of Surelease:Opadry I	

coated minitabulet showing the image before (left) and after (right) the domains were selected.....	141
Figure. 4.2. Screen in SPM labs to set Z threshold	142
Figure 4.3 L-TMA of minitablets film coated with Opadry I, Opadry II and Surelease	144
Figure 4.4 MTDSC of an uncoated powdered minitabulet	145
Figure 4.5 MTDSC of Opadry I coated minitablets.....	145
Figure 4.6 MTDSC of Surelease coated minitablets.....	146
Figure 4.7 MTDSC of Opadry II coated minitablets	146
Figure 4.8 L-TMA of Opadry I, Opadry II and Surelease cast films	147
Figure 4.9 MTDSC of Opadry I cast films	147
Figure 4.10 MTDSC trace of Surelease cast film	148
Figure 4.11 MTDSC of Opadry II cast films	148
Figure 4.12. SEM of film coated minitablets. Clockwise from top left: Surelease-Opadry I 50:50, Surelease Opadry I 70:30, Surelease-Opadry I 70:30 alternate view, Surelease-Opadry I 90:10.....	149
Figure 4.13 MTDSC trace of a minitabulet coated with Surelease and Opadry I 50:50 blend.....	150
Figure 4.14 MTDSC trace of a minitabulet coated with Surelease and Opadry I 70:30 blend.....	152
Figure 4.15 MTDSC trace of a minitabulet coated with Surelease and Opadry I 90:10 blend.....	152
Figure 4.16 50:50 Blend of Surelease and Opadry I analysed with Wollaston Probes	154
Figure 4.17 L-TMA of minitablets coated with a 50:50 Surelease:Opadry blend...	155
Figure 4.18 AFM contact image (left) and L-TMA results (right) for 50:50 Surelease:Opadry I blend	155
Figure 4.19 L-TMA of minitablets coated with a 70:30 Surelease:Opadry blend...	156

Figure 4.20 AFM contact image (left) and L-TMA results (right) for 50:50 Surelease:Opadry I blend	156
Figure 4.21 L-TMA of minitablets coated with a 90:10 Surelease:Opadry blend...	157
Figure 4.22 AFM contact image (left) and L-TMA results (right) for 50:50 Surelease:Opadry I blend	157
Figure 4.23 Correlated transitions of L-TMA and MTDSC for film coated minitablets.....	158
Figure 4.24 SEM image of Surelease:Opadry I 50:50 blend.....	158
Figure 4.25 Heated Tip Tapping Mode images of a Surelease coated minitablet (topography – left, phase image – right): From top to bottom 25°C, 30°C (continues overleaf)	160
Figure 4.26 Heated Tip Tapping Mode images of a 50:50 blend of Surelease:Opadry I coated minitablet (topography – left, phase image – right): From top to bottom 25°C, 70°C, 80°C and 90°C (continues overleaf).....	164
Figure 4.27 Heated Tip Tapping Mode images of a 70:30 blend of Surelease:Opadry I coated minitablet (topography – left, phase image – right): From top to bottom 25°C, 70°C, 80°C and 90°C (continues overleaf).....	168
Figure 4.28 Heated Tip Tapping Mode images of a 90:10 blend of Surelease:Opadry I coated minitablet (topography – left, phase image – right): From top to bottom 25°C, 30°C, 40°C (continues overleaf).....	171
Figure 4.29 MTDSC trace of a minitablet coated with Surelease and Opadry II 50:50 blend.....	174
Figure 4.30 MTDSC trace of a minitablet coated with Surelease and Opadry II 70:30 blend.....	175
Figure 4.31 MTDSC trace of a minitablet coated with Surelease and Opadry II 90:10 blend.....	176
Figure 4.32 L-TMA of minitablets coated with a 50:50 Surelease:Opadry II blend	177
Figure 4.33 AFM contact image (left) and L-TMA results (right) for 50:50 Surelease:Opadry II blend.....	177

Figure 4.34 L-TMA of minitablets coated with a 70:30 Surelease:Opadry II blend	178
Figure 4.35 AFM contact image (left) and L-TMA results (right) for 70:30 Surelease:Opadry II blend	178
Figure 4.36 L-TMA of minitablets coated with a 90:10 Surelease:Opadry II blend	179
Figure 4.37 AFM contact image (left) and L-TMA results (right) for 90:10 Surelease:Opadry II blend	179
Figure 4.38 Heated Tip Tapping Mode images of a 50:50 blend of Surelease:Opadry II coated minitablet (topography – left, phase image – right): From top to bottom 25°C and 30°C (continues overleaf)	180
Figure 4.39 FTIR Spectra of minitablets coated with Surelease, Opadry I and their blends	183
Figure 4.40 FTIR Spectra of minitablets coated with Surelease, Opadry II and their blends	184
Figure 4.41 FTIR spectra of Surelease-Opadry II 50:50 blend from 3000cm ⁻¹ to 3900cm ⁻¹	185
Figure 4.42 L-TMA of cast films of a 50:50 Surelease:Opadry blend	186
Figure 4.43 L-TMA of cast films of a 70:30 Surelease:Opadry blend	186
Figure 4.44 L-TMA of cast films of a 90:10 Surelease:Opadry blend	187
Figure 4.45 MTDSC trace of cast films of a Surelease and Opadry 50:50 blend	188
Figure 4.46 MTDSC trace of cast films of a Surelease and Opadry 70:30 blend	188
Figure 4.47 MTDSC trace of cast films of a Surelease and Opadry 90:10 blend	189
Figure 4.49 MTDSC trace of cast films of a Surelease and Opadry II 50:50 blend	194
Figure 4.50 MTDSC trace of cast films of a Surelease and Opadry II 70:30 blend	194
Figure 4.51 MTDSC trace of cast films of a Surelease and Opadry II 90:10 blend	195
Figure 4.52 L-TMA of cast films of a 50:50 Surelease:Opadry II blend	195
Figure 4.53 AFM contact image (left) and L-TMA results (right) for 50:50 Surelease:Opadry II blend	196
Figure 4.54 L-TMA of cast films of a 70:30 Surelease:Opadry II blend	196

Figure 4.55 AFM contact image (left) and L-TMA results (right) for 70:30 Surelease:Opadry II blend.....	197
Figure 4.56 L-TMA of cast films of a 90:10 Surelease:Opadry II blend.....	197
Figure 4.57 AFM contact image (left) and L-TMA results (right) for 70:30 Surelease:Opadry II blend.....	197
Figure 5.1 L-TMA of minitablets film coated with Opadry I, Opadry II and Surelease	203
Figure 5.2 Tapping mode image of Surelease minitablets cured for 6 hours showing topography (left) and phase (right)	204
Figure 5.3 Heated tip tapping mode image with the probe held at 80°C of Surelease minitablets cured for 6 hours showing topography (left) and phase (right).....	204
Figure 5.4 Tapping mode image of Surelease minitablets cured for 12 hours showing topography (left) and phase (right)	205
Figure 5.5 Heated tip tapping mode image with the probe held at 80°C of Surelease minitablets cured for 12 hours showing topography (left) and phase (right).....	205
Figure 5.6 Tapping mode image of Surelease minitablets cured for 24 hours showing topography (left) and phase (right)	205
Figure 5.7 Heated tip tapping mode image with the probe held at 80°C of Surelease minitablets cured for 24 hours showing topography (left) and phase (right).....	206
Figure 5.8 L-TMA of Surelease coated minitablets cured for 6 hours.....	207
Figure 5.9 Contact AFM image of Surelease coated minitablets cured for 6 hours, numbers denote locations of L-TMA.....	207
Figure 5.10 L-TMA of Surelease coated minitablets cured for 6 at locations specified in Fig 5.9	208
Figure 5.11 L-TMA of Surelease coated minitablets cured for 12 hours.....	209
Figure 5.12 Contact AFM image of Surelease coated minitablets and cured for 12 hours, numbers denote locations of L-TMA	209
Figure 5.13 L-TMA of Surelease coated minitablets cured for 12 hours at locations specified in Fig. 5.12	210

Figure 5.14 L-TMA of Surelease coated minitablets cured for 24 hours, showing transitions associated with Surelease circa 90°C and EC circa 130°C.....	211
Figure 5.15 Contact AFM image of Surelease coated minitablets and cured for 24 hours, numbers denote locations of L-TMA.....	211
Figure 5.16 L-TMA of Surelease coated minitablets cured for 24 hours at locations specified in Fig. 5.15.....	212
Figure 5.17 Tapping mode image of minitablets coated with a Surelease and Opadry I 50:50 blend cured for 6 hours showing topography (left) and phase (right).....	213
Figure 5.18 Heated tip tapping mode image with the probe held at 100°C of minitablets coated with a Surelease and Opadry I 50:50 blend cured for 6 hours showing topography (left) and phase (right).....	213
Figure 5.19 Tapping mode image of minitablets coated with a Surelease and Opadry I 50:50 blend cured for 12 hours showing topography (left) and phase (right).....	214
Figure 5.20 Heated tip tapping mode image with the probe held at 100°C of minitablets coated with a Surelease and Opadry I 50:50 blend cured for 12 hours showing topography (left) and phase (right).....	214
Figure 5.21 Tapping mode image of minitablets coated with a Surelease and Opadry I 50:50 blend cured for 24 hours showing topography (left) and phase (right).....	215
Figure 5.22 Heated tip tapping mode image with the probe held at 100°C of minitablets coated with a Surelease and Opadry I 50:50 blend cured for 24 hours showing topography (left) and phase (right).....	215
Figure 5.23 L-TMA of minitablets coated with a Surelease and Opadry I 50:50 blend cured for 6 hours.....	216
Figure 5.24 Contact AFM image of minitablets coated with a Surelease and Opadry I 50:50 blend and cured for 6 hours, numbers denote locations of L-TMA.....	217
Figure 5.25 L-TMA of minitablets coated with a Surelease and Opadry I 50:50 blend and cured for 6 hours at locations specified in Fig. 5.24.....	217
Figure 5.26 L-TMA of minitablets coated with a Surelease and Opadry I 50:50 blend cured for 12 hours.....	218
Figure 5.27 Contact AFM image of minitablets coated with a Surelease and Opadry I	

50:50 blend and cured for 6 hours, numbers denote locations of L-TMA.....	218
Figure 5.28 L-TMA of minitablets coated with a Surelease and Opadry I 50:50 blend and cured for 6 hours at locations specified in Fig. 5.27	219
Figure 5.29 L-TMA of minitablets coated with a Surelease and Opadry I 50:50 blend cured for 24 hours	220
Figure 5.30 Contact AFM image of minitablets coated with a Surelease and Opadry I 50:50 blend and cured for 24 hours, numbers denote locations of L-TMA.....	221
Figure 5.31 L-TMA of minitablets coated with a Surelease and Opadry I 50:50 blend and cured for 24 hours at locations specified in Fig. 30	221
Figure 5.32 Tapping mode image of minitablets coated with a Surelease and Opadry II 50:50 blend cured for 6 hours showing topography (left) and phase (right).....	222
Figure 5.33 Heated tip tapping mode image with the probe held at 70°C of minitablets coated with a Surelease and Opadry II 50:50 blend cured for 6 hours showing topography (left) and phase (right).....	222
Figure 5.34 Tapping mode image of minitablets coated with a Surelease and Opadry II 50:50 blend cured for 12 hours showing topography (left) and phase (right).....	223
Figure 5.35 Heated tip tapping mode image with the probe held at 70°C of minitablets coated with a Surelease and Opadry II 50:50 blend cured for 12 hours showing topography (left) and phase (right).....	223
Figure 5.36 Tapping mode image of minitablets coated with a Surelease and Opadry II 50:50 blend cured for 24 hours showing topography (left) and phase (right).....	224
Figure 5.37 Heated tip tapping mode image with the probe held at 70°C of minitablets coated with a Surelease and Opadry II 50:50 blend cured for 24 hours showing topography (left) and phase (right).....	224
Figure 5.38 L-TMA of minitablets coated with a Surelease and Opadry II 50:50 blend cured for 6 hours	225
Figure 5.39 Contact AFM image of minitablets coated with a Surelease and Opadry II 50:50 blend and cured for 6 hours, numbers denote locations of L-TMA.....	225
Figure 5.40 L-TMA of minitablets coated with a Surelease and Opadry II 50:50 blend and cured for 6 hours, at locations specified in Fig. 5.39	226

Figure 5.41 L-TMA of minitablets coated with a Surelease and Opadry II 50:50 blend cured for 12 hours	227
Figure 5.42 Contact AFM image of minitablets coated with a Surelease and Opadry II 50:50 blend and cured for 12 hours, numbers denote locations of L-TMA.....	227
Figure 5.43 L-TMA of minitablets coated with a Surelease and Opadry II 50:50 blend and cured for 12 hours, at locations specified in Fig. 5.41	228
Figure 5.44 L-TMA of minitablets coated with a Surelease and Opadry II 50:50 blend cured for 24 hours	229
Figure 5.45 Contact AFM image of minitablets coated with a Surelease and Opadry II 50:50 blend and cured for 24 hours, numbers denote locations of L-TMA.....	229
Figure 5.46 L-TMA of minitablets coated with a Surelease and Opadry II 50:50 blend and cured for 24 hours, at locations specified in Fig. 5.44	230
Table 6.1 Process conditions for film coating of minitablets.....	237
Figure 6.1 MTDSC trace of iron oxide powder	239
Figure 6.2 Iron oxide Powder analysed by L-TMA.....	240
Figure 6.3 MTDSC of Opadry I cast film with 10% w/w iron oxide	242
Figure 6.4 MTDSC of Opadry I cast films	242
Figure 6.5 L-TMA of Opadry I with 10% w/w iron oxide cast films	243
Figure 6.6 L-TMA trace of Opadry I cast film.....	243
Figure 6.7 AFM image in contact mode of Opadry I with 10% w/w iron oxide, area 1 represents an area of suspected Opadry I and area 2 suspected iron oxide.....	244
Figure 6.8 L-TMA of Cast Opadry I films with 10% w/w iron oxide	244
Figure 6.9 Tapping mode AFM images of Opadry I with 10% w/w iron oxide, showing topography (left) and phase (right).....	245
Figure 6.10 L-TMA results of Opadry I with 10% w/w iron oxide performed in tapping mode.....	246
Figure 6.11 Tapping mode AFM images of Opadry I with 10% w/w iron oxide, showing topography (left) and phase (right) with numbers denoting locations of L-TMA.....	247

Figure 6.12 L-TMA of Cast Opadry I films with 10% w/w iron oxide performed in tapping mode.....	247
Figure 6.13 MTDSC of Opadry II cast films	248
Figure 6.14 MTDSC of Opadry II cast film with 10% w/w iron oxide.....	249
Figure 6.15 Cast films of Opadry II in tapping mode showing topography (left) and phase (right)	249
Figure 6.16 L-TMA of Opadry II cast films	250
Figure 6.17 L-TMA of Cast films of Opadry II with 10% w/w iron oxide	251
Figure 6.18 Contact AFM image of Opadry II with 10% w/w iron oxide, with area 1 representing suspected iron oxide and area 2 suspected Opadry II	252
Figure 6.19 L-TMA of cast films of Opadry II with 10% iron oxide performed on a suspected area of iron oxide and Opadry II	252
Figure 6.20 Tapping mode image of Film coated minitables of Opadry I with 10% w/w iron oxide showing topography (left) and phase image (right).....	253
Fig 6.21 L-TMA of minitables film coated with Opadry I and 10% iron oxide. With L-TMA performed on an area of suspected iron oxide and L-TMA 2 on an area of suspected Opadry I.....	254
Figure 6.22 Tapping mode image of film coated minitables of Opadry II with 10% w/w iron oxide showing topography (left) and phase image (right).....	255
Figure 6.23 Contact AFM image of film coated Opadry II minitables with 10% iron oxide.....	255
Figure 6.24 L-TMA of minitables film coated with Opadry II and 10% iron oxide. With L-TMA performed on an area of suspected Opadry II and L-TMA 2 on an area of suspected iron oxide.....	256
Figure 6.25 AFM contact images of Opadry I with 10% w/v of the underside (left) and top (right) of the film.....	257
Figure 6.26 Diagram depicting likely positioning of iron oxide to produce the L-TMA in the bottom right (see text for full explanation).....	259
Fig 6.27 Diagram depicting likely positioning of iron oxide to produce the L-TMA in	

the bottom right (see text for full explanation)	261
Figure 7.1 GLA style probes used in SThM showing the different in tip compared to NanoTA probes.....	267

CHAPTER 1

1. Introduction

Film coats form an integral element of solid dose forms, and are applied for a number of reasons including taste masking, stability (protection of the tablet from light, moisture and air), ease of swallowing, identification and sustained, enteric or controlled release (Miller and McGinity, 2008, Sakellariou Rowe, 1995a). Films are typically composed from polymers which are formulated into a coating solution and then applied by spray coating to the solid dosage form being coated. The film coated dosage forms in some cases need to be treated after coating, for example curing in an oven, to ensure the coat is fully formed to provide the desired release characteristics.

Within the pharmaceutical industry there is a need for the in-situ analysis of pharmaceutical dosage forms. This is in part to the drive towards Process Analytical Technology (PAT) which requires a scientific understanding of how formulation and process factors affect performance and the continuous real time quality assurance during manufacturing (FDA, 2004). Therefore there is a need for the in-situ analysis during the development and manufacturing of pharmaceuticals to ensure a quality product is produced.

There is considerable interest in the characterisation of tablet film coats, with this interest ranging from how films are formed to how they behave *in-vivo*. There are a number of techniques used to analyse films including thermal, mechanical and spectroscopy methods (Felton, 2007). Unfortunately many techniques, by their very nature, preclude the in-situ testing of pharmaceutical film coats, for example it would be extremely difficult to use Differential Scanning Calorimetry (DSC) as an in-situ method, due to the need for small sample sizes and uniform contact with the bottom of the sample pan. Therefore many techniques analysing polymer films are performed on cast free films which potentially use considerably different process conditions to form the film.

Therefore this project aims to perform in-situ analysis of film coated solid dosage forms through the use of atomic force microscopy (AFM) and thermal analysis techniques to determine the behaviour of pharmaceutical film coats in-situ. Comparison will be made to cast free films to assess the equivalence of these films to those produced by spray coating.

The following chapter will review the available literature on film coating, taking into consideration the polymers and additives used, the types of solid dosage forms that tend to be film coated and the coating process. The remainder of the chapter discusses the techniques used to analyse film coated solid dosage forms, and the merits and drawbacks of each technique.

1.1 Components of the Coating Solution

There are often multiple components within a coating solution, each there to optimise the quality of the final film. The most basic coating solution involves a polymer dissolved in either an organic solvent or water, which is then applied to the substrate. Many film coating solutions systems however require the addition of further materials to aid in a variety of processes that occur during film coating such as adhesion to the substrate and the actual film forming. Additionally some additives are present to enhance the final appearance of the film, for example pigments and opacifiers.

1.1.1 Polymers

Sugar coatings were traditionally used to coats tablets however sugar coats cannot be used for functional coatings such as controlled release and the long process times were significant drawbacks compared to polymers (Hogan, 2002). Since the 1950s polymers have succeeded sugar coatings as the material of choice for tablet coatings, however tablets such as ibuprofen are still sugar coated. There are many different types of polymers used to create films with myriad functions, for example allowing a variety of release patterns, from immediate to sustained release and targeted delivery

via enteric coating. This variety in turn presents many problems and considerations during formulation as to which polymer or even grade of polymer to select.

One of the most important considerations in the choice of polymer is the glass transition, T_g , of the polymer or coating system used. As the majority of polymers used in the pharmaceutical industry are amorphous in nature, meaning that they have no long-range molecular order once formed into a film, and they therefore possess a T_g as opposed to a melting temperature (T_m). This is due to the high molecular weight and molecular flexibility of polymers resulting in a reduced tendency to form lattices. Below the glass transition temperature of a material it displays a glassy brittle nature; however above the T_g the material changes to a rubbery state. This transition differs from the T_m associated with crystalline substances, as it is not a solid to liquid transition, because the glassy state is a highly viscous liquid (Craig, 2008). T_g is a kinetic parameter as it is associated with a change in molecular mobility, rather than bond breaking as in T_m . When a material undergoes the transition from the rubbery to glassy state there is a dramatic reduction in the translational and rotational motions, with vibrational motions generally remaining below T_g (Craig *et al.*, 1999). As with the melting point of crystalline materials the glass transition is an important physicochemical property of a material. The T_g is of importance in film coating, as the polymer has to be in the rubbery state when it is applied to the substrate, therefore it is of importance to know the T_g of the polymer. The theory of glass transitions will be discussed further in Chapter 2.

As discussed above polymers are employed for a number of different purposes, with different polymer structures used for a number of functions described below. The polymer structure has the largest effect on film coat behaviour, but often different grades of the same polymer are employed to provide finer control. With different polymer grades tending to retain the same chemical structure but with varying molecular weight, which alters a number of the polymers properties, including T_g and the flexibility of the final polymer film.

1.1.1.1 Immediate Release Polymers

Film coats used for immediate release tend to be used to improve the appearance of the final tablet, to aid swallowing or for odour or taste masking (Dow, 2002). One of the most common polymers used for the immediate release of the active pharmaceutical ingredient is the cellulose ether hydroxypropyl methylcellulose (HPMC). HPMC is soluble in water and certain organic solvents, is a good film former, and is readily soluble in gastric juices making it ideal for immediate release coatings. HPMC also aids swallowing by beginning to hydrate in the mouth causing the surface to become slick and therefore easier to swallow. The most prominent HPMC product is MethocelTM, which is produced by the Dow Chemical Company[®], Midland, Michigan, U.S.A. It is available in a range of different viscosities, and for solid dosage form coating, typically low viscosity grades of Methocel E are used, with the letter after Methocel denoting the degree of methoxyl substitution on the cellulose backbone. Colorcon[®], Inc., West Point, Pennsylvania, U.S.A. produce a fully formulated film coating system called Opadry[®], which contains all the necessary plasticisers to produce a satisfactory film coat, with the option to add pigments and opacifiers.

The Eudragit[®] polymer range manufactured by Evonik Industries[®], Essen, Germany, have a wide range of functions including, controlled release, immediate release and enteric coating. Eudragit E 100 is a cationic aminoalkyl methacrylate copolymer, used in immediate release coatings and has a dimethyl aminoethyl functional group and an average molecular weight of approximately 150,000 kDa. The 'E' simply denotes the polymer is intended for immediate release. The polymer is used as a protective coating for odour/taste masking and to protect the substrate from moisture or light (Evonik, 2008). The mechanism of the polymers odour and taste masking is different to HPMC; Eudragit E100 is insoluble above pH 5, making it insoluble in saliva (which is pH 6.8). Once the polymer enters the low pH (pH 1-2) of the gastric fluids the dimethyl aminoethyl groups are protonated causing an increase in hydrophilicity of Eudragit E 100 leading to a swellable and permeable film to exist in these conditions (Chourasia and Jain, 2003).

Cerea *et al* (2004) demonstrated the use of a novel dry powder coating process using Eudragit E PO, which is the micronised form of Eudragit E 100, to form films for taste masking and moisture protection. The film coating process dispensed with the need for organic or aqueous solvents, instead the Eudragit powder was applied to the substrate under increased temperature forming a loose film coat. Further coalescence was achieved during curing, and although there was the advantage of no solvents, relatively high curing temperatures were needed for complete coalescence of the films. This can be a disadvantage in pharmaceutical formulation with many drugs being thermolabile, thus requiring the avoidance of excessive temperatures during processing to avoid their degradation.

1.1.1.2 Sustained Release Polymers

There are a number of polymers used for sustained drug release, and as for immediate release preparations methacrylate copolymers and cellulose derivatives are important polymers.

Ethylcellulose (EC) has a widespread and longstanding use as a polymer for sustained release film coating. EC is produced from natural cellulose, which is alkalisied and then reacted with ethyl chloride, to produce crude ethylcellulose, and is subsequently purified. It is a hydrophilic polymer which is practically insoluble in water, but when formed into a film is however permeable to water (Dow, 2005a). Ethylcellulose is soluble in a wide variety of organic solvents including chlorinated solvents, natural oils and aliphatic alcohols; as such ethylcellulose has historically been dissolved in ethanol prior to coating (Bodmeier and Paeratakul, 1989). As ethylcellulose is practically insoluble in water this prevents the coating of ethylcellulose simply dissolved in an aqueous medium. Therefore to avoid the use of organic solvents aqueous dispersions are used, where the water insoluble polymer is incorporated into a colloidal structure which is then dispersed in an aqueous medium. There are two aqueous dispersions of ethylcellulose available, Aquacoat[®] and Surelease[®], which are discussed further in section 1.2.2. Surelease, which is produced by Colorcon, is manufactured by melt extruding the EC with oleic acid and dibutyl sebacate (or fractionated coconut oil). The raw materials are heated, mixed and then homogenised in an extruder then the resulting mix is introduced to

ammoniated water. On mixing an emulsion is formed and ammonium oleate is produced which acts as a stabiliser of the colloidal structure (Colorcon, 2006a; 2006b).

There has been much interest in determining the mechanism of drug release from various dosage forms coated with ethylcellulose films (Ozturk *et al.*, 1990, Frohoff-Hulsmann *et al.*, 1999a, Frohoff-Hulsmann *et al.*, 1999b). The ethylcellulose coating around the substrate provides the main method of controlling drug release rate and is termed a reservoir system. It is understood that for substrates coated with ethylcellulose which use organic solvents in the coating solution drug release is via diffusion through the continuous polymer phase. When the tablet comes into contact with an external dissolution medium the liquid passes into the tablet matrix through molecular sized gaps between polymer chains and dissolves the drug in the core. The drug then diffuses through the membrane and out into the dissolution medium. The release rate for diffusion controlled release can be given by the following equation:

$$J = \frac{p_m}{\delta} (C_s - C_b) \quad (1.1)$$

where J is the flux, C_s is the concentration of drug at the drug-film interface and C_b is the bulk concentration of drug δ represents the film thickness and p_m the permeability coefficient, which is derived:

$$P_m = \frac{D\varepsilon}{\tau\beta} K \quad (1.2)$$

D equals molecular diffusivity, ε the volume fraction of the gaps, τ the tortuosity (the ratio of the transport distance in the gaps compared to the distance in solution, β represents the degree of cross-linking crystallites in the polymer and K the distribution coefficient of the drug between the film and water (Ozturk *et al.*, 1990).

Ozturk *et al* (1990) reported that the mechanism for drug release in ethylcellulose films produced from Aquacoat[®] is mainly via osmotic pressure, which is generated due to the high concentration of drug and tablet core excipients within the film relative to the dissolution medium. The osmotic pressure results in water diffusing

into the film and drug release occurring through aqueous pores in the film coat, which are generated via incomplete coalescence of the film or the leeching out of water soluble additives and polymers. The authors noted there was a small contribution of drug diffusion through the polymer film and diffusion through aqueous pores. The following equation was proposed to describe the mechanism of release from pellets coated with an aqueous dispersion of ethylcellulose.

$$J = \left[\alpha \Delta \Pi + \frac{P_p + P_m}{\delta} \right] (C_s - C_b) \quad (1.3)$$

where α is the osmotic force, $\Delta \Pi$ is the difference in osmotic pressure across the coating, P_p is the permeability coefficients for the aqueous pores and P_m is the permeability coefficient of the membrane, δ represents film thickness, C_s is the core surface concentration and C_b is the bulk drug concentration. This equation assumes however that drug release via the three mechanisms mentioned above occurs independently and in parallel.

Varying the molecular weight of ethylcellulose can control the drug release rate, and Rowe (1986) studied the effects of different molecular weights of ethylcellulose finding that as molecular weight increased drug release decreased. The principle conclusion from the study was that at lower molecular weights the internal stresses present during manufacturing caused flaws in the film surface. As molecular weight increases the polymer becomes more resistant to these stresses up to a limit of 35,000 Da where no more reduction in drug release occurs. Variance of molecular weight is not the only method to modify drug release. Increasing film thickness tends to retard drug release, and conversely decreasing thickness increases release. However thin coats have a greater degree of variability in drug release, therefore thicker coats are often applied with an immediate release polymer incorporated into the coating solution to prevent excessively long drug release times. This is discussed further in section 1.1.1.4.

There are also a number of Eudragit preparations that are designed for sustained release drug delivery. For these coating systems, as for Eudragit E100, release is mediated through the changing pH of the gastrointestinal tract (GIT). Examples of

Eudragit preparations designed for sustained release include Eudragit RL 100, Eudragit RS 100 and Eudragit NE30D.

Zein proteins, which are produced from maize seeds have gained interest as a pharmaceutical excipient, with interest as both a matrix in monolithic controlled release tablets (Georget *et al.*, 2008) and as a film former in controlled release coatings (Guo *et al.*, 2008). As Zeins are produced from a food product they are generally regarded as safe and due to their hydrophobic nature are suited to controlled release applications, and could potentially provide an alternative to Lactose as a pharmaceutical excipient. Similar to ethylcellulose Zeins are insoluble in water but freely soluble in ethanol, therefore there is interest to incorporate Zeins into aqueous dispersions (Guo *et al.*, 2008, Bisharat *et al.*, 2011).

1.1.1.3 Enteric Coating Polymers

Enteric coats are designed to protect drugs that are acid labile/irritant to the gastric mucosa by allowing minimal drug release in the stomach, followed by rapid release in the intestine. The majority of enteric coated dosage forms that are coated in a polymer that is sensitive to changes in pH, therefore exploiting the increasing pH of the gastrointestinal tract, which increases from pH 1-2 in the stomach to pH 6-7 in the small intestine, and finally in the distal Ileum pH 7-8 (Chourasia and Jain, 2003). The polymers used are designed to be insoluble at gastric pH and, depending on their chemical composition, they dissolve in the region of pH 5 to 7 (Friend, 2005). Thus the drug is not released in the stomach or distal ileum, but in the terminal ileum or ileocaecal junction, and therefore protects either the acid labile drug or the gastric mucosa. One of the most commonly used pH-dependent polymer is Eudragit[®], which is present in a number of preparations e.g. Asacol (Eudragit S) and Colpermin (Eudragit[®] S100 and Eudragit[®] L30 D55) (EMC, 2010 and EMC, 2013).

1.1.1.4 Polymer Blends

Alteration of the formulation is the primary method to alter the delivery characteristics of a tablet. For example the addition of plasticisers, altering the amount of the film coat that's applied or even changing the type of polymer. All

these options present problems however, in the case of altering the polymer there are only a certain number of approved polymers, and there is an optimum concentration of plasticisers and thickness of the film coating. Siepmann *et al* (2008) have described polymer blends in detail in a recent review article, so only a brief overview will be given here.

A major use of polymer blends is to improve the drug release profiles of coated tablets. By the use of more than one polymer it is possible to achieve a number of different release profiles other than immediate, delayed or sustained release. Pulsatile drug delivery is one possibility, where the drug is released in pulses. An example of this is by the use of a capsular system which combines immediate release portion, a “plug” and a controlled release portion of the dosage form. The immediate release component results in an initial release of drug once the dosage form comes into contact with the dissolution medium, then the plug which is often a hydrogel swells and expands eventually forcing itself out of the capsule exposing the controlled release component to the dissolution medium. A similar approach is a combination of immediate release followed by a period of controlled release which removes the initial lag observed with some controlled release preparations. The release characteristics can be customised for the designated purpose.

A well-established polymer blend is to mix a soluble and insoluble polymer together. There has been extensive study into HPMC and EC blends (Frohoff-Hulsmann *et al.*, 1999a, Frohoff-Hulsmann *et al.*, 1999b, Lippold *et al.*, 1989). It was found that in films using a water soluble plasticiser such as triethyl citrate (TEC) or diethyl phthalate (DEP) the HPMC and plasticiser dissolve and leach out of the film when exposed to dissolution media, leading to aqueous pores being formed in the EC matrix. In this instance HPMC is described as a pore former. In this system zero order kinetics were observed, however if plasticisers such as dibutyl sebacate (DBS) and dibutyl phthalate (DBP) were employed a two-phase release profile is observed. This is due to the HPMC dissolving and leaching out as observed with TEC and DEP, causing an initial burst of drug release. However the plasticiser remains in the EC portion of the film, and along with water trapped in the pores plasticises the film, causing a lowering of the T_g . The authors argued that the T_g of the film was then

below body temperature and thus the film was in a rubbery state causing closure of the pores, and therefore the rate of drug release is reduced.

Other examples of polymer blends include the mixing of Eudragit® RL 30D, which is insoluble but readily permeable, and the less permeable Eudragit® RS 30D. Amighi and Moës (1995) investigated this blend, as can be seen in Fig. 1.1. With 100% of the tablet coated in RL 30D drug release was slowed to a small degree, however by increasing the less permeable RS 30D component of the film drug release can be decreased significantly, and controlled accurately by using a number of different blends.

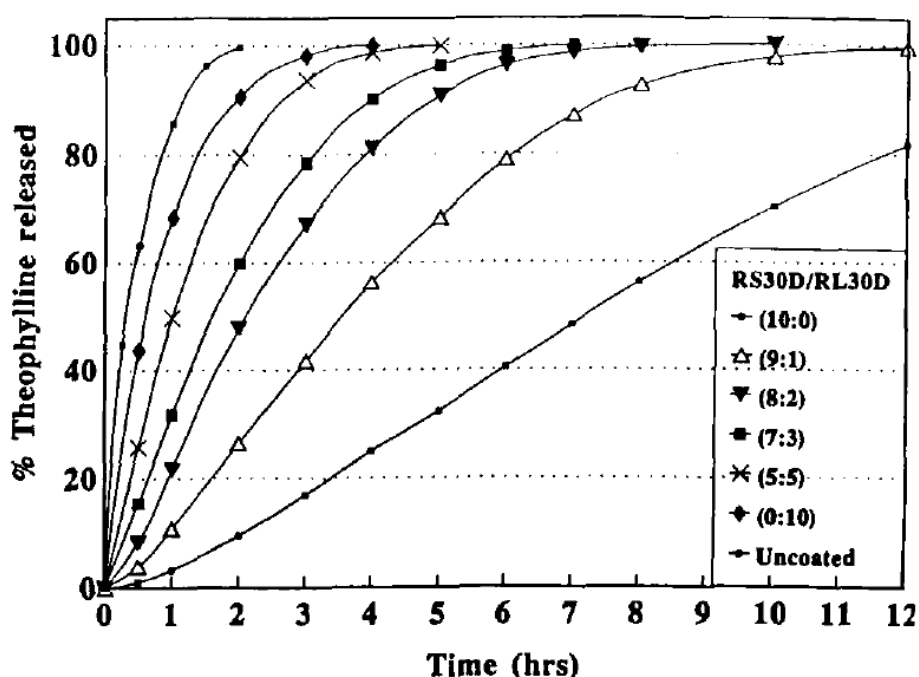


Figure 1.1 Showing Theophylline release from Eudragit RS30D and RL30D blends of varying proportions (Reproduced from Amighi and Moës, 1995)

Plasticisers play another important role in polymer blends, as plasticisers have different affinities for different polymers then unequal distribution between the two polymers by the plasticiser may be observed. Lecomte *et al* (2004a) observed that due to the partition coefficient of DBS being different between EC and Eudragit® L then redistribution of the plasticiser occurred and that drug release was slightly altered. By the use of different preparation techniques and curing parameters the effects could be negated.

A major disadvantage to polymer blends is that most polymers are incompatible and undergo near complete phase separation, due to a decrease in combinatorial entropy due to the large molecular weight of polymers. As mixing is governed by the Gibbs free energy equation:

$$\Delta G_m = \Delta H_m - T\Delta S_m \quad (1.4)$$

where ΔG_m corresponds to the free energy of mixing, ΔH_m represents the enthalpy of mixing, T is the absolute temperature and ΔS_m denotes the entropy of mixing. The negative ΔG_m required for mixing to occur spontaneously favours a large and positive ΔS_m . The most common expression of Gibbs free energy for polymer blends is the Flory-Huggins equation (Flory, 1966):

$$\Delta G_m = kT(N_1 \ln v_1 + N_2 \ln v_2 + \chi_1 N_1 v_2) \quad (1.5)$$

where k is the Boltzmann constant, T is absolute temperature, N_i is the number of molecules of species 1 and 2, v_i is the volume fraction of polymer 1 and 2, and χ_1 is the Flory-Huggins interaction parameter. The first two terms in equation (1.5) are entropic terms and as χ_1 is derived thus:

$$\chi_1 = \frac{\Delta H_M}{kTN_1v_2} \quad (1.6)$$

Then it can be seen that by rearranging equation (1.6) that χ_1 is an enthalpic term. In the case of mixing the large polymer molecules, there are fewer ways to organise the molecules and thus ΔS_m is small, making χ_1 the most important term. Miscibility between two polymers can be calculated by using the following equation:

$$\chi_{crit} = \frac{1}{2} \left(\frac{1}{\sqrt{v_1}} + \frac{1}{\sqrt{v_2}} \right)^2 \quad (1.7)$$

where χ_{crit} is the critical polymer interaction parameter, and for the polymers to be miscible then $\chi_1 < \chi_{crit}$. χ_{crit} for larger molecular weight polymers tends to be close to zero, so negative χ values are required for miscibility (Ougizawa *et al* 1999).

This has been demonstrated by Sakellariou and Rowe (1995b) in EC and HPMC blends, where χ_1 for the mix was given as 1.04, and the χ_{crit} was equal to 0.04. This was explained by the lack of dipole-dipole/induced dipole and hydrogen bonding occurring between EC and HPMC.

If two different polymers do interact then they are likely to phase separate at a higher temperature (contrary to many other systems where phase separation occurs at lower temperatures), giving rise to a lower critical solution temperature (LCST) (Sperling, 2006). This is due to the Flory-Huggins interaction parameter increasing with an increase in temperature therefore making it more likely to exceed χ_{crit} .

Other factors to consider when blending polymers is the colloidal latex particles becoming unstable leading to flocculation and sedimentation within the dispersion, which will be described below in section 1.2.2.

1.2 Solvents

A number of polymers are water soluble and require simply mixing with water to produce a solution; however many polymers are not soluble in water and historically organic solvents were utilised as solvents to dissolve these polymers. There are, however a number of drawbacks regarding the use of organic solvents, and over the past couple of decades aqueous colloidal dispersions have come to the fore and both methods will be described below.

1.2.1 Organic Solvents

Organic solvents have the advantage of a low latent heat of vaporisation, in the region of 200kcal/kg for ethanol, compared to around 540 kcal/kg for water (Mehta, 2008); therefore requiring less thermally efficient forms of coating equipment. However organic solvents are highly flammable so there is a notable safety and financial aspect, due to the need for more expensive facilities to be built. Disposal of the end solvent adds to the financial and environmental cost. Invariably a proportion

of the solvent remains in the film, which has to be accounted for, and may pose a risk to the patient. This has led to the utilisation of aqueous coating of film coats even for polymers that are insoluble in water which require more complicated formulation and process conditions.

1.2.2 Aqueous Colloidal Dispersions

Aqueous dispersions are a method of incorporating polymers, which usually require organic solvents, into aqueous media. There are two forms of aqueous dispersions, latexes and pseudolatexes, which differ in their method of production. Latexes are produced from emulsion polymerisation, whereas pseudolatexes are preformed polymers, which are then emulsified (Bodmeier and Paeratakul, 1989). The production of latexes involves the addition of surfactants and initiators to an aqueous monomer solution. The surfactant, for example sodium lauryl sulphate, forms micelles and monomers diffuse into them. When an initiator enters the micelle, which is typically a free radical source, polymerisation of the monomers occur (by free radical polymerisation if a free radical initiator is used). Polymerisation is terminated when a second free radical enters the micelle. Pseudolatexes however are manufactured by making a polymer solution in an organic solvent, which is then emulsified in an aqueous phase containing surfactants and stabilisers. Homogenisation followed by solvent removal forms the aqueous colloidal dispersion. An example of this type of aqueous colloidal dispersion is the FMC Biopolymer manufactured Aquacoat[®] ECD.

Surelease[®] is an ethylcellulose pseudolatex produced by Colorcon; however it is manufactured in a slightly different manner. Oleic acid and dibutyl sebacate are mixed with ethylcellulose and the resultant blend is melt-extruded. The melt is then emulsified in ammoniated water producing ammonium oleate which reportedly acts as a stabiliser to the dispersion.

Latex and pseudolatex dispersions are generally adjusted to around 30% solids, without excessive increases in viscosity, which is a major advantage over organic solvent systems. Particle size is important; as if it is too high the colloidal dispersion

may become unstable leading to caking, so the particle size is usually on the sub-micron scale, approximately 0.1-0.3 μ m.

A disadvantage of aqueous dispersions is they are sensitive to fluctuations in pH, temperature and electrolytes. Bodmeier and Paeratakul (1989) described latex flocculation or coagulation between sodium lauryl sulphate and ammonium oleate in Aquacoat[®] and Surelease[®] respectively with the anionic drugs chlorpheniramine maleate and propranolol HCL, when drugs were mixed with the latex.

The sensitivity of aqueous dispersions to alterations in pH has been reported in Zein polymeric systems (Guo *et al.*, 2008). Stability of aqueous dispersions can be described by the zeta potential (ζ), which is a measure of repulsion, in this instance, between latex particles. A high ζ indicates the dispersion will be stable, as the particles will repel each other, however if the ζ is low then attractive forces overcome the repulsion and flocculation will occur. As the ζ can be positive or negative, only the magnitude not the sign dictates whether the dispersion is stable. It can be seen from Fig. 1.2 that the ζ is at a maximum circa pH 3 but above and below

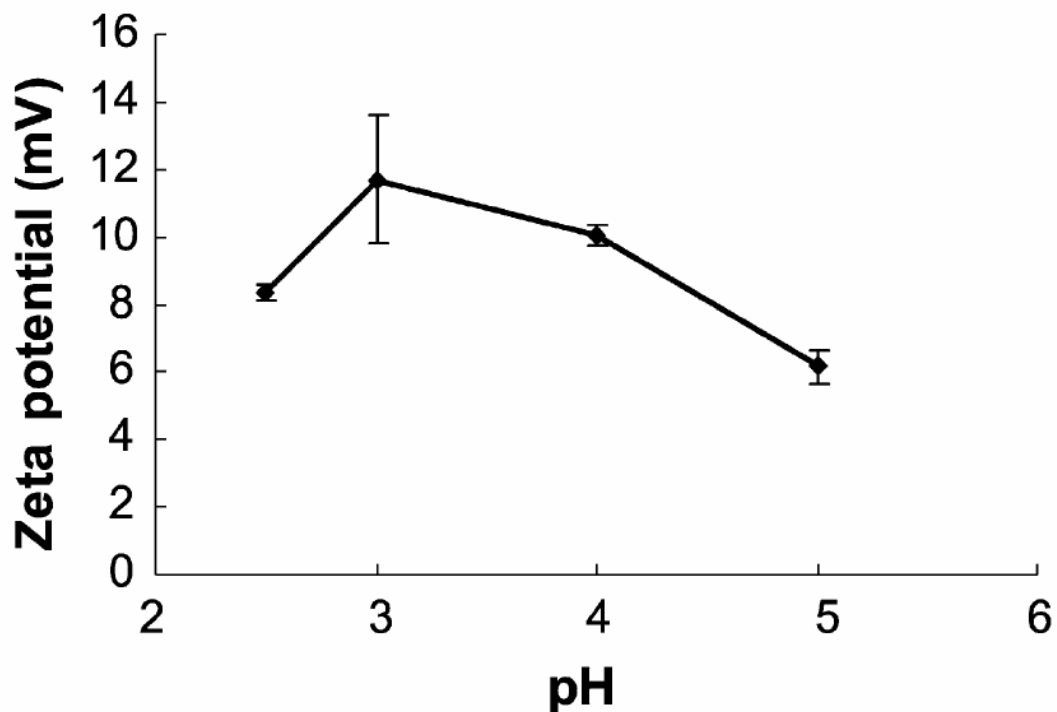


Figure 1.2 showing the zeta potentials of zein dispersions from pH 2.5-5 (Reproduced from Guo *et al.*, 2008)

pH 3 ζ declines, indicating a less stable dispersion. These factors are important during formulation as destruction of the colloidal structure will have a detrimental effect on film formation, however these incompatibilities can be overcome by modifying the formulation of the aqueous dispersion, for example changing the surfactant for a non-ionic alternative.

Neither method of aqueous dispersion manufacture is ideal with emulsion polymerisation potentially resulting in excess monomers and free radicals, and the emulsification of preformed polymers tending to involve organic solvents. However they do provide a very useful method to avoid the use of organic solvents during the film coating process.

1.3 Additives to Coating Solutions and Dispersions

A handful of coating systems consist solely of the polymer and a solvent, however the majority require additives to be added to allow or improve the film forming process. Although additives allow for the formation of the film, their inclusion increases the complexity of the coating system, through such issues as compatibility and stability. Below are a number of commonly used additives, and issues surrounding them.

1.3.1 Plasticisers

With the exception of polymers, plasticisers are the most commonly used excipients in polymeric films. This is especially true of latex dispersions, as plasticisers are often required to achieve coalescence during film formation. Plasticisers are generally small molecular weight compounds, which are employed to improve the mechanical properties of dried polymer films by allowing tough and flexible films to be formed. They achieve this through reduction in the glass transition (or in semi crystalline polymers through a reduction in crystallinity or melting temperature) of the polymer. Plasticisers affect the mechanical properties of the films by decreasing the elastic modulus and tensile strength, and through increasing the percentage elongation (Felton and McGinity, 1997).

There are a number of theories of the mechanism of action of plasticisers, including lubricity theory where the role of the plasticiser is to decrease the internal friction between polymer chains sliding over each other when put under stress and gel theory where the plasticiser reduces intermolecular polymer bonding therefore reducing the rigidity of the polymer structure and the free volume theory. They all agree that plasticisers penetrate the polymer mass, disrupting interpolymer bonds and therefore decreasing intermolecular forces and increasing polymer backbone mobility. Of the theories, free volume theory arguably most accurately describes plasticiser behaviour. Free volume describes the internal space within a polymer that the polymer chain can move in, therefore if the free volume increases this allows for increased molecular mobility of polymer chains. As plasticisers increase molecular mobility in the polymer then it follows that an increase in free volume occurs. Motion of the end group, side chains, or the main chain can all cause an increase in free volume, thus any factor to increase these motions will increase the free volume (Marcilla and Beltrán, 2004). Such factors include, increasing the temperature of the system, increasing the number of end groups (i.e. a lowering of the polymers molecular weight) or increasing the number or length of side chains. The last point here is an example of internal plasticisation, i.e. the addition of a compound to the polymer, which is not an ideal solution in the pharmaceutical industry due to regulatory restrictions on the polymers available to use as pharmaceutical excipients. However the same effect can be achieved by the inclusion of an external plasticiser, which is a compound not molecularly bound to the polymer. It can be seen from the above statement that due to plasticisers being smaller molecules than polymers this increases the free volume due to an increase in end groups in the system (Mark, 2004). In addition branched plasticisers are more effective than linear plasticisers, due to the presence of side chains.

The effectiveness of plasticisers depends on a number of factors, including their solubility and interaction parameters. Compatibility between the plasticiser and polymer can easily be observed via thermal techniques, as a single, intermediate T_g will be observed if the two are miscible, which will decrease with increasing plasticiser content up to a point where increasing the plasticiser content will no longer reduce the glass transition temperature (Miller and McGinity, 2008).

There are numerous plasticisers available in the chemical industry; however there is a limited number for use in pharmaceuticals due to the toxic nature of many plasticisers. Plasticisers are generally divided into water soluble or insoluble. In polymer solutions the plasticiser is incorporated directly into the polymer, but when plasticisers are added to aqueous dispersions the incorporation process is more complex. After dispersion or dissolution in the aqueous phase the plasticiser has to diffuse into the latex particles where it can then exercise its plasticising effect on the polymer. Depending on the affinity of the plasticiser to the polymer phase and the plasticisers hydrophilicity there will be different rates and extents of plasticiser uptake by the latex particles. This creates the need to allow adequate time for the plasticiser to partition into the polymer phase. Plasticisers are of particular importance in functional coatings such as enteric coats and sustained release preparations where continuous non-cracked films are required. Furthermore the addition of plasticisers tends to retard drug release, because of the formation of more continuous films, due to better coalescence of the latex particles (Lippold *et al.*, 1989).

Plasticiser content is usually circa 20% of the polymer weight, and there is an optimal mass of plasticiser that is added, as if too much plasticiser is added then when the substrate is coated the film may become tacky due to the temperature being above the polymers glass transition temperature, and can lead to film defects, which are discussed in more detail in section 1.7.

There has been extensive research into the role of plasticisers in film coating, varying from the choice of plasticiser and the effects of different plasticisers (Lecomte *et al.*, 2004a, Repka *et al.*, 1999), to novel plasticising agents. Regarding the use of novel plasticisers Wu and McGinity (1999) observed the drugs methylparaben, ibuprofen and chlorpheniramine maleate acting as plasticisers of Eudragit® RS 30D polymeric films. The authors reported that all reduced the glass transition of the films, with methylparaben and ibuprofen also decreasing the Young's modulus of the polymer films. The plasticising effect was attributed to ammonium and ester groups in the polymer interacting with the drugs via hydrogen bonding, causing disruption of interpolymer hydrogen bonding.

1.3.2 Other Additives

Several other additives are sometimes needed in the formulation. Detackifiers are one such example, and are often needed in aqueous coating solutions. Due to plasticiser content and the relatively high temperatures used during the coating process films can become tacky which can lead to defects and even agglomeration of substrates. Several detackifiers exist including talc and magnesium stearate.

Pigments are often added to coating formulations for several reasons including improving the appearance of the final tablet, as tablet cores sometimes have a mottled appearance due to the different components of the substrate formulation. Other reasons include product identification, and as pigments are often opacifiers, to protect photo-sensitive drugs from photolytic degradation. The amount of pigment added depends on the final colour required, but large quantities are often necessary for example in a typical Methocel formulation the pigment weight is from 50-200% of the polymer weight (Dow 2002).

1.3.3 Drugs

High potency drugs are sometimes not incorporated into the substrate; instead, the substrate is inert and is essentially a carrier for the drug loaded film, and the possibility exists for free films to be used for buccal delivery (Peh and Wong, 1999). In addition drugs occasionally partition into films from the tablet core during the coating process and storage. Therefore there has been attention in determining how drugs behave in polymer films.

When drugs are incorporated into films depending on the solubility parameters of the polymer and drug, either the drug is molecularly dispersed as a solid solution within the polymer forming a transparent film, or the drug and polymer are in two phases, either in crystalline or amorphous form embedded within the polymer producing an opaque film (Wu and McGinity, 2001).

As discussed previously for spontaneous mixing to occur the Gibbs free energy must be below zero and as mixing generally produces an increase in entropy then,

especially, in polymer systems where entropy tends to be relatively low the enthalpy of mixing is a crucial term in Gibbs free energy equation. Okhamafe and York (1987) described the following equation to calculate the enthalpy of mixing:

$$\Delta H_m = V_m(\delta_1 - \delta_2)^2 \varphi_1 \cdot \varphi_2 \quad (1.8)$$

with V_m the total volume of the mixture, δ_x the solubility parameter with x representing either component 1 or 2, and φ_x the volume fraction. The solubility parameter is calculated through the following equation:

$$\delta_x = \left(\frac{\Delta E^x}{V^x} \right)^{1/2} \quad (1.9)$$

where ΔE is the energy of vaporisation and V the molar volume. Therefore it can be seen from equation 1.8 if the two solubility parameters are numerically close a low enthalpy of mixing will result leading to the probable mixing of the two components.

A common phenomenon is that the drug is present as a solid solution up to its solubility limit in the polymer, and then above the solubility limit any extra drug content is then present as a separate, often crystalline, phase. Whether a drug is present as a solid solution, or in two phases can greatly affect the properties of the film, for example it can affect the films mechanical properties, the stability of the drug in the film, and drug release from the film. If drugs are incorporated into a latex dispersion then interactions between the dispersion and drug need to be considered as flocculation (the contact and adhesion of the colloidal particles into larger clusters) of latex particles can occur when additives are added (Bodmeier and Paeratakul, 1989).

There is a possibility of drug migration into the film coat, especially during the coating process or on storage. There may be dissolution of small amounts of the drug and/or additives due to the solvent in the coating process or residual solvent or moisture during storage, which can again affect the final properties of the film. This effect is much more likely to occur if the drug or excipient is soluble in the coating

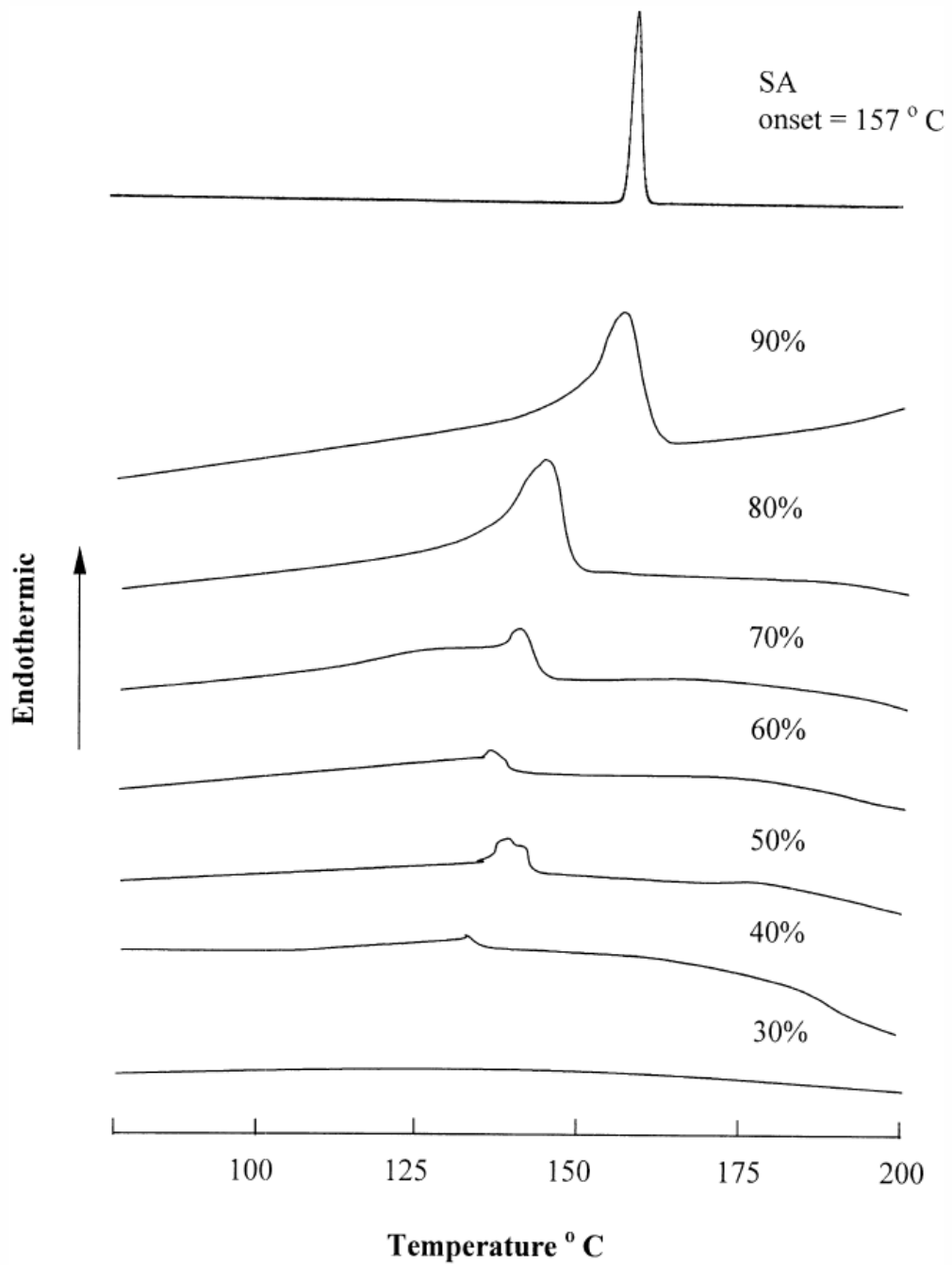


Figure 1.3 Showing phase separation occurring with increasing concentration of salicylic acid (SA) in chitosan films (reproduced from Puttipatkhachorn et al., 2001)

solution. Dansereau *et al* (1993) reported that by using a low spray rate to decrease particle size, or by increasing the inlet air temperature, migration was decreased.

However it was noted that other authors have found that decreasing air inlet temperature decreases migration, which would be a more logical proposition as many additives, can melt at temperatures used in film coating and therefore increase

the chance of migration. To prevent drug migration seal coats can be used such as an immediate release coat, such as HPMC, which does not retard drug release but can stop migration. Wu and McGinity (2001) reported an example of drug release from polymer films being affected by drug incorporation into the film. In the study, non-pareil beads were coated with Eudragit[®] RS 30 D containing ibuprofen and drug release was determined for differing levels of drug concentration. The findings indicate that increasing concentrations of ibuprofen retarded drug release from the film due to the plasticising effect of ibuprofen on the films causing an increase in Eudragit coalescence.

Conversely Bodmeier and Paeratakal (1989) reported that increasing the load of propranolol HCL above 100mg in Eudragit[®] NE 30D films caused a rapid initial drug release followed by a similar release rate to films loaded with 100mg and under. This indicates that drug release is constant out of the film when present as a solid solution, but once the solubility limit is reached the drug is present in a separate phase, resulting in rapid release. Fig. 1.3, from Puttipipatkachorn *et al* (2001), shows the phase separation occurring with increasing salicylic acid concentrations in chitosan films. At concentrations above 30% a melting endotherm is observed indicating that below this concentration the salicylic acid is dissolved in a solid solution but above this the salicylic acid existed as a separate crystalline phase.

1.4 Substrates

Polymer films for the most part are applied to a substrate, although there has been work in the use of free films for buccal delivery through mucoadhesive films and for transdermal application (Lieb *et al.*, 2002). In this section, however the focus will be on application of polymer films to solid dosage forms.

1.4.1 Tablets

Tablets are the most well-known and wide spread solid dosage form, and as such the majority of the literature regarding film coating to solid substrates concerns the coating of tablets. However there are issues with film coating tablets. Most tablets

have relatively sharp edges, which can lead to inconsistent deposition of the coat. Other considerations in the development of film coats are logos and break lines on the tablet, which with a poor formulation, can be filled with the coating solution leading to a poor appearance of the finished coat.

1.4.2 Pellets

Multiparticulate drug delivery systems offer a number of advantages over monolithic devices, such as quicker gastric emptying and more reproducible gastric transit times. They can also be utilised to give a constant level of drug release through a mix of immediate release fractions and sustained release fractions of the multiparticulate, providing an alternative option if blending polymers is not possible. Pellets are typically produced via extrusion spheronisation, although there are a number of other methods including spray drying and spray-congealing. Extrusion spheronisation has several advantages including the equipment's ease of use, high throughput, and the production of uniform spheres with low friability (Ghandi *et al.*, 1999). Extrusion spheronisation involves preparation of a wet mass in a granulator, which is then extruded in the extruder. The extruder shapes the plastic mass into long rods through the use of a singular or multiple Archimedes screws that drives the granulation liquid through an extrusion screen. The rods are then placed on a rotating friction plate called a spheroniser, which through frictional forces shapes the rods into spheres. The spheres then need to be dried in an oven to expel residual moisture from the pellets.

The process of extrusion spheronisation needs to be optimised to form good quality pellets. For example the water content of the wet mass must be within limits, if there is too little water there will be excess dust production, and with too much water agglomeration of the pellets can occur. Similarly the speed of the spheroniser also requires upper and lower limits. If the friction plate is moving too slow then round pellets will not form; however if it is too fast then again agglomeration may result (Vervaet *et al.*, 1995).

Pellets are often incorporated into hard gelatine capsules, but can also be compressed into tablet form. In granular form they can easily be film coated due to their spherical shape as there are no sharp corners which are present with traditional tablet shapes.

1.4.3 Minitablets

Minitablets are a relatively new form of multiparticulate drug delivery system, which have attracted recent attention. They are generally 2-5mm in diameter and weigh in the region of 10-100mg, depending on the molecular weight of the components and the minitables dimensions (Lopes *et al.*, 2006, Siepe *et al.*, 2008). Minitablets are generally prepared via direct compression and then incorporated into a hard gelatin capsule in a similar method to pellets (Ishida *et al.*, 2008); however they present a number of advantages over pellets. One advantage is that direct compression produces a stronger substrate than granulation, which increases the robustness of minitables during the film coating process. Another advantage presented by direct compression is that variations between batches tend to be smaller than with pellets, and more reproducible sizes of tablet and strength of the active pharmaceutical ingredient is achieved (Lennartz and Mielck, 1998). Additionally less coating material is required to coat minitables than pellets due to the relatively smaller surface area. However the shape of tablets makes minitables harder to coat and the direct compression introduces an extra step into the manufacturing process, and the need for specialist equipment.

1.5 Film Coating

As described earlier film coats are applied to solid dosage forms for a variety of reasons. This section will describe the equipment used to film coat the chosen substrate, how the films are formed and adhere to the substrate, curing of the coated substrate and common defects associated with coating.

1.5.1 Film Forming

The film forming process differs between organic solvents and aqueous based polymer systems. Due to the reduction in the widespread use of organic solvents in

film coating, a brief outline of film formation using organic solvents is provided followed by a more in depth description of film forming in aqueous systems.

1.5.1.1 Film Forming from Organic Solvents

Film formation from organic solvent based systems is considerably different from aqueous dispersions. The organic solvent begins to evaporate from the solution and when the polymer concentration reaches a certain concentration an intermediate stage analogous to a gel is formed. The solvent continues to evaporate eventually causing the polymer particles to become immobile (which is known as the solidification point), at which the polymer film is formed. However not all of the organic solvent is removed, and more of the solvent continues to diffuse through and evaporate from the film. In addition the quality of the final film is dependent on the compatibility of the polymer and the solvent, with components of similar solubility parameters allowing maximum extension of the polymer chains allowing strong interaction between the polymer chains in the resultant film (Porter, 1989).

At this point it is worth noting that the differences in film formation can have an effect on the drug release behaviour. It has been noted that films prepared from organic solvents retard drug release more significantly than those of aqueous dispersions. Lecomte *et al* (2004b) compared polymer blends cast from aqueous dispersions and organic solutions, suggesting the reason for retardation of drug release of propranolol-HCl from layered sugar cores coated with an EC and Eudragit[®] L blend is the increased mobility of the two polymers during the film forming process. When the organic solvent evaporates the increased mobility allows for a homogenous mix of the two polymers, so when the film comes in contact with a dissolution medium, Eudragit[®] L, which normally swells and becomes increasingly permeable to drugs, is impeded by the EC. Conversely with aqueous dispersions there is limited interdiffusion during the drying stage, with interdiffusion limited to the surfaces of latex particles. Although continuous films are formed, the microstructure is far different in these films with distinct regions of Eudragit[®] L and EC, allowing for swelling of the Eudragit[®] L and therefore increased drug release.

1.5.1.2 Film Forming from Aqueous Dispersions

Aqueous dispersions are considerably different to polymer solutions composed of organic solvent and therefore the film forming mechanism is significantly different. Because of the colloidal structure present in aqueous polymer dispersions the polymer chains are separated by surfactant molecules and need to coalesce to produce a continuous homogenous film. If the film does not coalesce sufficiently a brittle film that does not adhere to the substrate surface may result, which is of particular importance in functional film coats, as if the film is not continuous the film may not provide its intended function. For example if a sustained release solid dosage form film is not formed correctly it can lead to failure of the film and the entire dose being released immediately, which can lead to potential overdose and patient harm.

Films produced from aqueous polymer dispersions undergo three major steps (Chevalier *et al.*, 1992), which are described below, and shown in Fig. 1.4;

1. Concentration of the aqueous dispersion – as water evaporates from the dispersion, the latex particles are forced closer together as film volume decreases. Eventually, as the latex particles make contact they order themselves trapping water between them
2. Deformation of the latex particles – the residual water evaporates, and the spherical particles are deformed into polyhedral cells through interfacial and capillary forces. This is the beginning of particle coalescence and is denoted as the foam structure in Fig 1.4.
3. Particle coalescence continues to proceed through interdiffusion of polymer chains to eventually form a homogeneous mix. Polymer chains must be adequately mobile for interdiffusion to occur, and therefore must be above the polymers glass transition temperature (Hahn *et al.*, 1986).

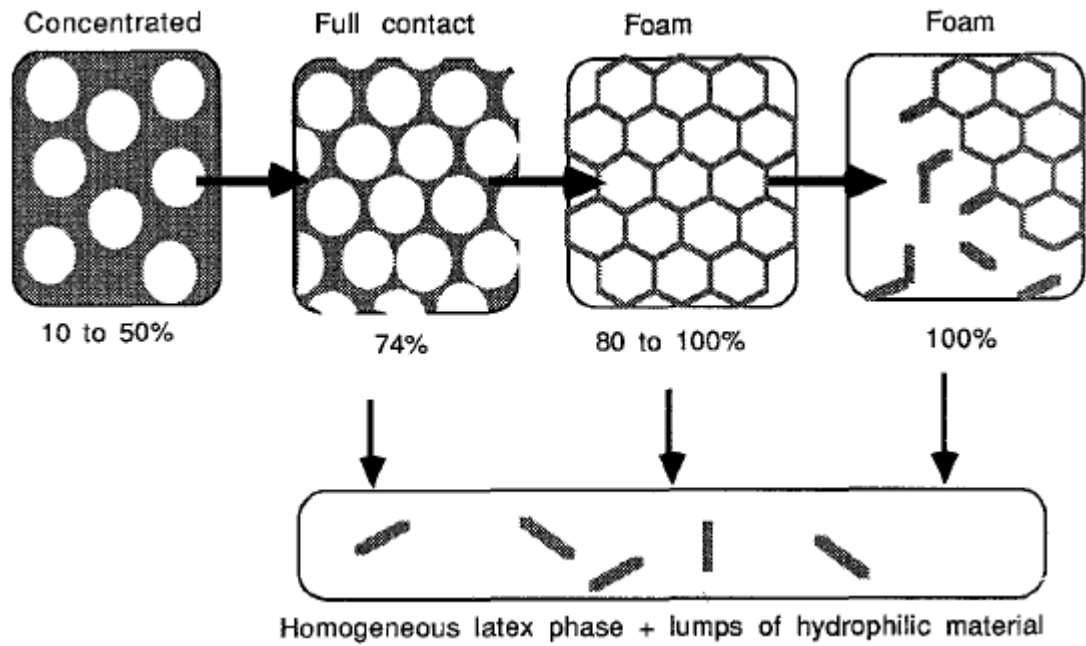


Figure 1.4 Film forming from aqueous latex particles (reproduced from Chevalier *et al.*, 1992)

In addition an increase in the polymer molecular weight will result in a decrease in interdiffusion due to a reduction in molecular mobility, requiring thermal post treatment of the polymer film to achieve an acceptable film coat (Hahn *et al.*, 1988).

1.5.1.3 Minimum Film Forming Temperature

Minimum film forming temperature (MFT) is the minimum temperature needed for films composed of aqueous dispersions to coalesce. If coating conditions are below the MFT then a powder will tend to form on the substrate surface, however if conditions are above the MFT then a continuous film is formed.

The MFT can be determined experimentally through use of a temperature gradient plate. The polymer dispersion is poured onto a plate of varying temperature with hot air blown across it, and the minimum temperature required for film formation can be observed. As the MFT is related to polymer chain mobility then the MFT corresponds to the T_g of the polymer; however MFT tends to be lower than the polymer T_g due to plasticisation from the absorbed aqueous phase and colloid stabilisers (Blackley, 1997). The MFT is important in manufacturing processes as it determines the minimum temperature of the fluid bed that can be set, therefore the

lower an MFT the more advantageous it is financially as the bed temperature can be set at a decreased level. The bed temperature is often set 10°C above the MFT to ensure adequate molecular mobility of the polymer chains to produce a good quality film coat (Frohoff-Hulsmann *et al.*, 1999b). If the coated dosage form requires curing it is also important in determining the temperature a film should be cured at.

1.5.2 Adhesion

Adhesion of the film to the substrate is vital. If a complete loss of adhesion occurs then a loss of film function may ensue, for example the film may no longer be able to protect moisture sensitive drugs, as moisture is able to accumulate in the interfacial region between the film and tablet (Felton and McGinity, 1999). There are two main modes affecting adhesion of the polymer film to the tablet surface, the interfacial work of adhesion, with the main mechanism of interfacial bonding being through hydrogen bonds, but internal stresses within the film are also an important factor (Rowe, 1977).

The following equation derived by Okutgen *et al* (1995), represents a method to calculate the internal stresses within a film coat.

$$P = \frac{E}{3(1-\nu)} \left[\frac{\Phi_s - \Phi_r}{1 - \Phi_r} + \Delta\alpha_{(cubic)}\Delta T + \frac{\Delta V}{V} \right] \quad (1.10)$$

where P is the total value of internal stresses within the film, E denotes the elastic modulus of the film, ν is the Poisson's ratio of the film, Φ_s and Φ_r represent the volume fraction of the solvent at the solidification point and the remaining solvent in the dry film when dried in ambient conditions. $\Delta\alpha_{(cubic)}$ is the change in cubical thermal expansion coefficients of the substrate and the film. ΔT is the difference between the polymer's T_g and the temperature during manufacture and storage of the film. ΔV is the change in volume of the substrate core and V the original volume of the substrate core.

It can be seen from the equation that the elastic modulus of the film coat, the shrinking of the film during coating, differences in thermal expansion coefficients of the film and substrate and changes in volume of the substrate core (during storage) all contribute towards the internal stresses of the film. Therefore any alteration to the formulation, including the formulation of the tablet core, to lower the internal stresses will increase the likelihood of producing films with good mechanical properties. A number of investigations into the effect of adding plasticisers to coating solutions have been published with a paper by Felton *et al* (1996) reporting a decrease in modulus through the addition of plasticisers led to increased adhesion.

1.5.3 Curing

Aqueous film coats in certain cases require a curing step after the film coating process. When the film coat is applied coalescence does not necessarily complete and for a continuous film to form thermal post treatment is used. The film coated substrate is held at a temperature above the MFT of the polymer in either an oven or by leaving the substrates in the coating equipment, i.e. in the coating pan or fluidised bed. The effect of curing is generally to retard drug release through the formation of a continuous film; it is therefore an important step in sustained release coatings to achieve the desired release profile. If curing does not take place then physical aging of the film can occur, where coalescence of the film occurs during storage of the substrate, which can alter the drug release profile over the age of the substrate.

As mentioned above curing tends to retard drug release. However Bodmeier and Paeratakul (1994) found that the curing could enhance or retard release depending on the physicochemical properties of the drug, plasticiser concentration and the curing conditions. For example chlorpheniramine maleate has a low affinity for ethylcellulose and curing slowed drug release. Ibuprofen on the other hand has a higher affinity to ethylcellulose and the researchers found ibuprofen crystals on the film surface, which were ascribed to the drug diffusing through the film, and in this case curing actually increased drug release.

1.6 Film Forming Techniques

A number of techniques are used for film coating although spray coating with a fluidised bed has gained widespread use in recent years. Although there is high mechanical stress directed at the substrate using a fluidised bed this can easily be compensated for during formulation.

1.6.1 Spray Coating

Spray coating of solid dosage forms involves atomising the coating solution and then spraying the atomised solution onto the solid dosage form within a specific area of the film coater. This area known as the coating zone has to have the solid dosage form moved through it to allow coating to take place then removal of the substrate to allow drying to occur before more coating solution is applied. The two most common methods of moving the substrate through the coating zone is through rotation of a pan or use of a fluidised bed.

Pan coating or perforated pan coating have traditionally been utilised to coat pharmaceutical solid dosage forms. Both methods employ a rotating pan placed on a tilted rotating shaft, with a top spray coater used to coat tablets as they are rotated into the coating zone. Pan coaters have the disadvantage of only applying air flow to the surface of the tablet bed, which perforated pan coaters avoid by drawing air through the bed. This achieves the improved drying times required of aqueous film coating, with several variations on air flow depending on the nature of the film coat being applied, e.g. enteric, modified release and aesthetic.

More recently fluid bed designs have been used to coat pharmaceutical dosage forms, especially for aqueous film coating due to the increased drying efficiency, which is required to the higher latent heat of vaporisation of water compared to organic solvents. Fluid bed coaters tend to be either top spray coaters, similar to pan coaters, or bottom spray coaters which come in the form of Wurster coating systems. Wurster coaters have the spray nozzle located in the centre of a distribution plate

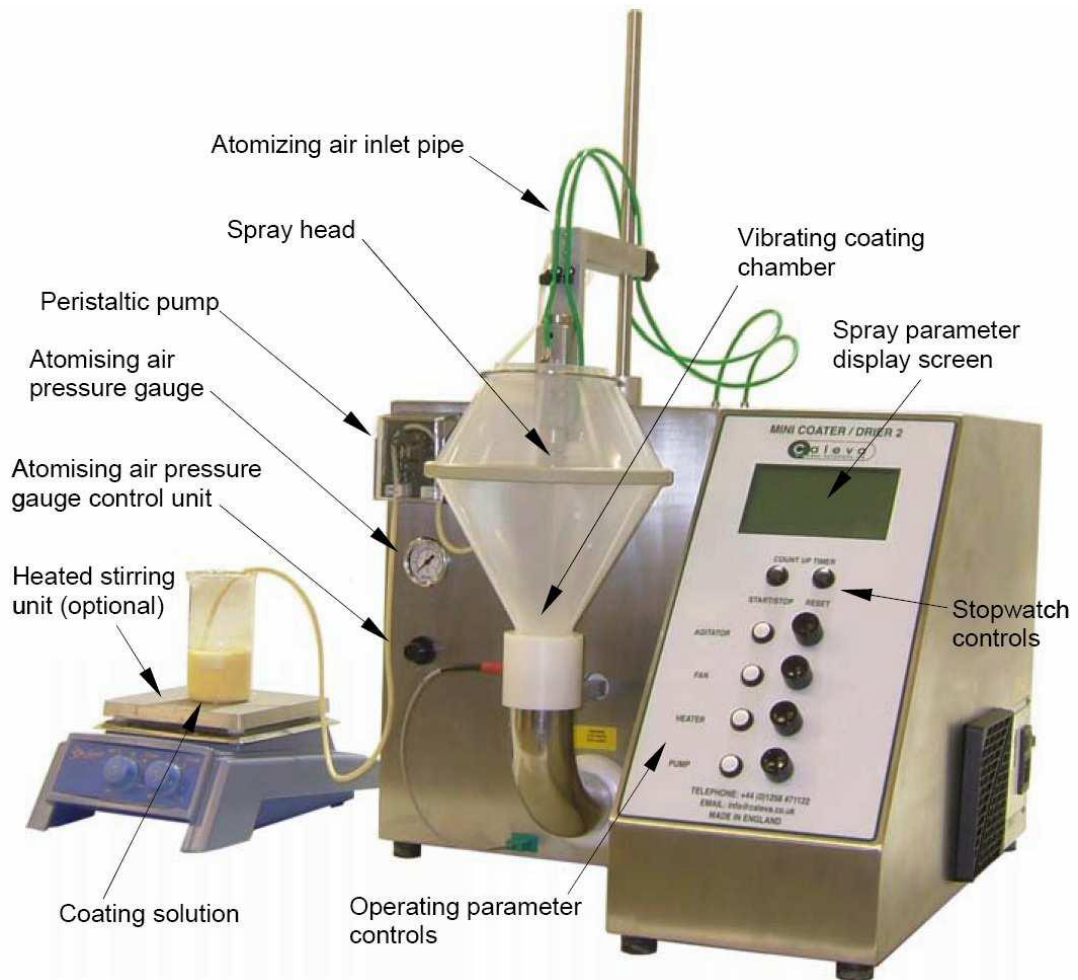


Figure 1.5 Caleva Mini Coater Drier 2 (reproduced from Caleva 2013)

which forces air through a central partition causing fluidisation. This central area of the coater is the location of the coating zone with the area outside allowing the substrates to descend outside the partition. The Wurster process tends to be of particular use to coat small particulates such as pellets, spheres or minitables (Rajabi-Siahboomi and Farrell, 2008).

Fig. 1.5 shows an annotated picture of the Caleva mini coater-drier 2 (MCD-2) The MCD-2 is a bench-top fluid bed coater/drier used to coat a variety of substrates on a laboratory scale of up to around 100 tablets. The MCD-2 is used as an example as it can demonstrate a number of considerations needed in equipment and formulation parameters. Tablets are placed in the vibrating coating chamber, vibration is used to help maintain the fluid bed, and air is forced into the bottom of the chamber, termed



Figure 1.6 Spray head from the Caleva Mini Coater Drier 2 (reproduced from Caleva 2013)

process air, to provide the fluid bed. The coating solution can be placed on a hot plate stirrer, which is used to avoid sedimentation of the coating solution, especially if aqueous dispersions are used, and also to pre-heat the solution. It is fed to the spray head through a peristaltic pump. Peristaltic pumps are used due their low pressure, which is of particular use for latex and pseudolatex dispersions as these are sensitive to the high pressures in other pumps such as gear and piston pumps and can result in coagulation of the dispersion.

The disadvantage of peristaltic pumps though is the long tube which may lead to sedimentation in systems containing solid elements such as opacifiers (Felton, 2004). The coating solution is pumped into the spray head, see Fig. 1.6, where the solution

is mixed with atomising air and is then forced through a needle valve via compressed air, which produces a fine spray directed at the fluidised bed. The substrates of the fluid bed are in constant motion the spray comes into contact with all sides of the substrate and film forming occurs as described in section 1.5.1.1 and 1.5.1.2. There are several parameters important in film coating that can be controlled by the operating parameter controls. The first parameter to consider is the fan speed, which alters the volume of process air passed over the substrates. As the process air is used to dry the film then increasing the air speed will increase the energy available to evaporate the solvent from coating solution. The process air can be heated to achieve the MFT (see section 1.5.1.3) needed for film formation from aqueous dispersions, which is the second parameter that can be altered. Pump speed determines the amount of coating solution delivered to the spray head, and has an important role in preventing defects, described in further detail in section 1.7.

As with many processes the parameters need to be optimised to gain an acceptable film coat. The process air needs to be sufficient to create the fluid bed and therefore optimise heat and mass transfer, but if the fan speed is set too high this can result in significant turbulence in the coating chamber causing fouling of the nozzle and the side of the chamber being coated. Therefore a balance needs to be struck between the temperature and air speed to achieve the optimal coat (Jones, 2008). Alterations in the formulation can also have an effect on the final coat with, for example, an ideal viscosity of polymer solution to use. If the viscosity is too low brittle films will be formed, but if it is too high manufacturing costs will increase (Dow, 2002). In addition increasing the solids content in the coating solution can alter the uniformity and film quality. With an increase in solids less time is required to produce the film; however a rougher coat is produced, so again an optimal concentration needs to be found.

1.6.2 Film Casting

For analytical purposes free films are often produced via casting. The films are generally prepared by pouring of the coating solution onto a Teflon plate or Petri dish allowing the solvent to evaporate, sometimes aided by oven drying. This method negates the need for expensive equipment and makes the analysis of the

films easier as they are free films. However there are several problems with cast films. Due to the long drying times required in cast films sedimentation of film components may occur, with this especially true for aqueous dispersions. Films of multiple layers are also difficult to produce because the solvent added to create subsequent layers may dissolve or interact with the previous layer (Obara and McGinity, 1994). Films produced by spray coating tend to be more porous due to air pockets being left behind during film formation, with cast films tending to be denser. Obara and McGinity (1994) compared the mechanical properties of cast films to sprayed films finding that any mechanical differences observed were unique to each polymer. For example there was little difference in tensile strength, elongation and Young's modulus for Eudragit[®] L 30D, but significant differences in the tensile strength and elongation between ethylcellulose films produced by the different methods.

1.6.3 Spin Coating

Spin coating provides an alternative to film casting in the analysis of film coats. Spin coating allows for fast drying times associated with spray coating of substrates, but provides a free film that allows the film to be analysed in a wider range of equipment.

The coating solution is deposited onto a disk which is then rotated at circa 500rpm resulting in radial movement of the coating solution due to centrifugal forces. The fluid spreads to, and eventually off, the spinning disk leading to the coating solution covering the whole of the disk. Subsequent to this step the rotating disk tends to be accelerated to between 1500-6000rpm where solvent evaporation dominates the drying process leading to production of the final film (Hall *et al.*, 1998).

The final film thickness depends on a number of factors, with spin speed arguably the most important factor, as this affects both the shear force applied to the solution to cause spreading of the solution and the drying rate through evaporation. Other factors resulting in alterations to the final film include the viscosity and solids content of the initial solution, which will affect the initial thinning of the film; the

spin time and the rate of solvent removal through any exhaust system present (Temple-Boyer *et al.*, 2010).

Spin coating has the advantage of being able to produce thin films in the region of a few hundred microns, therefore similar to the thicknesses observed for controlled release coatings, with similar drying times to those observed in spray coating. There can be issues with the reproducibility of spin coated films owing to the fact that subtle variations in spin coating parameters can have a larger bearing on the final thickness and properties of the film.

1.7 Defects in Film Coats

Various defects can occur during film coating, most however can be negated by changes in process parameters, such as air inlet temperature or fan speed, or by changing the formulation of the coating solution.

Some of the most common defects are cracking, chipping and splitting, which when minor in nature are generally caused by attrition during the coating process, with the solution being to reduce the fan speed in the fluidised bed coater, thus decreasing the force of substrate impact in the fluid bed (Aulton and Twitchell, 2002). If severe cracking, chipping and splitting occur this can be a symptom of incomplete film formation, which can be overcome by increasing plasticiser content or the inlet air temperature to achieve the minimum film forming temperature. Another cause of severe cracking, chipping or splitting of the film is poor overall toughness of the film. This can be corrected by changing the grade or by increasing the molecular weight of the polymer. In cases of extreme cracking, chipping or splitting, peeling or flaking of the film coat may occur, where whole portions of the film detach from the substrate. This again can be remedied by altering the above parameters but it may require significant reworking of the coating parameters and formulation (Rowe, 1997).

As discussed above the parameters set on the coating machine such as inlet air speed and pump speed needs to be optimised rather than maximised or minimised. As an example the air inlet temperature needs to be sufficient to form the film, and if the temperature is not high enough then picking may occur. When two substrates collide and their film surfaces agglomerate and are then pulled apart, producing pick marks on the substrate surface. If the air inlet temperature is set too high then pitting, wrinkling and an increase in surface roughness may be observed. Pitting arises from the melting of substrate components such as stearic acid and polyethylene glycol (Rowe, 1983), which have melting points close to the temperatures used in aqueous film coating. Occasionally gases are trapped in between the substrate and the film, and if the air inlet temperature is too high expansion of the gas can occur. Eventually the film can rupture leading to the film collapsing back onto the substrate causing a wrinkle effect. To reduce the chances of a film wrinkling the air inlet temperature can be reduced and/or the formulation altered to increase the adhesion of the film to the substrate. Increasing surface roughness can often result from atomised droplets drying in flight and then not fully coalescing on the substrate surface, leading to a spray drying effect.

Another common defect is bridging, which is where break lines or monograms are “bridged” by the film coating. Bridging results from the drying process when internal stresses exceeding adhesive forces, therefore any means to decrease the internal stress of the film coat will reduce the incidence of bridging, for example through the addition of plasticisers (Okhamafe *et al.*, 1987).

The above discussion shows the potential problems associated with film coating, but also highlights that most defects can be overcome by changes in formulation or operation parameters of the coating equipment. This is in preference to changes in the formulation of the coating solution, as this tends to be more costly both in monetary terms through increased amounts of regulation and in the time taken to alter the formulation.

1.8 Previous Research

Previous research analysing film coated solid dosage forms has shown that analysis of polymer films in-situ is possible, but there is a paucity of research using thermal and mechanical methods with the main thrust of research being through spectroscopy techniques. In the article by Podczeck and Almeida (2002) it was shown that polymer films can be analysed after application to a substrate through the use of dynamic mechanical analysis (DMA) to measure the difference in viscoelastic response of coated and uncoated pellets.

1.8.1 Microscopy Techniques

Microscopy encompasses a wide range of techniques, not limited to traditional optical microscopy, with modern microscopy also incorporating electron and atomic force microscopes. Although optical microscopy can have a role in tablet film coating, it is limited in its resolution by the diffraction limit of light, which atomic force microscopy and electron microscopy are not concerned by. This results in the foremost use of optical microscopy being in analysis of pigmented film coats and in visual inspection of defects. Atomic force and electron microscopy both have a far higher resolution than optical microscopy, but the huge differences in the principles of the techniques results in far different utilisation.

1.8.1.1 Atomic Force Microscopy

Atomic Force Microscopy (AFM) is a well-established technique for the analysis of surfaces. Introduced by Binnig, Quate and Gerber (1986), AFM is capable of imaging single atoms. To provide a notion of the area of scrutiny for AFM imaging in pharmaceutical research the usual image size produced ranges from $100\mu\text{m}^2$ down to 100s of nanometres for biological samples. In contact mode imaging the probe is brought into contact with the sample surface and a constant force is applied to the cantilever. A topographic image is obtained by a scanner moving the probe tip in a

raster pattern in the x , y direction, with z displacement measured through deflection of the cantilever.

There are a number of different modes of operation for AFM. The simplest being contact mode AFM, and as the name suggests the probe is in continuous contact with the sample and kept at a constant height above the surface. With the probe being in constant contact it is the easiest mode to operate and produce images with, however due to the higher forces needed to keep the probe in contact with the sample it can be limited by the type of sample being analysed, with particularly soft samples being susceptible to damage by the probe tip. Additional information to the standard topographic image can be generated in contact mode through the use of lateral force microscopy (LFM), where frictional forces are measured by the “twist” of the cantilever when the tip comes into contact with areas of higher/lower friction. In this mode the topographic image is constructed in the normal fashion, with frictional forces plotted through the deflection of the laser onto the left or right hand side of the photodiode detector.

AFM can also be used in noncontact mode, which as the name suggests means the tip is further away from the sample surface than in contact mode. Because of the increased distance between the tip and the surface the tip is in a region where van der Waals forces are attracting it to the surface. The tip is also fed an AC current causing it to oscillate, and as it moves across the surface any changes in attractive forces cause a change in oscillation which is then smoothed out via the feedback unit. Due to the probe not being in contact with the sample surface it is ideal for relatively soft samples, such as biological samples, as there are no lateral forces. However the tip needs to avoid the fluid layer present on most materials so a slower scan speed is required, and only relatively hydrophobic samples can be imaged. A related mode is intermittent contact mode, patented as and often referred to as tapping mode (TM-AFM). As in non-contact mode the probe is oscillated near its resonant frequency, but the probe is held closer to the surface and the probe tip lightly taps the surface of the sample, which again is ideal for soft samples as the force between the probe tip and the sample is lower than in contact mode. As with non-contact mode there are no lateral forces; however, unlike non-contact mode where the lateral resolution

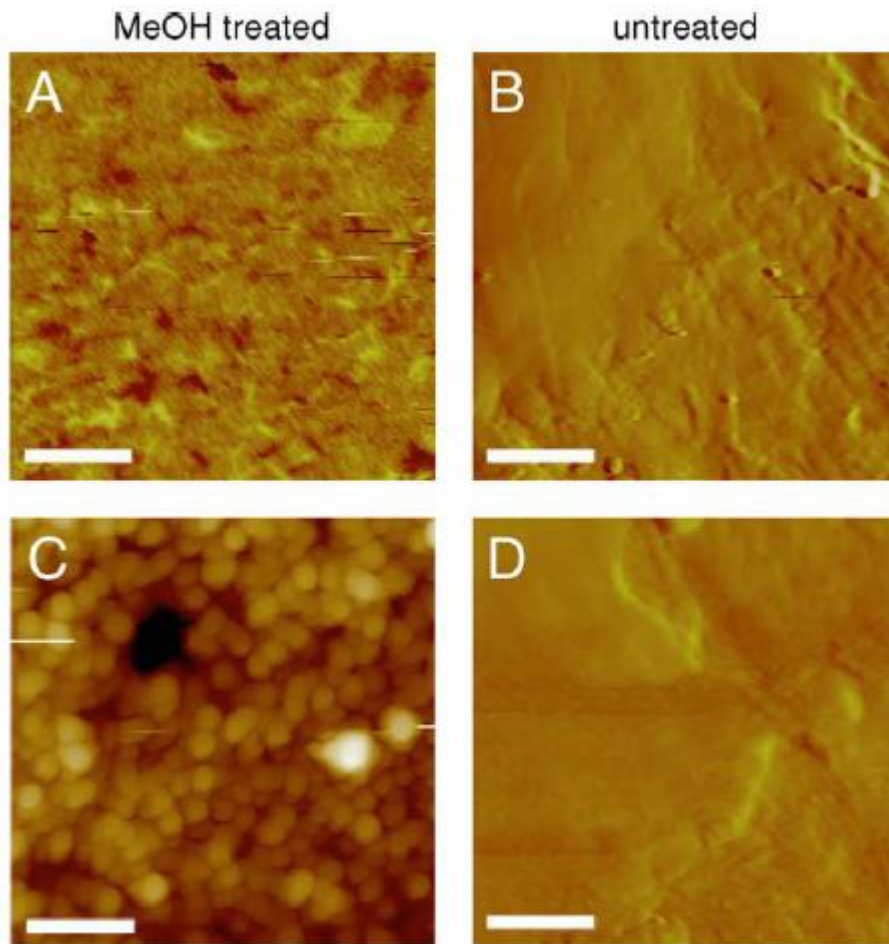


Figure 1.7 AFM images of Silk Fibroin films either treated with MeOH or untreated. Scale bar length in images A and B is 2.5 μ m and C and D it is 0.5 μ m (reproduced from (Hofmann *et al.*, 2006))

is relatively poor due to tip-sample separation the tip intermittently comes into contact with the sample allowing for an increase in lateral resolution. In non-contact and intermittent contact the user is able to use the secondary imaging mode of phase imaging. In this mode information about differences across the sample surface such as adhesion, composition and viscoelasticity can be determined, through changes in observed cantilever oscillation compared to the driving signal. A complete explanation of phase imaging along with the operation of AFMs is provided in Chapter 2.

Apart from the obvious benefit of being able to image at the molecular level another advantage of AFM is that it is not sample destructive, offering a considerable advantage over many of the spectroscopic and other microscopy techniques outlined.

There has been interest in using AFM to investigate polymer films. A recent paper by Hofmann *et al* (2006) used AFM to image films made from silk fibroin. Silks are high molecular weight organic polymers made from repetitive hydrophobic and hydrophilic peptide sequences that are analogous to block co-polymers. Fig. 1.7 shows AFM images comparing the morphologies of films treated with Methanol (A and C) or water (C and D) and it can be seen that a globular structure can be observed when treated with methanol. The bar length in images A and B is 2.5 μm and C and D it is 0.5 μm , which gives an indication of the scale of AFM.

Micro-thermal analysis is an AFM technique where the ultrasharp tip is replaced with a thermal probe, which is produced from a Wollaston wire allowing resistive heating of the probe, by passing a current through the wire. Two major techniques have been developed, that of Localised Thermomechanical Analysis (L-TMA) and Scanning Thermal Microscopy (SThM). In L-TMA the probe is heated in a linear ramp analogous to conventional DSC, when the material undergoes a softening transition the probe indents into the sample which can be measured through the z piezo. The related technique of SThM holds the probe at a constant temperature and as the probe passes over areas of differing thermal conductivity the power required to maintain a constant temperature alters and is recorded for each x, y coordinate. A more detailed explanation of AFM thermal probe methods is provided in Chapter 2.

In a paper by Royall *et al* (2001a) the use of micro-thermal analysis was employed to garner information about sugar coated ibuprofen tablets. One of the major weaknesses of thermal probe methods was highlighted in the study, which is the varying topography of samples causing the probe tip to be in contact to varying degrees with the sample. Differences in thermal conductivity when the probe is at a peak and trough are observed, as when the probe is at a peak there is high thermal conductivity resistance due to the insulating effect of air around the probe. Conversely when the probe is in a trough there is high thermal conductivity from the sample around it. In the paper Royall suggested the use of a pixel intensity histogram which presents a histogram of the distribution of pixel intensity in an area, which was used for both conductivity and topographic images. The topography showed no distinct variance and as such only one peak is shown, however with conductivity two peaks are observed indicating two distinct areas of conductivity. This however gives

no spatial resolution of the areas, so by analysing the histogram a cut-off point of power consumption can be determined, with any pixel over this cut off ascribed one colour and any below another colour, as seen in the top right hand corner of Fig 1.8. This still however does not provide a clear analogue image and further work to compensate for this effect was described by Harding *et al* (2007), through the use of

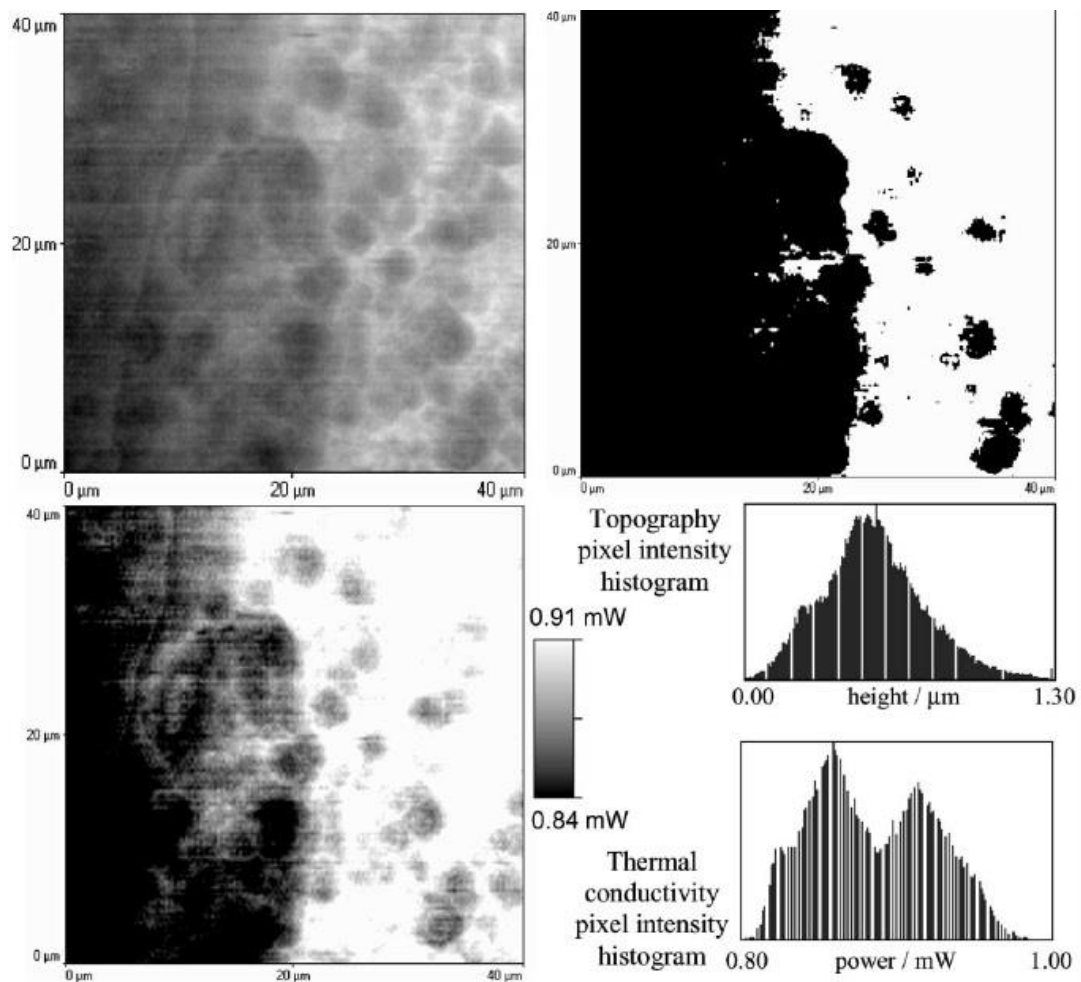


Figure 1.8 various thermal conductivity images. Of note is the image in the top right, which is explained in the text. (Reproduced from Royall *et al.*, 2001a)

statistical modelling. This paper also described a novel three dimensional imaging technique employing L-TMA which allowed the mapping of areas of paracetamol in an HPMC matrix. This was achieved through performing a number of L-TMA experiments across the sample surface and then analysing the results to produce a three dimensional image of the location of areas of paracetamol within the HPMC matrix.

1.8.2 Spectroscopy Techniques

Spectroscopy techniques involve the use of the electromagnetic spectrum to garner information about samples through the electromagnetic waves interacting with samples. Although the visible spectrum is used in analysis, for example inspecting pigments in films coats, areas of the non-visible spectrum are more often used to analyse pharmaceuticals. Many different frequencies are used, including those in the x-ray, ultraviolet, infrared and terahertz regions. Discussed here are the most common techniques used in the analysis of film coats.

Microscopy and changes in the weight of the uncoated substrate have been the traditional method of analysing film thickness. Rowe (1996) provided a method to estimate the thickness of a film coat through treating the tablet as a cylinder and two hemispheres:

$$T = \frac{v}{S} \quad (1.11)$$

where v is the volume of the film and S is the surface area of the tablet. The volume is calculated through the following equation:

$$v = \frac{m}{p} \quad (1.12)$$

where m is mass which is calculated by the percentage weight increase of the tablet during coating and p is the density of the film. The surface area of the tablet is calculated from the following equation:

$$S = \pi dh + 4\pi Rz \quad (1.13)$$

S is surface area, d is the tablet diameter, h is the height of the tablet edge, R is the radius of curvature of the tablet cap and z is the height of the tablet cap, and both R and z are published by the tablet press manufacturers. This provides a simple mathematical model to estimate the thickness of a film coat on a tablet; however there are a number of variables in the equation that are estimates. For example

weighing the tablets only provides an estimate of the amount of coat applied to the substrate, as it does not take into account weight loss of the tablet during coating. Weighing also provides no information regarding the uniformity of the film, and as described above electron Microscopy is laborious and sample destructive. Spectroscopy methods conversely can be relatively quick and non-sample destructive. The combination of these factors has led to spectroscopy becoming an important tool in determining the thickness and uniformity of film coated dosage forms.

1.8.2.1 Near Infrared

Near-infrared (NIR) is a technique that has attracted much attention for analysing tablet coats, especially the in-line measurement of the film coating process. Near-infrared is a vibrational spectroscopic technique that has traditionally been used to characterise products in the food, textile and agricultural industries (Watson, 2003), but has found an increasing use in the pharmaceutical industry. The infrared spectral

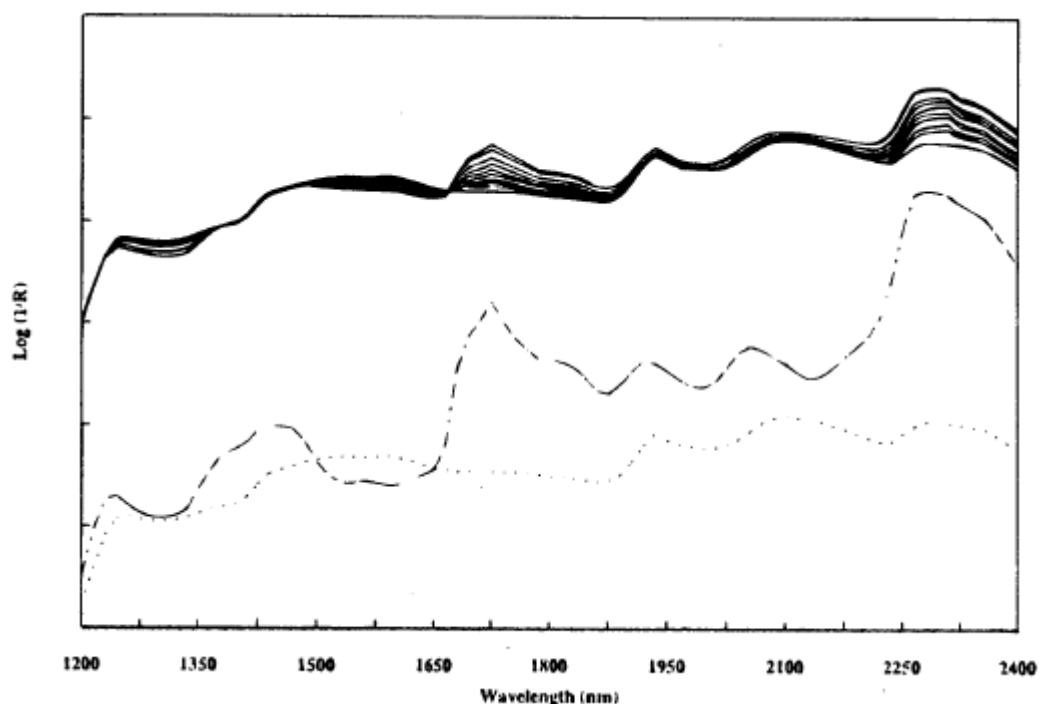


Figure 1.9 Near-IR spectra of a cast EC film (dot-dash line), an uncoated tablet core (dotted line) and film coated tablets (solid line) taken at various times during the coating run. Reproduced from (Kirsch and Drennen, 1996)

region ranges from 0.8-1000 μm with the near-infrared region lying between 0.8-2.5 μm . NIR absorbance spectra result from overtones and combinations of vibrations occurring in the mid-infrared region (2.5-50 μm). Due to the low incidence of these vibrations absorbance signal is around 1000 times weaker than bands observed in the midinfrared, allowing for no sample preparation, as opposed to mid-infrared analysis which requires dilution owing to strong absorbance (Gendrin *et al.*, 2008). Along with the decreased intensity NIR peaks overlap more, and tend to be broader, often necessitating statistical analysis. Due to the complex calculations required to deconvolute data there is a requirement of powerful computer hardware and software, which caused NIR to only be used from the 1980s onwards (MacDonald *et al.*, 1993). The absence of sample dilution and the allowance of measuring in the presence of or direct measurement of water allows NIR to be a viable option for in-line analysis. There has been interest in using NIR to analyse film coats. Kirsch and Drennen (1995), used NIR to evaluate the film thickness of theophylline tablets, and in a further study the technique was employed at-line to measure the amount of film coat applied during a coating run (Kirsch and Drennen, 1996). Fig. 1.9 is taken from the study, with the dotted line representing the uncoated tablet core, the dot-dashed line a cast EC film, and the solid lines are a series of near-IR spectra collected from a coating run. It can be seen there is a peak ca. 1650-1800nm and 2250-2400nm in the cast ethylcellulose film, and there are corresponding peaks in the coating, which increase during the course of the run. This study also shows an advantage of NIR in that with calibration the technique can provide quantitative information; however the calibration can be complex and time consuming.

Recently NIR has been used to measure the formation of a gel layer in an HPMC matrix and dissolution of an API from the tablet (Avalle *et al.*, 2011). Fig 1.10 shows the tablet core at the top of the each image, with the dissolution medium occupying the bottom. The gel layer can be seen forming and eroding, and the API can also be seen to be removed from the tablet matrix. Dissolution testing (USP I) complemented the NIR technique and showed zero order dissolution supporting the NIR results that drug release is controlled by polymer erosion. Although this paper did not use film coated tablets there is scope for this technique to be applied to film coated tablets.

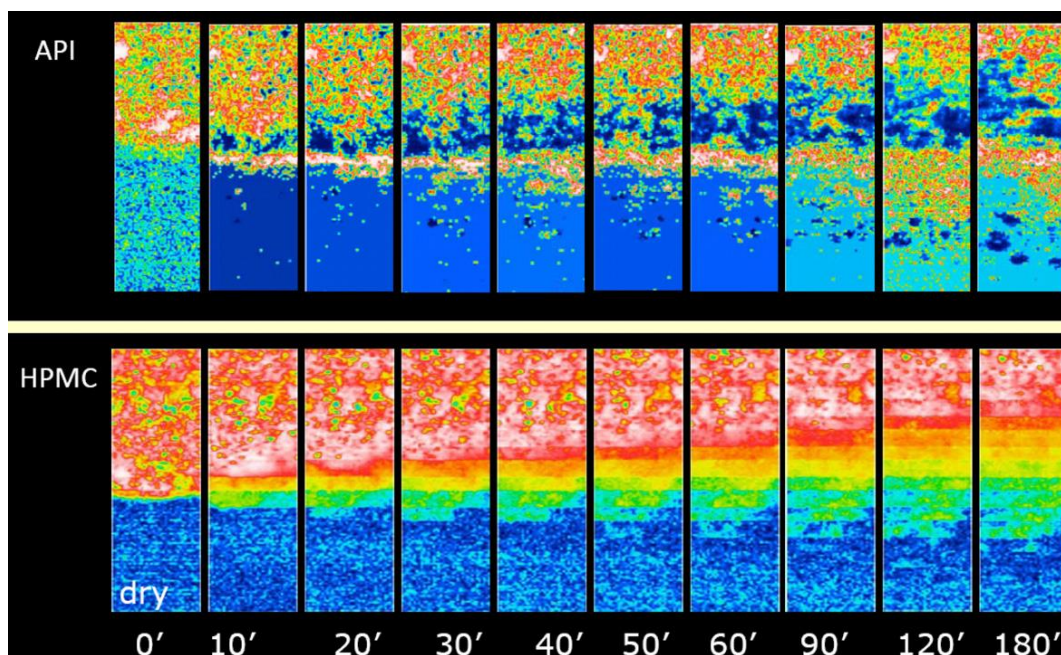


Fig 1.10 Formation and erosion of the gel layer in a HPMC matrix (bottom), and dissolution of the API. Reproduced from (Avalle *et al.*, 2011)

Advantages of NIR include that it is relatively quick, and is non-invasive and non-destructive. However unlike terahertz pulsed imaging (see section 1.8.2.3) and other techniques it can only provide information in two dimensions

1.8.2.2 Raman Spectroscopy

Raman spectroscopy is closely related to infrared, in that bands are observed as a function of energy; however it provides complimentary information to infrared and generally if a band absorbs weakly in mid-IR, then it is likely to produce a strong response to Raman.

Raman spectra therefore are similar to IR spectra, with the bands of the spectra representative of molecular vibrations; however Raman is a scattering phenomenon not an absorbance phenomenon (McGoverin *et al.*, 2008). Energy transfer is between the laser and the molecule causing inelastic scattering of light, conversely to when light is scattered most photons undergo elastic (Rayleigh) scattering, with all photons having the same energy. With the Raman effect the photons have a different, usually lower, energy to the incident photons; therefore an energy shift in cm^{-1} is measured.

The Raman effect is therefore weak due to the lower proportion of photons used, but is proportional to the intensity of energy.

There are a number of advantages to using Raman spectroscopy over NIR. To begin with water is a poor Raman scatterer; therefore samples with high water content can be used without any adverse effects on the response. This also means there is less sample preparation needed. Another advantage to Raman is it being a non-invasive technique, but can only produce 2D images, even though it can penetrate the sample surface (Zeitler *et al.*, 2007a). However due to the fact it is based on scattering phenomenon these are generally weak events, therefore signal enhancement may be required.

Raman spectroscopy is starting to find an increasing role in pharmaceutical analysis, with one area being the analysis of film coat thickness. In a paper by Romero-Torres *et al* (2006), Raman spectroscopy was used to successfully analyse film coats up to 151 μ m thick. The researchers used fluorescent ingredients, either the food colorant Alphazurine FG or D&C Blue No. 4, as fluorescence can be a major source of interference in Raman spectroscopy; however reasonable results were achieved.

1.8.2.3 Terahertz Pulsed Imaging

A recent non-destructive approach to determining film thickness and uniformity in pharmaceutical film coats is Terahertz Pulsed Imaging (TPI). The technique involves using radiation in the terahertz region of the electromagnetic spectrum, which is between 60 GHz–4 THz, which locates it in the far-infrared region. In the case of the Imaga 2000 (Teraview Ltd) a femtosecond laser is used to produce a short pulse of terahertz radiation which is transmitted towards the tablet (Zeitler *et al.*, 2007b). When a pulse incidents onto a suitable semiconductor, such as a polymer, a portion of the pulse is reflected back and this is detected by the equipment. Most polymers appear semi-transparent to Terahertz radiation allowing the terahertz pulse to penetrate the sample, and at interfaces in the tablet, i.e. between the film and the substrate there is a change in refractive index, causing a portion of the pulse to be reflected.

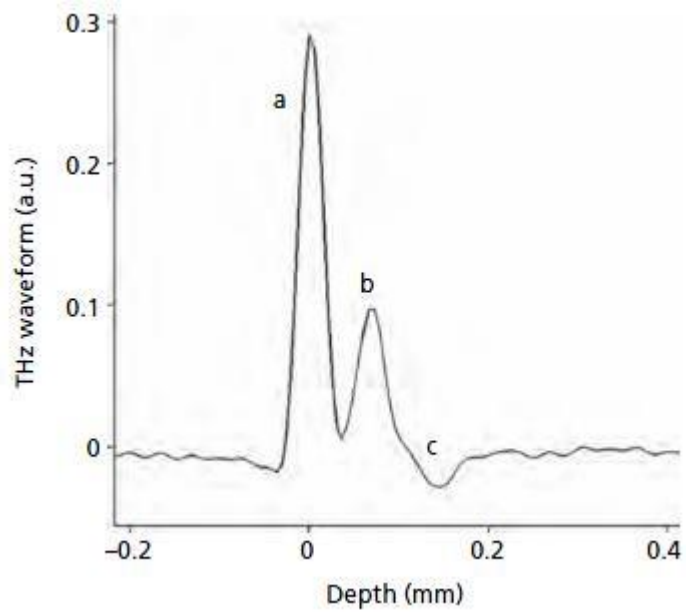


Figure 1.11 A typical terahertz waveform. See text for explanation. Reproduced from Zeitler *et al* 2007a)

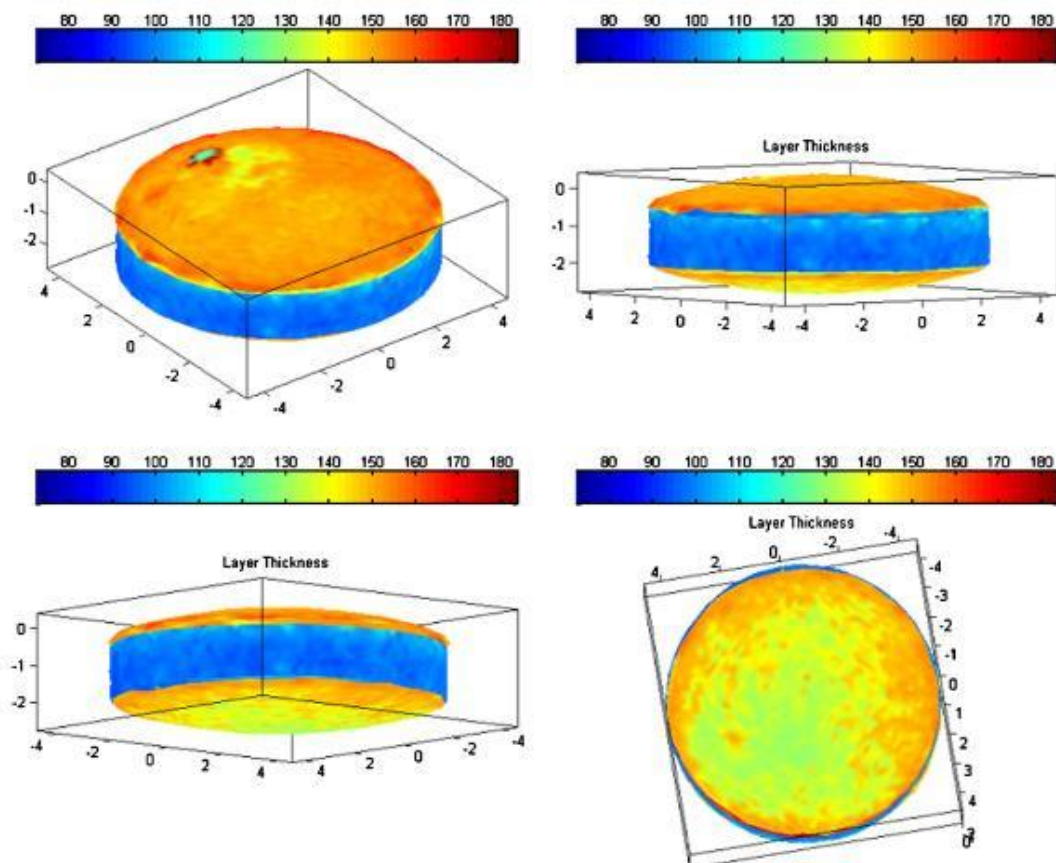


Figure 1.12 A spatially resolved 3D image of a tablet coat. Reproduced from Ho *et al.*, 2008)

Fig. 1.11 shows a typical terahertz waveform. The letters a, b and c each relate to an interface with the tablet. The first at 0mm is the air-tablet interface, and the other two are for interfaces within the tablet, e.g. between film layers (Zeitler *et al* 2007a).

There is a time delay between the surface reflection and reflections from interfaces, which is used to produce spatially resolved 3D images. Depending on the duration of the pulse, depth of penetration is currently up to around 3mm.

Ho *et al* (2007; 2008) have used TPI to construct 3D images of tablets. Figure 1.12 shows a spatially resolved 3D image showing the differences in the coating uniformity over the entire tablet surface. The colour scale is in microns, and it can be seen that the central band of the tablet has a thinner layer of coat applied than the rest of the tablet. In addition there is a defect observable on the top left hand image, again showing a reduced thickness in the coat. The maximum resolution attainable by TPI is dependent on the frequency of the pulses, which when analysed at 3THz can be as small as 150 μ m (Fitzgerald *et al.*, 2005). TPI is also relatively quick, as only a single run is needed, which take approximately 20-50 minutes to cover both sides of a tablet and the central band.

1.8.2.4 Laser Induced Breakdown Spectroscopy

Laser Induced Breakdown Spectroscopy (LIBS) is another technique that has been applied to the pharmaceutical analysis of tablet coat thickness and uniformity. It is an elemental analysis technique that employs a high energy pulsed laser to ablate the sample material and produce a plasma containing excited ions and electrons of the elements present in the sample (Madamba *et al.*, 2007). When the plasma cools the excited elements atomic emission occurs at wavelengths characteristic of the components of the sample. The emission is also proportional to the concentration of the elements present in the plasma, and therefore the sample. As LIBS is an elemental analysis technique it requires distinct elements to be present. It is therefore unsuitable to detect many polymers, active pharmaceutical ingredients and other additives, due to their abundance of carbon, hydrogen and oxygen, as the technique would not be able differentiate between them (Mowery *et al.*, 2002).

An important parameter with LIBS is the laser energy, which needs to be optimised, as the signal intensity of the atomic emission increases when the energy of the laser is ramped, however at higher levels the emission lines become saturated. Also with regard to the analysis of coat thickness at lower energies the laser penetrates to a lesser degree and therefore improves the depth resolution. Madamba *et al* (2007) reported that a laser energy of 25mJ could produce observable signal intensities of tablet coats containing Opadry II containing iron and titanium. However if the energy was increased to 150mJ the signal intensity was greater, but saturated emission lines were observed.

Mowery *et al* (2002) used LIBS to determine tablet coat thickness, by the number of laser pulses required to penetrate the coat. As calcium was included in the tablet core this could be measured via LIBS, and when the intensity of calcium increased over 100,000 the laser was deemed to have penetrated through the core. The LIBS data provided good correlation with SEM data and in addition to qualitative data that SEM can provide, LIBS can generate quantitative data on the components of the film coat. It is also rapid and in comparison to atomic force microscopy and microthermal analysis, multiple areas of a single tablet coat can be tested to build a picture of the entire coating. However, as described above, although there is relatively little preparation required compared to some techniques LIBS requires the core of the tablet and the coat to be prepared with specific targets included, and it is sample destructive.

1.9 Research Objectives

As can be seen, film coating is an important element in the formulation of solid dosage forms and there are numerous and wide ranging methods of analysing film coats available to the pharmaceutical scientist. All of these techniques have advantages and disadvantages associated with them, so it is important to not only select the correct method but quite often a number of techniques to fully understand the sample in question.

However a large number of these techniques cannot perform in-situ analysis of pharmaceutical dosage forms, and therefore need to have samples prepared that are able to be analysed in the equipment. In the case of polymer films this has historically led to cast films being analysed. Therefore the aim of the project is to develop techniques to allow the in-situ characterisation of film coated solid dosage forms.

The use of thermal analysis and AFM is a powerful combination, and has been used in other studies (Harding *et al.*, 2007, Royall *et al.*, 2001a, 2001b). Previous research has shown that although thermal probe techniques only provide semi quantitative information regarding the transitions of materials, it nonetheless offers a means of identifying material distribution on the microscale. AFM imaging can also achieve superior resolution compared to other microscopy and spectroscopy techniques and when coupled with spatially resolved thermal analysis it can produce data that other techniques cannot. MTDSC is a standard analytical technique that can be used to verify L-TMA results and will therefore be used alongside L-TMA in the study. Although other thermal analysis techniques, such as dynamic thermomechanical analysis can be used to determine the T_g of polymers, and is particularly useful when determining subtle glass transitions it cannot provide spatially resolved information. Chapter 3 characterises the samples used in the remainder of the study using thermal probe methods, coupled with standard thermal analysis techniques such as modulated temperature differential scanning calorimetry. This is to ensure the accuracy of the results produced by comparing them with quantitative data.

Also outlined in this chapter is the fact that many techniques used to analyse polymer films are either sample destructive or are unable to analyse the film coat in-situ, i.e. the coat that is present on the actual dosage form. This is particularly pertinent as historically analysis of films was undertaken on films that had been cast on Petri dishes, which has vastly different process conditions to produce the coat than by spray coating. There appears to be little data in the literature comparing cast free films to those films prepared by spray coating, which may be down to limitations in the techniques used to analyse films. Therefore although there is no proof that cast films and spray coated films behave differently, due to the vast differences in process conditions used to produce the two types of films it seems appropriate to question

the validity of using cast films. The comparison of polymer films produced by film casting and spray coating is one of the main objectives of the thesis and is dealt with in chapter 4, through the use of novel thermal probe methods.

Chapter 5 aims to investigate the behaviour of solid dosage forms coated with both individual polymers and polymer blends, with respect to aging and thermal post treatment. Due to the second law of thermodynamics most chemical systems are unstable over time, especially when heat is involved. As has been stated in the previous chapter most polymer systems phase separate due to the high molecular weight of both components making it entropically unfavourable for them to exist in one phase. Again AFM is combined with thermal probe methods and conventional thermal analysis techniques to investigate the behaviour of polymer blends in film coats after thermal stress is applied.

The final research chapter is interested in analysing the composition of film coats with pigments incorporated into them. As stated above many film coats incorporate pigments, among other additives, and many analytical methods currently employed either do not have the required resolution to image or detect these components or are unable to analyse the films in-situ.

CHAPTER 2

2. General Methods and Materials

2.1 Thermal Analysis of Pharmaceutical Materials

The field of thermal analysis refers to techniques that study a material's change in properties with respect to temperature and is a versatile tool used for sample identification, the measurement of purity, moisture content, polymorphism and the crystalline and amorphous content of the sample. Thermal analysis therefore has an important role in the characterisation and development of pharmaceutical materials and drug delivery systems.

The thermal analysis of materials is centuries old, however thermal analysis in its present form is a little over 100 years old. By this time the difference between heat and temperature was well understood, and the field of thermodynamics matured. Towards the end of the 19th century Le Chatelier had experimented with recording temperature as a function of time and in 1901 the concept of comparing the sample to a reference was used and differential thermal analysis (DTA) was introduced (Ozawa 2000). DTA was the first of a number of thermal analysis techniques introduced during the twentieth century, including thermogravimetric analysis (TGA) and differential scanning calorimetry (DSC) both of which are still both standard analytical techniques.

More recently modulated temperature DSC (MTDSC) was proposed and developed into a standard analytical technique allowing for increased sensitivity to subtle transitions and the ability to observe certain overlapping transitions. Within the last twenty years a novel technique for thermal analysis has been introduced based on atomic force microscopy (AFM) techniques. The early crude probes, which when combined with AFM was termed microthermal analysis (MTA) has now been

developed into micromachined probes with comparable imaging resolution to AFM but with an area of scrutiny for thermal analysis far superior to that of other techniques.

2.1.1 Theory of Thermal Analysis

When a sample is heated its temperature tends to rise and at a point the sample will undergo either a first or second order phase transition, or a number of different phase transitions at varying temperatures. There are a number of basic concepts to understand before considering thermal analysis techniques, such as definitions of temperature and heat, and other associated concepts.

Firstly temperature (T) is a measure of the tendency of a body to transfer heat to its surroundings; therefore if a body has a high temperature then it has a high tendency to give heat, and will appear “hot”. The standard absolute temperature scale is the Kelvin scale (designated K), but the Celsius scale (C) is commonly used, which has the same empirical intervals but the scale is zeroed at the freezing point of water; not absolute zero. Heat (often denoted as Q) is the transfer of energy between two bodies of, and heat tends to flow from the body with the higher temperature to the body with the lower temperature until thermal equilibrium is reached, with the time taken to reach thermal equilibrium being the relaxation time. The heat content, or enthalpy, of a sample can be confused with temperature; however enthalpy represents the total amount of energy contained in the bonds of the system. Enthalpy is an extensive property dependent on mass; therefore if the mass of the sample doubles then so will the enthalpy, and as such the SI unit of enthalpy is J/kg , although in pharmaceutical thermal analysis it is often presented in more appropriate units. Conversely the temperature of a sample is constant regardless of the mass or volume of the system.

As described above, on heating a substance its temperature tends to increase with the degree of temperature increase dependent on the heat capacity, which is derived thus:

$$C = Q/\Delta T \quad (2.1)$$

where C is the heat capacity, Q is the energy supplied as heat and ΔT is the change in temperature. The classical definition of heat capacity is the energy required to increase the temperature of a material by 1°C (or by 1K), and as Joules (J) and Kelvin (K) are the SI units for energy and temperature respectively, heat capacity therefore is measured in $J K^{-1}$. In resemblance to heat content the heat capacity is variable with the sample mass, and in order to make it an intensive property, in this case independent of mass, the specific heat capacity is used:

$$C_p = C/m \quad (2.2)$$

where C_p is the specific heat capacity and m is the mass, in grams (g), of sample (Atkins *et al.*, 2005).

2.1.2 Differential Scanning Calorimetry

Differential scanning calorimetry (DSC) and more recently modulated temperature DSC (MTDSC) have proven to be invaluable tools in the characterisation of polymer films, and have become arguably the most common thermal analysis method. In DSC a small sample, typically in the milligram range, is placed in a sample pan, usually made of aluminium, and then sealed either hermetically or via crimping. A heating signal is applied with the resulting temperature and energy being measured in relation to thermal events (Craig, 2008). DSC evolved from Differential Thermal Analysis (DTA), where a sample pan and an inert reference pan (the reference pan is generally empty) are subjected to a linear heating signal, and when a thermal event occurs in the sample such as melting or crystallisation a temperature difference between the sample and reference pan will exist. This is explained due to the endothermic and exothermic nature of melting and crystallisation respectively. On melting extra energy is required to break chemical bonds, and this extra energy is referred to as the latent heat of fusion, causing heat to be absorbed by the sample, with the reverse true of crystallisation.

DSC produces similar results to DTA; however DSC measures the heat flow into and out of the sample allowing for more accurate temperature control and therefore measurement of enthalpy and heat capacity. DSC measures heat flow through one of two methods, either heat flux or power compensation. In heat flux DSC a sample and a reference pan are placed symmetrically in a furnace and heated, with the differential temperature being measured via a pair of thermocouples. The following equation describes the heat flow from the furnace to both pans:

$$dQ/dt = \Delta T/R \quad (2.3)$$

where Q is heat, t is time, with dQ/dt representing the difference in heat flow between the sample and the reference, ΔT is the observed temperature difference, and R is the thermal resistance of the heat path between the furnace and the pan. It can be seen that the heat flow equation is analogous to Ohms law, and is derived from Newton's Law of cooling (Gill *et al.*, 1993). Heat flux DSC is analogous to DTA, however superior calibration allows for the measurement of heat flow and changes in temperature. It is also of note that the energy associated with thermal events can be derived from equation (2.3) above. Power compensation DSC involves the use of two isolated furnaces in which the sample and reference pans are located. The temperature difference between the reference and sample pan is maintained at zero. Power is applied to the reference and sample pan in a linear fashion as for heat flux DSC, however when a thermal event occurs, the power needed to keep the sample pan at the same temperature as the reference alters. As described above endothermic events absorb energy therefore more power is required when a sample melts, conversely less power is required when a sample crystallises as energy is evolved; although in reality more power is supplied to the reference pan (Coleman *et al.*, 1996). The following equation describes the power delivered to the furnace:

$$P = dQ/dt = I^2R \quad (2.4)$$

where P is power and I is the current supplied to the furnace. In practice both methods produce similar results. Due to the differential nature of the technique it is vital that the sample and reference pan match each other as closely as possible. To provide quantitative data the temperature must be calibrated. 99.9% indium is a

common calibration material as it has a known melting temperature and enthalpy of fusion, 156.6°C and 28.7 Jg⁻¹ respectively. Ideally a number of calibrants with a range of temperatures should be used, with benzoic acid and *n*-octodecane commonly used to provide a three point calibration over a range of melting points.

Fig. 2.1 represents a typical DSC trace. Power/heat flow is plotted as a function of temperature, producing a trace of the changes in heat flow following the heating signal.

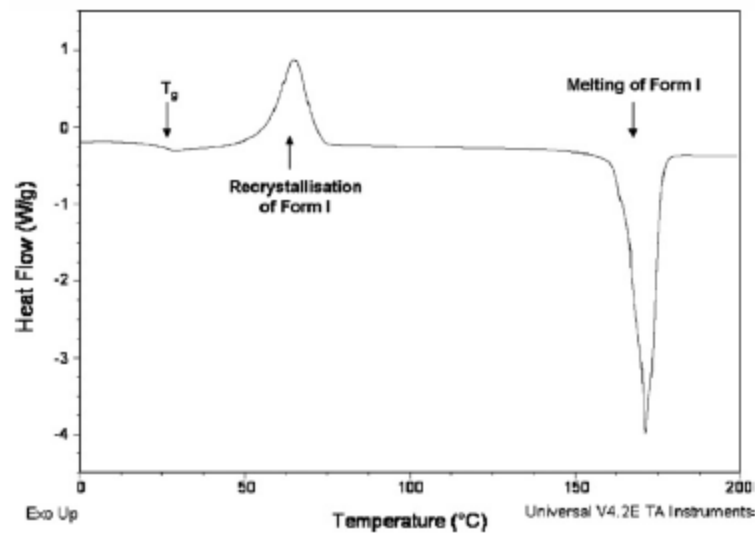


Figure 2.1 Common transitions on a DSC trace of quench cooled paracetamol (Qi *et al.*, 2008)

There are a number of different thermal events represented in Fig 2.1, which was performed on a quench cooled sample of paracetamol. A glass transition, crystallisation exotherm and a melting endotherm are all observed showing the wide range of transitions detectable by DSC. The baseline of the thermogram can be defined thus:

$$dQ/dt = C_p \cdot dT/dt \quad (2.5)$$

where dQ/dt represents heat flow, dT/dt the heating rate and C_p the heat capacity. It shows the power required to increase the temperature of the sample to adhere to the heating program, and as this is a function of heat capacity it is seen that the baseline is a measure of heat capacity. When a sample undergoes a thermal

transition such as melting, cold crystallisation or evaporation, kinetic events are introduced to the equation:

$$dQ/dT = C_p \cdot dT/dt + f(t,T) \quad (2.6)$$

The term $f(t,T)$ describes a function of time and temperature, and represents the heat flow associated with kinetic processes, and will be discussed further below. The heat flow associated with heat capacity and the heat flow from kinetic responses cannot be separated when using conventional DSC, which is a major drawback of DSC in polymer studies. The most common thermal transition measured using DSC is the first-order phase transition of melting. First-order phase transitions, as described by Ehrenfest, are associated with a discontinuation of either of the first derivatives of the Gibbs potential at the phase transition. The two partial first derivatives of the Gibbs potential are entropy and volume and are described in the following equations:

$$\partial G/\partial T = -\Delta S \quad (2.7)$$

$$\partial G/\partial P = V \quad (2.8)$$

This is simple to visualise, for instance when a liquid undergoes a phase transition to a gas the volume under constant pressure will increase, and the entropy of the system will also increase. The reverse is true for condensation. A melting endotherm can be observed in Fig. 2.1, and is characterised by a peak under the baseline. The reasons for this discontinuation from the baseline are described above. The area under the peak represents the enthalpy of change associated with the transition, which is calculated from the heat capacity, the mass of the sample and temperature change. Another type of phase transition frequently observed is the glass transition, which is a second order phase transition. In second-order phase transitions a discontinuation in the partial first derivatives is not observed, instead the discontinuation is observed in a second derivative. In the glass transition the second derivative with respect to temperature is:

$$\partial^2 G / \partial T^2 = -\Delta C_p / T \quad (2.9)$$

Thus it can be seen that with respect to second-order transitions a change in heat capacity of the sample must be observed. The glass transition does not fit ideally with a second order transition, as by definition they should be rate independent. T_g is dependent on heating rate however (see below), therefore other explanations must be explored.

There are a number of theories including considering the relaxation processes and free volume changes observed; however there is no uniform explanation of the glass transition. In Fig. 2.1 the glass transition is represented by a step change in the heat flow and therefore the heat capacity of the sample. T_g is a kinetic event, and as such, its measurement is dependent upon heating rates and thermal history. For example if an amorphous material is produced via cooling a liquid, slower cooling rates will produce lower apparent glass transitions. This can be explained in terms of relaxation processes. When the temperature is above the T_g the relaxation processes are rapid compared to the rate of cooling and therefore molecular mobility is relatively high. As the temperature decreases relaxation will slow a point is reached where the relaxation rate equals the rate of cooling (which is the T_g). With a slower cooling rate the temperature at which these equilibrate will be lower.

Modulated temperature DSC (MTDSC) is a variation of standard DSC that aims to increase the sensitivity of the instrument especially with respect to the measurement of glass transition temperatures. This technique differs from DSC in that a sine wave heating pattern is applied to the sample and a discrete Fourier transform is applied to the data to separate the responses. The average (or underlying) heating rate is analogous to the linear rate in a conventional DSC experiment. From equation (2.6) there are two components on the right side of the equation, $C_p \cdot dT / dt$ and $f(T,t)$, which correspond to heat capacity and kinetic responses respectively. The heat capacity represents the energy stored in molecular motions (such as vibrations, rotations and translations) of the sample, and as according to the second law of thermodynamics the same amount of energy will be released when the sample is cooled at the same rate as it is heated. Therefore the energy is stored reversibly.

Conversely the kinetic components are representative of the enthalpy of the thermal event, which is often irreversible. This allows MTDSC to distinguish heat capacity and kinetic components, as the reversibly stored energy will be released during the cooling portion of the sine wave. Thus for every MTDSC experiment three traces are produced; the total heat flow, which is equal to a conventional DSC experiment, the reversing heat flow corresponding to the $C_p \cdot dT / dt$ term and non-reversing heat flow which is equal to $f(T,t)$ (Craig *et al.*, 1998).

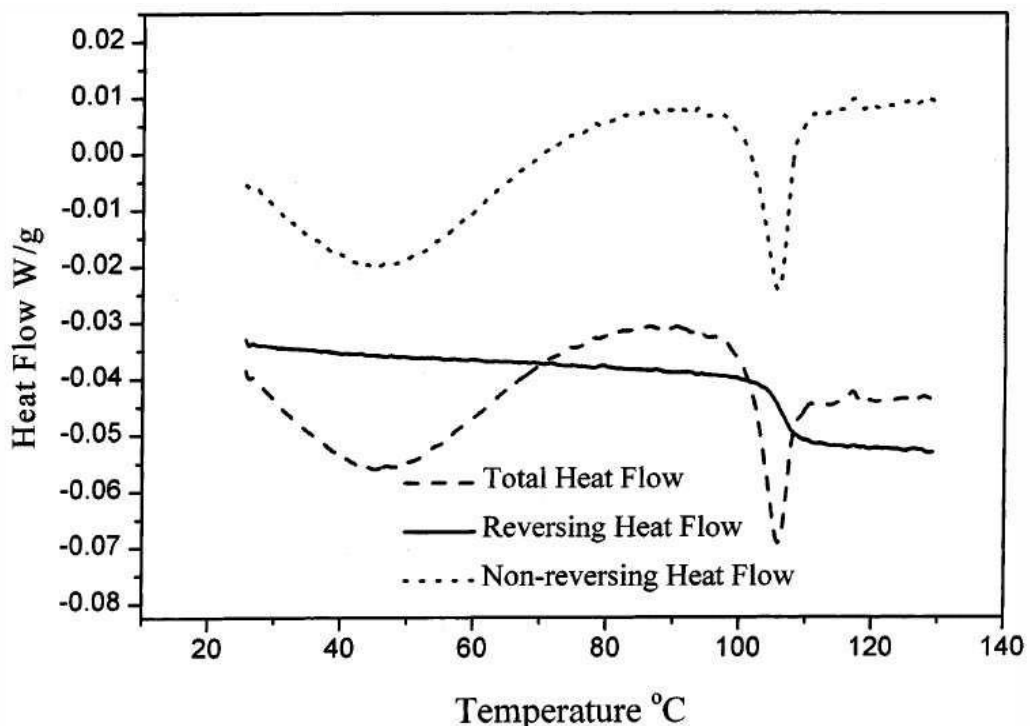


Figure 2.2 Common transitions on a MTDSC trace. See text for explanation (reproduced from Royall *et al.*, 1999a)

Fig. 2.2 shows one of the advantages of MTDSC over conventional DSC. The total heat flow displays an endothermic peak; however it can be seen in the reversing heat flow that a glass transition occurs over this temperature range. The endotherm shows a phenomenon known as endothermic relaxation, which is caused due to a reduction in enthalpy on storage, and as the glass goes through its glass transition this enthalpy is regained through absorbing heat energy. Other advantages of MTDSC include the use of relatively high heating rates during the heating phase of modulation allowing for increased sensitivity, which is a result of the term $C_p \cdot dT/dt$ of equation (2.6). A

larger heating rate will produce a larger value of this term. However the overall, or underlying, heating rate of MTDSC tends to be slower than that of DSC.

2.2 Atomic Force Microscopy

As mentioned in Chapter 1, Atomic Force Microscopy (AFM) is a powerful tool for imaging microscopic areas of sample surfaces. AFM is closely related to stylus profilometry and scanning tunnelling microscopy (STM), however AFM is many orders of magnitude more sensitive than stylus profilometry and measures variations in force rather than current as in tunnelling microscopy (Binnig 1987). This allows AFM to image electrical insulating materials as well as conductive materials, which STM is restricted to.

The technical challenge upon inception of AFM was to produce a cantilever with a spring constant weaker than the spring constant between atoms to avoid the probe tip simply pushing atoms away. To calculate the spring constant the following equation is used;

$$k = \omega^2 m \quad (2.10)$$

The angular frequency (ω) of crystalline bound atoms is approximately 10^{13} Hz and the mass (m) of an atom is around 10^{-25} kg, resulting in the interatomic k being around 10 N/m. Of note aluminium foil with dimensions of 4mm x 1mm has a spring constant around 1 N/m, therefore short lengths of metal can be used as cantilevers for force measurements, and in fact the first probe (the general term for the tip and cantilever assembly) produced for AFM was constructed from gold foil (Rugar *et al.*, 1990, Bushan and Marti, 2010). This first probe had a diamond stylus glued to it to produce the tip, but most modern probes are microfabricated from a single piece of silicon, silicon oxide or silicon nitride using photolithographic techniques producing a pyramidal shaped probe tip (Rugar *et al.*, 1999, Edwardson *et al.*, 2004). These techniques can produce tips with a radius of curvature in the region of 5-10 nanometres (Sanders *et al.*, 2000). Even though atoms are sub nanometre in diameter

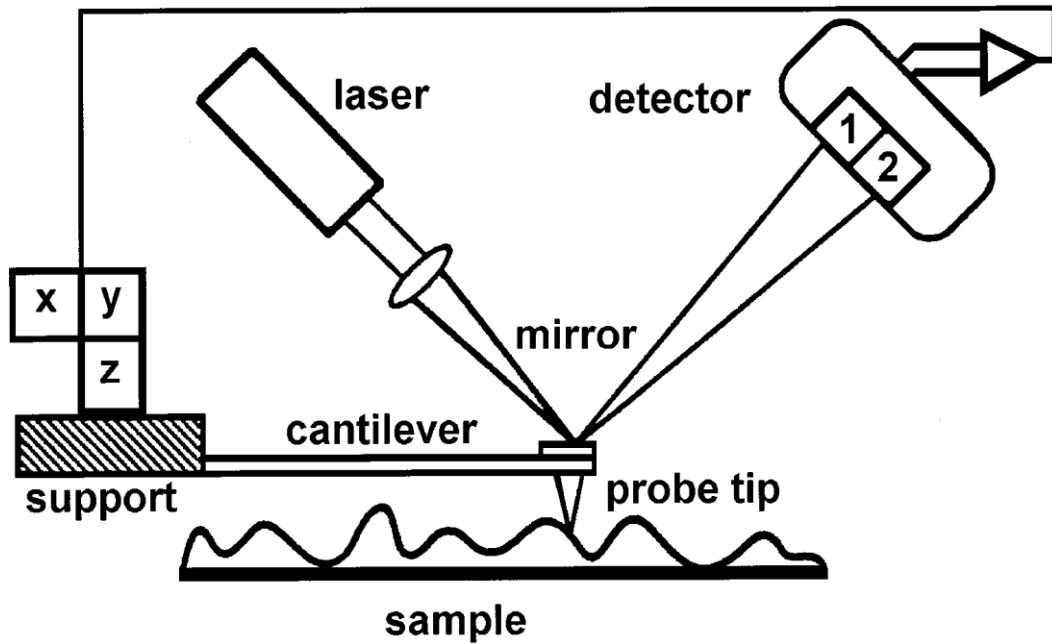


Figure 2.3 Schematic of AFM (Price *et al.*, 1999a)

AFM can produce images on this scale through a minute loading force of between 10^{-7} to 10^{-11} N allowing a smaller area of contact between the tip and the sample.

The upper side of the cantilever is then usually coated with a reflective material such as gold or aluminium. This is because the most common method to detect cantilever position in the z axis is through beam deflection, which usually takes the form of a laser. Another method to detect z height is through interferometry; however this is generally used in magnetic and electrostatic imaging where thin wire cantilevers are used so there is no reflective surface. Deflection of the cantilever in the z axis can be measured down to approximately 0.1\AA , through the use of a split photodiode detector. Once the laser beam is reflected off the cantilever surface a mirror is used to align the beam onto a photodiode detector, which is split into four quadrants. To detect changes in cantilever deflection the laser is initially aligned to fall in the centre of the photodiode. To detect changes in the z axis the photodiode quadrants depicted in Fig (2.4) are merged into two sections (1 + 2 and 3 + 4) with the amount of reflected light falling on either the top or the bottom of the photodiode being detected. The output signal is measured by a differential amplifier which takes the bottom signal from the top and then normalises the deflection through division with the sum of the top and bottom signal.

This differential measurement provides the basis of measuring the z axis during imaging. When the probe is brought into contact the user determines the degree to which the cantilever deflects, termed the set point. This is then compared to the output of the differential amplifier and when they are equal the probe is in contact with the sample surface. As the cantilever is deflected by a known amount and the spring constant of the cantilever is known then the force between the probe tip and the sample can be calculated by Hooke's Law:

$$F = -kx \quad (2.11)$$

Where F is the force, k is the spring constant, and x represents cantilever deflection. Spring constants of cantilevers tend to be in the ranges on 0.01 to 1.0N/m, and the deflections of the cantilever in nanometres so the forces acting on the probe tip have a tendency to be in the nN to μ N range (Thornton, *et al.*, 2000) As the probe is scanned over the surface changes in topography alter the cantilever deflection which changes the output value from the differential amplifier, and the discrepancy between this value and the setpoint is calculated and referred to as the error signal, which can provide the information in the z axis. However in many modes of AFM a feedback loop is used to maintain a constant force between the probe tip and the sample by moving the probe in the z axis in response to changes in topography. By altering the probe height the cantilever deflection is changed and a constant force kept between the probe and the sample. The voltage applied to the probe to either move it closer or further from the surface at each x,y coordinate is then used to construct the topographic image. Of note is that AFM images can be constructed without the use of a z feedback loop, and can in fact be turned off in most AFMs. Images are obtained through the error signal, and although it allows faster scanning of surfaces due to there being fewer processing steps, and the physical time taken to adjust the height, only relatively smooth samples can be imaged without damage to the tip occurring (“A Practical Guide to SPM” 2005, Bushan and Marti, 2010).

The probe is moved in all axes by piezoelectric scanners, able to move the probe in the x , y and z directions by altering their dimensions on application of a voltage. Piezoelectric materials are ceramics that are fabricated into a cylindrical shape

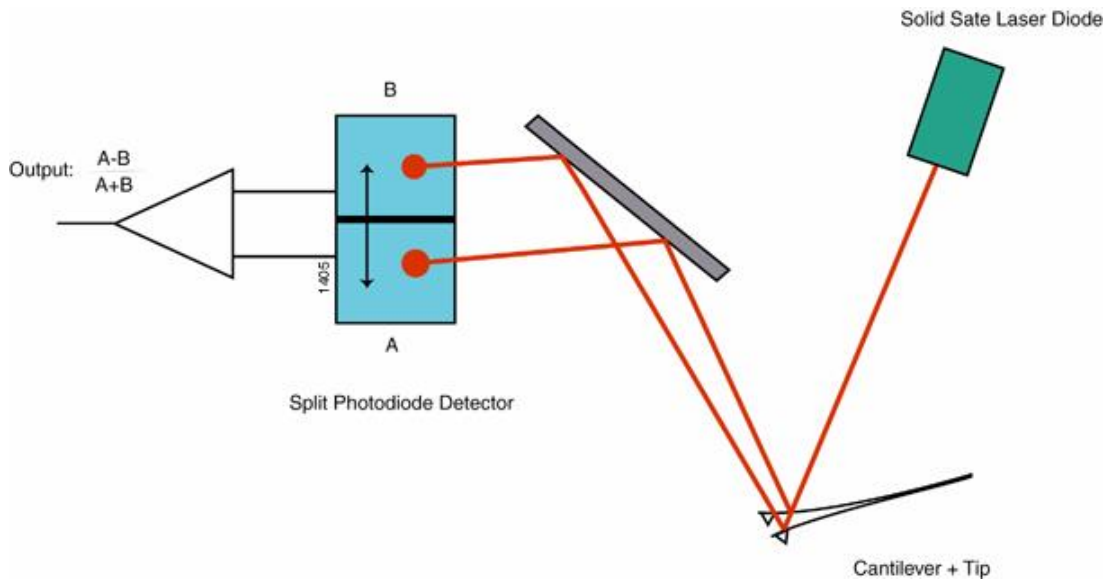


Figure 2.4 Schematic of laser and photodiode detector (Thornton *et al.*, 2000)

generally through sintering of lead zirconium titanate. After sintering a polycrystalline material is produced with each crystal having a separate dipole moment, which needs to be aligned to allow the scanner to move the probe. The alignment is performed by heating the scanner to around 200°C and a DC voltage applied. Electrodes are placed on the outside splitting the scanner tube into four quadrants allowing movement in $+x$, $+y$, $-x$ and $-y$, with an extra electrode attached in the centre of the scanner to control the probe in the z direction. Piezoelectric materials are chosen as they can be spatially controlled down to a sub-angstrom level and generally have a maximum range of movement up to 100 μm in the x , y plane and around 10 μm in the z . The limitations of piezoelectric scanners include varying sensitivity to applied voltages leading to movement hysteresis and age related depoling of the piezoelectric crystals, both of which can be overcome by calibration against a grid of known pitch (Thornton *et al.*, 2000, “A Practical Guide to SPM” 2005, Bushan and Marti, 2010).

2.2.1 Tapping Mode AFM

Tapping mode AFM is a technique where the cantilever is driven near to its resonant frequency, ω_0 , at a constant amplitude, A_0 . The probe is then brought close to the sample, and the probe tip lightly taps the surface with a predetermined set-point

amplitude A_{sp} . The probe is then rastered over the sample surface as in contact mode, and a topographic image can be constructed. The probe is kept in feedback by maintaining a constant A_{sp} . By lightly tapping the surface with the probe tip it gives tapping mode AFM the advantage of having lower loading forces than for standard contact AFM. Another advantage of this mode is access to the secondary imaging technique termed phase imaging. The information of different phases is derived from the differences observed between the drive frequency and the observed frequency of the cantilever. The differences in frequency arrive from tip-sample interactions; therefore it is of importance to understand how the phase angle of the cantilever is affected by tip-sample interactions.

In a freely oscillating cantilever the resonant frequency ω_0 is related to the mass m and the spring constant k of the cantilever, and is shown in equation 2.12 below:

$$\omega_0 = (k / m)^{1/2} \quad (2.12)$$

The phase angle, which is the fraction of a wave cycle that has elapsed relative to an arbitrary point, can be described in radians thus:

$$\phi = \tan^{-1} \left(\frac{m\omega\omega_0}{Q(k - m\omega^2)} \right) \quad (2.13)$$

Where ω is vibrational frequency, Q is the quality factor, which is a dimensionless parameter describing how quickly an oscillator loses energy. The phase angle, denoted ϕ , describes the fraction of a wave cycle which has passed relative to an arbitrary point. Equation 2.13 also describes the behaviour of the phase angle in relation to the vibrational frequency, with ϕ being $\frac{\pi}{2} rad$ at the cantilevers resonant frequency, which is an angle of 90° . At frequencies below the resonant frequency the phase angle is below $\frac{\pi}{2} rad$ and above the resonant frequency ϕ is greater than $\frac{\pi}{2} rad$ (Magonov *et al.*, 1997). The sharpness of this transition is determined by the Q factor of the cantilever, with higher Q factor values giving sharper transitions, as seen in fig 2.5.

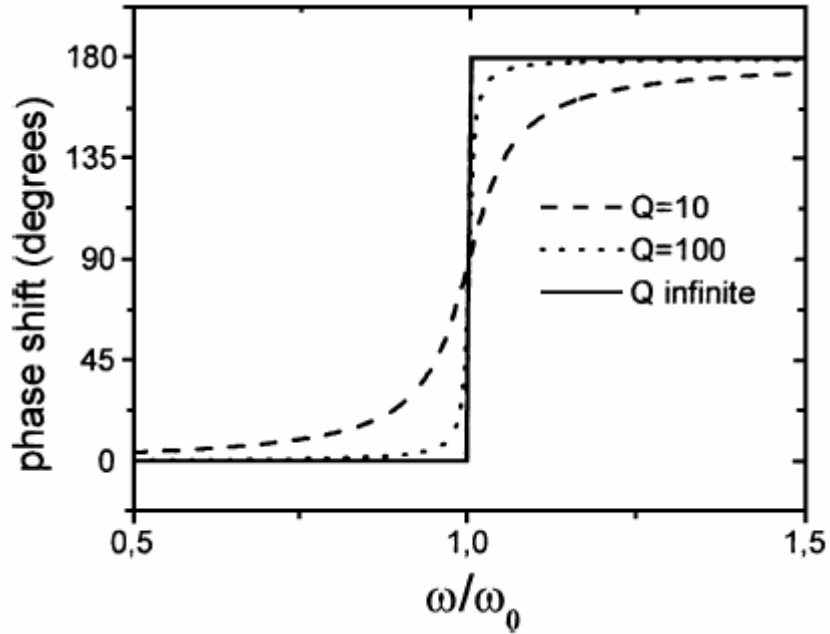


Figure 2.5 Diagram with frequency plotted on the x axis. The dotted line represents phase angle with respect to frequency, and the solid line represents amplitude of the freely oscillating cantilever (reproduced from Garcia *et al.*, 2002)

When a freely oscillating cantilever approaches the sample surface it begins to interact with the sample surface, with the main forces involved being long range attractive interactions such as Van der Waals and short range repulsive forces resulting from Pauli and ionic interactions. In addition long range electrostatic and capillary forces, arising from water adsorption on hydrophilic surfaces, are present but of less concern (Garcia *et al.*, 2002).

The result of these interaction forces is that the force constant changes to a new effective value, which can be described by:

$$k_e = k + \sigma \quad (2.14)$$

where k_e is the effective force constant and σ representing the forces acting on the cantilever:

$$\sigma = \sum \frac{\partial F_i}{\partial z} \quad (2.15)$$

F_i denotes all the forces acting on the cantilever and z the relative displacement

between the tip and the sample. Therefore σ describes the sum of the force derivatives of all the forces acting on the cantilever as a function of relative displacement. This allows the relative strength of different forces at varying relative displacements to be taken into account when calculating the change in force constant.

This alteration in the force constant therefore alters the resonant frequency of the cantilever described below:

$$\omega_e = \left(\frac{k - (\partial F_i / \partial z)}{m} \right)^{1/2} \quad (2.16)$$

with ω_e representing the effective resonant frequency.

In addition by taking equation 2.13, it can be seen that the alteration of the force constant will affect the phase angle:

$$\Delta\phi = \tan^{-1} \left(\frac{m\omega\omega_0}{Q(k + \sigma - m\omega_0)} \right) \quad (2.17)$$

Where $\Delta\phi$ represents the phase angle shift resulting from k_e . If σ is considerably smaller than k then the phase angle shift at the cantilevers resonant frequency, denoted $\Delta\phi_0$, can be described below:

$$\Delta\phi_0 = \tan^{-1} \left(\frac{k}{Q\sigma} \right) \approx Q\sigma/k \quad (2.18)$$

As the probe further approaches the sample and the tip and sample come into contact the repulsive forces indent the surface. As the stiffness of the sample and the tip determine the magnitude of these repulsive forces and indentation into the sample surface, then σ can be approximated by using the Hertz theory of contact mechanics (Magonov *et al.*, 1997):

$$S = \frac{\partial F}{\partial d} = \epsilon a E^* \quad (2.19)$$

S is the stiffness, F the force, d the depth of indentation, which is analogous to σ . If it is assumed a spherical tip indents leading to a circular contact area, then S can also be described by the right hand side of equation 2.19, with ε being a number between 1.9 and 2.4 (Kendall *et al.*, 1971), a is the radius of the contact area, which is derived via:

$$a = \sqrt{Rd} \quad (2.20)$$

with R representing the radius of the tip. The area that the probe tip is in contact with the sample is denoted A , but is not of concern here. The term E^* from equation 2.19 is the effective modulus, which is found by the following equation:

$$\frac{1}{E^*} = \left(\frac{1-\nu_1^2}{E_1} \right) + \left(\frac{1-\nu_2^2}{E_2} \right) \quad (2.21)$$

where ν is the Poissons ratio, which is a measure of the change in the material perpendicular to the applied stress or strain, with 1 denoting the tip and 2 the sample. In AFM E^* is generally dominated by the modulus of the sample as the tip is generally much harder than the sample, especially when analysing polymer systems.

These measures for S are only applicable for contact mode however, as due to the probe moving in and out of contact in tapping mode the contact area becomes larger and smaller throughout the course of the oscillation. This requires the use of time averaged values of a and S , denoted $\langle a \rangle$ and $\langle S \rangle$:

$$\sigma \approx \langle S \rangle = \varepsilon \langle a \rangle E^* \quad (2.22)$$

The phase shift can then be calculated:

$$\Delta\phi_0 \approx \langle S \rangle \left(\frac{Q}{k} \right) = \varepsilon \langle a \rangle E^* \left(\frac{Q}{k} \right) \quad (2.23)$$

This shows that a phase image can be created showing a map of stiffness across the sample surface. Also from equation 2.23 it can be seen that the more stiff the sample

is then the more positive the phase shift will be, and in practical terms this results in lighter areas of the image.

Tip-sample interactions can be increased by alterations in the parameters controlling tapping mode, i.e. A_o and A_{sp} . By raising A_o the increase in amplitude causes an increase in S resulting in a larger $\Delta\phi_0$. Similarly if the A_{sp} is reduced then this too increases the forces acting on the surface. Conversely if A_o is decreased and A_{sp} is increased the tip-sample interactions will be decreased. For phase imaging it is desirable to maximise $\Delta\phi_0$ to provide adequate images, however in soft materials $\langle A \rangle$ (the area the probe tip is in contact with) can be relatively large, resulting in the stiffness of the sample being dominated by the area of contact rather than E^* . In this event the contrast of the phase image is reversed, showing the importance of the correct parameters being employed (Whangbo *et al.*, 1997).

The above equations are all force based, which is a sensible approach based on the name of the technique. There are limitations to this approach, including that it is only applicable when $A \rightarrow 0$, but in reality the amplitude is in the region of 100 to 200nm (Holscher *et al.*, 1999).

Another method of analysing mechanical systems is through Hamiltonian as opposed to Newtonian mechanics and looking at energy dissipation when the tip interacts with the sample.

If it is assumed that the system is in equilibrium the energy required to oscillate the cantilever is equal to the energy dissipation out of the system, which consists of the motion of the cantilever and the tip sample interaction:

$$\overline{P_{in}} = \overline{P_0} + \overline{P_{tip}} \quad (2.24)$$

$\overline{P_{in}}$ represents the average energy required to drive the oscillating cantilever and $\overline{P_0}$ is the energy dissipated through cantilever motion. $\overline{P_{tip}}$ is the term of interest as it represents the energy lost through tip-sample interactions:

$$\overline{P}_{tip} = \frac{1}{2} \frac{kA^2 \omega_0}{Q} \left[\left(\frac{QA_0}{A} \right) \sin \phi - 1 \right] \quad (2.25)$$

with A_0 the free oscillation amplitude and A being the oscillation amplitude once the probe is interacting with the sample surface. As can be seen the phase angle can be derived from equation 2.25 and therefore the phase shift can be determined.

This model of energy loss shows good correlation with experimental results (Anczykowski *et al.*, 1999), and does not require the solution of the differential equation of motion (Anczykowski *et al.*, 1999). However this method does assume that the cantilever oscillations remain approximately sinusoidal (Cleverland *et al.*, 1998). Both methods for determining phase shifts have their merits, however the force model provides a good explanation of how phase images are produced.

2.3 Thermal Probe Methods of AFM

Standard thermal analysis techniques such as differential scanning calorimetry (DSC), modulated temperature DSC (MTDSC) and thermogravimetric analysis (TGA) have been used extensively to study pharmaceutical systems (McPhillips *et al.*, 1999, Royall *et al.*, 2001a). These techniques identify substances through their distinctive transition temperatures, however they can only provide a system averaged response, i.e. any thermal response at a known temperature or time is representative of the entire system, not individual entities. Furthermore mapping of spatial distribution of phases and components may not be achieved, simply due to the nature of the techniques, and for this to be achieved; some form of microscopy is required.

Microthermal analysis (MTA) was introduced in the mid-1990s and permits the thermal characterization of spatially distinct entities in a multicomponent system. The term MTA describes a number of techniques, which use near-field thermal probes to perform highly localised (up to submicrometre scale) characterisation. The instrumentation is based on the near-field imaging technique of atomic force microscopy (AFM); a thermal probe however replaces the conventional ultra-sharp



Figure 2.6 A Wollaston wire probe (reproduced from Royall *et al.*, 2001b)

SPM tip used in AFM. The thermal probe acts as a miniature temperature sensor and a heat source. In MTA a Wollaston wire probe is employed, which is composed of a platinum/10% rhodium alloy core (with an approximate diameter of 3-5 μ m), coated with a silver sheath (circa 75 μ m diameter). A length of wire is bent into a sharp V shape, and braced with a bead of epoxy resin. The silver sheath at the apex is etched away, exposing the platinum filament, and producing a pointed tip (Reading *et al.*, 2001, Craig *et al.*, 2002), as seen in fig. 2.6. A mirror is glued to the wires, which acts as the fulcrum for the optical lever deflection feedback system and the whole assembly is then attached to a cantilever mount for connection to the piezoelectric scanner (Moon *et al.*, 2000).

It is possible to achieve topographic images as per standard contact mode AFM, although at a lower resolution, as AFM tips have radii of curvature in the range of 5-10nm compared to the 100nm of the thermocouple probes used in MTA (Sanders *et al.*, 2000).

Another possibility afforded by the technique is localised thermal studies. A facet of this is local thermomechanical analysis (L-TMA); usually, after a topographic image

is obtained, the probe can be moved to an area of interest, an initial force applied to deflect the probe, and temperature ramping applied linearly.

The heating of the tip occurs due to its decreased diameter and the increased specific electrical resistance of the platinum core, which has a much higher resistance (approximately 2-3 Ω) than silver and, therefore, the rest of the Wollaston wire. This results in Joule heating of the tip when a current is passed through it.

Within the range of 300-600K the resistance of platinum has an almost linear relationship with regards to temperature, and is described in the following equation.

$$R_p = R_{p0}[1 + \alpha(T_p - T_0)] \quad (2.26)$$

with R_p representing the probe resistance, R_{p0} the probe resistance at room temperature, α the platinum wire temperature coefficient, T_p the probe temperature and T_0 room temperature. The resistance of the lead wires and the untreated Wollaston wire are not considered as their value is so low compared to the resistance of the tip (Moon *et al.*, 2000). It can therefore be deduced that if the resistance of the wire is known then the temperature of the probe can be calculated.

The probe still requires calibration, and this is usually achieved by a series of three calibration standards composed of organic polymers with known transition temperatures. A room temperature “kick-in” point is used to provide a fourth temperature, due to the fact that the probe tip is at room temperature when zero voltage is applied to the tip. Wollaston probes are run in dual probe mode permitting differential temperature measurements, with the second probe held in air away from the sample, in a similar manner to DTA.

The heat flow from into the sample can be illustrated by Fourier’s Law of conduction as described by Wang:

$$\frac{\Delta T}{\Delta t} = -\kappa \nabla T \quad (2.27)$$

where $\frac{\Delta T}{\Delta t}$ represents the change in temperature with respect to time, ∇T , the temperature gradient between the tip and the sample, and κ the thermal diffusivity, which is calculated:

$$\kappa = \frac{\lambda}{\rho C_p} \quad (2.28)$$

with λ being the thermal conductivity, ρ the density, and C_p the specific heat capacity. If it is assumed that heat transfer is negligible in every direction apart from vertical the heat transfer can be modelled thus:

$$\frac{\partial T(z,t)}{\partial t} = \kappa \frac{\partial^2 T(z,t)}{\partial z^2} \quad (2.29)$$

with z representing heat transfer in the vertical direction. The model can be adapted to a three dimensional model, in which the probe, for simplicity, is assumed to be a perfect hemisphere, and that heat transfer is equal in all directions:

$$\frac{\partial T(z,t)}{\partial t} = \kappa \left(\frac{\partial^2 T}{\partial z^2} + \frac{2\partial T}{r\partial r} + \frac{\cos\theta}{r^2 \sin\theta} \frac{\partial T}{\partial\theta} + \frac{\partial^2 T}{r^2 \partial\theta^2} \right) \quad (2.30)$$

With r being the distance between the centre of the probe and the sample, which is effectively the radius of the tip and θ the polar angle.

The materials mechanical properties may alter on heating, if it undergoes a phase transition thermal expansion will occur, forcing the cantilever upwards, the degree to which this occurs depends on the materials thermal expansion coefficient, thermal conductivity, and heat capacity. If the melting or glass transition temperature of the material is reached softening of the material occurs, the tip indents the sample, and the cantilever movement can be measured via the optical lever. Therefore force feedback is usually disabled, as the z -piezo would drive the tip through the sample as it softens in a bid to re-establish feedback. This results in application of controlled heating signal to a highly specific area of a few microns, and information about thermal transitions to be garnered.

As opposed to conventional DSC the information regarding thermal transitions is not quantitative, as the sample mass is unknown, due to the large size of the sample in comparison to the probe tip (Price *et al.*, 1999b). This only permits qualitative information to be provided, however this often suffices for characterisation purposes, for example two different phases can be characterised and distinguished with this data.

More recently nano-TA probes have been introduced which are more similar in shape to traditional AFM probes; however the probe tip is constructed from silicon doped with either boron or phosphorous resulting in probe becoming electrically conductive (Nelson *et al.*, 2007). The tip contains a reduced level of doping than the cantilever, which acts in a similar fashion to the Wollaston probe, resulting in resistive heating (Harding *et al.*, 2007). The cantilever is in a U shape, as seen in Fig. 2.7, allowing current to flow through the probe tip, and Joule heating to occur.

These improved probes have a profile comparable to traditional AFM probes, with a tip radius of around 30nm, which is considerably improved on the 1 μ m radius of

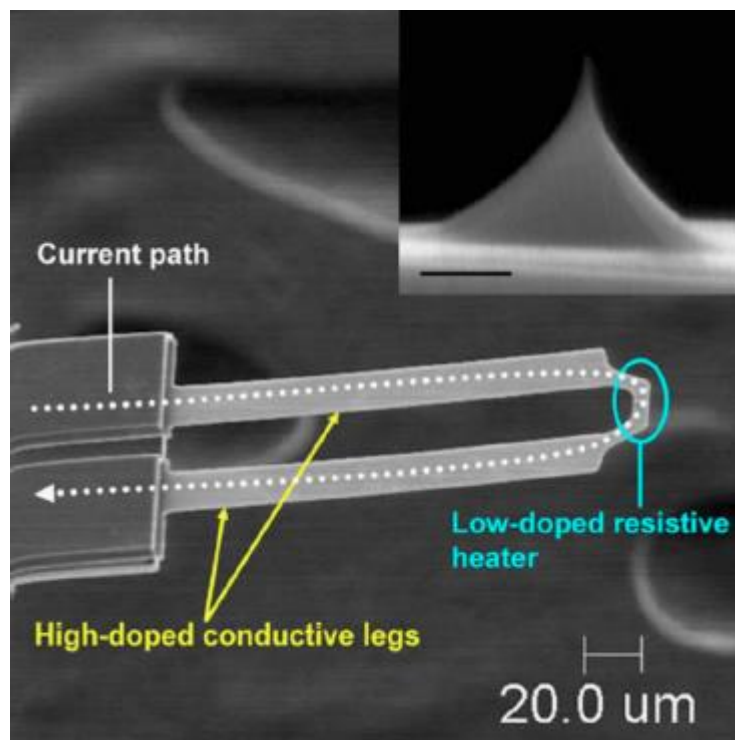


Figure 2.7 SEM image and diagram of the current flow in a nano-TA probe (reproduced from Nelson *et al.*, 2007)

Wollaston probes. This allows for an area of indentation of $<100\text{nm}$ (Nelson *et al.*, 2007), which in practical terms indicates the size of crater resulting from an L-TMA experiment. This allows the area of scrutiny to be considerably smaller with nano-TA probes and should enable more measurements to be made in the same region of the sample. Another advantage of nano-TA probes is that they are considerably stiffer than Wollaston probes, which permits non- and intermittent contact modes to be opened up for use.

As stated above there is a whole family of techniques encompassed by MTA and nanothermal analysis. These include scanning thermal microscopy (SThM), where the probe is used in an active (constant temperature), or passive (constant current) mode. Constant temperature mode measures the voltage required to keep the tip at a constant temperature, through balancing of a Wheatstone bridge circuit. In Fig 2.8, R_1 , R_3 and R_4 are of known resistance, with R_4 being a variable resistor, and R_p the

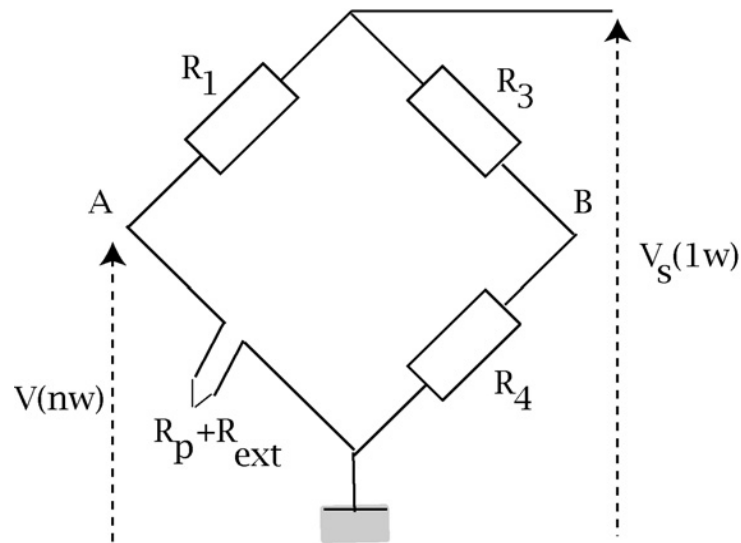


Figure 2.8 Schematic of the Wheatstone bridge circuit employed in SThM (reproduced from Gossel *et al.*, 2007)

probe resistance. The ratio $\frac{R_p}{R_1}$ is compared to $\frac{R_4}{R_3}$, and if the ratios equal each other then no current will flow between points A and B. If the circuit is unbalanced current will flow, and the direction of flow indicates if R_4 is tuned too high or low, and can be adjusted back to zero. Through ohms law the voltage required to keep the tip at a

constant temperature is derived and this provides a feedback circuit from which to construct a map of thermal conductivity (Reading *et al.*, 2001).

As mentioned above L-DTA measurements can be performed, with the power required to keep the probes adhering to the temperature ramp measured. This provides similar information to traditional DTA measurements, however again the information gathered is only semi qualitative.

A sinusoidal heating pattern similar to MTDSC can also be applied through the use of alternating current (AC), rather than direct current (DC) to the probe, allowing information about the depth of samples to be acquired.

Harding *et al.* (2007) have previously described the use of heated tip pulsed force mode (PFM) AFM. PFM-AFM is an Intermittent contact technique using low frequency modulation (around 100-2000Hz) at an amplitude of 10-5000nm. The images produced using PFM-AFM relate to topography, stiffness and pull off force (adhesion). The technique was able to create a highly localised amorphous region using L-TMA then differentiate between crystalline and amorphous regions of indomethacin based on the adhesion between the tip and the probe. As the probe was scanned across the sample the adhesion could be measured at each location allowing the production of a topographic image and a map of surface adhesion. After each image was obtained the probe temperature was increased by 10°C, showing the changes in adhesion as the amorphous region recrystallised.

These techniques have been reviewed in detail elsewhere in the literature (Price *et al.*, 1999a; Reading *et al.*, 2001; Pollock *et al.*, 2000; Craig *et al.*, 2002), and will not be discussed in detail here.

2.4 Fourier Transform Infrared Spectroscopy

As molecular bonds vibrate they have a resonant frequency and at this resonant frequency the bonds will absorb energy causing a transition in the vibrational state.

For a bond to be visible in the IR spectrum it must have a dipole moment, and it must change during the vibration, for example through stretching or bending of the bond. Molecular bonds tend to have resonant frequencies in the infrared spectrum, so if a source of infrared light is emitted towards a sample the amount of energy absorbed can be measured.

The vibrational energy of the bonds is determined by the following equation:

$$E_{vib} \propto \sqrt{\frac{k}{\mu}} \quad (2.31)$$

With k representing the bond force constant, which dictates the strength of the bond and μ which is the reduced mass of the two atoms in the bond, and is calculated thus:

$$\mu = \frac{m_1 m_2}{m_1 + m_2} \quad (2.32)$$

m_1 and m_2 are the masses of the two atoms. It is therefore apparent that the highest energy bonds are those that contain a hydrogen atom. In the electromagnetic spectrum energy is directly proportional to wavelength; therefore bonds with a higher vibrational energy will appear at a lower frequency on the spectrum. This means that each molecular bond has a unique frequency that it absorbs light at, so if a range of frequencies in the infrared spectrum are transmitted at the sample and a spectra of absorption peaks can be constructed.

Infrared spectrometers consist of a source of infrared light, which transmits infrared light towards the sample and a detector which detects the amount of energy absorbed by the sample. Most modern infrared spectrometers use an interferometer to allow for all frequencies to be collected simultaneously, as opposed to traditional IR spectrometers which used dispersive techniques to measure each frequency individually. Once the infrared light has reached the detector the signal produced then undergoes a Fourier transform to deconvolute the interferogram into a final infrared spectrum. This not only increases the speed of measurements, but also the signal to noise ratio, as many spectra can be taken in a short space of time. Also by

increasing the speed of measurements, a larger number of spectra can be taken thus reducing any errors in the signal (Alemeida *et al.*, 2002).

A further improvement on traditional IR spectroscopy is the use of attenuated total reflectance (ATR) FTIR. This is based on the phenomenon of total internal reflectance, which occurs when light incidents on a boundary between two materials of differing refractive indices above a critical angle all light is reflected. For total internal reflection to occur the sample must have a far lower refractive index than the material it is in contact with, which generally entails the use of a zinc selenide or germanium crystal (Offermann *et al.*, 1995). Although all light is reflected a near field standing wave is created running parallel to the boundary and penetrates somewhat into the sample. This wave is termed the evanescent wave, and as it penetrates into the sample the wave is attenuated by the sample absorbing energy in the same fashion as in traditional IR spectroscopy. The infrared radiation is reflected along the interface and collected by a detector, from which a spectrum is constructed (Hind *et al.*, 2001).

The penetration depth of the evanescent wave can be defined by the following equation:

$$d_p = \frac{\lambda}{2\pi\eta_1\sqrt{\sin^2\theta - (\eta_2/\eta_1)^2}} \quad (2.33)$$

d_p is defined as the distance where the amplitude of the electric field drops to e^{-1} of its surface value. The wavelength, λ , has an important effect of the depth of penetration as the amount of energy in the wave is inversely proportional to its wavelength and θ is the angle of incidence of the IR radiation (Hind *et al.*, 2001). This is required to be greater than the critical angle required for total internal reflection, which is found:

$$\theta_c = \sin^{-1}\left(\frac{\eta_2}{\eta_1}\right) \quad (2.34)$$

where η_1 and η_2 are the refractive indices of the crystal and the sample respectively.

As \sin^{-1} , to be defined, has to be <1 then η_1 must be $\geq \eta_2$, which is needed for total internal reflection to occur. As can be seen in equation 2.33 the refractive indices of the materials also have a bearing on the penetration depth of the evanescent wave which in turn has an effect on the spectrum produced, as different structures within the sample may be probed at varying depths (Grosse *et al.*, 1995). The typical penetration depth is in the region of 0.5 to 5 μm .

Traditional IR requires samples to be prepared prior to analysis, often by grinding the sample in a mortar and pestle with a salt, often KBr, and then pressing the sample into a disk, which allows IR radiation to pass through. ATR-FTIR removes this requirement as it is not transmission based, which is of note to this thesis, as it allows for samples to be analysed in-situ. Providing there is sufficient contact between the ATR crystal and the sample, there is no destructive preparation and, within reason, there is little limitation on the sample geometry.

2.5 Scanning Electron Microscopy

Traditional optical microscopes use reflected light focused and magnified by optical lenses to create images. Microscopes are limited by the wavelength of incident source, which is known as the diffraction limit, and can be calculated through the following equation:

$$d = 0.61 \frac{\lambda}{NA} \quad (2.35)$$

Where d is the diffraction limit, λ the wavelength of light, and NA the numerical aperture, which is the relationship between the radius of the objective lens aperture and the working distance. From this calculation it can be shown that optical microscopes can achieve a minimum resolution of around 200nm. Scanning Electron Microscopy (SEM) however use accelerated electrons as opposed to light to create an image. Electrons are used as under quantum theory electrons can be treated as waves and have a considerably lower wavelength than light. Their wavelength can be found:

$$\lambda = \frac{h}{p} = \frac{h}{\sqrt{2m_c E_b}} \quad (2.36)$$

with h representing Plank's constant and p the momentum of an electron. The momentum of an electron can be calculated from the right hand side of the equation, with m_c corresponding to the rest mass of the electron and E_b the energy of the electron beam. Thus it can be derived from the following equation that at 1 eV the electron will have a wavelength in the nm range, and as the E_b is increased then the wavelength decreases (Bozzola and Russell, 1998). At accelerating voltages seen in SEM, which are typically in the tens of kilovolts, the wavelength of the electron is in the μm range. By substituting these values into the equation 2.36, it can be seen that the diffraction limit for electron microscopes is far lower than for that of traditional optical microscopy, allowing for much increased levels of magnification.

The electron beam is usually created through the use of a tungsten or lanthanum hexaboride filament, which is heated to lower the work element of the filament until it is possible to draw electrons off the material using an electric field. The electrons pass through a number of lenses, which work in the same manner as optical lenses but focus the beam using magnets. The electron beam incidents onto the sample, which is held in a vacuum and coated in a conducting material. A vacuum is used because the molecules in air would disrupt the flow of electrons, and also as the filament is heated it could become contaminated. The sample is coated in a conductive material, usually gold, and grounded to avoid the accumulation of electric charge on the surface which can produce artefacts in the image (Goldstein *et al.*, 2003, Reed 2005).

The sample is located on a stage which can be rotated in three dimensions allowing for most areas of the sample surface to be imaged through movement of the stage. SEM allows precise spatial measurements of surface structures to be determined as the working distance and lens aperture is known the length of surface features can be calculated.

2.6 Materials

2.6.1 Opadry I

Opadry I is a fully formulated dry blend system used for aqueous film coating consisting Hydroxypropyl methylcellulose (HPMC), as the film forming polymer, and polyethylene glycol (PEG) as a plasticiser. Opadry I tends to be used as an immediate release coating with or without pigments to enhance the visual appearance of solid dosage forms or to provide taste masking. HPMC is a hydrophilic, propylene glycol ether of methyl-cellulose, derived from cellulose with the chemical name 2-hydroxypropyl cellulose methyl ether. HPMC is freely soluble in water, of note though it is insoluble in hot water, and if added to cold water incomplete wetting of the HPMC occurs and a lumpy solution may be produced. This has led to the hot/cold dispersion technique where around 1/3 of the water is heated to 90°C and the HPMC is added under agitation until all the HPMC is wetted. The remainder of the water is then added as either cold water or ice to lower the temperature and allow for solubilisation of the HPMC (Dow, 2005). The polymer is also soluble in certain organic solvents and binary solutions, however for pharmaceutical purposes it is almost invariably dissolved in water.

HPMC can be incorporated into the tablet matrix providing a controlled release function by hydrating and forming a gel layer whereby the API dissolves through. When HPMC comes into contact with an aqueous medium there is rapid uptake of

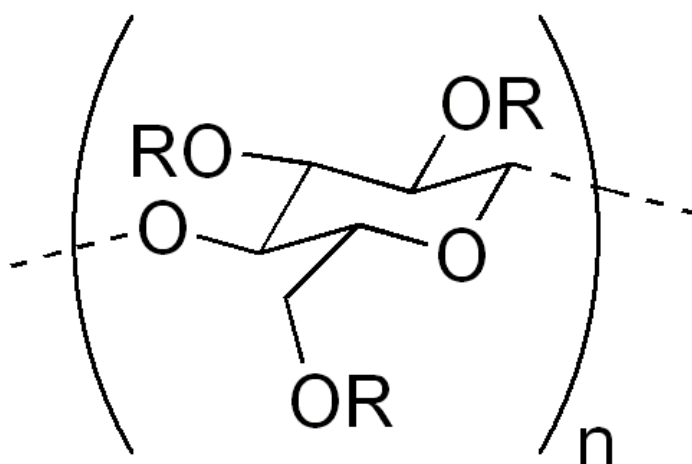


Figure 2.9 Structure of HPMC

water causing hydration of the polymer. The polymer coil begins to uncoil and extend, causing inter-polymer hydrogen bonds to break, thus allowing further sites for water to enter (Li *et al.*, 2005). This forms a hydrated layer on the outside of the tablet. This hydrated layer retards further uptake of water into the rest of the tablet, and hence slows drug release. Drug release is controlled by drug diffusion through the gel layer and, by erosion of the gel layer (Colombo *et al.*, 1996). The rate of drug release is then dependent on the rate of drug diffusion through the gel, and the rate of matrix erosion, which is influenced by polymer grade, drug loading, drug/polymer ratio and the amount and type of tablet filler (Ebube *et al.*, 2004).

There are numerous different grades of HPMC which contain different ratios of hydroxypropyl and methyl substitution which, amongst others, affects organic solubility and the thermal gelation temperature of aqueous solutions. Another factor that influences the properties of HPMC is viscosity which ranges from 3 to in excess of 200,000 mPa's with the grade used depends on the purpose that HPMC is used for. When incorporated into matrix tablets the viscosity tends to be in the region of thousands or tens of thousands millipascals, however for film coating a viscosity in the hundreds of millipascals is more suitable.

2.6.1.1 The Glass Transition of HPMC

The glass transition of HPMC is notoriously difficult to ascertain. Aside from the typical issues of polydispersity, water sorption, differing molecular weight grades and residual solvent when measuring the glass transition of polymers, HPMC is also a strong glass former. As described above when using MTDSC to determine the glass transition of a material the change in heat capacity associated with the glass transition is measured. In a strong glass former there tends to be some local to intermediate range order resulting in relatively stable structures which tends to lead to Arrhenius-like changes in molecular mobility with regards to temperature and a relatively small change in heat capacity. Fragile glasses on the other hand tend to consist of nondirectionally, noncovalently bonded molecules, which leads to a deviation from the Arrhenius curve which results in rapid changes of molecular mobility and heat capacity around the T_g (Angell *et al.*, 1995, Borde *et al.*, 2000, Hancock *et al.*, 1996).

This difficulty in determining the T_g of HPMC has been well documented in the literature (Sakellariou *et al.*, 1985, McPhillips *et al.*, 1999). Strong glass formers such as HPMC benefit enormously from MTDSC, where the subtle glass transition can be resolved in the reversing signal. However McPhillips highlighted the difficulties of T_g measurement, even when using MTDSC, with numerous sets of parameters having to be investigated to achieve the best resolution and sensitivity. This included increasing the underlying heating rate, which as can be seen in equation 2.6, the term $C_p \cdot dT/dt$ will be increased with higher scan rates. The scan rate is limited however by the requirement of four modulations through the thermal event (McPhillips *et al.*, 1999).

Strong glass formers highlight an important limitation in DSC and MTDSC, as they rely on heat capacity changes to detect the glass transition. This shows the need to use a variety of techniques when analysing samples, as there is unlikely to be one piece of analytical equipment that can analyse every sample and produce meaningful data. In the case of HPMC it has been reported that torsional braid analysis and thermomechanical analysis can be more sensitive methods to detect its T_g (Sakellariou *et al.*, 1985).

2.6.2 Polyethylene Glycol

Polyethylene glycol (PEG) is a widely used excipient in pharmaceuticals and associated industries such as cosmetics and as a food additive. The chemical structure of PEG is $H(OHCH_2CH_2)_nOH$ where n represents the average number of

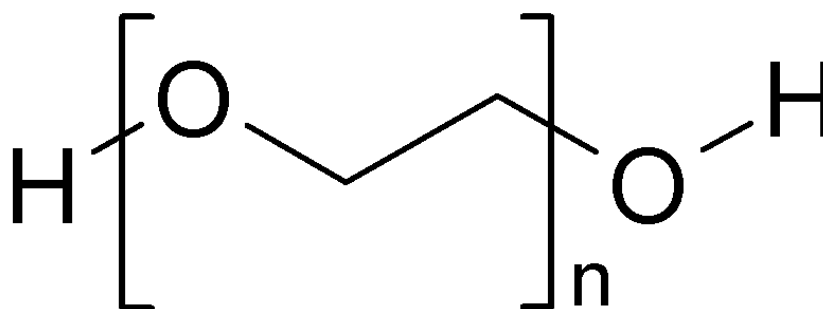


Figure 2.10 Structure of PEG

oxyethylene groups. Depending on the molecular weight of the PEG in question will either be a clear viscous liquid ($M_w < 200$), white or off-white waxy flakes (M_w 200-2,000) or opaque white crystalline solid at higher molecular weights.

As a synthetic polymers PEGs have numerous advantages, including being non-toxic, non-immunogenic, non-antigenic and approved by the FDA. Due to these benefits PEGs have myriad pharmaceutical applications ranging from bases in ointments and suppositories, a lubricant in eye drops and as tablet binders. PEGs are also used therapeutically for constipation with PEG of molecular weight 3350 formulated into oral powders and marketed in preparations such Movicol and Laxido (British National Formulary 2011). There is also considerable interest in the use of PEGs in drug delivery due to their non-immunogenic and non-antigenic properties PEGs can reduce the immunogenic and antigenic properties of drugs. This technique is termed PEGylation and was first described in 1977 by Aubrochovic (1977a, 1977b). Functionalising APIs with PEG also increases the hydrodynamic size of the API, reducing renal clearance and therefore prolonging residence time in the body resulting in less frequent administration (Veronese 2005).

In polymer film coats PEG is employed as a plasticiser to improve the quality of the finished film and is incorporated into both Opadry I and Opadry II. The M_w is circa 3000-4000, therefore appearing as white flakes and a melting point of around 60°C (Sigma-Aldrich, 2011).

2.6.3 Opadry II

Opadry II is based on poly (vinyl alcohol) (PVA), which is a non-toxic water soluble polymer produced by the hydrolysis of poly (vinyl acetate). In addition to PVA, Opadry II consists of PEG as a plasticiser, polysorbate 80 to aid dispersion of the plasticiser and Talc as a glidant. PVA has myriad functions in pharmaceuticals including as a lubricant in eye drops, however PVA's role in film coating is as a film forming polymer for tablet coatings. PVA has uses in many other fields including producing biodegradable films, water soluble packaging, and as a raw material for other

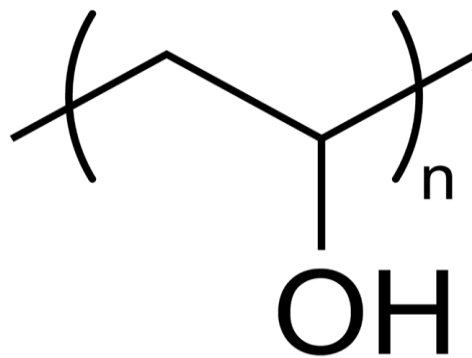


Figure 2.11 Structure of PVA

polymers such as polyvinyl nitrate. In film coating Opadry II is used as an immediate release film coating and is typically applied for taste and odour masking, or to achieve an improved visual appearance through increased gloss.

Vinyl alcohol, the monomer of PVA, is present almost completely as its tautomeric form acetaldehyde, therefore, unlike other polymers is not synthesised from its monomer but is prepared from partial or complete hydrolysis of poly (vinyl acetate) (PVAc) (Bohlmann, 2005). The percentage of poly (vinyl acetate) hydrolysed to PVA can be controlled, which alters the properties of the final PVA. For example if over 70% of PVAc is hydrolysed to PVA the resulting PVA will be biodegradable. Thus alongside altering the MW of PVA the percentage hydrolysed also has a bearing on the final properties of the polymer.

As with many polymers the properties for different uses are controlled by altering molecular weight, with the degree of hydrolysis also being altered. PVA has a relatively simple structure compared to the cellulose derivatives, with just a hydroxyl group attached to the carbon-hydrogen backbone. PVA forms a semi-crystalline structure as the small nature of the OH group allows a planar zig-zag conformation to be formed.

PVA has a number of advantages over HPMC, which include a lower viscosity allowing for optimal droplet spreading resulting in tablets with a smoother appearance and higher gloss. Also PVA has higher adhesion than PVA leading to improved logo and break line definition. Another key advantage over HPMC is that

when blended with aqueous dispersions of ethylcellulose flocculation can occur at relatively low concentrations of HPMC; however this is less of an issue when PVA is used (Siepmann *et al.*, 2007).

2.6.3.1 Thermal Transitions of PVA

Due to the semicrystalline nature of PVA there are several transitions seen for this polymer. Mucha *et al.* (2005) described the T_g of cast films of PVA as 45°C, using DSC. The authors noted this was a low value due to the plasticising effect of water and once this had been driven off in the initial DSC run, the glass transition value increased to circa 70°C. The paper also described the use of DMTA to analyse PVA which gave the T_g as 40-50°C from α -relaxation. Again the T_g increased to 65-75°C on the second scan once water was removed. Okhamafe (1988) also used DSC to describe the T_g of PVA as 70°C, with the experiment containing an isothermal step of 125°C to remove any excess water. The paper also described the crystalline melting temperature of PVA as between 150-215°C.

Park *et al.* (2000) described the use of DMTA and DSC to determine the thermal transitions of PVA films. When films were analysed using DMTA a peak in $\tan \delta$ was observed at 85°C which was attributed to the T_g of PVA as there was also a large decrease of E' corresponding to this temperature. Another small peak was observed at 143°C and was assigned to β_c relaxation caused by alterations in motions of the PVA chains. A larger transition was seen between 220-260°C and is the result of crystalline phase of PVA undergoing its T_m . DSC showed the melting point to be 228°C. There was no mention of the glass transition being detected by DSC, however as DSC opposed to MTDSC was employed then the T_g may not have been detected.

Other authors (Jones *et al.*, 2005), have described similar transitions using MTDSC, with a T_m between 170-220°C and two lower transitions of 70°C and 116°C. The authors noted that the higher of the two transitions is relatively small and is not always noted in papers. Also of interest was that with increasing hydrolysis of the polymer the first glass transition was also increased, as by removing increasing

amounts of acetate from the chain increases the crystallinity of PVA and therefore decreases the mobility of chains in the amorphous phases thus increasing the T_g .

2.6.3 Surelease

Surelease is an ethylcellulose pseudolatex produced by Colorcon[®], and is typically used for controlled release coatings of solid dosage forms. Ethylcellulose is derived from cellulose through the addition of ethyl groups onto the hydroxyl groups present on the cellulose backbone, as can be seen in the figure below. Similar to other polymers altering the molecular weight of ethylcellulose will alter the polymer

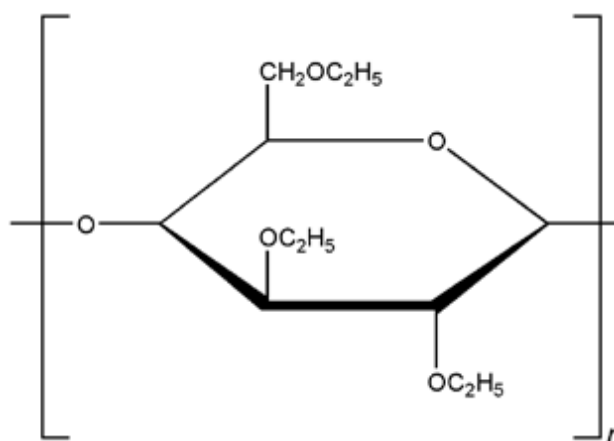


Figure 2.12 Structure of Ethylcellulose

viscosity, but in addition variation in the ethoxyl content can produce differences in physical properties (Porter *et al.*, 1989). An interesting property of ethylcellulose is that it is water insoluble, however due to the presence of ethoxyl and hydroxyl groups, it is hydrophilic so can absorb water (Dow, 2008). This property is of particular use for controlled release film coats, as it allows water absorption into the film allowing the film to become permeable to the active drug, but results in the film retaining mechanical integrity. Ethylcellulose is soluble in a wide variety of organic solvents including chlorinated solvents, natural oils and aliphatic alcohols; as such ethylcellulose was historically dissolved in ethanol prior to coating (Bodmeier *et al.*, 1989).

Ethylcellulose has many applications apart from film coating of pharmaceuticals. Within the pharmaceutical industry it is also employed as a controlled release matrix in tableting and outside of pharmaceuticals ethylcellulose is often used to create films and as a rheology modifier in industries such as food, personal care and printing inks. It has numerous advantages including being one of a limited number of water insoluble polymers approved for pharmaceutical use and being relatively easy to manufacture.

Surelease is manufactured by melt extruding the ethylcellulose with oleic acid and dibutyl sebacate (or fractionated coconut oil) then the resulting melt is introduced to ammoniated water. On mixing an emulsion is formed and ammonium oleate is produced which acts as a stabiliser of the colloidal structure. Purified water is then used to adjust the dispersion to a final solids content of 25%, producing a coating solution of the correct viscosity and solids content for aqueous film coating.

2.6.3.1 Thermal Transitions of Ethylcellulose

Ethylcellulose, similar to HPMC, is a strong glass former, and therefore has a subtle glass transition temperature when analysed with MTDSC, due to the small heat

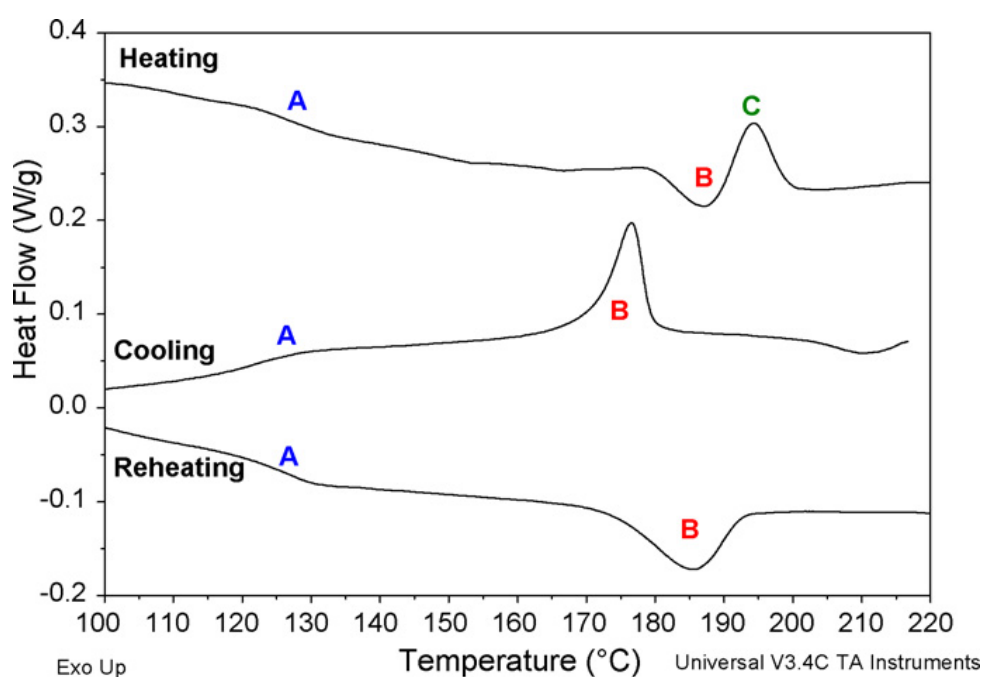


Figure 2.13. MTDSC trace showing ethylcellulose transitions. See text for explanation (Reproduced from Lai *et al.*, 2010)

capacity change. The T_g of ethylcellulose is generally accepted to be circa 130°C, though, as with other preformulated coating systems this will most likely be decreased due to the presence of plasticisers. In the case of ethylcellulose the degree of ethoxyl substitution can also alter T_g (Sakellariou *et al.*, 1985).

Another interesting aspect of the thermal transitions of ethylcellulose is the presence of a high temperature endothermic and exothermic response above the T_g , circa 175°C. Lai *et al.*, (2010) accredited the endotherm, denoted B in Fig. 2.13, to microcrystals present in the polymer, which underwent melting, and the exotherm to oxidative degradation, denoted C in Fig 2.13. This is a sensible conclusion as other cellulose derivatives contain some crystalline structure. However the ethylcellulose used in the study was analysed in powder form, so there may well be some microcrystals present, however once the ethylcellulose is processed into a pseudolatex and dried to form a film there may be less chance of these crystals being present.

CHAPTER 3

3. Characterisation of Materials

3.1 Introduction

As discussed in previous chapters L-TMA can only produce semiquantitative data, due to the sample mass being unknown. Alongside the influence of sample roughness and other factors, it is necessary to confirm any transitions seen in L-TMA with a standard analytical technique such as DSC or D-TMA.

This chapter therefore is concerned with the determination of thermal transitions for the three chosen coating systems of Surelease, Opadry I and Opadry II through the use of L-TMA and MTDSC. This will provide a basis for future chapters, as once the polymers are blended, pigments are added or the minitablets cured there is likely to be alterations to the glass transitions of the individual polymers. Additional characterisation will be undertaken by AFM imaging in contact mode to provide information on the surface structure of the polymer films as again changes in film morphology would be expected once the polymer films have been blended, cured or had pigments added.

Both cast films and film coated minitablets will be analysed, thus ascertaining if AFM and L-TMA are suitable for use in the in-situ analysis of polymer film coats. Film coated minitablets are likely to have a different morphology than cast films due to the different process conditions in the production of the films therefore a comparison between the two is prudent.

There has been some debate as to whether L-TMA measures the glass transition or melting point of a material (Royall *et al.*, 2001b), or whether it measures a softening point, and data is included to add to this discussion.

3.2 Materials and Methods

3.2.1 Preparation of Films

The coating systems Surelease (E-7-19040), Opadry (OY-29020) and Opadry II (85F19250) were kindly supplied by Colorcon (Dartford, England). Surelease contains ethylcellulose as the film forming polymer, HPMC forms the basis of Opadry and poly (vinyl alcohol) is the film forming polymer of Opadry II. Both Opadry I and Opadry II are plasticised with polyethylene glycol with Opadry II also containing polysorbate 80 to aid dispersion of the plasticiser and Talc as a glidant. 8% w/v solutions of Opadry and Opadry II were prepared by adding Opadry powder to distilled water under gentle agitation and mixing for 45 minutes. Surelease is supplied as a 25% (by solid weight) dispersion which requires dilution with distilled water to 15% prior to coating.

Cast films were prepared by pouring 15ml of coating solution into a 9cm Petri dish and drying in an oven for 24 hours at 45°C. After drying the Petri dishes were stored in desiccators, to avoid any water sorption onto the film, until analysed.

Placebo bi-convex minitables containing lactose monohydrate (Friesland Foods Domo UK Ltd, Netherlands), cellulose powder elcema F150 (J Rettenmaiers & Sohne Gmbh, Germany), Starch 1500 (Colorcon Ltd, UK), Magnesium Stearate (Peter Greven, Holland) and Aerosil 200 (Evonik, Germany) were prepared on a Riva Piccola rotary tablet press and were also gifts from Colorcon. 20g batches of minitables were coated in a Caleva Mini Coater Drier-2 (Caleva Sturminster Newton, Dorset).

Parameter	Opadry I	Opadry II	Surelease
Air Inlet Temperature (°C)	40	45	45
Process Air Flow (m/s)	12	12	12
Atomising Air Pressure (bar)	0.7	0.7	0.7
Flow Rate (ml/hr)	23	23	23*
Process time (min)	45	45	90

Table 3.1 Process conditions for film coating *flow rate increased to 30ml/hr after 15 minutes

Process conditions for each coating solution are given in Table 3.1. Opadry I and Opadry II solutions were applied to give a final weight gain of 2%, with Surelease solutions applied so as to achieve a 10% increase. This is generally the weight gain observed when the coating systems are applied in industry, thus providing an accurate estimation of how the film coats appear in practice. The process time for Surelease was only twice that of Opadry I and Opadry II as once a layer of film has been deposited on the minitablet surface the flow rate can be increased, thereby applying the solution more quickly but without any associated tacking.

3.2.2 Atomic Force Microscopy and Thermal Probe Methods

Thermal nanoprobes (AN-2 probes, Anasys Instruments, Santa Barbara, CA) were used throughout the study. Additionally Wollaston wire thermal probes (Veeco Santa Barbara, CA) were also used and are specified in the text where these were employed. Samples were attached to a metal stub using double sided sticky tape and then placed onto an X-Y translating microscope stage. Minitablets had one end cap removed with a scalpel, to allow adequate contact with the tape to avoid the sample moving during scanning. To analyse cast free films a small section of film was cut using a scalpel and attached to the metal stub in the same fashion. AFM images were acquired with a Veeco (Santa Barbara, CA) Explorer AFM head, or with a Veeco Caliber head. The two AFMs used in the study were of a similar nature, however tapping mode was not enabled on the Explorer AFM, therefore tapping mode images were acquired using the Caliber head. A minimum of three images were acquired for each minitablet or section of cast film and in addition three different minitablets or sections of cast films were analysed. L-TMA was carried out using these AFM heads connected to a nano-TA system (Anasys Instruments Santa Barbara, CA) with the explorer also connected to a TA instruments (New Castle, DE) 2990 μ TA Microthermal analyser. A minimum of 20 L-TMA measurements were acquired for each sample. Temperature calibration was carried out in the nano-TA software using a room temperature “kick-in” point along with Polycaprolactone (PCL, 60°C), Polyethylene (PE, 130°C) and Poly(ethylene terephthalate) (PET, 238°C). The calibration materials are supplied by Anasys Instruments and their onset melting temperature is determined using a DSC by the manufacturer. All experiments were carried out with a heating rate of 25°C/s, unless otherwise stated, and a set point of 5nA for nano-TA probes and 15nA

when using Wollaston probes. These values were obtained from initial experiments indicating these experimental parameters produced the most consistent L-TMA traces and images. L-TMA experiments were also calibrated so that it was possible to observe the transitions in microns rather than volts, which is usually displayed in the program. L-TMA results were recorded and analysed using NanoTA software (Anasys Instruments, CA), and graphs were plotted using a spread sheet.

3.2.3 Modulated Temperature Differential Scanning Calorimetry

All measurements were carried out using a Q2000 DSC (TA instruments, Newcastle, USA). The instrument was calibrated for temperature using *n*-octadecane (28.24°C), benzoic acid (122.37°C) and indium (156.61°C), and the heat capacity was calibrated using aluminium oxide. Samples of 2-5mg were analysed in aluminium pin-holed hermetic pans and a minimum of three repeats were performed. When cast films were used samples were cut of the cast films and placed in the bottom of the DSC pans to a weight of 2-3mg, by stacking the cut films on top of one another. When peeled films were analysed, a scalpel was used to cut the tablets and expose the film, with any residual tablet core removed with the scalpel. It was not possible to remove the entire core; therefore some residue may be present on the MTDSC thermograms. To identify if there were any transitions associated with the residue that would interfere with the transitions of the polymer film coats a sample of minitables were gently ground in a mortar and pestle and analysed through MTDSC. An underlying heating rate of 5°C/min, a modulation frequency of 40 seconds and a modulation amplitude of 0.5°C was used. The MTDSC conditions were the same as described by McPhillips *et al* (1999), and Lai *et al* (2010) These conditions were used for Opadry I, Opadry II, however for Surelease samples the parameters were a heating rate of 2°C/min, a modulation frequency of 40 seconds and an amplitude of 0.212°C.

3.2.4 Scanning Electron Microscopy

Coated mini tablets were axially bisected, and mounted onto an aluminium stub then sputter coated with a gold layer of approximately 50nm in a Polaron SC7640 sputter

coater (Edwards, UK). The samples were then imaged using a JEOL JSM-5900LV SEM (Oxford Instruments, Abingdon, England), equipped with a Tungsten filament using a 20kV accelerating voltage at a number of locations along the core-film coat interface and of the intact film surface.

3.2.5 Fourier Transform Infrared Spectroscopy

Fourier Transform Infrared (FTIR) Spectroscopy was performed on an IFS/66 S spectrometer from Bruker Optics (Coventry, U.K.). Whole minitablets were placed on the ATR crystal and pressed down to ensure a good contact between the surface of the film coat and the ATR crystal. Whole minitablets could be used as the penetration of the IR evanescent wave is only in the order of tens of microns, therefore there should be limited interference from the tablet core.

Each sample was run with a resolution of 4cm^{-1} with an average of 32 spectra being taken. The empty ATR crystal was used as a reference spectrum, which was determined before each sample was placed on the crystal.

3.3 Results

3.3.1 Cast Films

3.3.1.1 AFM Images

AFM images produced in contact mode of Surelease, Opadry I and Opadry II are shown in Fig. 3.1 and did not produce many surface features. The contact mode images provide little information on any phase separation or miscibility between the polymers and other components of the coating system. Images for Opadry II however do show some areas of interest present in the form of light areas at the top of the image which may be related to phase separation of the polymer and plasticiser, or another component of the coating system; however this is unlikely as PVA and PEG tend to be miscible.

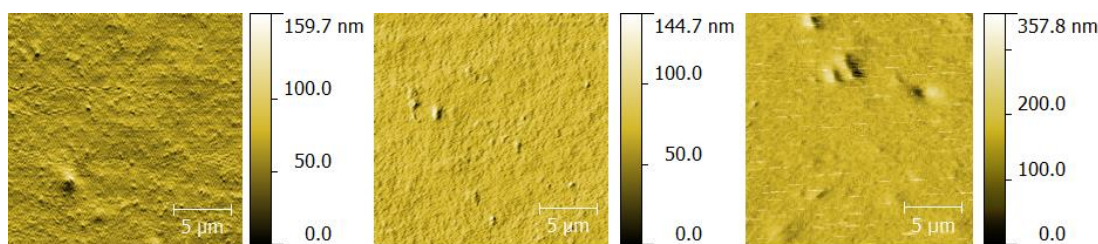


Figure 3.1 AFM images of cast polymer films (from left to right) Surelease, Opadry I, Opadry II

There is also the possibility of a semi crystalline structure being formed of PVA, and this area may be an area of crystal structure in the amorphous polymer. Depending on the process conditions to produce the film, different degrees of crystallinity are observed, with a range from circa 15-50% (Lewin, 2007). This is mainly dependent on the temperatures employed to anneal the films, as the higher the temperature (but below the melting point) the higher the degree of crystallinity observed. In addition plasticisers can reduce the degree of crystallinity in the film, as does the degree of hydrolysis of the PVA. As the preparation of the film was at 45°C, and there are plasticisers incorporated into the coating system, this would lead to the assumption that a relatively small percentage of the film will be crystalline. Therefore these areas may just be a defect on the film surface; however L-TMA experiments should be able to determine whether this is correct.

3.3.1.2 Thermal Analysis

3.3.1.2.1 Opadry I

The glass transition of Opadry I was observed at 166.3°C ($\pm 0.4^\circ\text{C}$; $n=3$) using MTDSC, as seen in Fig 3.2, which is somewhat different than other literature values for HPMC which has previously been reported as 162°C (McPhillips *et al.*, 1999). Comparison to the literature values of these systems however is problematic for a number of reasons. Firstly polymers tend to be classified into different grades, often based on their molecular weight; therefore each grade possess a slight variance in their

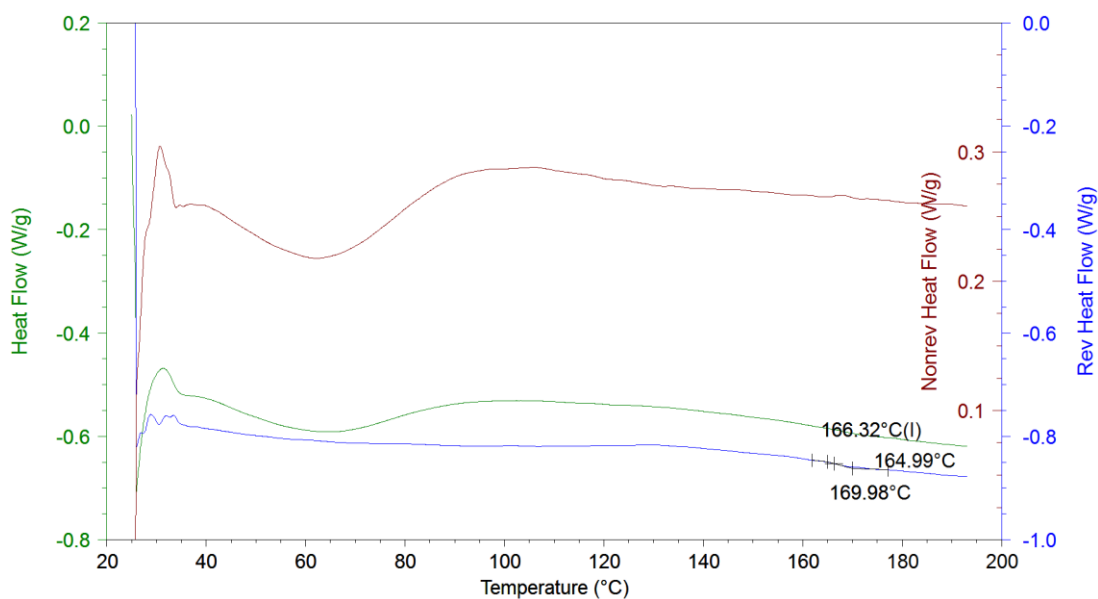


Figure 3.2 MTDSC of Opadry I cast films

transition temperature. Also due to the polydispersive nature of polymers the different grades of polymers contain a range of molecular weights, giving scope for differences in thermal transition values. Another problem with comparison to literature values is that the polymer systems analysed are plasticised. The intent of plasticiser addition is to lower the glass transition of the material to improve the materials physical properties, such as increasing its flexibility. Therefore it is more important to determine the T_g of the system studied and compare any future experiments to these values, rather than rely too heavily on literature values.

As described previously in this work and in previous studies the difficulty of measuring the glass transition of HPMC was apparent. Even by using the parameters outlined by McPhillips *et al.*, (1999), there was still only a relatively small change in heat capacity around the T_g .

Another issue associated with the thermal analysis of cast polymer films is that of residual water trapped within the film. As water acts as a plasticiser this has the effect of depressing the observed glass transition temperature and production of an extra endotherm on the MTDSC trace possibly masking other transition temperatures. As can be seen in Fig. 3.2 there is a broad endotherm present in the non-reversing heat flow signal which is typical of trapped water. This endotherm can be reduced by drying the films in an oven to aid driving water off, and storing the

films in a desiccator to help prevent adsorption of water vapor into the film from the environment. Due to the nature of cast films however it is difficult to drive all the water from the film and often there is residual water trapped in the film that can potentially alter results.

Due to the residual water present in the films hermetic pin-hole pans were used in the study, which have a pin-hole drilled in the lid allowing for the controlled and reproducible loss of water. These pans also have the advantage of having a larger volume and greater surface area at the bottom of the pan allowing for a greater sample mass to be placed in the pan, which is advantageous when measuring subtle glass transition temperatures.

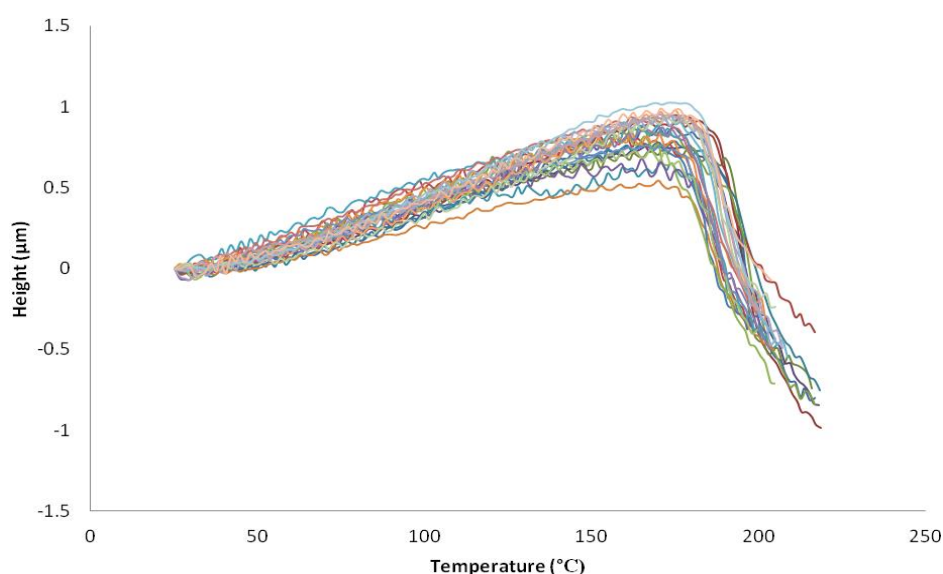


Figure 3.3 L-TMA results of Opadry I cast films

Although this effect should be the same for both L-TMA and MTDSC experiments on cast films, it may result in a slight discrepancy between film coated tablets, as through this method more water should be driven off during drying of the films.

Fig 3.3 shows a typical L-TMA trace for Opadry I, showing the glass transition to be around 164.2°C ($\pm 4.4^\circ\text{C}$ sd; $n=20$). It has been noted previously (Harding, 2006, Royal 1999) the difficulties in accurately determining the glass transition of HPMC using microthermal analysis. In both studies different grades of HPMC were used, but the issue lies with the nature of the polymer rather than the grade used in the

experiments. In these studies and others (Six *et al.*, 2003) that have analysed strong glass formers there has been difficulty in measuring the T_g using L-TMA.

Although the literature values for the glass transition of HPMC and Opadry I are relatively close the presence of one T_g indicates miscibility between HPMC and PEG in Opadry I.

3.3.1.2.2 Surelease

The glass transition temperatures for surelease analysed using MTDSC was 85.1°C ($\pm 0.6^\circ\text{C}$; n=3) and for L-TMA it was 89.8°C ($\pm 4.2^\circ\text{C}$ sd; n=20), shown in Fig. 3.4 and 3.5.

The glass transition for unplasticised ethylcellulose tends to be in the region of 130°C (Lai *et al.*, 2010), therefore the single lower glass transition indicates that Surelease forms a molecularly dispersed system with its plasticisers resulting in a considerable lowering of the T_g .

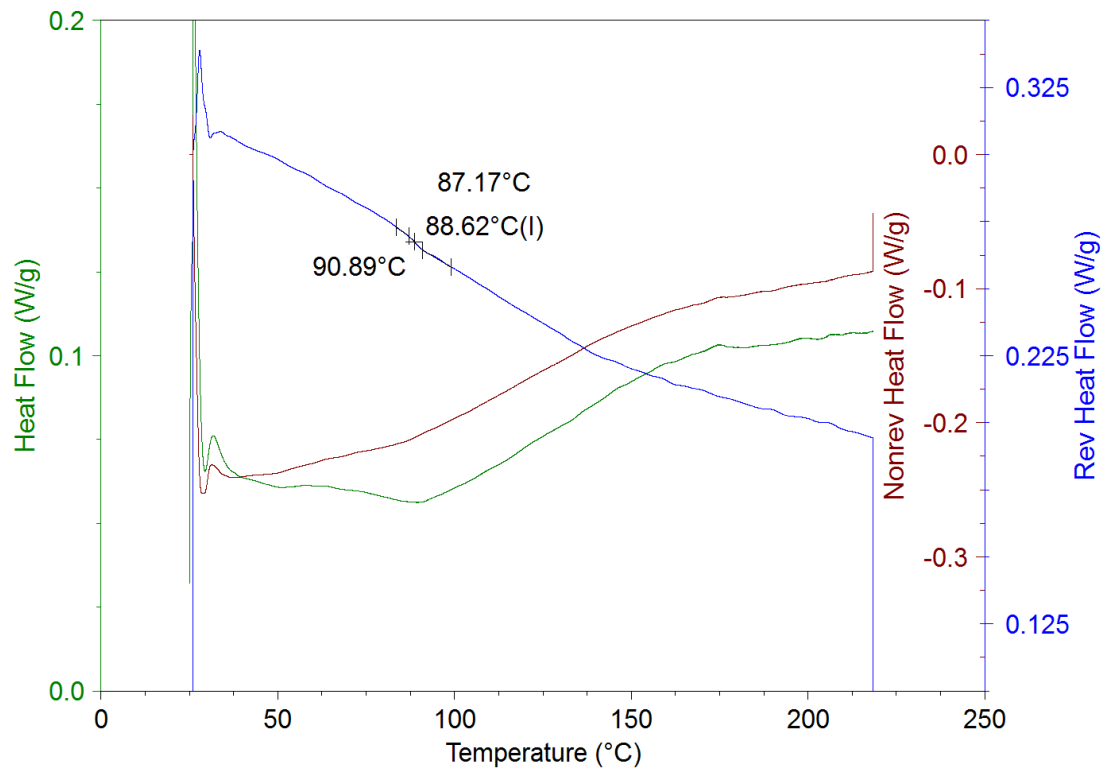


Figure 3.4 MTDSC trace of Surelease cast film

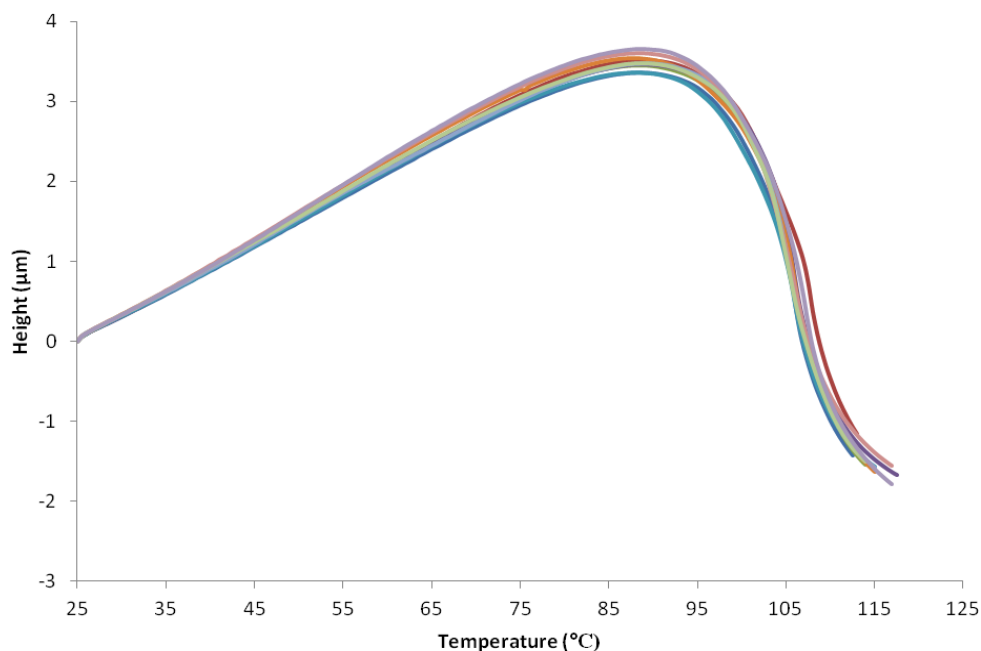


Figure 3.5 L-TMA of Surelease cast film

The L-TMA and MTDSC results agree very well, and indicate that the increased transition temperature observed for the L-TMA results in Opadry I measurements are possibly due to the issues surrounding L-TMA measurements. This highlights the importance of using a number of analytical techniques when analysing samples, especially when using L-TMA.

3.3.1.2.3 Opadry II

Results for Opadry II cast free films are shown in Fig. 3.6 indicating the semi-crystalline nature of PVA. There is an initial peak at 47.8°C ($\pm 1.4^\circ\text{C}$ sd; n=3), which on first inspection appears to be a melting peak, however on closer inspection of the baseline there is a shift analogous to that observed during a glass transition. This apparent “melting” is termed a relaxation endotherm and is often present in semi-crystalline materials; however it does not represent the glass transition temperature of the material, and will be discussed in more detail in the discussion.

The glass transition temperature of PVA is somewhat lower than literature values, with previous papers reporting the glass transition to be in the region of 75-85°C (Mucha *et al.*, 2005, Park *et al.*, 2000, Sudhamani *et al.*, 2003). There have been reports of a transition around 45°C in the literature, which authors

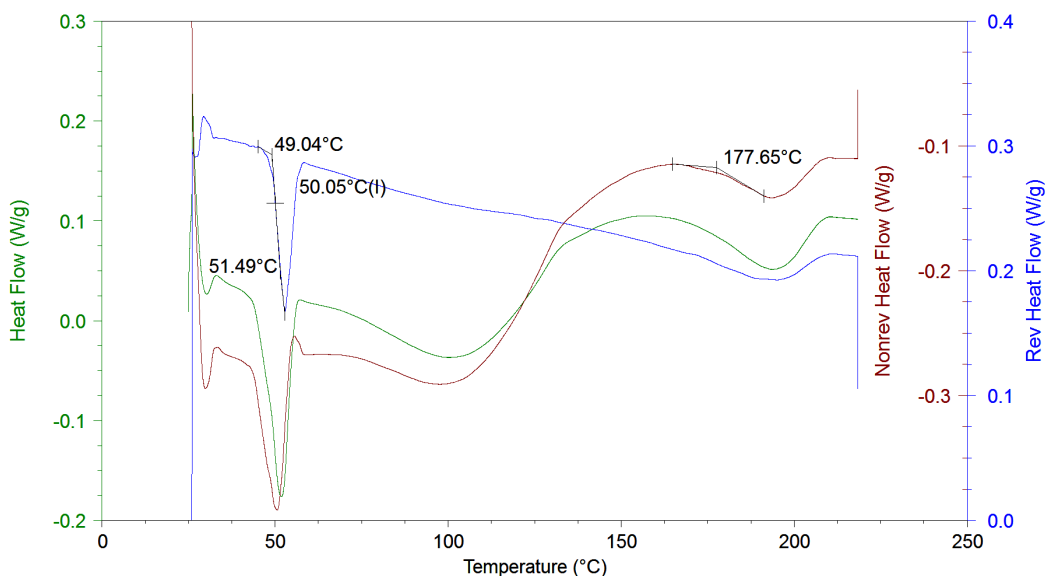


Figure 3.6 MTDSC of Opadry II cast films

have attributed to trapped water in the sample acting as a plasticiser (Mucha *et al.*, 2005). This may provide the explanation here too, especially with the cast films, as there may be residual water in the film. There is a broad endotherm circa 100°C in Fig. 3.6 indicating the presence of trapped water. Also in the papers mentioned above pure PVA was used, however the films here contain a plasticizer, which will have the same effect of lowering the glass transition as trapped water.

A wide melting endotherm around 175.1°C ($\pm 3.7^\circ\text{C}$ sd; n=3) is seen for the crystalline part of the PVA. This is also in agreement with literature values reported in the papers previously mentioned.

The L-TMA results for cast Opadry II cast films, shown in Fig. 3.7, display similar results to the MTDSC, with a sharp transition at 48.1°C ($\pm 4.8^\circ\text{C}$ sd; n=20) and a higher broader softening at 152.9°C ($\pm 11.4^\circ\text{C}$ sd n=20). This higher broader softening can be seen in Fig. 3.7 in the traces that indent to a lesser degree where the probe can be seen gradually indenting into the sample at a higher temperature than the initial transition at 48°C. Although the broader softening occurred at a slightly different temperature to that observed by MTDSC, as stated earlier the broad nature of this transition can make the determination subjective. This is exemplified by the considerably larger standard deviation seen for these results.

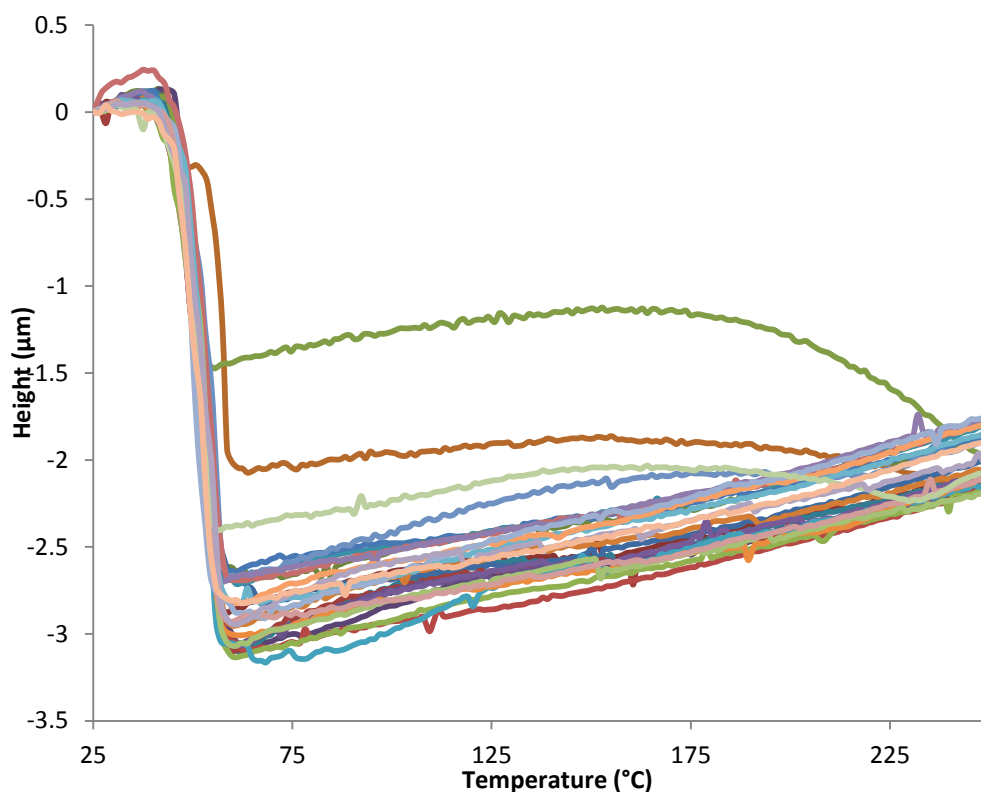


Figure 3.7 L-TMA of Opadry II cast films

This does highlight a limitation of L-TMA regarding identification of different solid states. MTDSC highlighted the presence of amorphous and crystalline components of the material; however the L-TMA results cannot differentiate between amorphous and crystalline components. Indeed often a sharp transition is seen for crystalline materials and a slow softening observed when a material undergoes a glass transition. Although these are present here, MTDSC showed the glass transition to be the lower transition and the higher transition to be crystalline melting. Additionally a crystalline melting point present at a lower temperature than a glass transition would be thermodynamically unfavourable.

3.3.2 Film Coated Minitablets

3.3.2.1 AFM Images

Fig. 3.8 shows AFM images from film coated minitables. It is immediately noticeable that the film morphology is visibly different from the cast films, with a number of round structures appearing on the film surface. The most likely

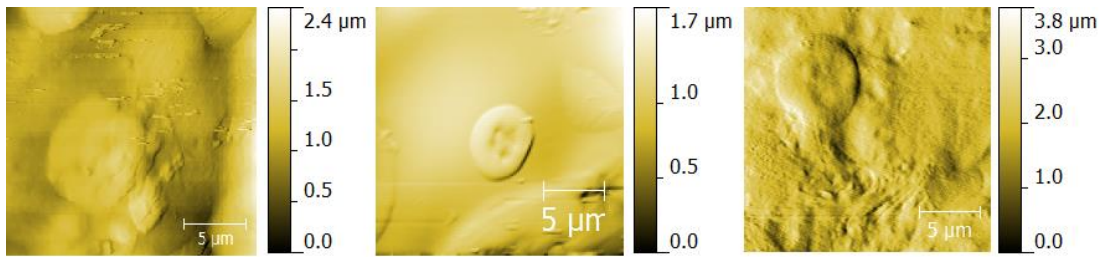


Figure 3.8 Contact mode AFM images of film coated minitables (from left to right) Surelease, Opadry I, Opadry II

explanation for this is due to the preparation of the films in the spray coater. As the film is constructed from myriad droplets of polymer solution and subsequent drying of these droplets on the surface, these structures are likely to be the last droplets to strike the minitabket during coating.

It will be interesting to note when analysing the films using L-TMA whether these areas produce the same thermal transitions as seen in other areas of the film, or whether the phase distribution changes in these droplets.

3.3.2.2. Scanning Electron Microscopy Images

Fig. 3.9 shows an SEM image of the cross section of an Opadry I film coated minitabket, indicating that the film thickness for the Opadry I coated minitables was

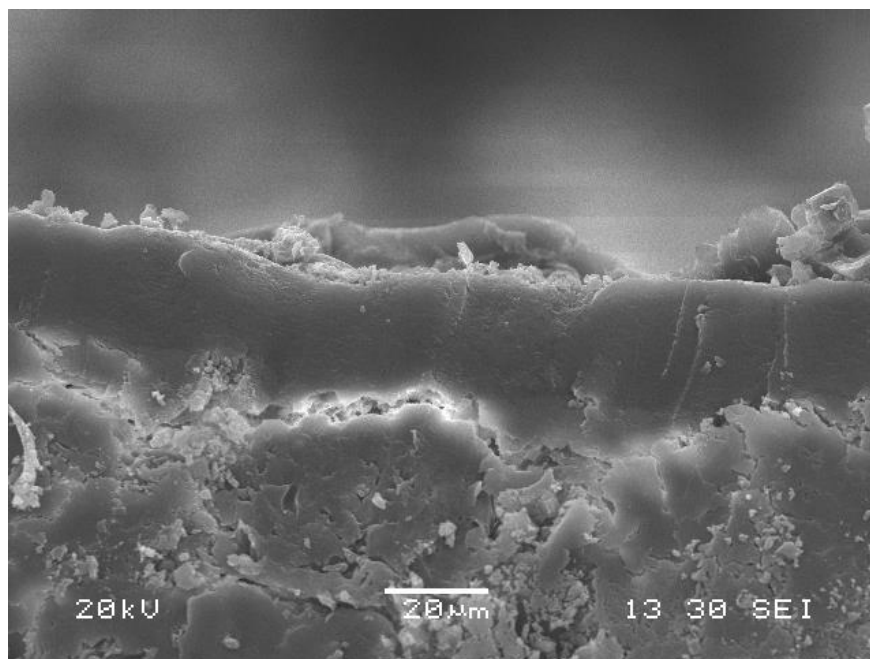


Figure 3.9 SEM image of Opadry I film coated minitabket cross section

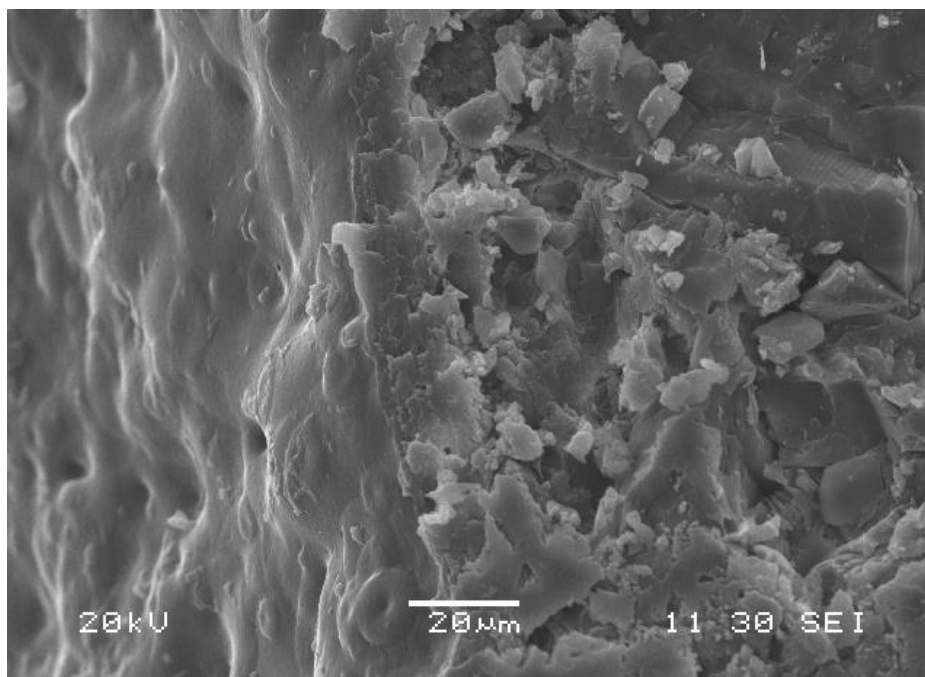


Figure 3.10 SEM image of Opadry I film coated minitabilet surface in the region of 20 μ m. The darker band in the middle of the image represents the film coat, with the lower third of the image showing the tablet core. The image also indicated that a good film was formed from the spray coating process with no air pockets present in the film and no space between the film and the minitabilet core indicating good adhesion of the film.

The SEM image in Fig. 3.10 shows a section of the surface of a minitabilet coated with Opadry I, with the droplet structure present in the contact AFM images also observed, which can be seen in the left hand side of the image. These images combined with the contact AFM images give a first indication that the films produced by spray coating and those by film casting exhibit at least topological differences.

3.3.2.3 Thermal Analysis

When films were peeled from minitablets there is likely to be some residual tablet core remaining on the peeled film. Washing the films after peeling with the scalpel was considered, however as many of the components of the films are soluble in both water and a number of organic solvents, the composition of the film is likely to change resulting in erroneous results. Therefore if any residual minitabilet core

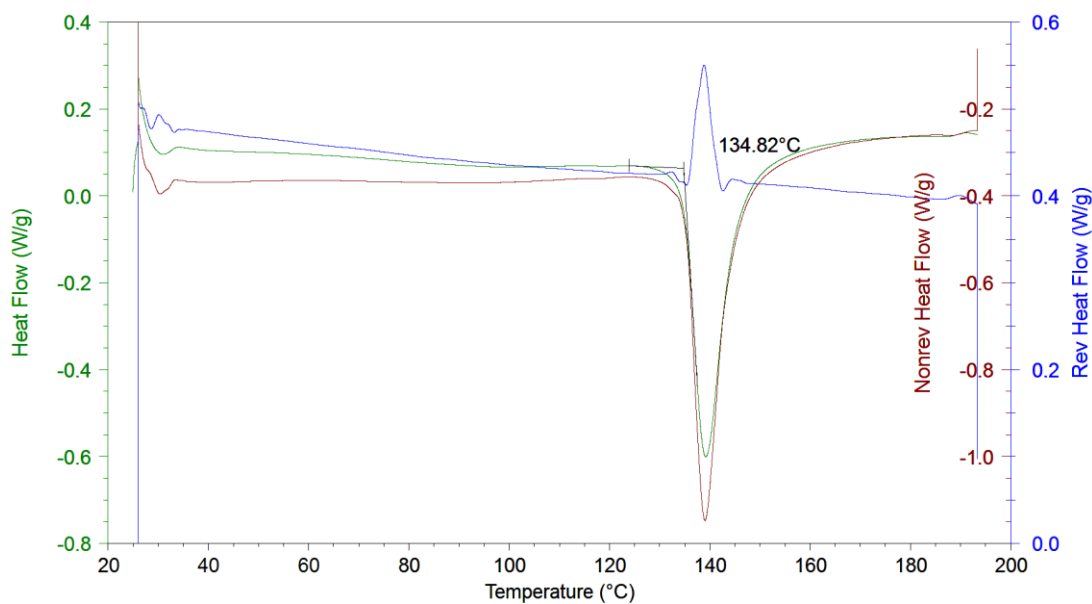


Figure 3.11 MTDSC of an uncoated powdered minitabket

remaining on the peeled film it is of importance to determine where the transitions were likely to appear, and with this consideration uncoated minitabkets were analysed by MTDSC. There was a prominent melting endotherm at 134.8°C ($\pm 0.8^{\circ}\text{C}$ sd; $n=3$) present in the powdered minitabket samples (Fig. 3.11). This transition appears to fall outside the regions of those observed on the cast films; therefore it should not affect the interpretation of MTDSC results for the peeled films. There was however a transition observed in the reversing heat flow, and although likely to be an artefact, could be problematic if any transitions do appear in this region; however it is unlikely unless the polymer systems prove to be miscible and produce intermediate glass transitions.

3.3.2.3.1 Opadry I

Fig. 3.12 shows an MTDSC trace for a minitabket coated with Opadry I, which displays the transition associated with the residual core around 130°C , and the glass transition of Opadry I at 162.5°C . As discussed above the glass transition temperature is not affected by the transition of the minitabket core due to the T_g being present in the reversing heat flow at a different temperature to the residual core.

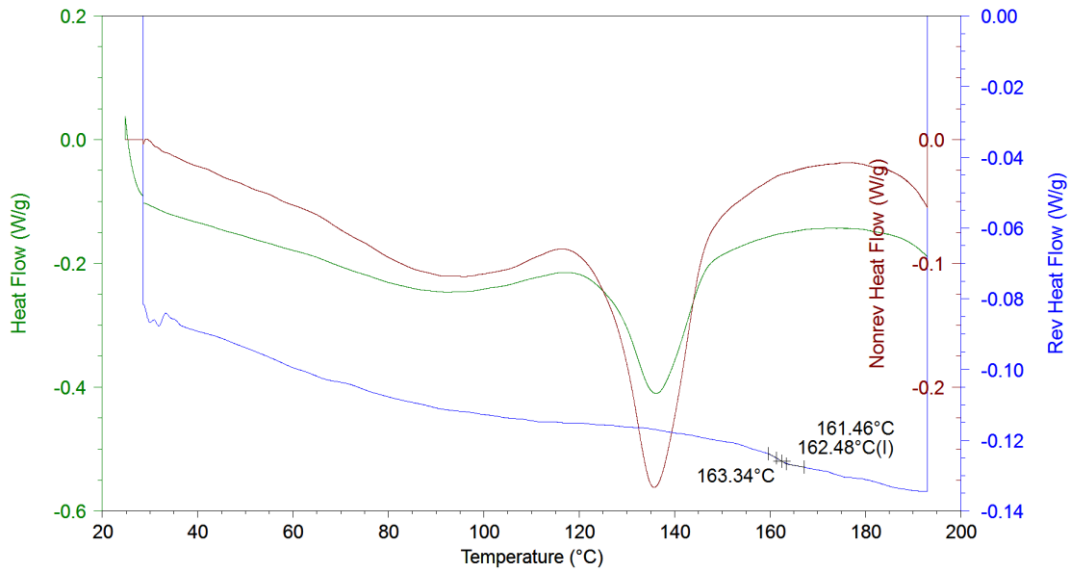


Figure 3.12 MTDSC of Opadry I coated minitables

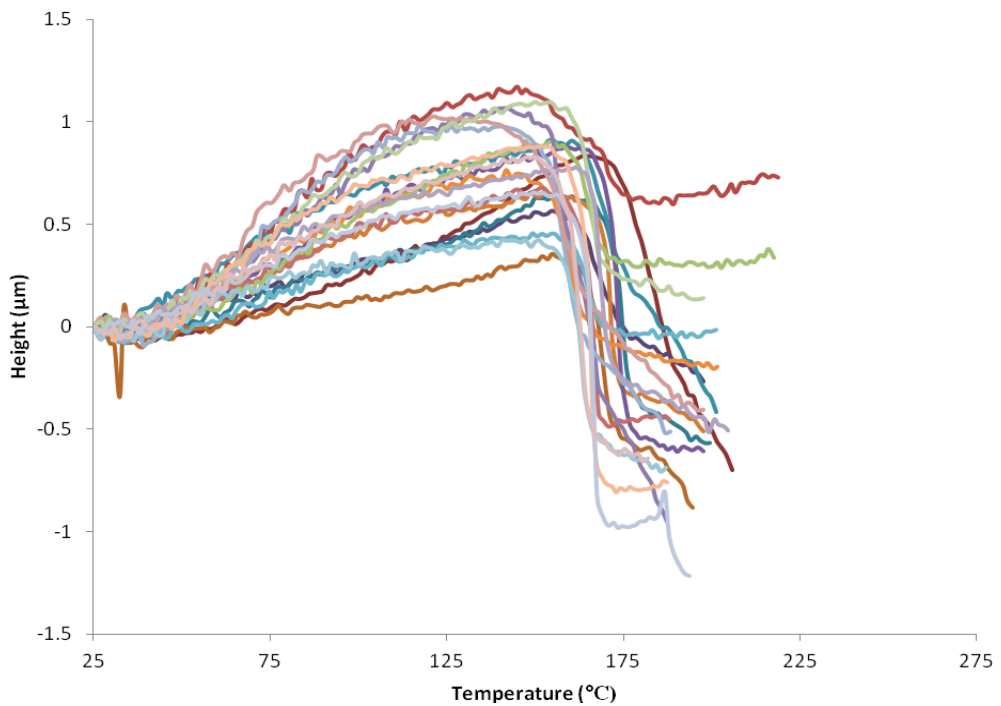


Figure 3.13 L-TMA of Opadry I coated minitables

L-TMA results for film coated minitables were comparable to the cast films with transitions observed at 161.6°C ($\pm 5.5^\circ\text{C}$ sd; $n=20$), as seen in Fig. 3.13. There is a slightly higher standard deviation of the results, which is possibly due to the increased surface roughness of the film coated minitables compared to the cast films.

3.3.2.3.2 Surelease

The MTDSC trace for Surelease coated minitables (Fig. 3.14) indicates a glass transition of 87.0 ($\pm 0.1^\circ\text{C}$ sd; $n=3$), which is in good agreement with the MTDSC results from the cast films. The melting endotherm at 135.0 $^\circ\text{C}$ (± 0.2 sd; $n=3$) corresponding to the observed endotherm on the crushed uncoated minitables

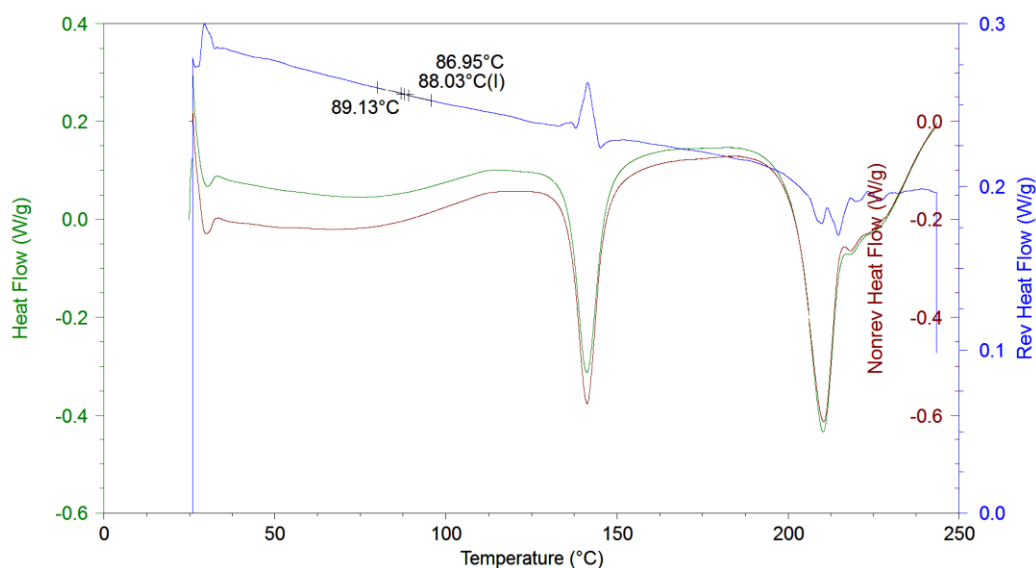


Figure 3.14 MTDSC of Surelease coated minitables

indicating there was some of the tablet core remaining on the peeled film. The glass transition of the Surelease was easily observed however as it can be seen in the reversing signal separate from the transitions seen for the tablet core. The additional endotherm present over 200 $^\circ\text{C}$ was due to components of the tablet core melting, however this endotherm is unlikely to provide any interference to the analysis of the film coats as it is above of the T_g values observed for the coatings.

Fig. 3.15 demonstrates that L-TMA traces for Surelease coated minitables also showed good correlation with cast films with a transition at 85.0 $^\circ\text{C}$ ($\pm 3.1^\circ\text{C}$ sd; $n=3$).

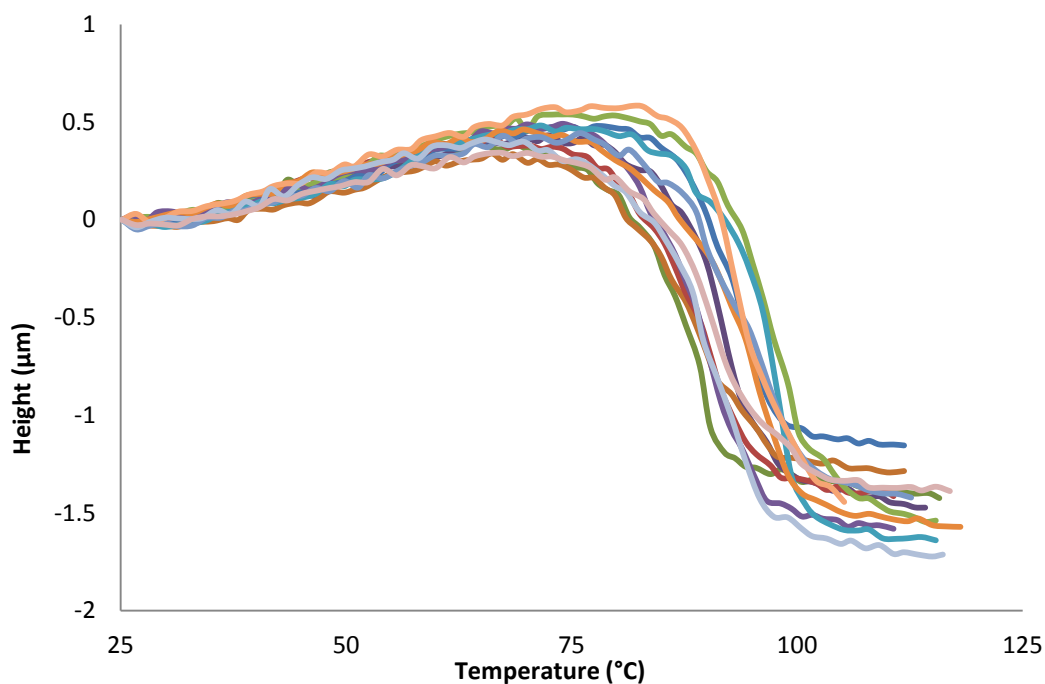


Figure 3.15 L-TMA of Surelease coated minitables

3.3.2.3.3 Opadry II

Fig. 3.16 shows a typical MTDSC result of peeled coats of Opadry II. These results showed the glass transition to be 48.4°C ($\pm 0.7^{\circ}\text{C}$ sd; $n=3$), again agreeing well with the result for the cast Opadry II films. The upper melting endotherm was recorded as being 193.6°C ($\pm 0.5^{\circ}\text{C}$ sd; $n=3$), which again is a slightly different temperature to that seen previously. This is possibly caused by alternative polymorphs of the crystal form of PVA being created during film coating as opposed to cast films. This is further supported by the two extra melting endotherms seen on the MTDSC trace. The endotherm at 132.0°C ($\pm 0.9^{\circ}\text{C}$ sd; $n=3$) can be attributed to the tablet core, however there is a further endotherm at 108.5°C ($\pm 1.2^{\circ}\text{C}$ sd; $n=3$), which was not present on any of the previous MTDSC results. This transition appeared to interfere with the endotherm from the tablet core observed at 132°C , however both transitions were still observable.

There has been evidence of extra endotherms observed around 120°C on PVA films with poly glycol or glycerol incorporated into them (Park *et al.*, 2005) which the authors attributed to a different polymorph of the crystalline part of the PVA being

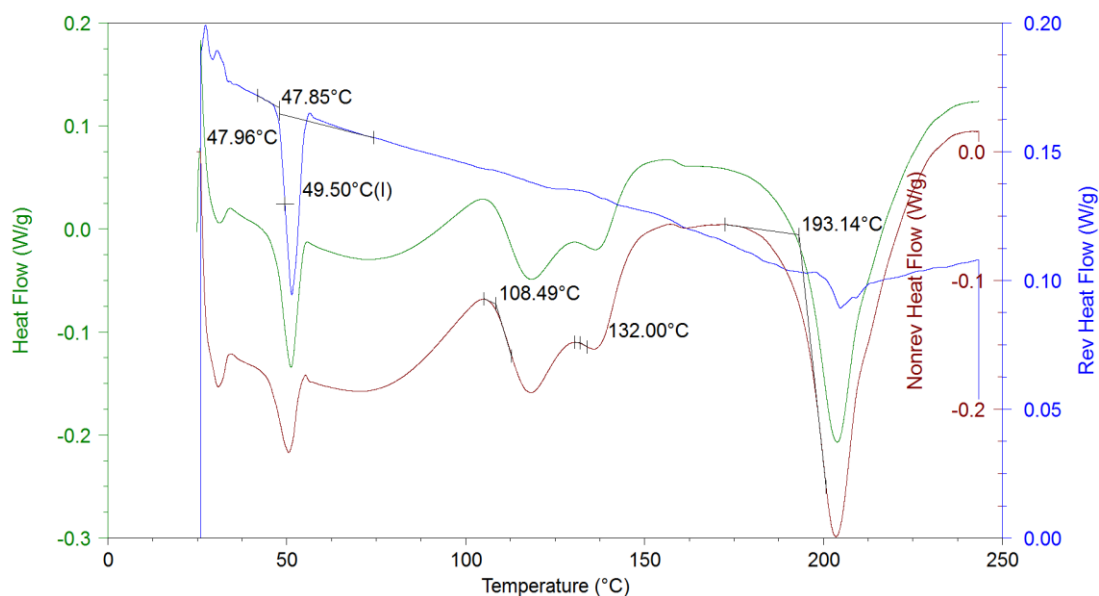


Figure 3.16 MTDSC of Opadry II coated minitablets

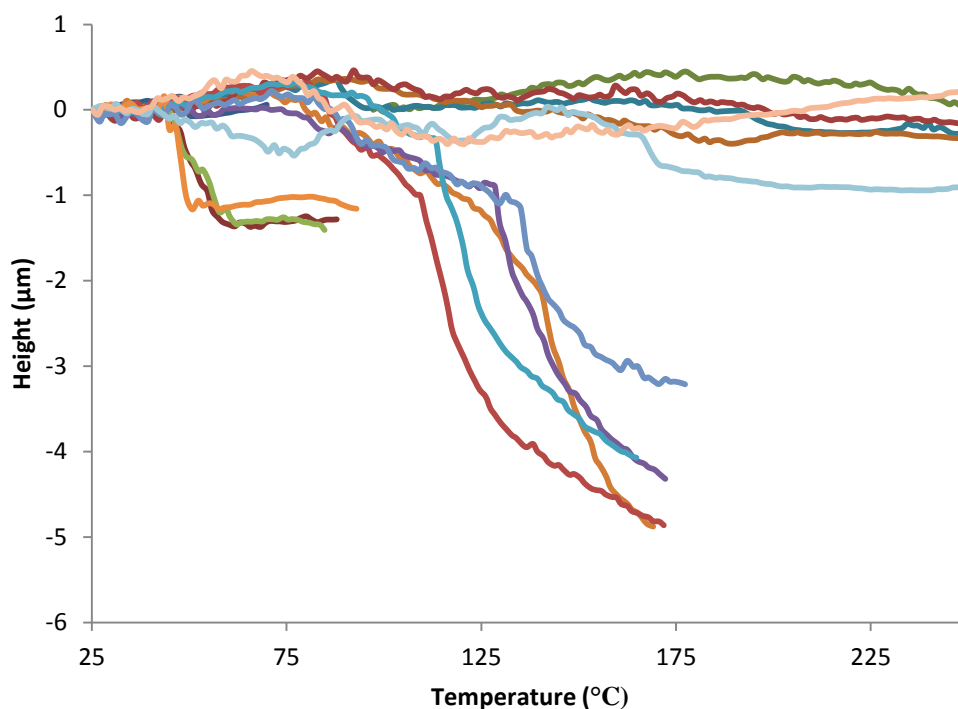


Figure 3.17 L-TMA of Opadry II coated minitablets with nano-TA probes

formed. This is a strong possibility in this case, and maybe unique to the method producing the films as these transitions were not obvious in the analysed cast films.

L-TMA traces for Opadry II coated tablets produced a glass transition of 48.8°C ($\pm 5.3^\circ\text{C}$ sd; n=6), as seen in Fig. 3.17. The number of L-TMA traces was only 6, as although the number L-TMA performed was twenty, there were only six transitions

observed in this temperature range. Although only three traces can be seen in Fig. 3.17 there were a number that are obscured by other traces, and as discussed below there often was not a large indentation into the sample by the probes, resulting in some transitions not appearing on the collated graph in Fig. 3.17. Similarly the melting temperature was 203.0°C ($\pm 10^{\circ}\text{C}$ sd; $n=4$); and as previously the same issues of the broad nature of this transition posed difficulties in accurately determining the transition.

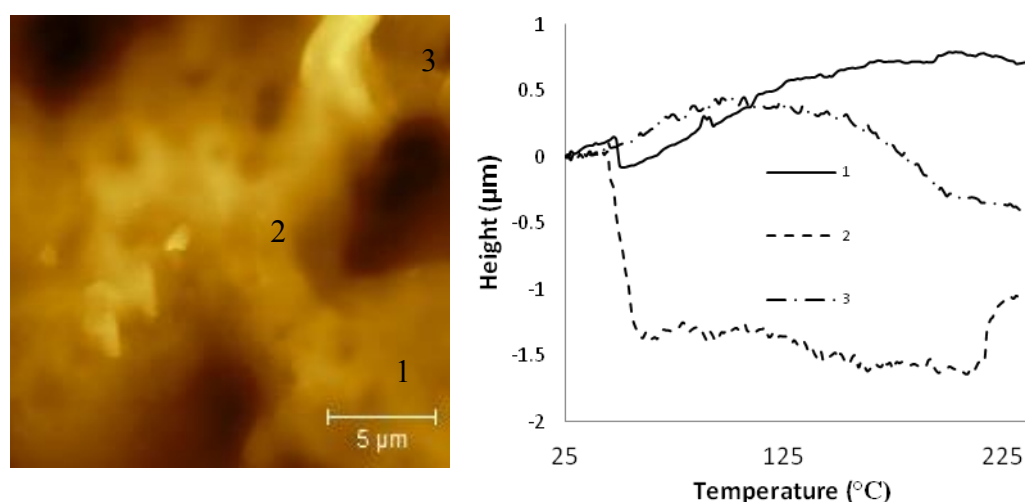


Figure 3.18 AFM image obtained in contact mode of film coated minitablet (left) and corresponding L-TMA result (right)

When all L-TMA of are grouped together it appears as though there are a number of traces that do not show any transitions, showing limited correspondence to the MTDSC results with some probe penetration occurring over a large range of transitions. However most do undergo softening, and it is merely due to the fact that the nano-TA probes tend to indent less into the samples because of the lower set point used. However there were some L-TMA results that indented far into the sample, giving the impression of no softening in some of the traces where the probe penetrated the sample to a lesser degree. As can be seen in Fig. 3.18, the three areas where L-TMA was performed on an Opadry II coated minitablet show the variations in probe penetration into the film. In this sample a transition is observed around 45°C , a transition circa 110°C , and a further transition is observed $>150^{\circ}\text{C}$, which correlates well to the MTDSC. L-TMA results also resembled the MTDSC results with a transition seen at 104.4°C ($\pm 7.5^{\circ}\text{C}$ sd; $n=8$) on a number of the experiments.

As discussed above this additional transition is likely to be present due to a different polymorph of PVA being formed when formulated into a film. Also of note is there were no transitions around 130°C, as was expected due to this transition being associated with the minitablet core.

3.3.3 FTIR Spectra

FTIR spectra were recorded for each of the coatings used in the study. Due to the small penetration of the evanescence wave (around 10microns), whole minitablets could be placed on the sample mount, allowing for there to be limited interference by the tablet core. The most important peak in the analysis is the one located between 3200-3600cm⁻¹, as this peak is attributed to hydrogen bonding of hydroxyl groups, which is the most likely bonding to occur if any of the polymer blends show miscibility. PVA particularly, and both HPMC and EC have numerous hydroxyl groups to participate in hydrogen bonding. Figures 3.19 through 21 show FTIR spectra for film coated minitablets, coated in each of the three systems.

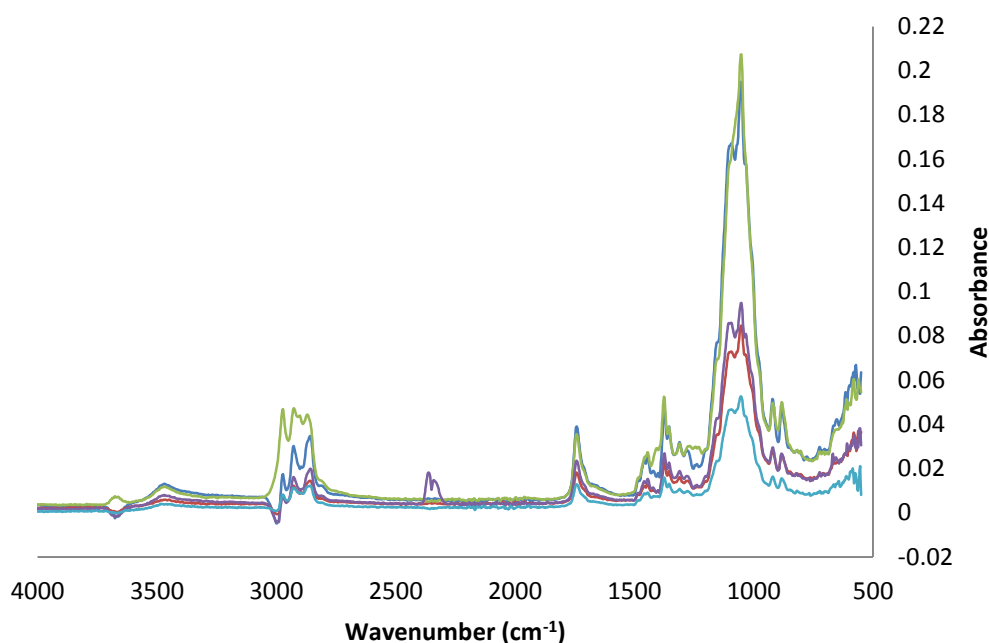


Figure 3.19 FTIR spectra of Surelease coated minitablets

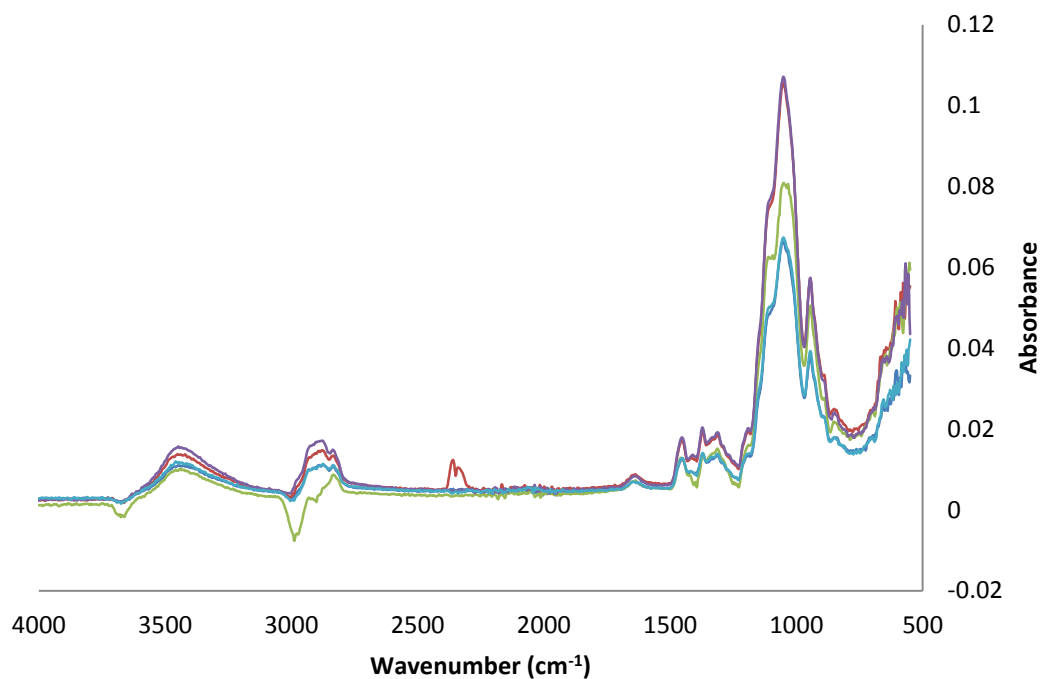


Figure 3.20 FTIR spectra of Opadry I coated minitables

There appears to be a peak between $3200\text{-}3600\text{cm}^{-1}$ for each of the polymers, suggesting there is hydrogen bonding present in the systems, and each polymer tended to have a distinct level of absorbance. Opadry I showed the peak to be at 3440cm^{-1} , Opadry II at 3320cm^{-1} and Surelease at 3370cm^{-1} . It will therefore be interesting to see if there is any change to the peaks in the blends.

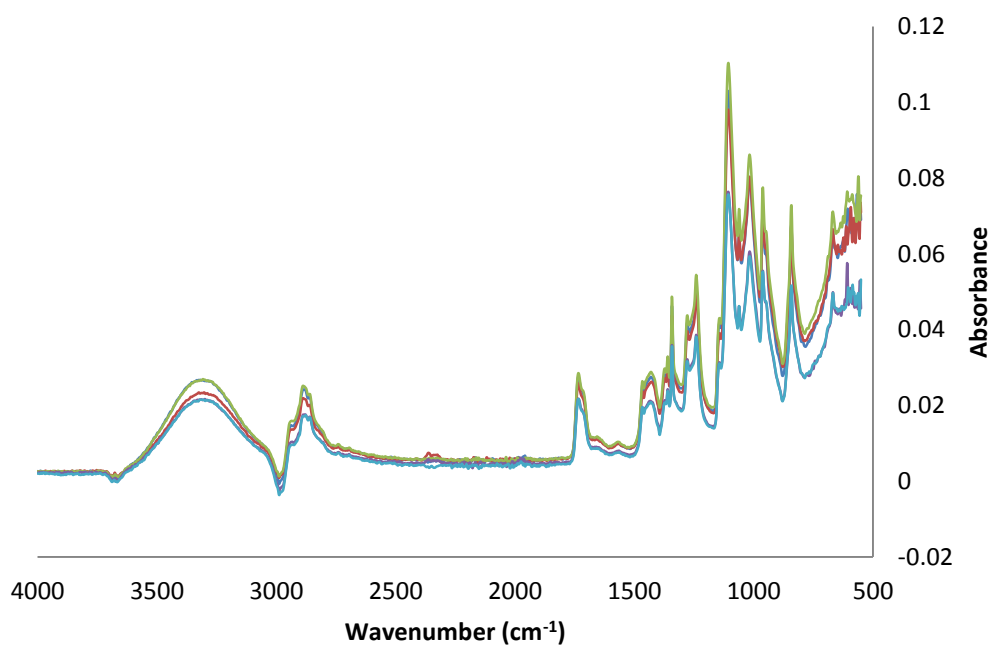


Figure 3.21 FTIR spectra of Opadry II coated minitables

In addition there was a degree of variation in the absorbance observed in the samples. This was likely to be due to the inconsistent contact between the crystal and the sample, as even with careful placement of the sample, the nature of analysing the film coats on a solid dosage form may lead to inconsistent contact across the crystal surface for different samples.

3.3.4 Area of Discrimination of Probes

A positive reason for using nano-TA probes over Wollaston probes is the increased resolution gained by smaller size of the probes. This in theory should allow for much smaller features on the sample surface to be analysed. Previously the area of discrimination for Wollaston probes has been reported to be in the region of 20 μm (Royall *et al.*, 2001b), however nano-TA probes in theory should allow for sub-

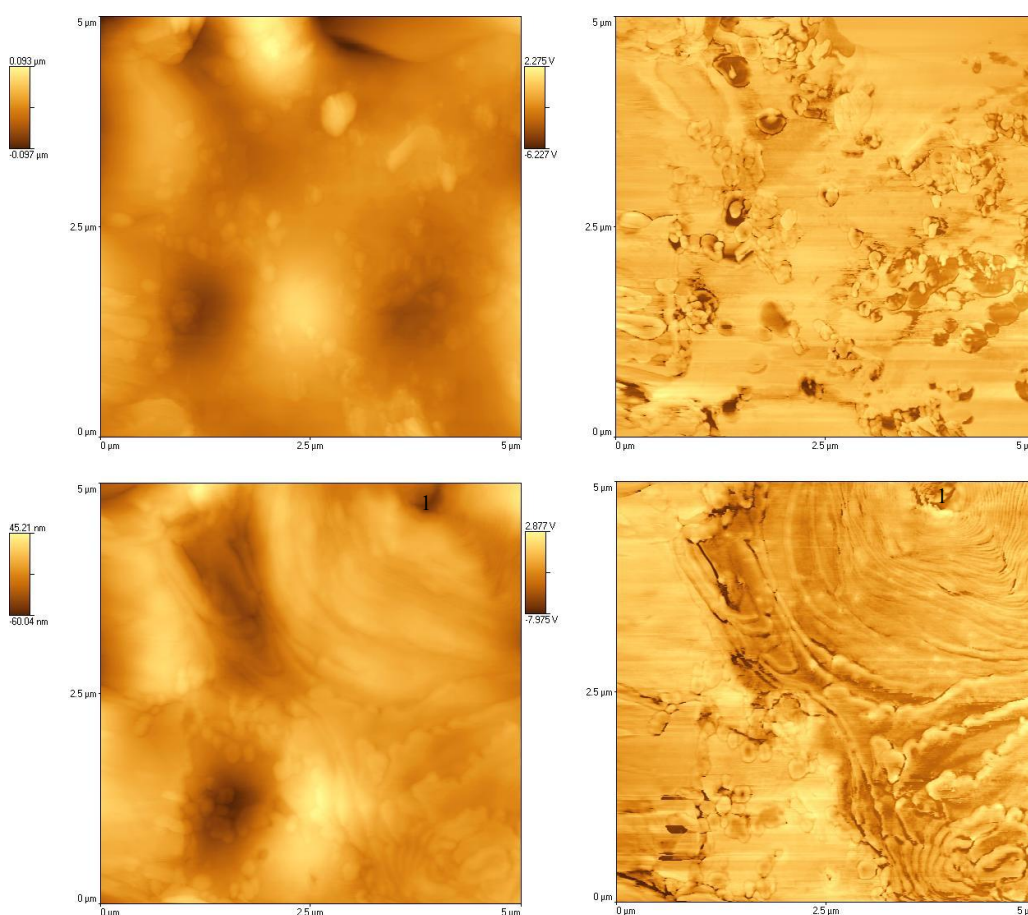


Figure 3.22 Topography (left) and phase images (right) of a 5 μm area of an Opadry II cast film, before (top) and after (bottom) an L-TMA measurement with 1 representing the L-TMA location

100nm features to be resolved. The authors in Royall *et al* stated the size and nature of the crater depends on a number of factors including the set point used and the nature of the sample being analysed Fig. 3.22 below shows an area of a cast Opadry II film before and after an L-TMA performed with nano-TA probes. The residual crater from the L-TMA can be observed in the top right hand corner of the topography and phase image from after the L-TMA experiment. As can be seen the area at the centre of the crater directly measured by the probe is relatively small, measuring circa 200nm, thus showing the improved resolution of the nano-TA probes. However the area affected by the L-TMA remains relatively large. Although this can be observed to a certain degree in the topography image, it is of interest to note in the phase image this area appears larger. This may be due to heat dissipating from the probe tip through the sample during the L-TMA.

Also stated in Royal *et al* (2001b) the possibility was discussed of the sample having the potential to “wick” along the wire if it is attracted to the platinum filament in the probe tip, leading to a peak as opposed to a crater.

It would be prudent therefore still not to perform L-TMA measurements within 10 μ m of another L-TMA to avoid there being any issues with previous L-TMA experiments altering the nature of the sample. This will be especially important when measuring thermal transitions in polymer blends as the previous experiment may alter the distribution and phase behaviour of the two polymers. In other systems this may also be an issue as glass transition temperatures are sensitive to the thermal history of polymer, which in this case the cooling rate after the L-TMA may be different to when the film was produced, therefore potentially altering the glass transition of the polymers. Also if one of the components of the system is thermolabile then the polymer may be decomposed during the first experiment, and therefore causing any further L-TMA experiments to be erroneous.

3.3.5 Effect of Heating Rate of the Softening Point

An area of L-TMA that is poorly understood is whether during the L-TMA experiment the probe measures the T_g of the material being analysed, or whether the

probe measures a softening temperature. It was noted by Royall *et al.* (2001b) that the onset of melting did not alter with increased heating rate of the probe, and other authors have questioned whether the probe is in fact measuring the softening point of the material rather than the glass transition. This has led to much discussion with many authors referring to the softening point rather than the glass transition when describing L-TMA experiments (Harding *et al.*, 2007, Nelson *et al.*, 2007).

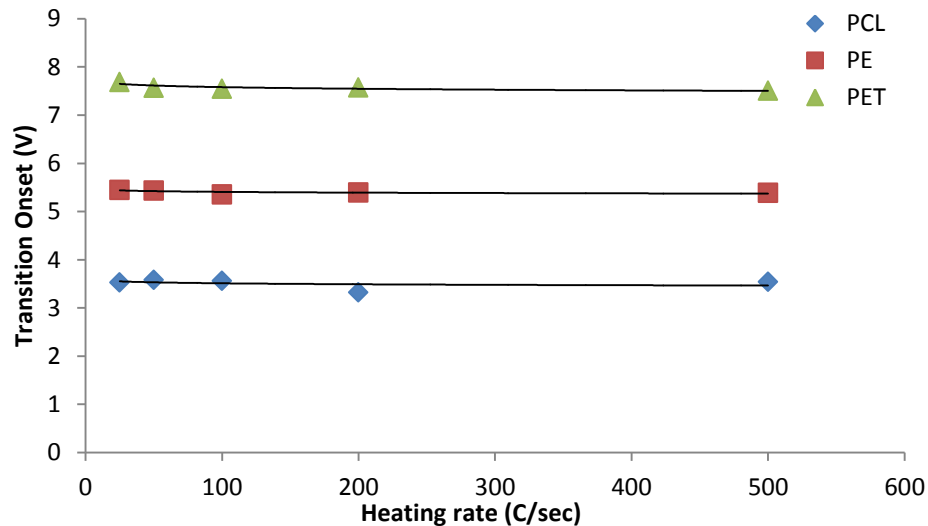


Figure 3.23 Onset voltages recorded at different heating rates for the calibration samples

Heating rates up to 500°C/s were used in this study on cast Surelease films, which of the systems studied displayed the most consistent glass transition temperature. The nano-TA probes were calibrated at heating rates of 25, 50, 100, 200 and 500°C to observe the effect of increasing the heating rate on the transition temperatures observed. As with any thermal calibration method standard samples with a known transition temperature are used to calibrate the probe. In nanothermal analysis three polymers are employed and the voltages they undergo a transition are measured and then plotted against the known temperature they should soften at to provide a calibration curve.

Polycaprolactone (PCL) tends to undergo a melting transition at 60°C, polyethylene (PE) at 130°C and poly(ethylene terephthalate) (PET) at 238°C (Anasys Instruments 2012). The voltages used to calibrate the probes are displayed in Fig. 3.23, with a transition observed with the tip voltage at 3.5V for PCL, 5.5V for PE and 6.5V for PET. Fig. 3.23 shows that the voltages where the probe indented tended to stay

consistent with increasing heating rates, as even though polymers are used to calibrate the probes they undergo a melting temperature at the temperatures used for calibration which does not alter with increased heating rates. As discussed above these polymers are used due to discrepancies observed when small molecular weight standards are used.

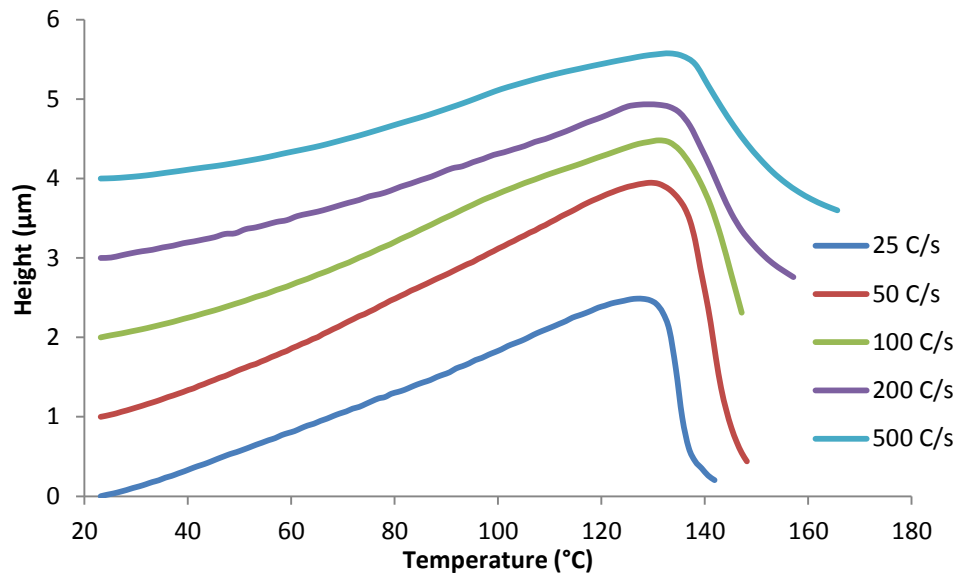


Figure 3.24 Transition temperature of PE calibrated at various heating rates

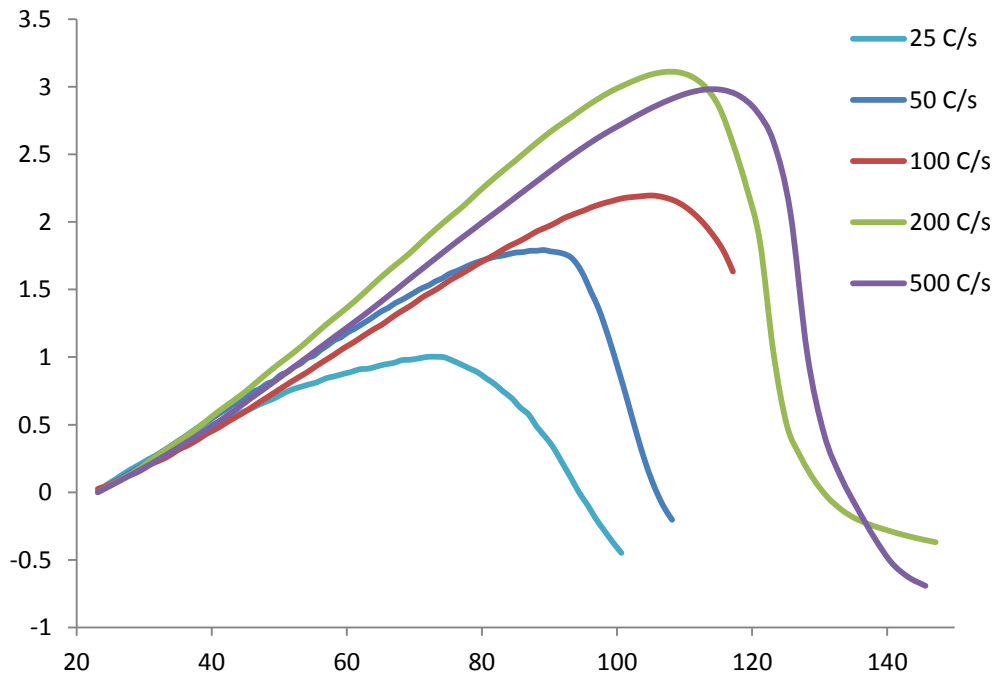


Figure 3.25 Transition temperatures of Surelease cast films with various heating rates

Once the probe was calibrated at each heating rate the PE calibration grid was analysed at each rate, and is shown in Fig. 3.24. The transition temperature observed for PE increased from 131°C to 135°C, however as can be seen in Fig 3.25, this is a relatively minor increase compared to those seen when the heating rate is increases when analysing Surelease.

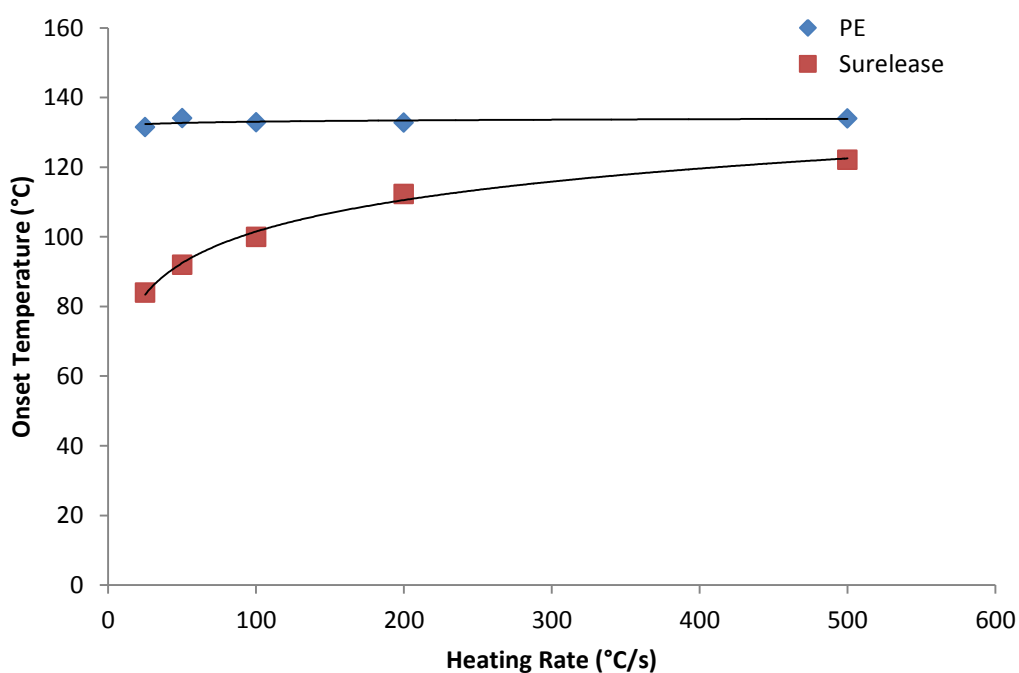


Figure 3.26 Comparison of transition temperatures observed for PE and Surelease at various heating rates

Fig 3.25 shows the effect of increasing the heating rate on Surelease samples where a noticeable increase in the transition temperature occurs with increased heating rate from 25°C/s to 500°C/s.

Fig. 3.26 shows a comparison between the transitions observed for PE and Surelease cast films at increasing heating rates, showing the increase in transition temperature observed for Surelease compared to the consistent temperature observed for PE.

Of note in the paper by Royall *et al.* (2001b) the author stated that rates of 2, 10 and 20°C/s were used with the probe calibrated between each heating rate employed. There can be issues with the probe remaining in contact with the sample at relatively low heating rates such as 2°C/s with L-TMA, due to feedback being disengaged, and

this was the case in this study with the probe drifting out of contact during lower heating rates. Therefore only higher heating rates were used, and these resulted in a considerable increase in the glass transition temperature observed for Surelease films.

As the transition temperature observed appears to increase with increased heating rates it appears that the softening observed is related to the glass transition temperature of the sample. However as only two samples were used and there was conflicting data with previous studies it would be prudent to test further materials, as the probe response may be specific to different materials.

3.4 Discussion

MTDSC and L-TMA results indicated transitions could be observed for all the coating systems used in the study; however as discussed previously in Chapter 2 HPMC and EC are strong glass formers, leading to subtle changes in heat capacity registered in MTDSC. Additionally as mentioned above previous research has reported that the determination the transition temperature of HPMC to be difficult using L-TMA. This can be related to the fragility index of the material, which is a measure of the temperature dependence of the molecular motions in the region of the materials glass transition (Hancock *et al.*, 1998). Therefore with a strong glass former where the molecular mobility may only alter by one order of magnitude for every 25°C, there is unlikely to be a dramatic change in the polymers mechanical properties around the T_g .

However when analysing Opadry I the HPMC is combined with a plasticiser (polyethylene glycol) and even though the L-TMA trace is not as smooth as other materials a clear glass transition can be observed for Opadry I. This appears to make sense as it has been reported that when mixed with plasticisers the fragility index of polymers decreases (Coca *et al.*, 2007). In this study Eudragit was mixed with triethyl citrate (TEC) at varying concentrations and a decrease in the fragility index was observed. The authors attributed this to the increase in free volume caused by the addition of the plasticiser leading to increased molecular mobility and therefore a

less fragile film being formed. Therefore when HPMC is mixed with PEG there may be a decrease in the fragility index leading to easier determination of the T_g using L-TMA.

Although L-TMA results are slightly different than MTDSC, they generally compare well, and this is to be expected due to the higher heating rates of LTMA. Although calibration issues with L-TMA have been reported (Harding 2006), this is generally with low molecular weight crystalline compounds, such as drugs, not for high molecular weight polymers. As the calibration of the probe is completed with polymers rather than low molecular weight compounds then due to the different softening characteristics of the two types of material the temperature calibration may not be accurate with low molecular weight compounds showing a lower transition temperature than expected.

The relaxation endotherm observed in Opadry II films is a commonly observed transition occurring due to the increased relaxation times often associated with physical aging of amorphous materials attempting to reach equilibrium. Relaxation endotherms are also commonly observed in semi-crystalline materials as the crystalline regions of the material can restrict segmental mobility of the amorphous phase and thus increase activation energy for the T_g of the polymer (Atkinson *et al.*, 2002). As relaxation time can be described by the following equation:

$$\tau = \tau_0 \exp\left(\frac{x\Delta h}{RT} + \frac{(1-x)\Delta h}{RT_f}\right) \quad (3.1)$$

Where τ is the relaxation time, τ_0 is a constant, $0 \leq x \leq 1$ is the nonlinear component, Δh the activation enthalpy, R the gas constant, T represents temperature, and T_f the fictive temperature, which is the temperature at which the glass would be in equilibrium. Therefore from this equation it can be seen that with an increase in activation enthalpy the relaxation time will also increase.

In materials which are physically aged a method to remove the relaxation endotherm is to heat the material through its T_g , then rapidly cool it and analyse the material immediately to prevent the development of the relaxation endotherm. However with

PVA being a semi-crystalline material this may not remove the relaxation endotherm as it may be present due to the crystalline areas of PVA. In addition once the blends of PVA are analysed this heating and cooling may alter the phase distribution of the polymer blend leading to incorrect assumptions being made regarding the behaviour of the polymer blend in-situ.

The relaxation endotherm present in the MTDSC is not typical as generally the glass transition can still be observed in the reversing heat flow of the MTDSC trace. However; as mentioned in chapter 2 previous papers have detected a glass transition temperature in the range of 45-50°C in samples of plasticised PVA. Additionally the other components of Opadry II will not undergo a melting transition in this temperature range, as the grades of PEG used in film coating tends to have melting points around 60°C, the melting point of talc is in excess of 1500°C and polysorbate 80 melts at -20°C. This leads to the conclusion that the transition present around 48°C in the MTDSC results does represent the glass transition of PVA.

3.5 Conclusions

L-TMA shows mainly good correlation with MTDSC, at least sufficient to compare between L-TMA results. It does however indicate some of the limitations associated with L-TMA, but also some of the strengths, most notably when compared to results taken with Wollaston probe.

Thermal analysis performed on minitables film coated with Opadry II produced interesting results, showing the semi-crystalline nature of the material. Additionally both MTDSC and L-TMA detected the presence an extra transition present in the film coated minitables but not the cast films. This is likely to have resulted from the differences in process conditions employed to produce the different types of film.

These results provide a good basis for the rest of the thesis, where any alterations concerning mixing in polymer blends or addition of pigments can be observed and commented on. They also provide preliminary results on whether L-TMA observes a softening point or the actual glass transition, however they are not conclusive results.

CHAPTER 4

4. Analysis of Polymer Blends and Comparison of Film Coated Minitablets to Cast Free Films

4.1 Introduction

There is growing interest in being able to analyse pharmaceutical films in-situ rather than as free films (Podczeck and Almeida, 2002, Felton, 2007). Historically, polymer films have been analysed as cast free films, which are comparatively easy to analyse but have different process conditions to spray coated films. Recently, films produced via spin casting have been utilised to provide a more accurate representation of polymer films when observed on solid dosage forms, as these have the advantage of being a free film but with more similar process conditions. However the process conditions and film deposition still deviate from the traditional spray coated films, and there can be issues with consistency in producing spin cast films as small variations in parameters can greatly affect the film produced (Temple-Boyer *et al.*, 2010).

For analytical purposes films are often produced via casting, and as discussed in Chapter 1 these films are generally prepared by casting onto a Teflon plate or into a Petri dish with subsequent drying producing the final film. The film can then be removed and altered to the correct dimensions to correspond to a variety of analytical techniques (Bodmeier and Paeratakul, 1993, Lafferty *et al.*, 2002). Spray coating of solid dosage forms involves atomising the coating solution and then spraying the atomised solution onto the solid dosage within a designated coating zone. The solid dosage forms require some form of agitation to move them into and out of the coating zone to allow drying of the film to take place before a further layer is applied. A number of factors affect the final film coat formed, with the atomising air pressure, the application rate of the coating solution, the process air flow and temperature all important factors. Compared to spray coating film casting has a

limited choice of process variables, with alteration of the oven temperature being the most important factor.

As can be seen there are vastly different process conditions between spray coating and film casting which tends to lead to the production of films with different qualities. Cast films tend to be denser and with the increased drying times sedimentation of components of the film can occur. Conversely spray coated films can be rougher and contain defects from the film coating process, which may cause failure of the dosage form if a specific release profile is desired.

The data in this chapter is concerned with the in-situ analysis of film coated minitables coated with polymer blends using the same methods as in Chapter 3. Comparison of these film coated minitables to films produced through casting will be made to ascertain any differences in the blend morphology resulting from the different process conditions of the two films.

4.2 Research Objectives

Due to the flexibility and lack of sample preparation allowed for by AFM the in-situ analysis of many pharmaceutical solid dosage forms is possible. Previous work includes the analysis of PLA microspheres (Bouissou *et al.*, 2006) and HPMC tablets (Royall *et al.*, 1999b); however to the authors knowledge there has been little work conducted on film coated solid dosage forms, in particular by nano-thermal analysis.

This chapter aims to explore the morphology of spray coated polymer films, especially with respect to the behaviour of polymer blends. The data should also provide information on any differences in the surface morphology of cast films and film coated minitables, providing evidence to whether cast free films can provide an accurate estimation of the film coats present in dosage forms. With the differences in process conditions between spray coated films and cast films it is envisioned that there will be differences observed, particularly with polymer blends, and will hopefully give an insight into how polymer blends alter the release rates of drugs.

4.3 Materials and Methods

4.3.1 Preparation of Film Coated Minitablets

Cast films were prepared from the film coating solutions by pouring 15ml into Petri dishes of 9cm diameter, which were then placed in an oven and held at 45°C overnight for 12 hours. The dried films were then placed in a desiccator until analysed. Samples were kept for up to one month, and if additional experiments were needed after this time further samples were prepared.

Bi-convex minitables were prepared on a Riva Piccola rotary tablet press and were also gifts from Colorcon. 20g batches of minitables were coated in a Caleva Mini Coater Drier-2 (Caleva Sturminster Newton, Dorset). Process

Parameter	Surelease and Opadry	
	I	II
Air Inlet Temperature (°C)	45	45
Process Air Flow (m/s)	12	12
Atomising Air Pressure (bar)	0.7	0.7
Flow Rate (ml/hr)	23*	23*
Process time (min)	90	90

Table 4.1 Process conditions for film coating *flow rate increased to 30ml/hr after 15 minutes

conditions for each coating solution are given in table 4.1, with an increase in weight of 10% w/w for both polymer blends. If the coating solution is applied too quickly the film can become tacky and cause picking and/or sticking of the solid dosage forms. To avoid this but to keep process time at a minimum the coating solution can be applied at a low rate initially and then the flow increased.

4.3.2 Atomic Force Microscopy and Thermal Probe Methods

Samples were attached to a metal stub using double sided sticky tape and then placed onto an X-Y translating microscope stage. Minitables had one end cap removed with a scalpel, to allow adequate contact with the tape to avoid the sample moving during

scanning. Cast films were cut from the Petri dish with a scalpel and carefully removed with tweezers and placed on the metal stub.

Contact images were obtained using AN2-200 nano-TA probes (Anasys instruments) mounted onto a Caliber AFM (Veeco), using a scan rate of 1.0 Hz, with a scan area between 5 μm and 20 μm . L-TMA experiments were carried out with a nano-TA2 box (Anasys Instruments) using a heating rate of 25 $^{\circ}\text{C sec}^{-1}$. Heated tip tapping mode images used a scan rate of 1.0Hz and a set point ratio between 0.3-0.5. The cantilever was tuned to determine the resonant frequency of the probe after each increase in probe tip temperature due to the possibility of a decrease in resonant frequency with increasing temperature.

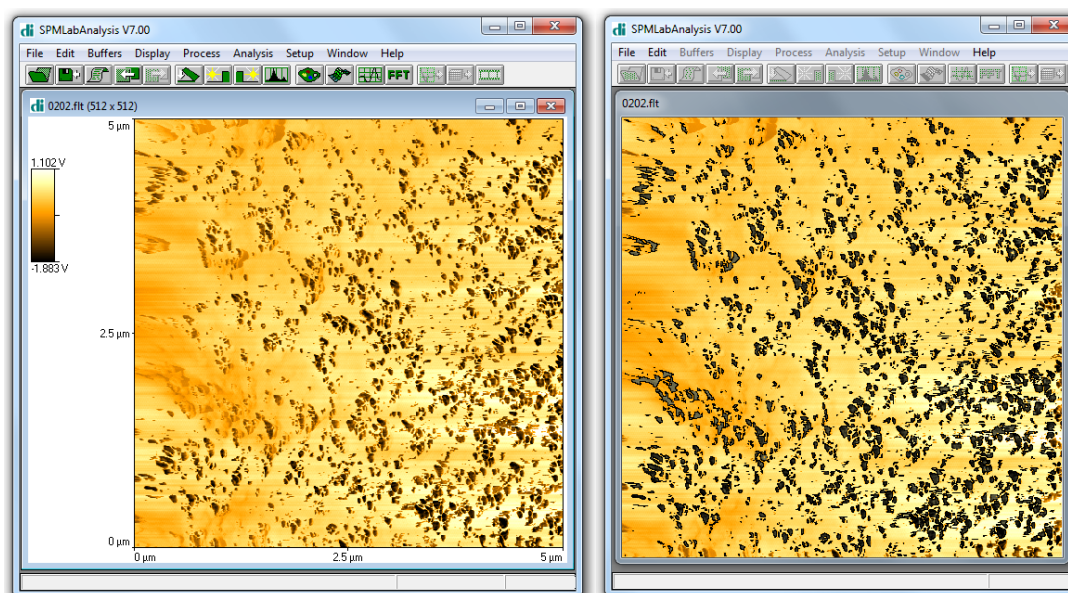


Figure 4.1 Heated Tip Tapping Mode images of a 50-50 blend of Surelease:Opadry I coated minitab showing the image before (left) and after (right) the domains were selected.

Grain analysis was performed in SPM labs to determine the size of domains in the polymer blends, with the edge of the domains being determined by marking a threshold in the Z axis of a certain parameter in the image. In the case of the phase images a certain voltage was set as the threshold with values above this attributed to one polymer and below this voltage attributed to the other polymer in the system. Fig. 4.1 shows the phase image before and after the domains were selected for analysis, with the darker areas in the right hand image indicating the “grains” that are analysed by the software.

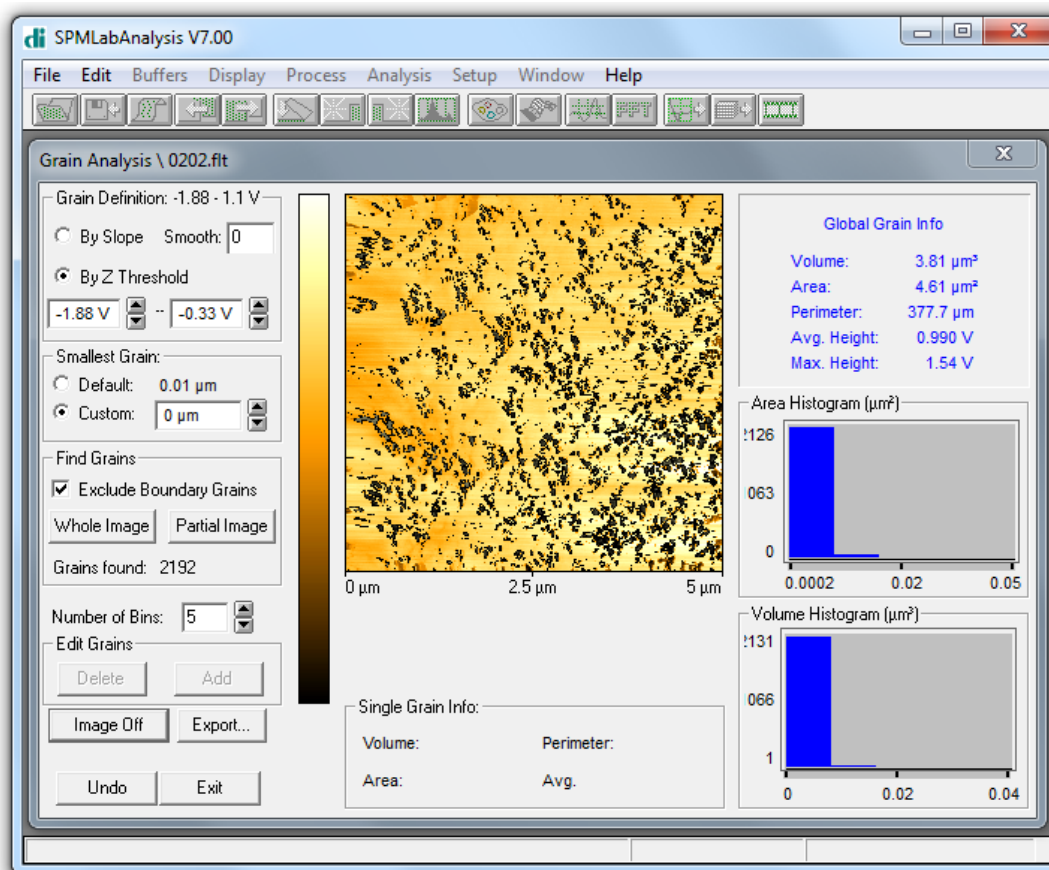


Figure. 4.2. Screen in SPM labs to set Z threshold

Fig. 4.2 displays the screen in SPM labs that allows the threshold in the Z axis to be selected. As can be seen the Z threshold is in volts and can be adjusted until corrected boundary is established between the suspected different phases. Once the Z threshold is set the grain analysis can be exported to a spread sheet. The analysis contains various data regarding the image including the circumference of each grain and their area. The grain analysis also allowed the determination of the percentage of the image attributable to each polymer.

4.3.3 Modulated Temperature DSC

MTDSC was carried out using the same method as previously stated with all measurements carried out using a Q2000 DSC (TA instruments, Newcastle, USA). When peeled films were analysed some residue may be present on the MTDSC thermogram, and this was confirmed in Chapter 3. The same experimental conditions

used in Chapter 3 were used for all MTDSC experiments.

4.3.4 Scanning Electron Microscope

Coated minitablets were axially bisected, and mounted onto an aluminium stub then sputter coated with a gold layer of approximately 50nm in a Polaron SC7640 sputter coater (Edwards, UK). The samples were then imaged using a JEOL JSM-5900LV SEM (Oxford Instruments, Abingdon, England), equipped with a Tungsten filament using a 20kV accelerating voltage at a number of locations along the core-film coat interface and of the intact film surface.

4.3.5 Fourier Transform Infrared Spectroscopy

Fourier Transform Infrared (FTIR) Spectroscopy was performed on an IFS/66 S spectrometer from Bruker Optics (Coventry, U.K.). Whole minitablets were placed on the ATR crystal and pressed down to ensure a good contact between the surface of the film coat and the ATR crystal. Whole minitablets could be used as the penetration of the IR evanescent wave is only in the order of tens of microns, therefore there is limited interference from the tablet core.

Each sample was run with a resolution of 4cm^{-1} with the average of 32 spectra being taken. The empty ATR crystal was used as a reference spectrum, which was performed before each sample was placed on the crystal.

4.4 Results

The individual coating systems (Surelease, Opadry I and Opadry II) of the polymer blends were analysed and presented in chapter 3. These data indicated a glass transition of Surelease to be around 90°C , depending on the analytical technique used, and 160°C for Opadry I. The results for Opadry II produced interesting results due to the semicrystalline nature of the polymer, with a glass transition around 50°C and a melting point above 150°C .

From these results a mixture of transitions associated with the two polymers or a single intermediate glass transition between those observed for the individual polymers would be expected.

A single glass transition at an intermediate value of the two component polymers, which increases or decreases with alteration of composition is generally indicative of phase miscibility, and the presence of two unaltered glass transitions tends to indicate immiscibility (Sperling, 2006). As discussed previously polymers are rarely miscible due to the long chain lengths of the polymers making it thermodynamically unfavourable for mixing to occur. Additionally in the literature ethylcellulose and HPMC have been shown to phase separate (Sakellariou *et al.*, 1986, Sakellariou *et al.*, 1995b). It is therefore expected that two distinct areas of polymers will be observed through thermal analysis.

4.4.1 Analysis of Individual Coating Systems

Fig. 4.3 shows typical L-TMA responses to film coated minitables coated with each polymer. The transition temperatures observed were 161.6°C for Opadry I, 48.8°C for Opadry II and 85.0°C for Surerelease. A higher melting temperature was observed

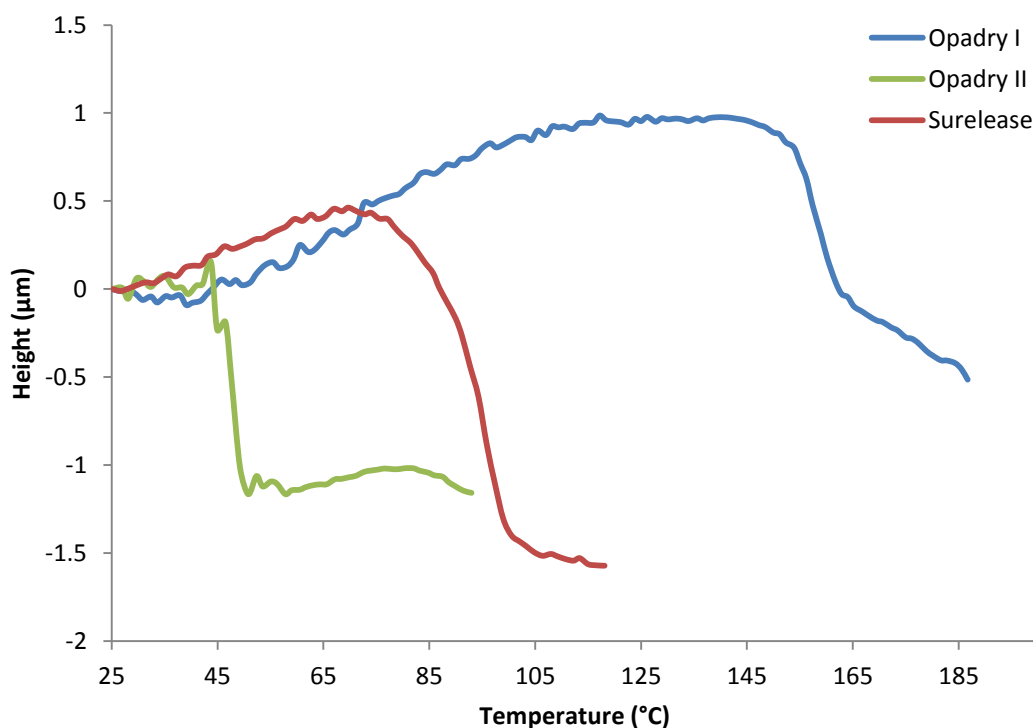


Figure 4.3 L-TMA of minitables film coated with Opadry I, Opadry II and Surerelease

for Opadry II, however if any miscibility is observed between the polymers then an alteration in the glass transition is more likely to occur so is of more concern to measure the glass transition.

The MTDSC thermogram in Fig. 4.4 was of an uncoated minitabilet showing a sharp melting endotherm at 134.8°C, which may be present in the MTDSC results for films peeled from minitablets. There is a discontinuation in the reversing heat flow which could potentially mask any glass transitions of the polymer; however as the transitions of Opadry I, Opadry II and Surelease are not in the vicinity of this transition then this should not be an issue.

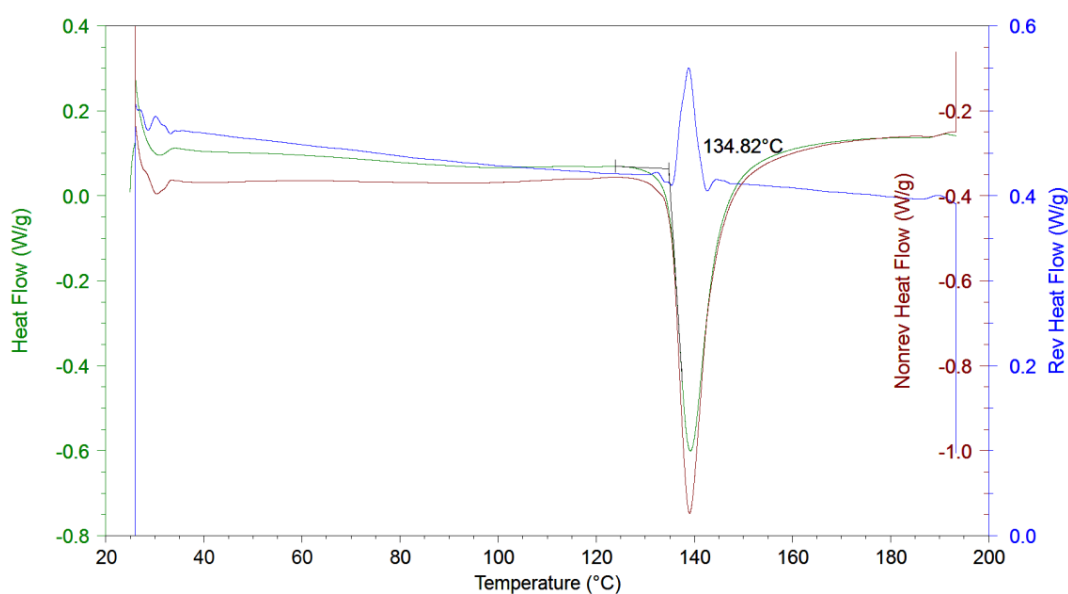


Figure 4.4 MTDSC of an uncoated powdered minitabilet

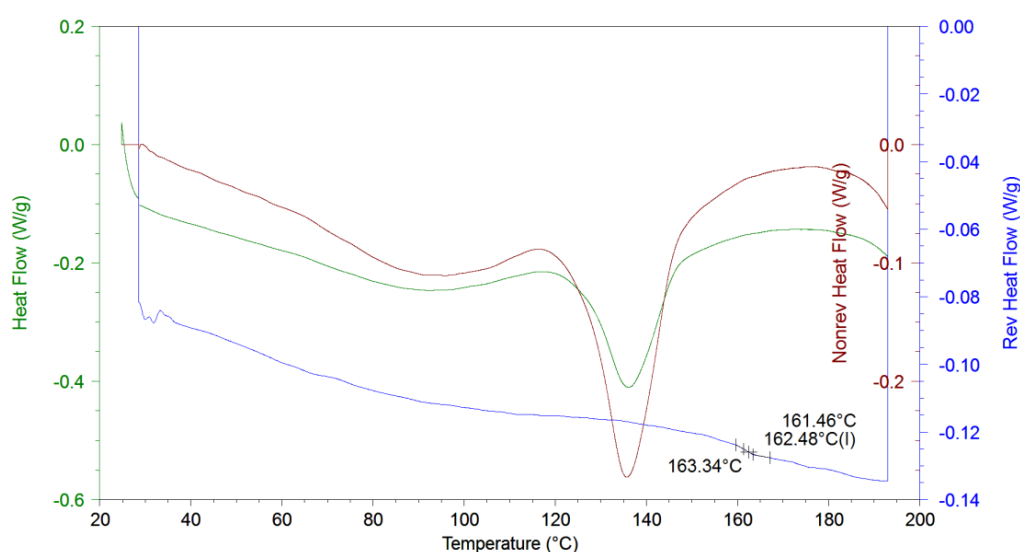


Figure 4.5 MTDSC of Opadry I coated minitablets

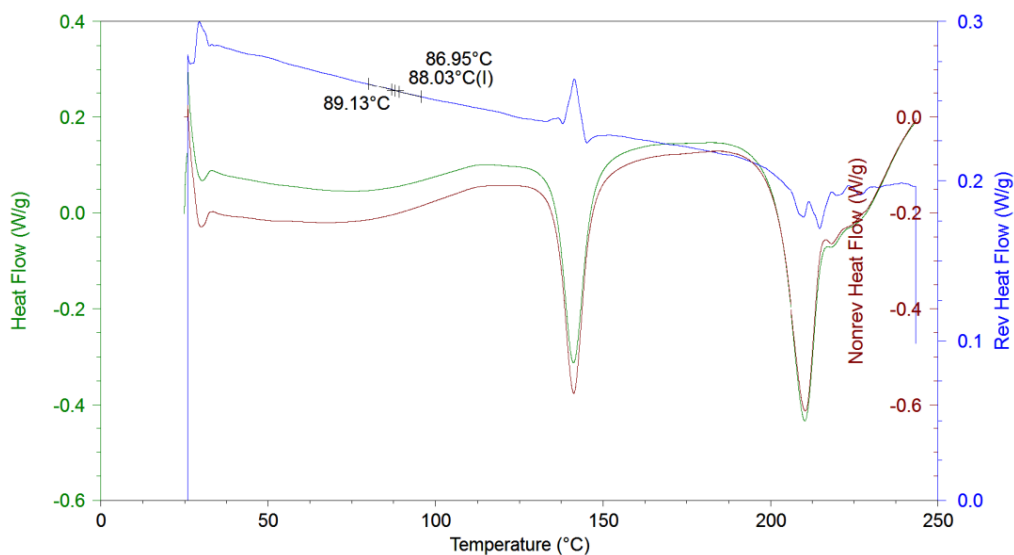


Figure 4.6 MTDSC of Surelease coated minitables

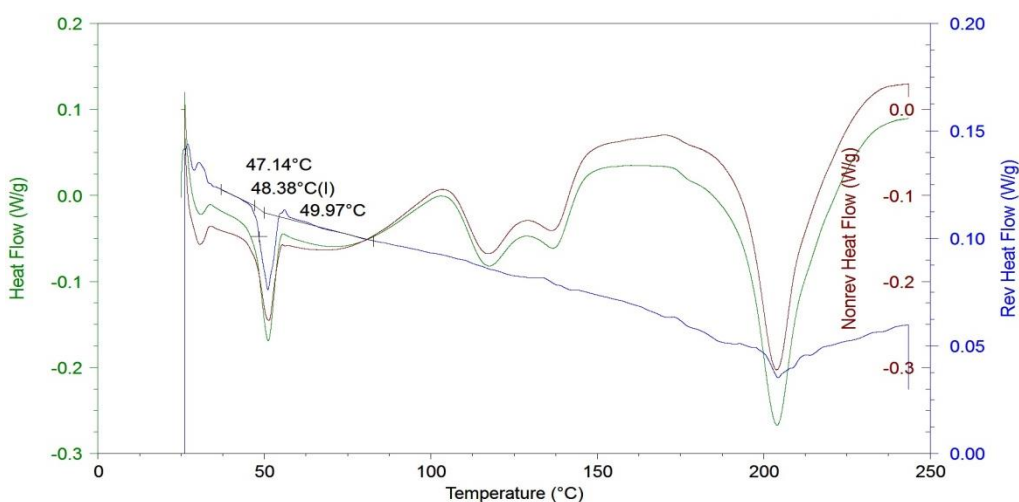


Figure 4.7 MTDSC of Opadry II coated minitables

Fig. 4.5 through 4.7 shows MTDSC thermograms for minitables film coated with each polymer and displaying glass transitions at 162.5°C for Opadry I, 48.4°C for Opadry II and 87.0°C for Surelease.

Cast films were also analysed by L-TMA and MTDSC, with L-TMA results shown in Fig 4.8 indicating transitions of Opadry I at 164.2°C, Opadry II at 48.1°C and Surelease at 89.8°C. Fig. 4.9 through 4.11 shows the glass transitions observed in MTDSC, with Opadry I being observed at 164.9, Opadry II at 50.0°C and Surelease at 85.1°C.

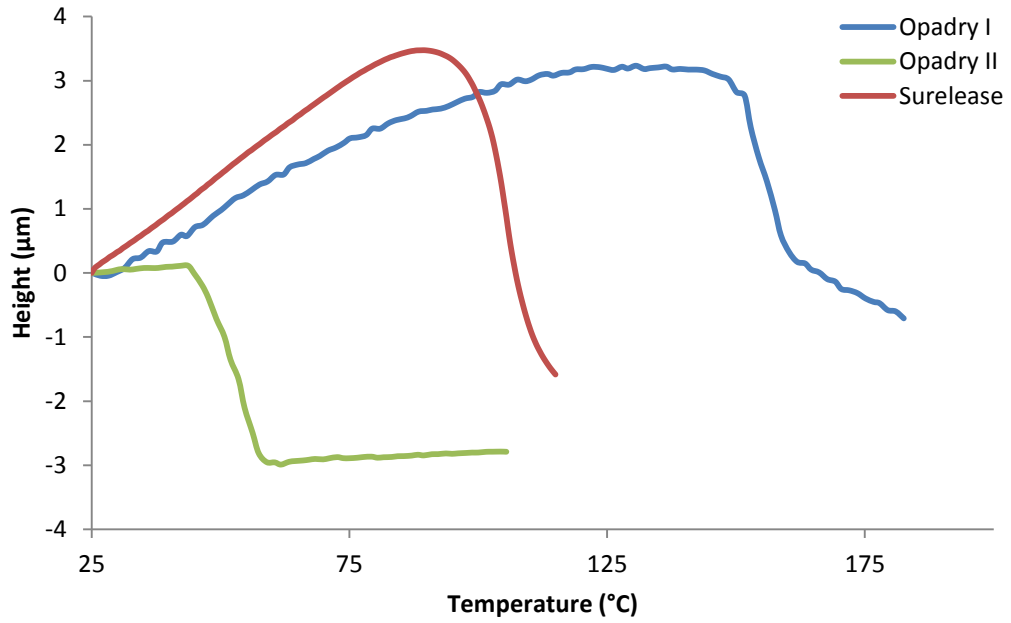


Figure 4.8 L-TMA of Opadry I, Opadry II and Surelease cast films

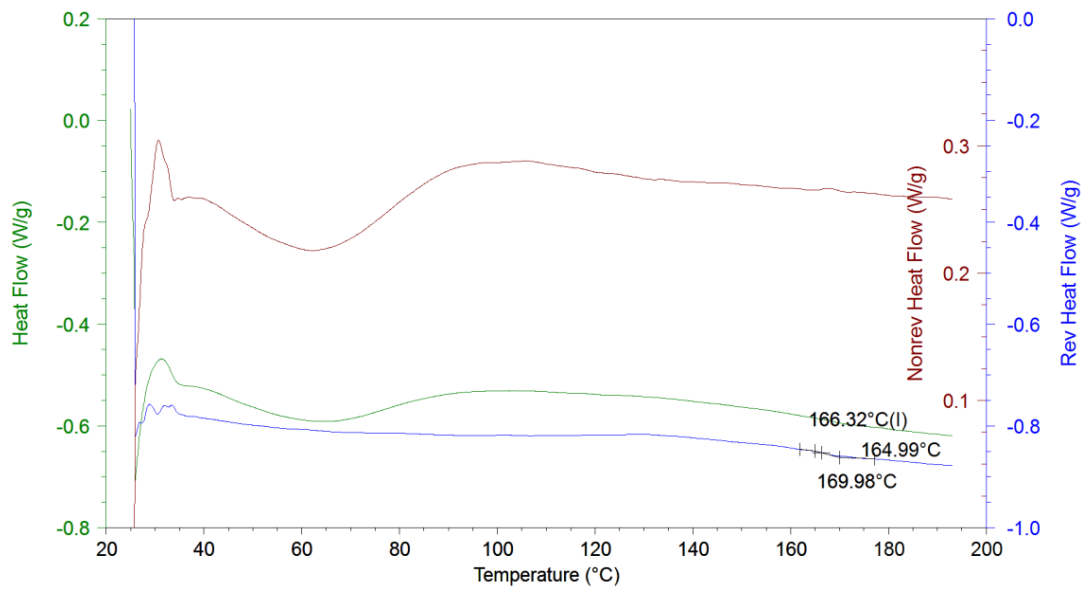


Figure 4.9 MTDSC of Opadry I cast films

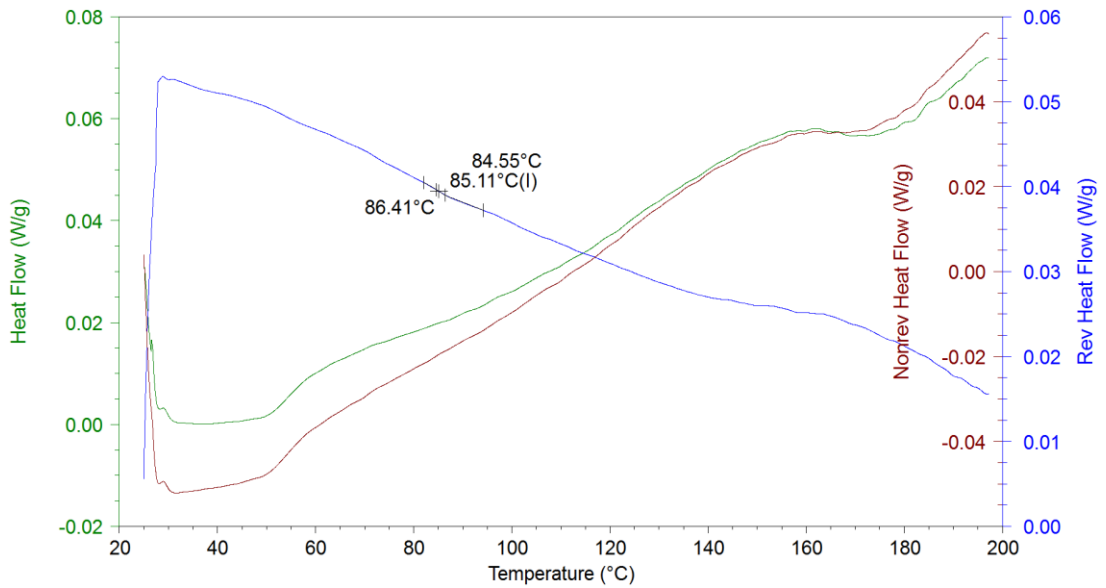


Figure 4.10 MTDSC trace of Surelease cast film

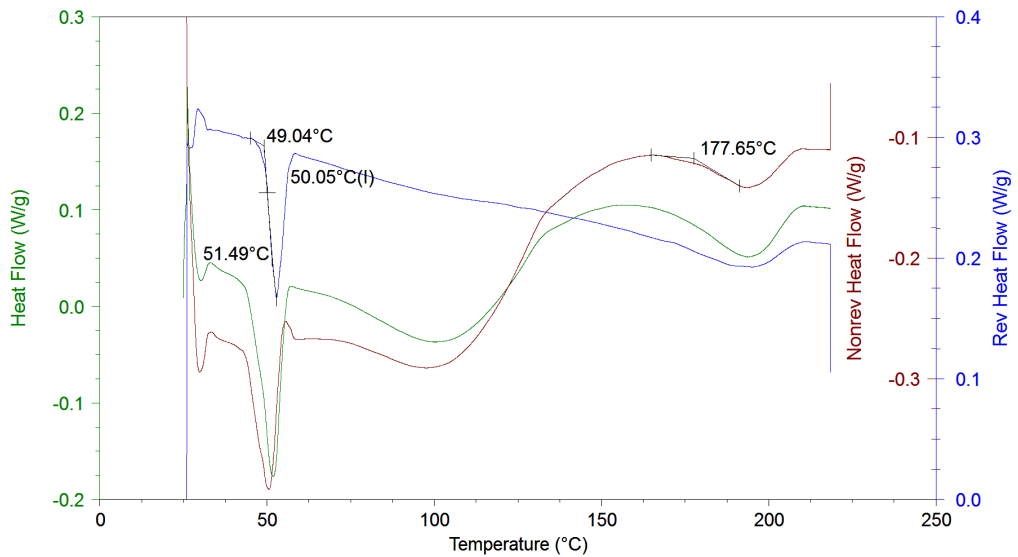


Figure 4.11 MTDSC of Opadry II cast films

4.4.2 Analysis of Film Coated Minitablets Coated with Polymer Blends

4.4.2.1 SEM

The coating thickness of the minitablets can be seen to be in the region of 50 μ m, which is in the region expected for the weight gain observed and the function of the film coat. With Lehmann (1994) and Lippold (2001) reporting similar thicknesses in film coated multiparticulate.

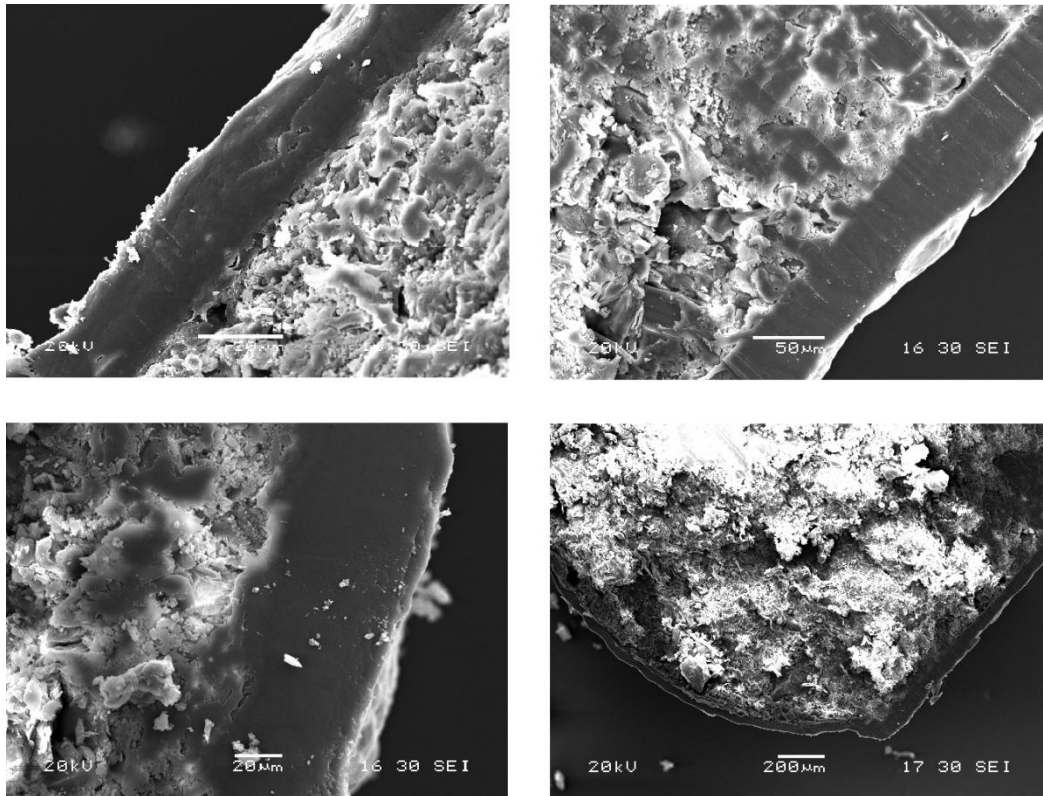


Figure 4.12. SEM of film coated minitables. Clockwise from top left: Surelease-Opadry I 50:50, Surelease Opadry I 70:30, Surelease-Opadry I 70:30 alternate view, Surelease-Opadry I 90:10

Alongside the coating thickness of the film coated minitables the quality of the film can also be assessed, allowing an indication of whether the film will perform its designated function. For controlled release coatings large variations in coating thickness or a porous film structure may lead to controlled release not being obtained. The film coats observed in Fig. 4.12 indicate a good film structure and additionally the image in the bottom right of Fig. 4.12 shows the film coat is a consistent thickness over the whole minitabket including the area where the crown and the central band meet. The data demonstrates SEMs strengths of being able to image a wide range of magnifications and angles of a single sample; however it cannot provide information on the phase behaviour of the polymer blends.

4.4.2.2 Surelease and Opadry I Film Coated Minitables

A 50:50 blend of Surelease and Opadry was chosen as it should provide a relatively easy sample to analyse. A 50:50 blend is not a composition used in industry, as the film coat will rupture and not provide any controlled release due to the high

concentration of immediate release polymer. This blend however will provide a test as to whether thermal probe techniques are suitable for the in-situ analysis of polymer film coats. 70:30 and 90:10 blends were also analysed to provide a more accurate representation of blend compositions used in industry.

4.4.2.2.1 Modulated Temperature DSC

The film coated minitables were analysed using MTDSC though peeling the film off the tablet core with a scalpel. As described in Chapter 3 there is an endotherm around 135°C indicating the presence of residual tablet core which has not been removed from the film coat. However the endotherm is present at a temperature not associated with the glass transition of any of the polymers, therefore allowing for any glass temperatures to be easily identified.

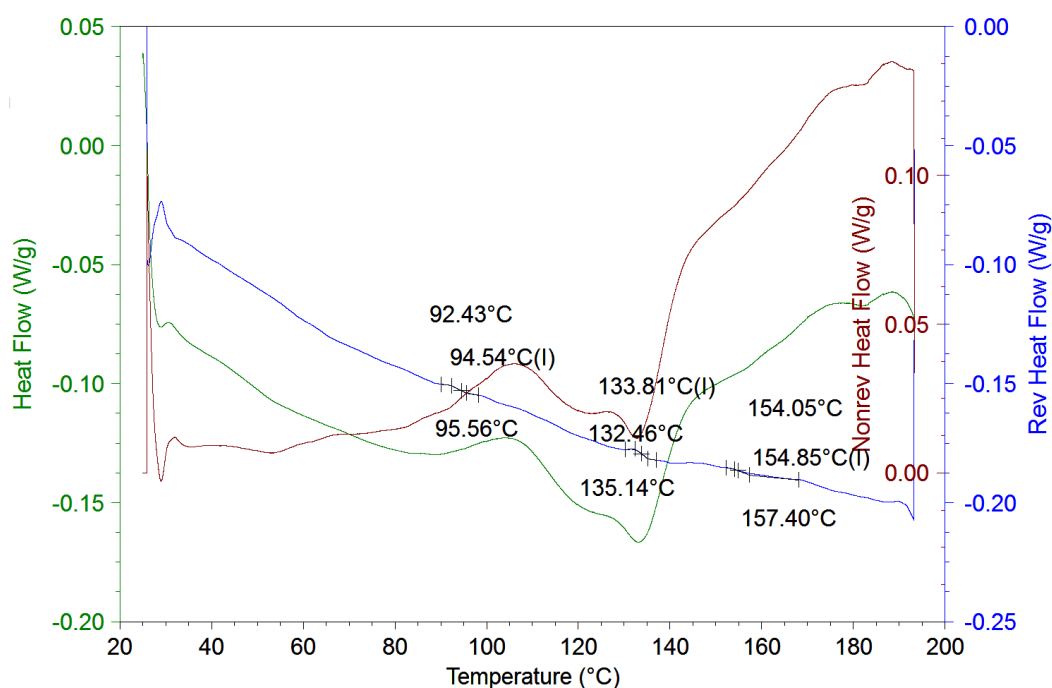


Figure 4.13 MTDSC trace of a minitabket coated with Surelease and Opadry I 50:50 blend

Also due to the preparation method of the films to be able to perform analysis by MTDSC only a small quantity of film could be analysed, due to the small nature of the minitables. The curvature of the minitables resulted in the peeled films also having a noticeable curve restricting the amount of film that could be placed in the pan before sealing, resulting in poor contact with the bottom of the pan. This also led

to a relatively small amount of film being able to be placed in the pan leading to an increase in the signal to noise ratio and therefore resulting in poor baselines. In addition a proportion of the weight of the film was contributed by residual minitablet core, and coupled with the strong glass forming nature of EC and HPMC made interpretation of MTDSC traces particularly difficult.

As discussed above both EC and HPMC are both strong glass formers, making glass transitions hard to detect, even when using MTDSC. Two clear transitions of EC and HPMC were expected to be present on the MTDSC trace as EC and HPMC are known to phase separate. In Fig. 4.13 there is a weak T_g value associated with Surelease at 91.4°C, indicating there are domains of Surelease observable. However a glass transition is also apparent at 154.9°C which is lower than that observed in the film coated tablets coated solely with Opadry I and is at an intermediate value between the two observed in the single films. This is a surprising observation given that ethylcellulose and HPMC tend to phase separate then two distinct glass transitions would be expected to emerge.

The dynamic nature of DSC may alter miscibility during the course of the experiment, and this has been reported in drug-polymer mixtures where the drug dissolves in the softened polymer upon heating (Qi and Craig, 2010). This may not be the case in this situation, especially with polymer blends tending to exhibit lower critical solution temperatures and therefore phase separate at elevated temperatures.

Additionally, previous DSC and MTDSC studies have produced single glass transitions in phase separated systems, with reports that if domain sizes of phase separated amorphous materials are sub 30nm (Newman *et al.*, 2008) or even below 70nm (Meulendijks *et al.*, 1989) then DSC cannot resolve the two glass transitions of the individual components.

In Fig. 4.13 there also appears to be a glass transition at 133.8°C, however this is present on the traces for every blend and therefore maybe present due to the transitions observed in non-reversing heat flow associated with the tablet core.

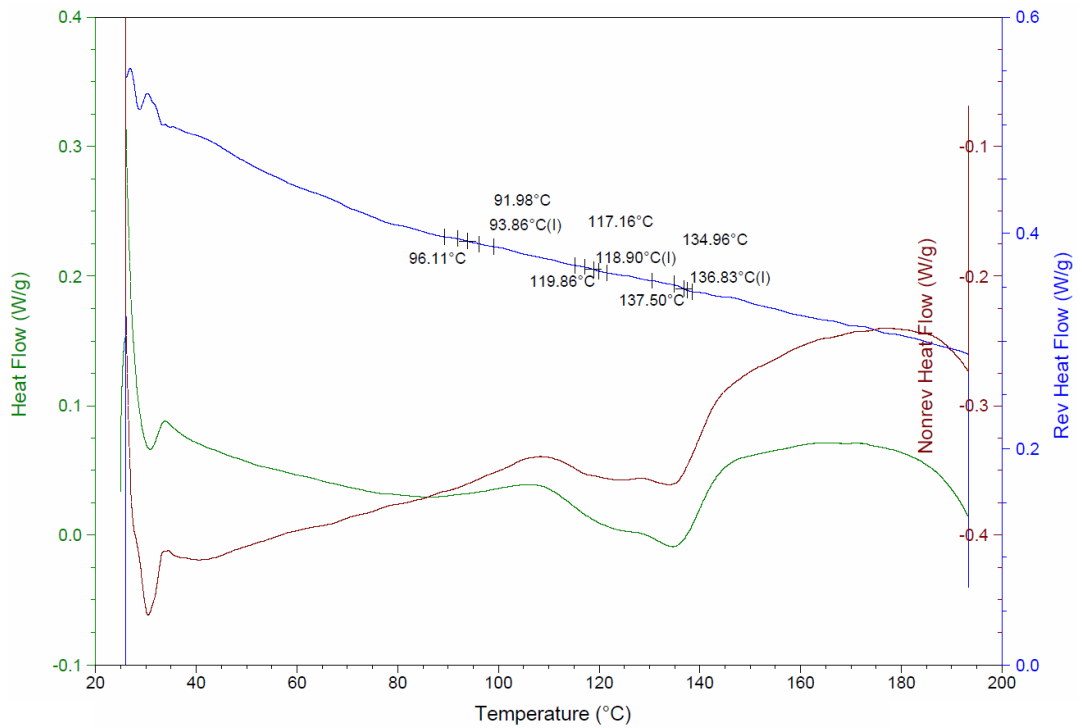


Figure 4.14 MTDSC trace of a minitabket coated with Surelease and Opadry I 70:30 blend

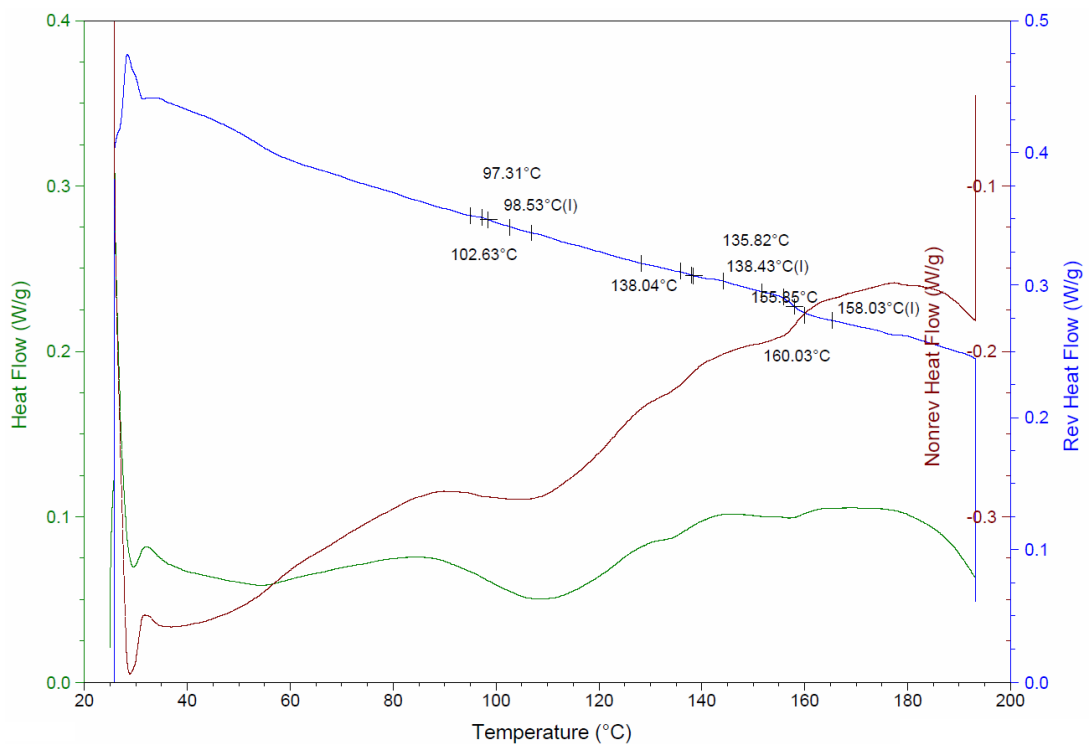


Figure 4.15 MTDSC trace of a minitabket coated with Surelease and Opadry I 90:10 blend

Indeed in Chapter 3 MTDSC of the tablet cores did show a discontinuation in the reversing heat flow present at the melting endotherm observed in the non-reversing heat flow.

The two other blends were also analysed by MTDSC, shown in Fig. 4.14 and 4.15, with the intermediate glass transition observed for the 50:50 blend also seen in the 70:30 and 90:10 blends decreasing from 118.6°C ($\pm 0.4^\circ\text{C}$ sd; n=3) to 100.9°C ($\pm 3.6^\circ\text{C}$ sd; n=3). For these blends there were also glass transitions present for both Surelease and Opadry I.

Intermediate glass transitions are generally indicative of a system where the components are miscible, with the two components molecularly dispersing and producing a glass transition between the two components. As stated above polymers tend to phase separate when blended and EC and HPMC in previous studies have been shown to phase separate; therefore this is an unexpected result. The presence of the intermediate glass transition coupled with the those of the individual polymers could indicate partial miscibility between Surelease and Opadry I as up to the solubility limit of miscible materials a single T_g is generally present, then once over the solubility limit an intermediate and the two original glass transitions are observed.

It has to be remembered though that MTDSC provides measurements over the entire sample being analysed and is not spatially resolved, so it is difficult to reach any firm conclusions regarding phase distribution from this data. L-TMA should be able to provide spatially resolved data and provide further information on the morphology of the blends.

4.4.2.2.2 Localised Thermomechanical Analysis

When analysing the samples using L-TMA Wollaston probes were initially used to analyse the blends. It is usually of value to conduct initial experiments with Wollaston probes for any new samples, as these probes are less delicate than the nano-TA probes. If the probe undergoes any unexpected or sudden transitions it is less likely to be damaged. However the disadvantage of Wollaston probes is their size is considerably larger than nano-TA probes reducing the spatial resolution of the probes for both imaging functions and L-TMA.

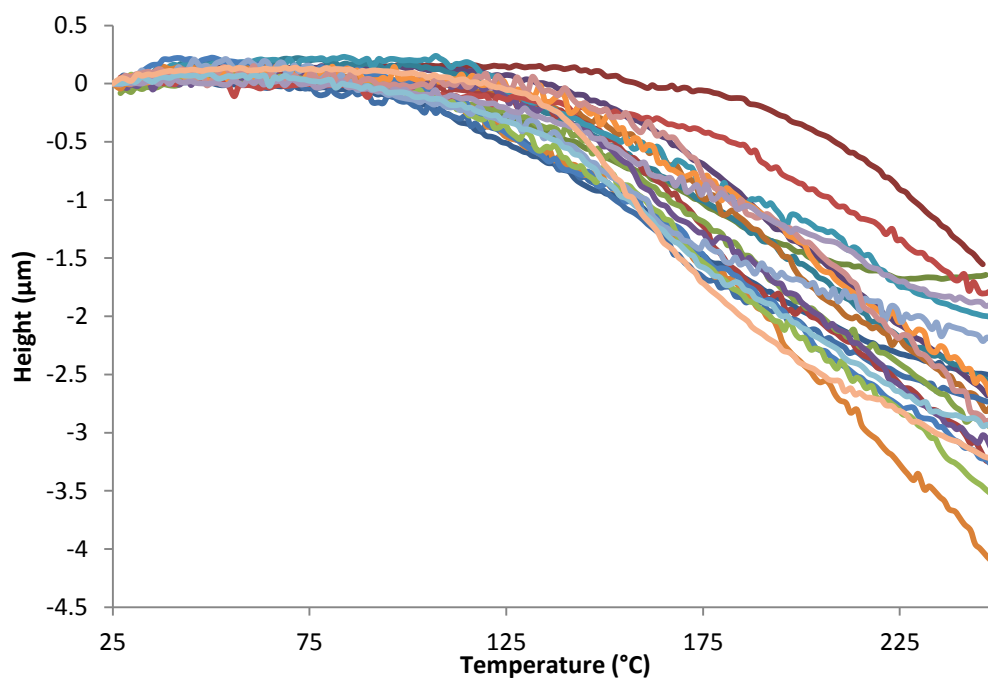


Figure 4.16 50:50 Blend of Surelease and Opadry I analysed with Wollaston Probes

The traces in Fig. 4.16 displayed the usual thermal expansion and indentation associated with L-TMA. However, as with MTDSC, only one intermediate glass transition is observed, again suggesting miscibility between the two polymers is occurring. The area analysed using a Wollaston probe is relatively large due to the area of the probe in contact with the sample being in the region of $1\mu\text{m}$, and MTDSC analyses samples in the bulk. These methods may not provide the resolution to determine different phases of the two polymers and thus produce a single glass transition. Therefore nano-TA probes were used to perform L-TMA on the polymers blends in an attempt to differentiate between the two. As can be observed in Fig. 4.17 the main transition observed is still an intermediate transition of 148.4°C ($\pm 5.2^\circ\text{C}$ $n=30$). However there are some transitions observed around 90°C and 160°C , indicating that the polymers may be phase separated but the domain size is at the limit of what nano-TA probes can detect.

Fig. 4.18 shows an AFM contact image and three L-TMA experiments performed at areas of interest. There appeared to be no correlation between lighter and darker areas, or any other features of the AFM contact image and the nature of the transition. This therefore indicates that any information in the sample topography is

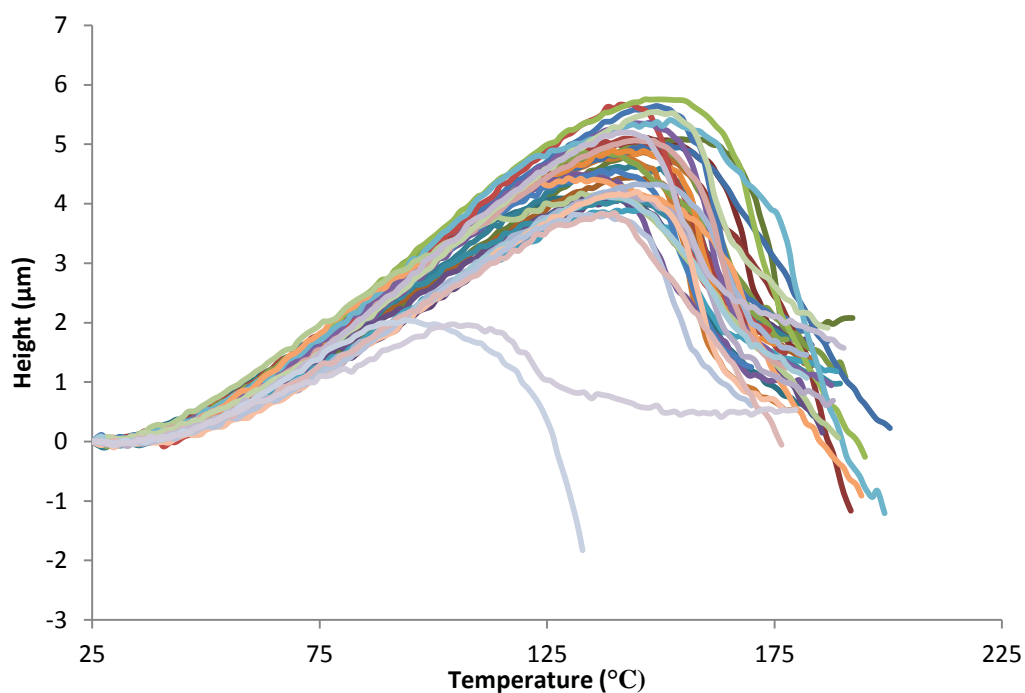


Figure 4.17 L-TMA of minitablets coated with a 50:50 Surelease:Opadry blend

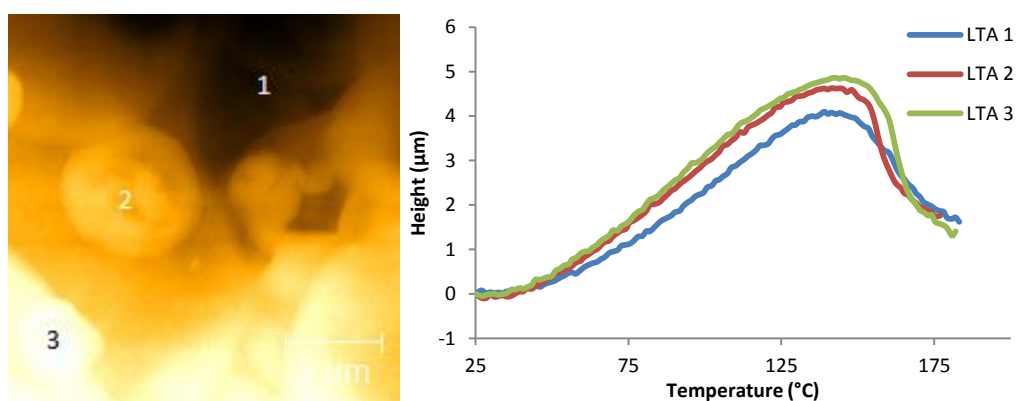


Figure 4.18 AFM contact image (left) and L-TMA results (right) for 50:50 Surelease:Opadry I blend

not related to the composition of the blend. As the domains cannot be observed in contact mode AFM then it is not possible to conclude that the intermediate transition is due to the presence of small domains, and therefore the potential of phase miscibility is still possible.

Figures 4.19 and 4.20 shows the glass transitions found when analysing Surelease:Opadry 70:30 blends. Again there is an intermediate transition temperature observed at 128.7°C ($\pm 9.1^{\circ}\text{C}$ sd; $n=30$), and as with L-TMA results of the 50:50 blend little correlation is observed between areas on the contact AFM image.

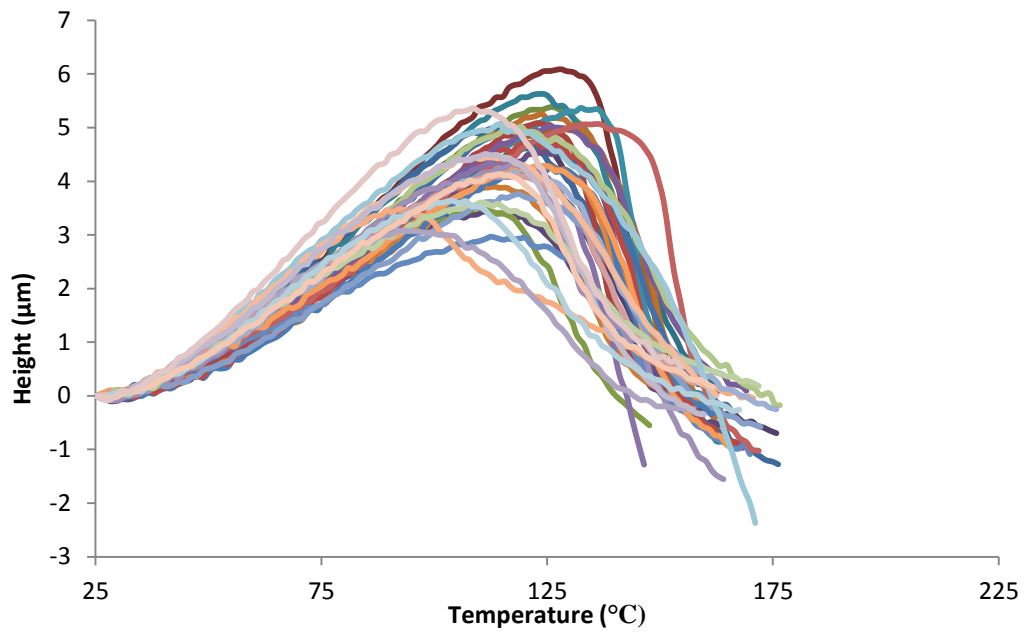


Figure 4.19 L-TMA of minitablets coated with a 70:30 Surelease:Opadry blend

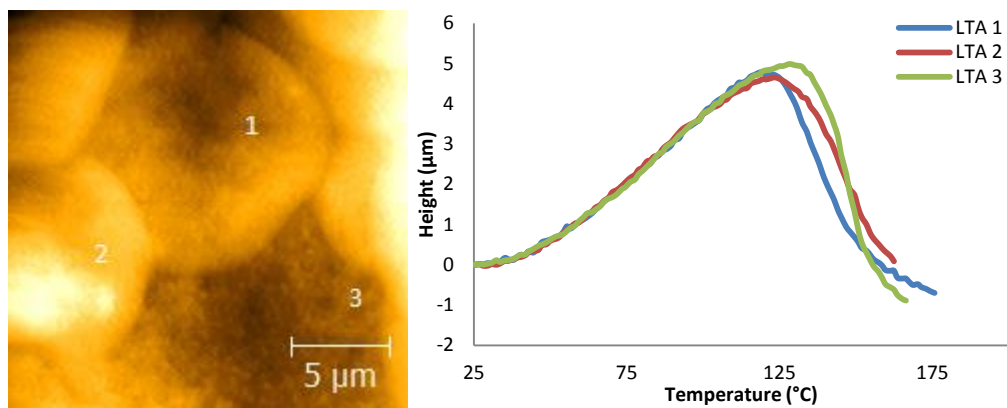


Figure 4.20 AFM contact image (left) and L-TMA results (right) for 50:50 Surelease:Opadry I blend

Analysis of the 90:10 Surelease:Opadry blend (Fig. 4.21 and 4.21) again produced similar result with an intermediate temperature observed at 103.5°C ($\pm 4.4^{\circ}\text{C}$ sd; $n=30$).

Of interest is the intermediate glass transition temperature appears to decrease with increasing Surelease content which can be seen in the graph in Fig 4.23 In the graph 0% Surelease indicates Opadry I coated minitablets and 100% Surelease indicates Surelease coated minitablets, with the blends falling between. The trend of the graph shows the gradual reduction in the intermediate glass transition when the ratio of Surelease to Opadry I is increased. The Gordon-Taylor equation provides a method

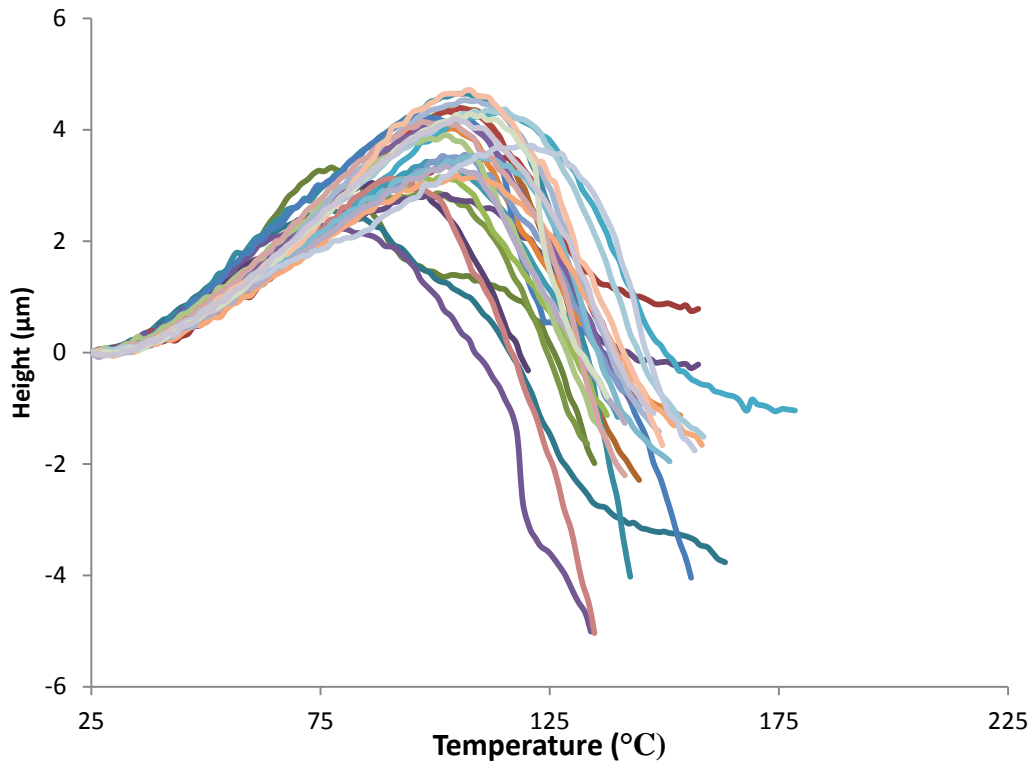


Figure 4.21 L-TMA of minitablets coated with a 90:10 Surelease:Opadry blend

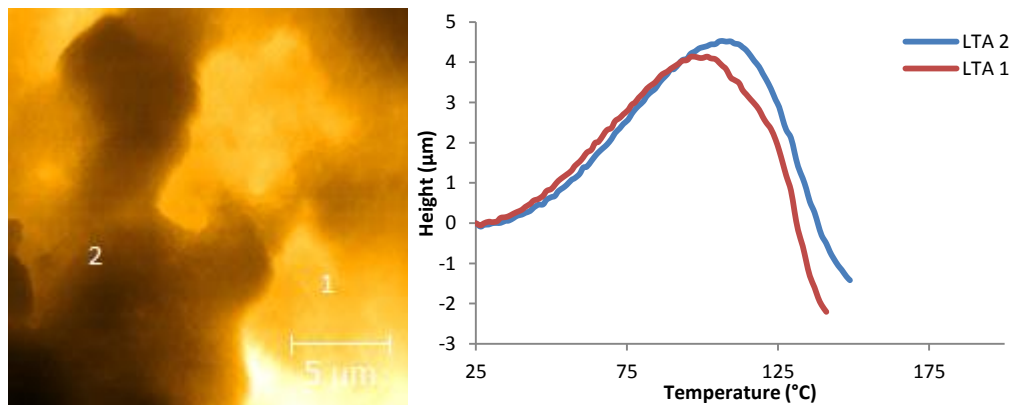


Figure 4.22 AFM contact image (left) and L-TMA results (right) for 50:50 Surelease:Opadry I blend

to predict the glass transition temperature of binary polymer blends:

$$T_{g_{mix}} = \Phi_1 T_{g1} + \Phi_2 T_{g2} \quad (4.1)$$

where $T_{g_{mix}}$ is the expected glass transition of the blend, Φ is the volume fraction and the subscripts denote the two components. As stated above a single transition at an intermediate value indicates one phase being present, however this is improbable as previous studies have indicated two phases, and the Flory-Huggins interaction

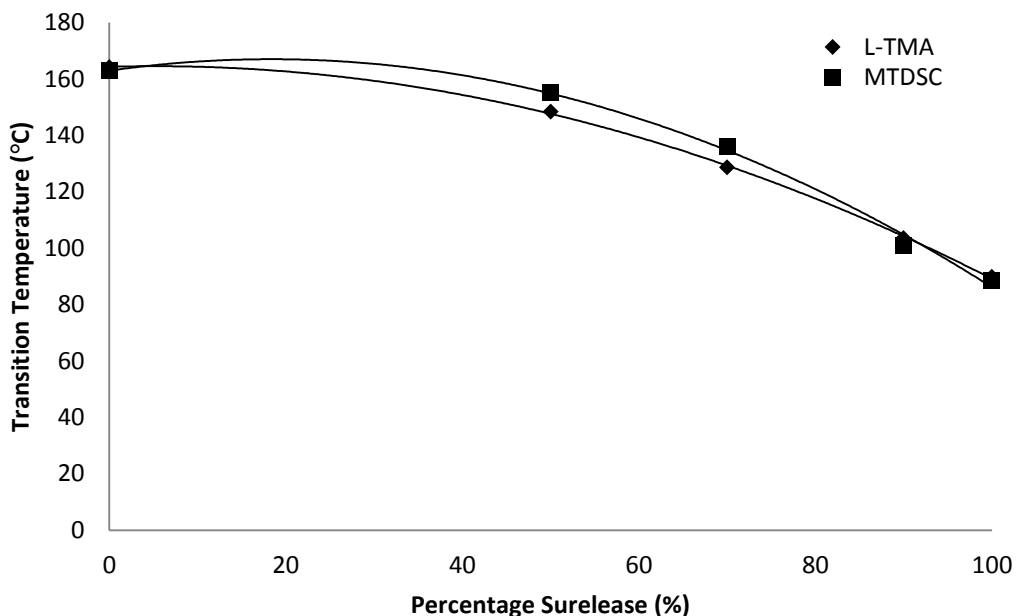


Figure 4.23 Correlated transitions of L-TMA and MTDSC for film coated minitablets

parameter for the two polymers indicates that they are not miscible. However the Flory-Huggins interaction parameter is applicable to binary mixes and may not be suitable in this instance due to Surelease being formulated as an aqueous dispersion. The extra excipients used to formulate the pseudolatex of Surelease could affect the phase separation of the EC and HPMC.

Another possibility could be down to the way that droplets spread on the surface of the tablet, causing very thin layers of the individual polymers that the AFM may not

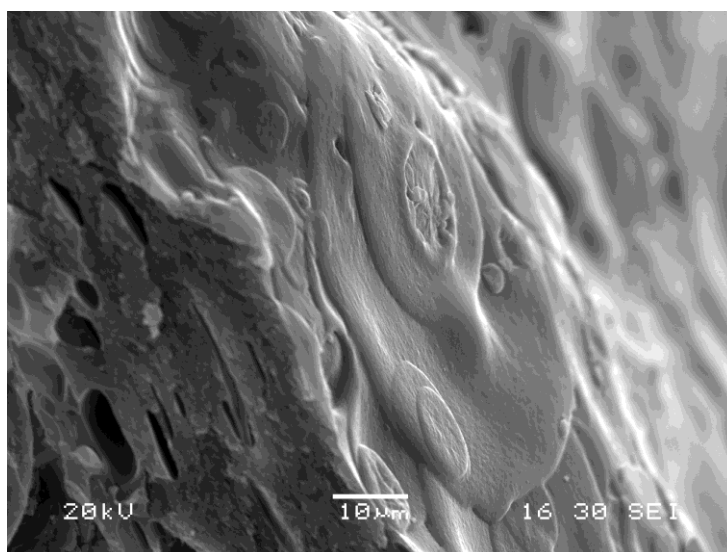


Figure 4.24 SEM image of Surlease:Opadry I 50:50 blend

resolve in the z axis when performing L-TMA. There are a number of L-TMA experiments that do hint towards layered polymers, with a transition around the temperature expected for Surelease, then further thermal expansion and another transition at a higher temperature. SEM images, seen in Fig. 4.24, show on the surface of the tablet show that droplets appear to be deposited in this manner. However this would not account for the transitions seen in the MTDSC results, where the sample is not spatially resolved. This leads to the reasoning that either the polymers are miscible or the spatial resolution of the techniques is not sufficient. However due to previous studies finding immiscibility between the two polymers it is more likely that there are distinct phases, but are too small to be resolved by the techniques employed thus far.

4.4.2.2.3 Heated Tip Tapping Mode AFM

These results lead to the hypothesis that even the spatial resolution of the nano-TA probes was not sufficient to resolve the size of the phase separated domains present in the film coated minitabket surface. Therefore the use of tapping mode AFM combined with the ability of the nano-TA probes could be utilised to provide the necessary resolution to determine the presence or absence of two phases. Tapping mode AFM, as described earlier in the work, is used to obtain topographic images on soft samples such as polymers but can also be operated in the secondary imaging mode of phase imaging. However as tapping mode AFM detects the differences in phases through different mechanical properties this can present a problem when attempting to detect different phases of polymers with similar mechanical properties. As Surelease and Opadry are both cellulose derivatives their Young's moduli are similar with Surelease reported to be in the region of 252 MPa (Rege *et al.*, 2006) and Opadry I 1900 MPa (Vesey, 2002). Although there is an order of magnitude between the two polymers their moduli are relatively close as steel has a Young's modulus in the region of 190,000 MPa (Rho *et al.*, 1993). As the mechanical properties of amorphous samples alter with temperature then a reasonable method to circumvent this is to raise the temperature of the system. Generally a two to three orders of magnitude decrease in the Young's modulus is observed around the T_g (Hale 2002). Therefore once the temperature approaches the T_g of the component with the lowest transition temperature then this component should soften

considerably, allowing for easier identification of the two polymers.

Previous research (Harding *et al.*, 2007) has used pulsed force microscopy (PFM) AFM for a similar effect. With this technique the probe comes in contact with the sample, whereas tapping mode AFM does not; however as tapping mode AFM measures stiffness of the sample then this should perform a similar function. An advantage of tapping mode AFM is that it is a widespread technique with most commercial AFMs having an intermittent contact option. PFM-AFM unfortunately requires extra specialist modules to control the drive of the cantilever as different frequencies and amplitudes are used. Although identical probes are used for both techniques the widespread application of tapping mode AFM makes it a more appealing technique to use. A major disadvantage of operating the AFM in any imaging mode at elevated temperatures is a potential reduction in image quality. Due to the higher temperatures softening the sample there is a higher possibility of tip

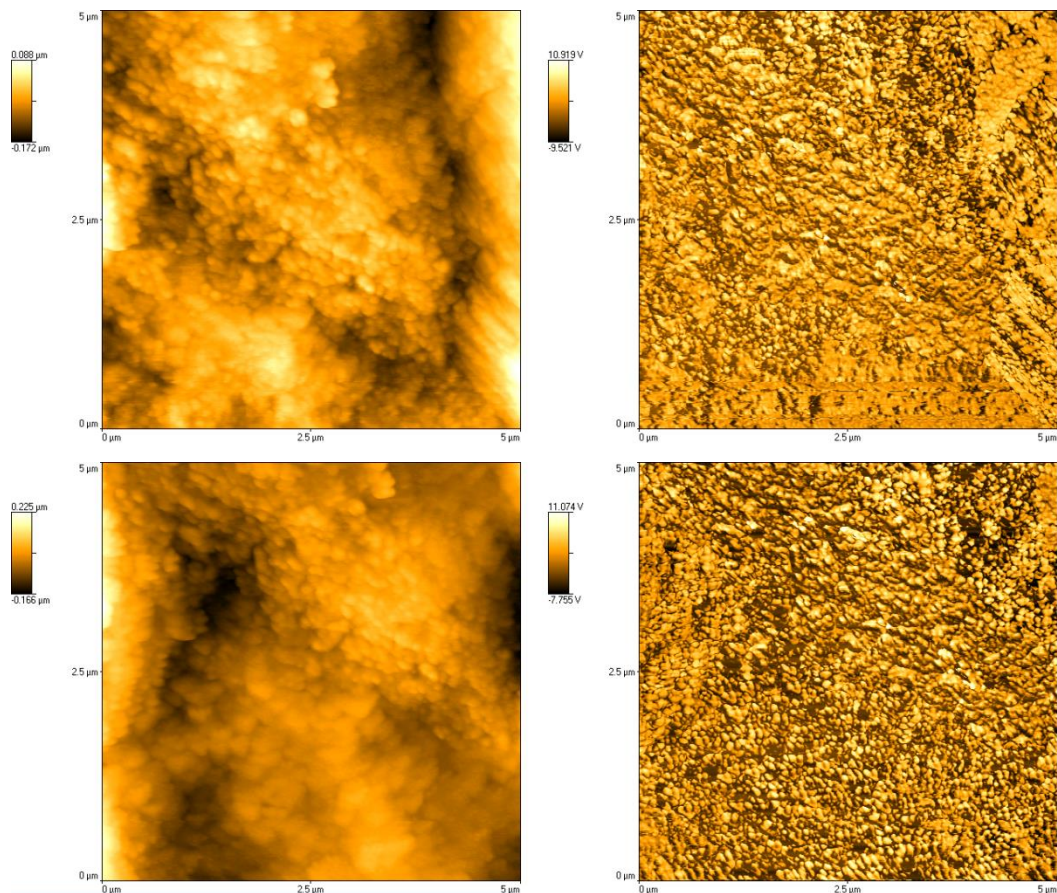


Figure 4.25 Heated Tip Tapping Mode images of a Surelease coated minitabket (topography – left, phase image – right): From top to bottom 25°C, 30°C (continues overleaf)

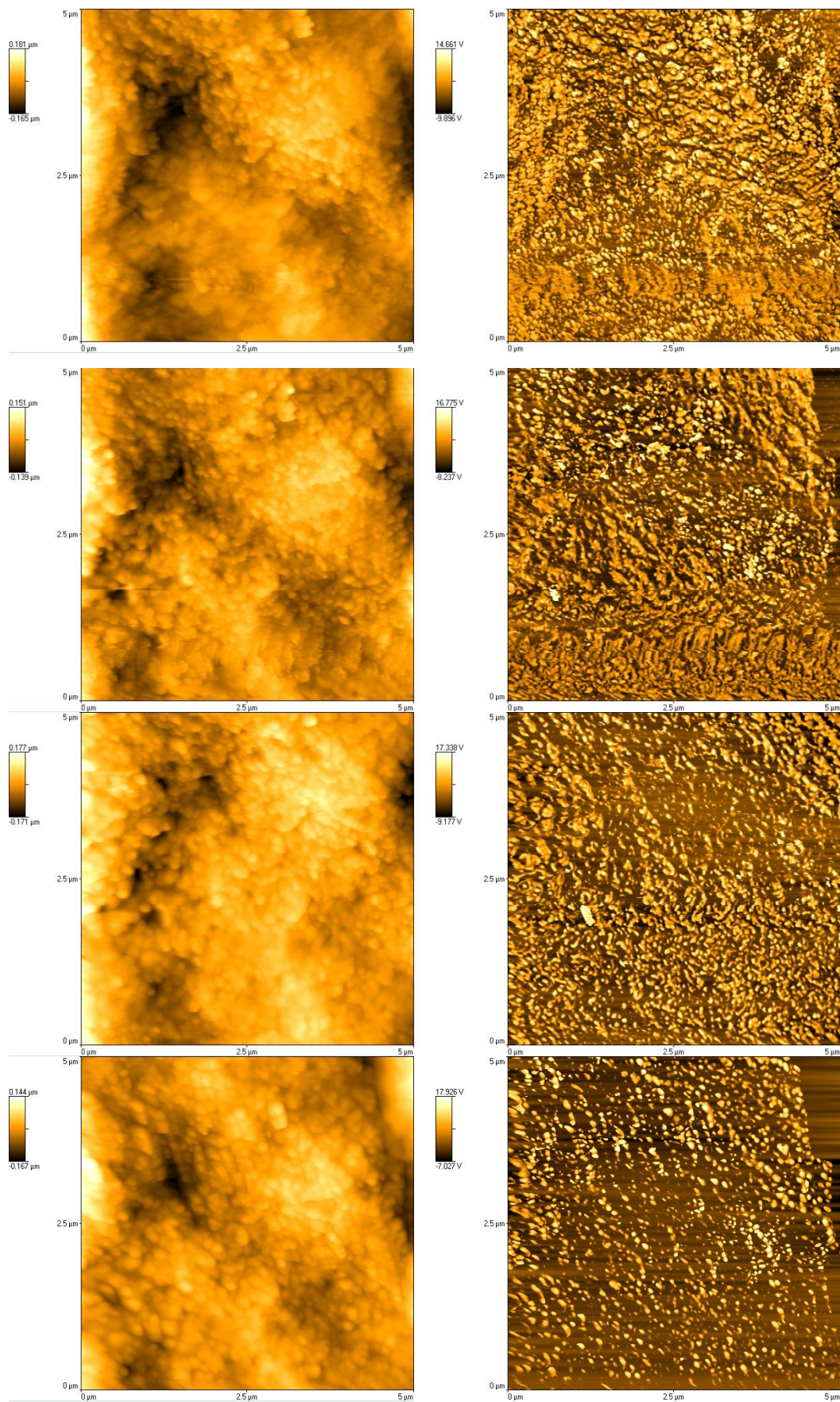


Figure 4.25 Heated Tip Tapping Mode images of a Surelease coated minitabilet (topography – left, phase image – right): From top to bottom 40°C, 50°C, 60°C and 70 °C (continues overleaf)

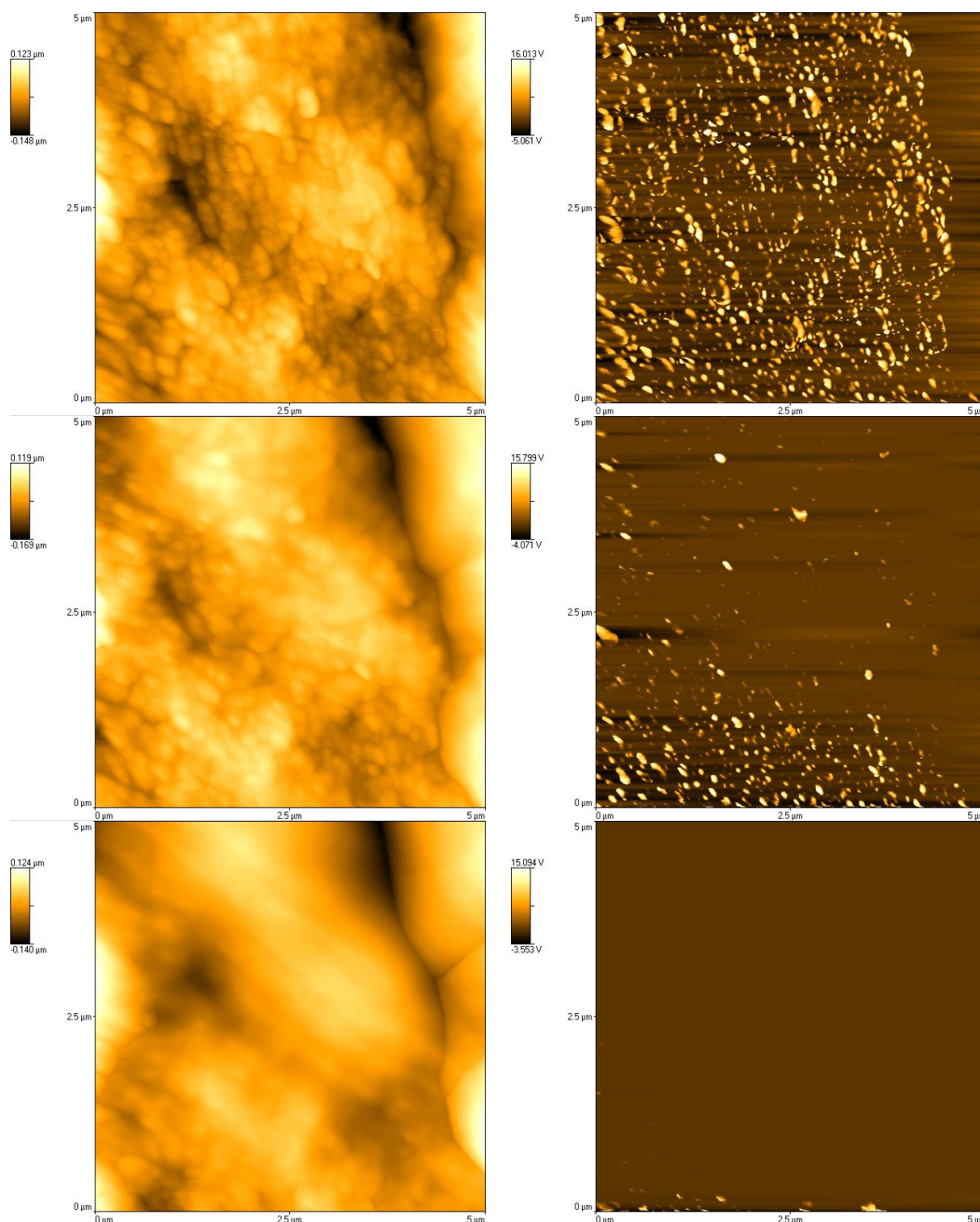


Figure 4.25 Heated Tip Tapping Mode images of a Surelease coated minitab (topography – left, phase image – right): From top to bottom 80°C, 90°C and 100°C

contamination and sample drift. Additionally the piezoelectric scanners are sensitive to temperature and the resonant frequency of the probe tends to decrease with increasing temperature (Broekmaat *et al.*, 2008). A number of these factors can be negated, such as the decrease in resonant frequency through retuning of the cantilever once the temperature of the probe tip is increased. However certain disadvantages of the technique, for example tip contamination, are inherent in heated tip experiments and need to be minimised through appropriate experimental

parameters. Apart from limited work carried out by Anasys instruments, to the author's knowledge there has been no in depth study on the use of heated tip tapping mode AFM.

A series of heated tip tapping mode images were acquired on a Surelease coated minitabket (Fig. 4.25). Compared to the contact images acquired the image size is smaller with 5 μm instead of 20 μm used. Intermittent contact modes of AFM require samples to be reasonably smooth, and the coated minitabkets in an AFM setting the roughness of the samples is relatively high requiring a smaller scan size to be able to acquire acceptable images. A 5 μm^2 area was chosen and an initial image was acquired with no voltage passed through the probe, thus obtaining the image at room temperature. A series of images were then acquired with a heated tip from 30°C increasing by 10°C per image up to 100°C.

The topography of the sample observed was considerably different to that observed in contact mode AFM, which is likely due to the lighter loading forces used in tapping mode not deforming the polymer surface, as can occur in contact mode. The topography image displays small spherical structures which are likely to relate to the pseudolatex particles.

Previous studies state the particle size of Surelease dispersions, and Surelease with up to 20% Opadry dispersed are in the region of 190nm (Rege *et al.*, 2006). Grain analysis of these spherical structures showed an average diameter of 60nm, which although smaller could be due compaction and deformation of the pseudolatex particles during drying of the film. Additionally many of the grains are not spherical due to deformation of the pseudolatex particles during film formation, which may cause errors with the computer program trying to determine the grain size.

The topography image at room temperature displays a broadly homogeneous surface, with any features complying with topographic changes. As the temperature increases the topography image appearance becomes "smoother" due to the polymer softening as the temperature approaches the T_g of Surelease, and this becomes most apparent at 100°C. As discussed in Chapter 3 softer areas of the phase image appear darker, and the phase images shows some areas becoming darker and therefore softer above

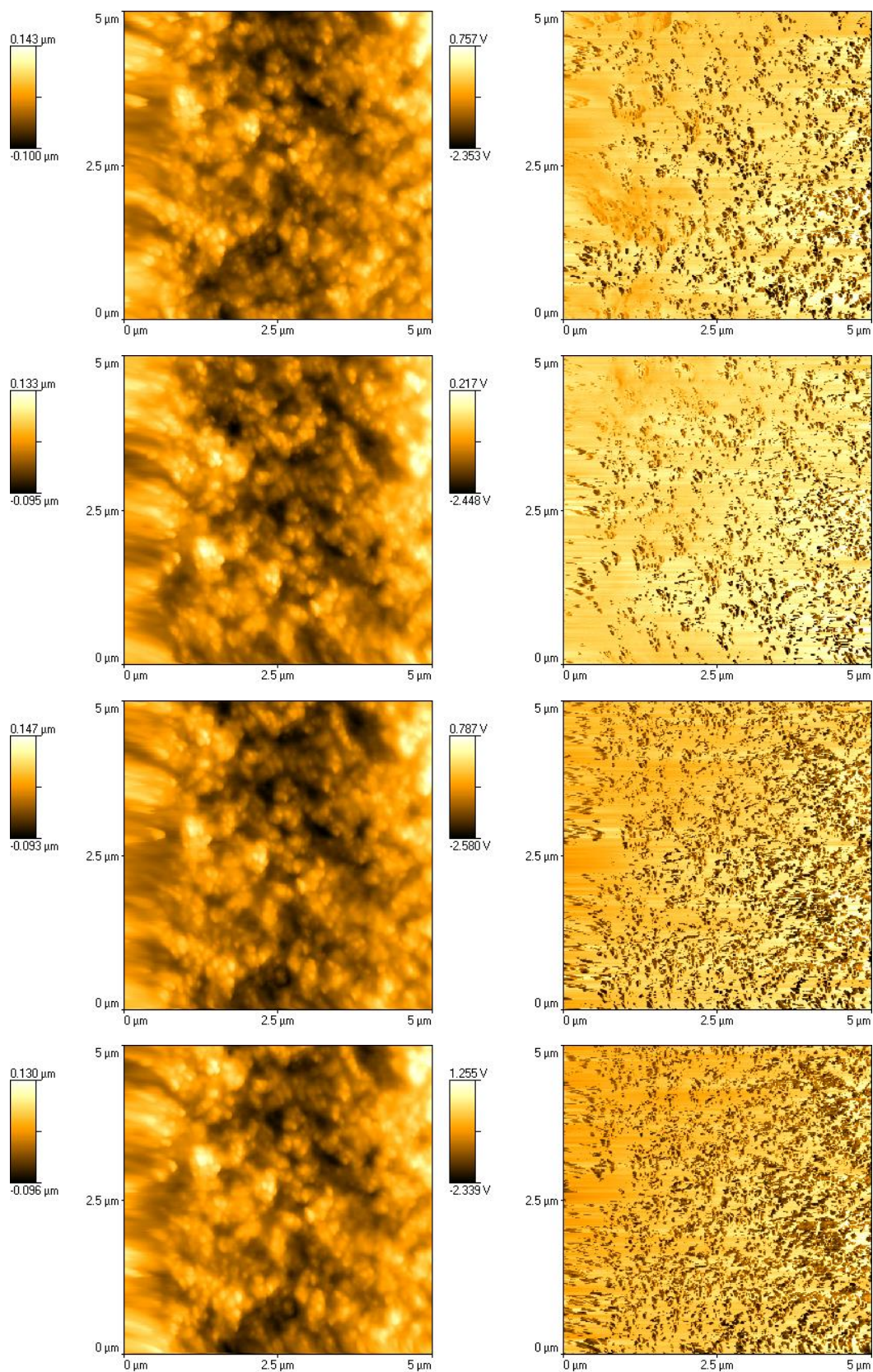


Figure 4.26 Heated Tip Tapping Mode images of a 50:50 blend of Surelease:Opadry I coated minitab (topography – left, phase image – right): From top to bottom 25°C, 70°C, 80°C and 90°C (continues overleaf)

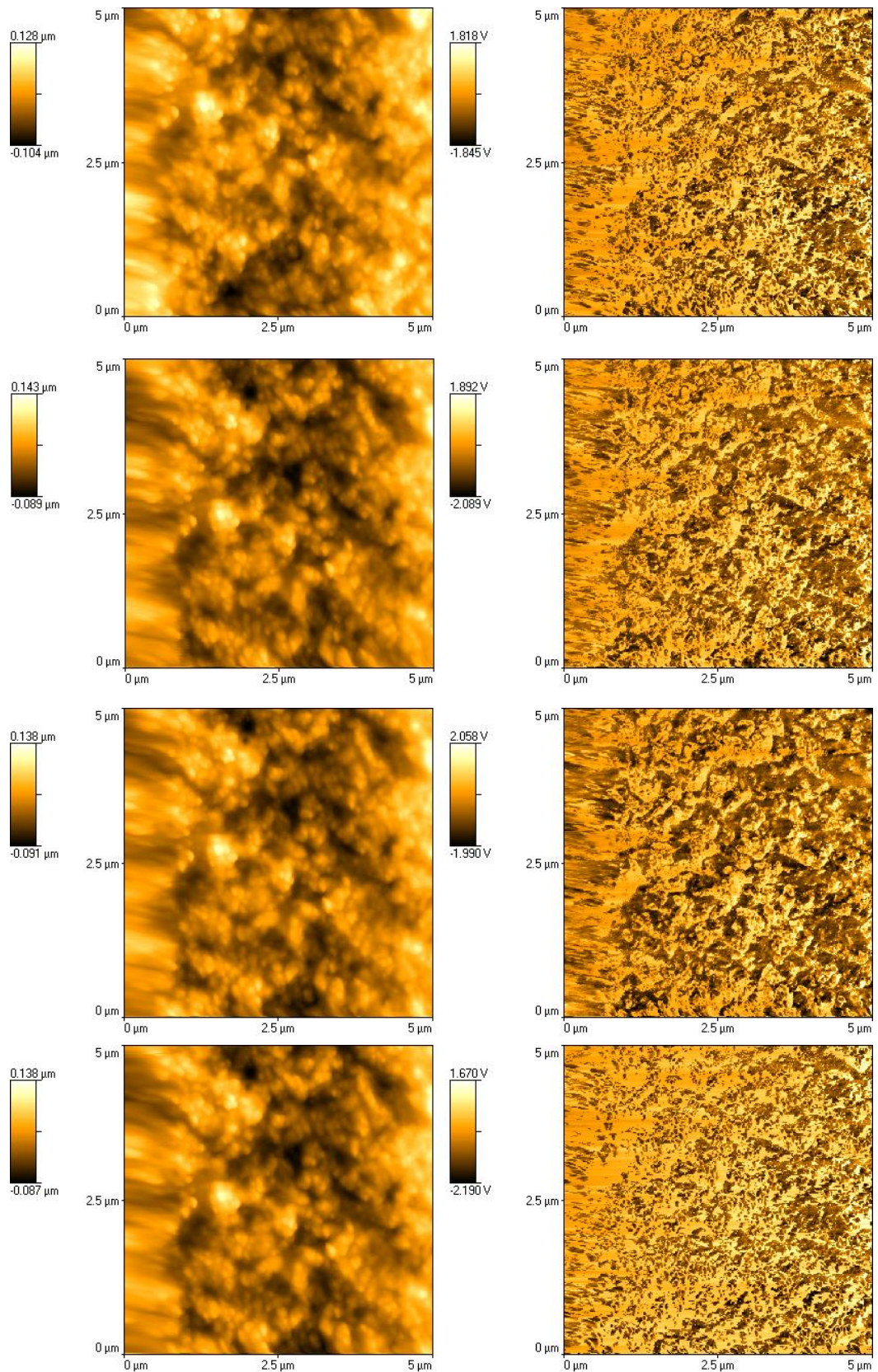


Figure 4.26 Heated Tip Tapping Mode images of a 50:50 blend of Surelease:Opadry I coated minitabiet (topography – left, phase image – right): From top to bottom 100°C, 110°C, 120°C and 130°C (continues overleaf)

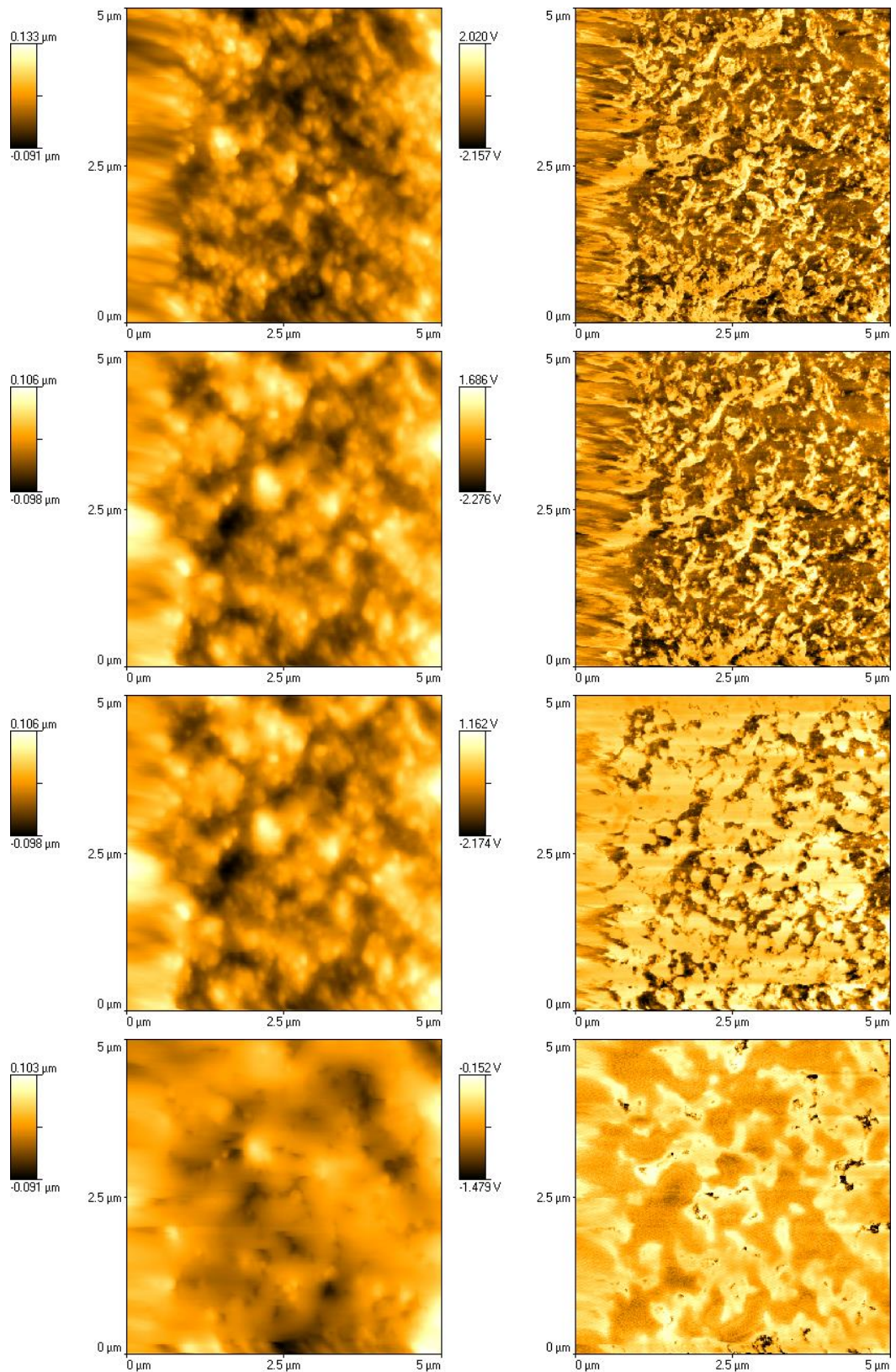


Figure 4.26 Heated Tip Tapping Mode images of a 50:50 blend of Surelease:Opadry I coated minitab (topography – left, phase image – right): From top to bottom 140°C, 150°C, 160°C and 170°C (continues overleaf)

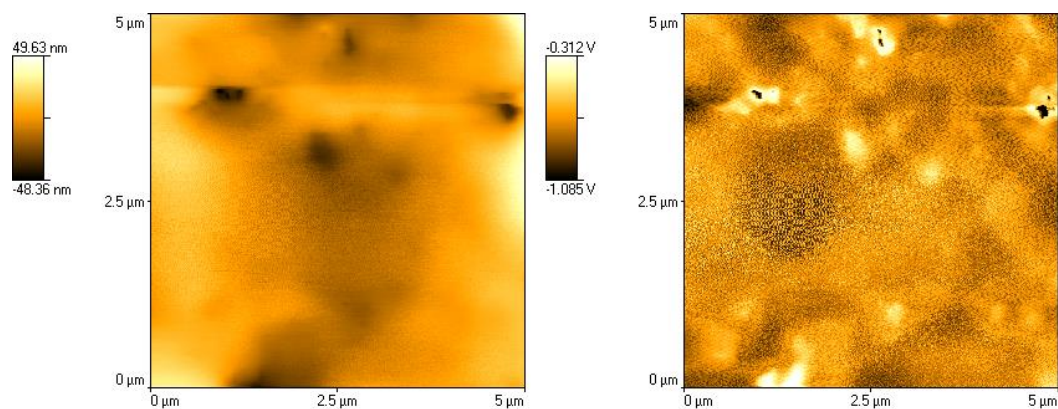


Figure 4.26 Heated Tip Tapping Mode images of a 50:50 blend of Surelease:Opadry I coated minitab. (topography – left, phase image – right): 180°C

60°C. The result is likely to be due to the polydispersive nature of polymers resulting in a spread of the glass transition.

Once the tip reaches 100°C however the majority of the sample appears to have softened, as the phase image is predominantly darker and the probe struggled to image at this elevated temperature.

Heated tip tapping mode experiments were then performed on minitab. coated with blends of Surelease and Opadry I, with the 50:50 blend seen in Fig 4.26. The darker areas would appear to represent Surelease, as this has the lowest glass transition temperature, and the lighter regions Opadry I. The darker areas of the image become more prominent as the glass transition of Surelease is approached, further indicating these areas represent Surelease. As mentioned previously a disadvantage of phase imaging techniques is sample topography influence the phase image, however of note is that the darker areas attributed to Surelease appear to bear little resemblance to the topographic features, indicating the features observed in the topographic image are likely to represent different polymer phases as opposed to the sample topography.

It can be seen that the domain size for the two phases is relatively small, with many of the phases in the sub-100 micron range. This level of scrutiny is beyond the capability of DSC and L-TMA with Wollaston probes, and is at the limit of what nano-TA probes can achieve. When performing grain analysis on the phases the

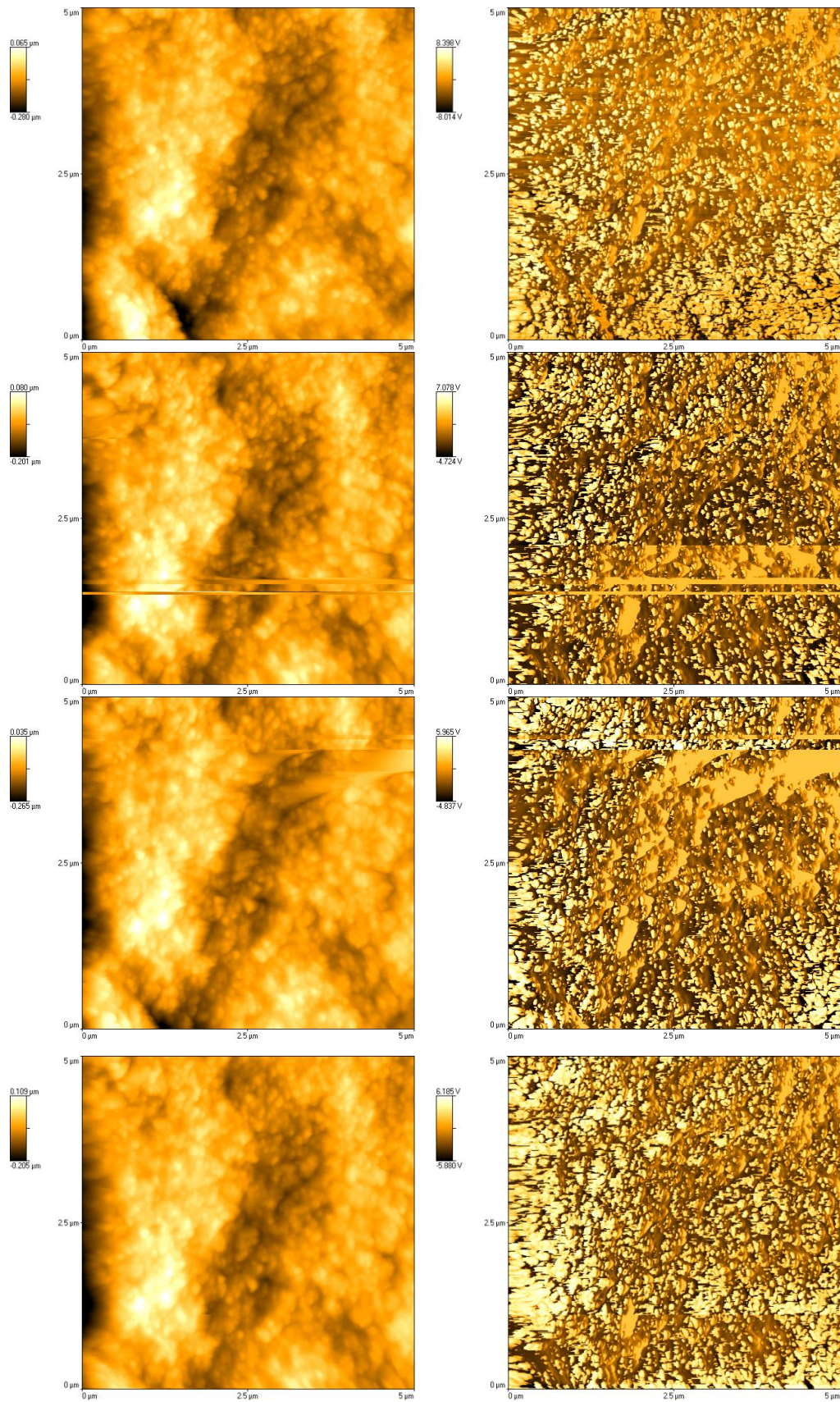


Figure 4.27 Heated Tip Tapping Mode images of a 70:30 blend of Surelease:Opadry I coated minitab (topography – left, phase image – right): From top to bottom 25°C, 70°C, 80°C and 90°C (continues overleaf)

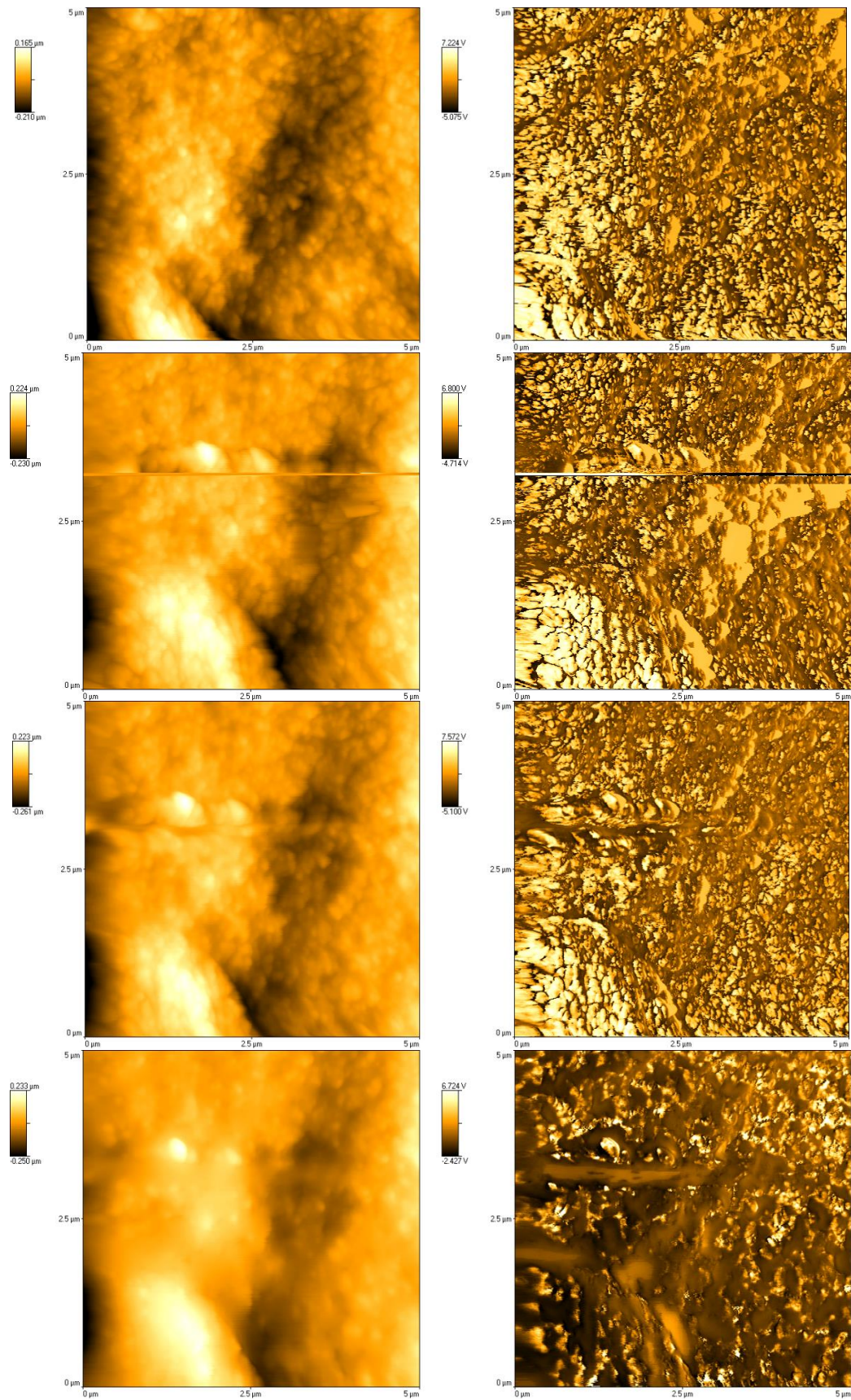


Figure 4.27 Heated Tip Tapping Mode images of a 70:30 blend of Surelease:Opadry I coated minitab (topography – left, phase image – right): From top to bottom 100°C, 110°C, 120°C and 130°C

average diameter of the phases is 20nm, thus confirming that the two polymers phase separate, but not to a sufficient degree to allow detection by traditional thermal analysis methods. These nanophases however can be resolved by the nano-TA tip in heated tip tapping mode.

Of note is the appearance that Opadry I forms the matrix and Surelease forms the “pores”. During the grain analysis of the image the area covered by Surelease was shown to be 46.4%, and is therefore probably due to this being a 50:50 mix and is highly improbable to occur at the 70:30 and 90:10.

The phase images for the 70:30 blend of Surelease and Opadry I (Fig. 4.27) shows that the Surelease has formed the matrix with Opadry I dispersed within. This is the phase distribution that must be present in controlled release coatings, as an Opadry matrix would not provide any delay in release of the drug.

Again on heating of the tip the two phases become clearer, and similar to the 50:50 blend that phases are relatively small, with grain analysis indicating an average diameter of 18nm. There does appear to be larger areas of Opadry I present however, indicating further phase separation in this blend, and this was evident in L-TMA results with a higher number of transitions associated with Opadry I present.

90:10 blends were also imaged using heated tip tapping mode, and the results are presented in Fig. 4.28. The phase image at room temperature appears to show little difference between the two polymers, although on heating the areas of Surelease and Opadry become easier to differentiate. As with the other blends the two phases appear clearest above the glass transition temperature of Surelease, which is expected as this will be when the Surelease has softened, but before Opadry I undergoes its T_g .

This shows the value of using heated tip tapping mode to differentiate between two polymers with similar mechanical properties, as if the sample was analysed in standard tapping mode the phase separation would not have been obvious.

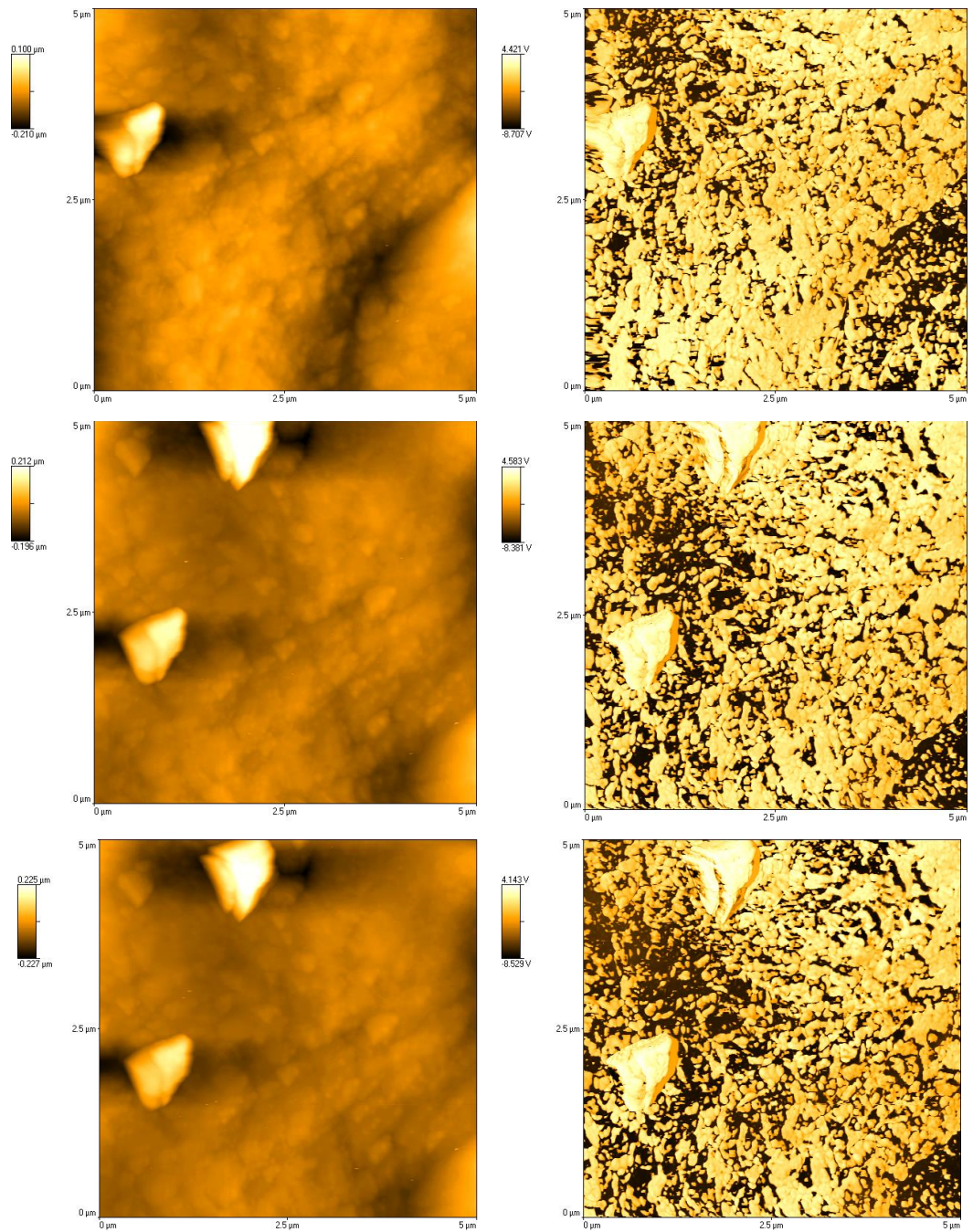


Figure 4.28 Heated Tip Tapping Mode images of a 90:10 blend of Surelease:Opadry I coated minitabilet (topography – left, phase image – right): From top to bottom 25°C, 30°C, 40°C (continues overleaf)

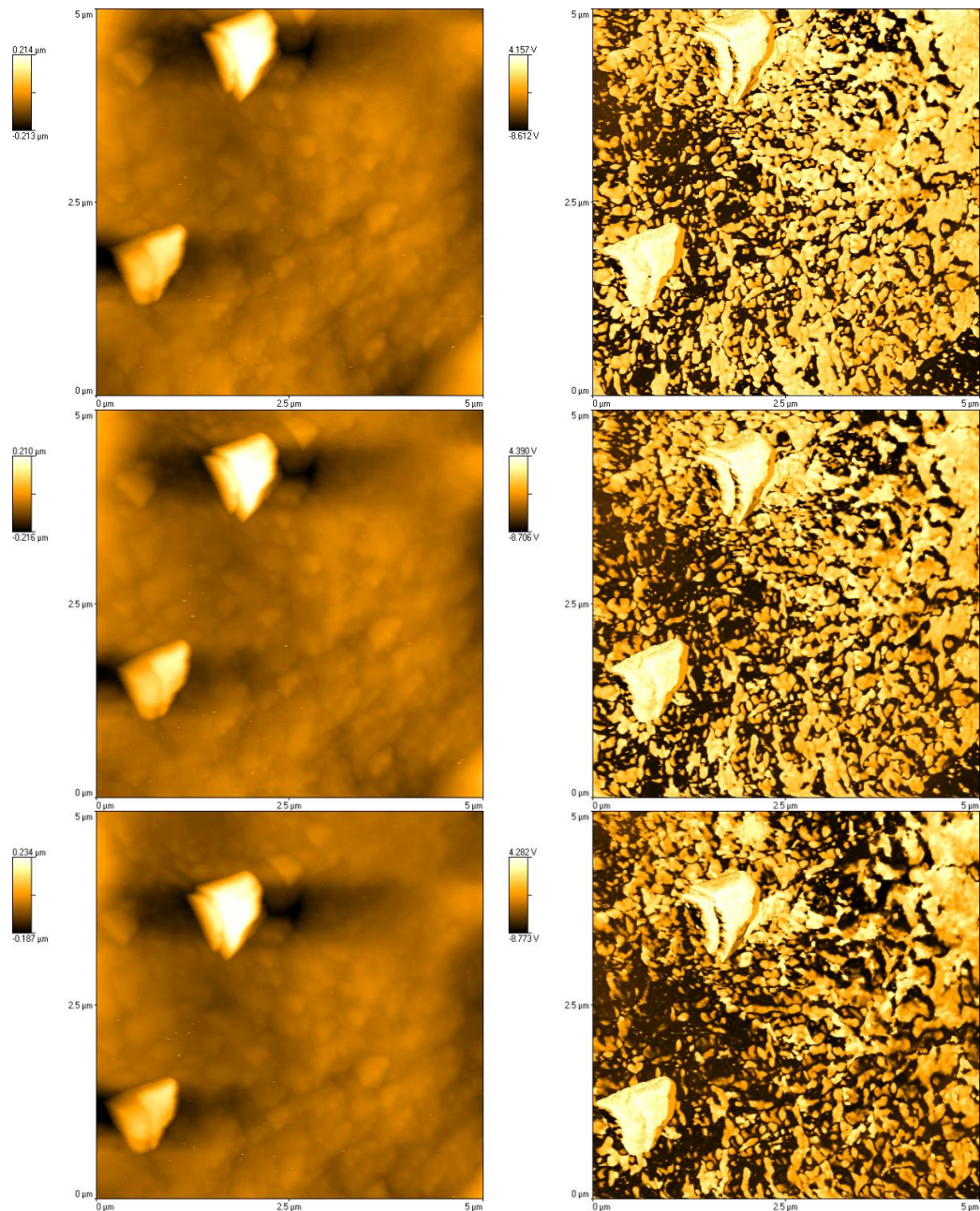


Figure 4.28 Heated Tip Tapping Mode images of a 90:10 blend of Surelease:Opadry I coated minitab (topography – left, phase image – right): From top to bottom 50°C, 60°C and 70°C (continues overleaf)

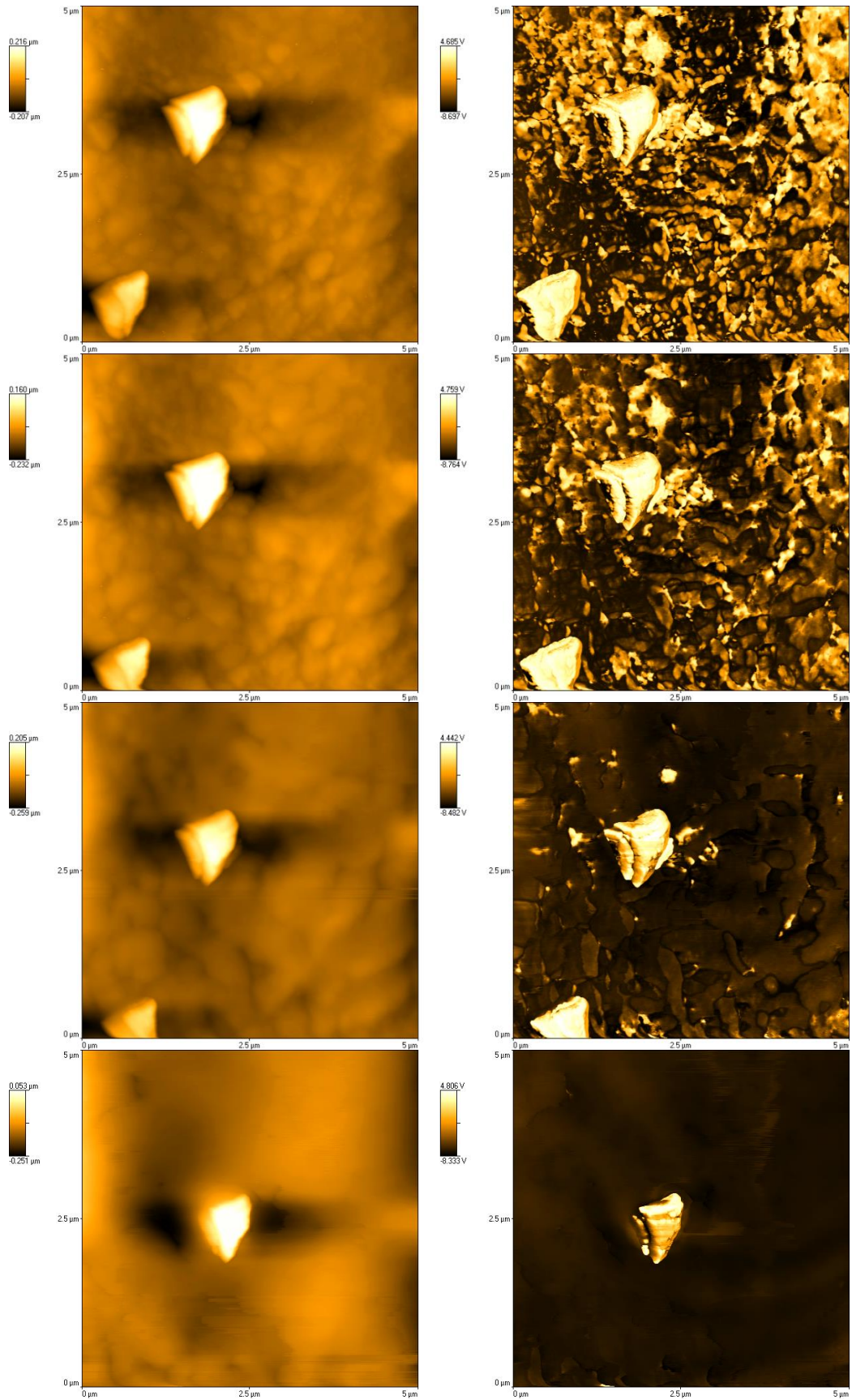


Figure 4.28 Heated Tip Tapping Mode images of a 90:10 blend of Surelease:Opadry I coated minitab (topography – left, phase image – right): From top to bottom 80°C, 90°C, 100°C and 110°C

Also of note is the large domain of Opadry I in the sample, which is larger than those seen in the other blends, and could lead to the “pores” allowing for drug release to occur, although this would need further investigation to confirm.

The movement of the suspected Opadry I could be due to the Surelease softening over its glass transition temperature, and the Opadry I freely moving. However it is more likely due to sample or probe movement when engaging and withdrawing the tip after each image, as the area moves constantly down the image at each temperature. As the probe is at an elevated temperature, when approaching the sample surface the sample may begin to soften as it is coming into contact leading to the probe making repeated attempts to enter feedback leading to differences in the location where the probe tip begins scanning the next image.

4.4.2.3 Surelease and Opadry II Film Coated Minitablets

4.4.2.3.1 Modulated Temperature DSC

Film coated minitables of Surelease and Opadry II blends were analysed in the same manner as the Surelease and Opadry I blends. It was possible to analyse the Surelease and Opadry II blends using films peeled from minitables, however there

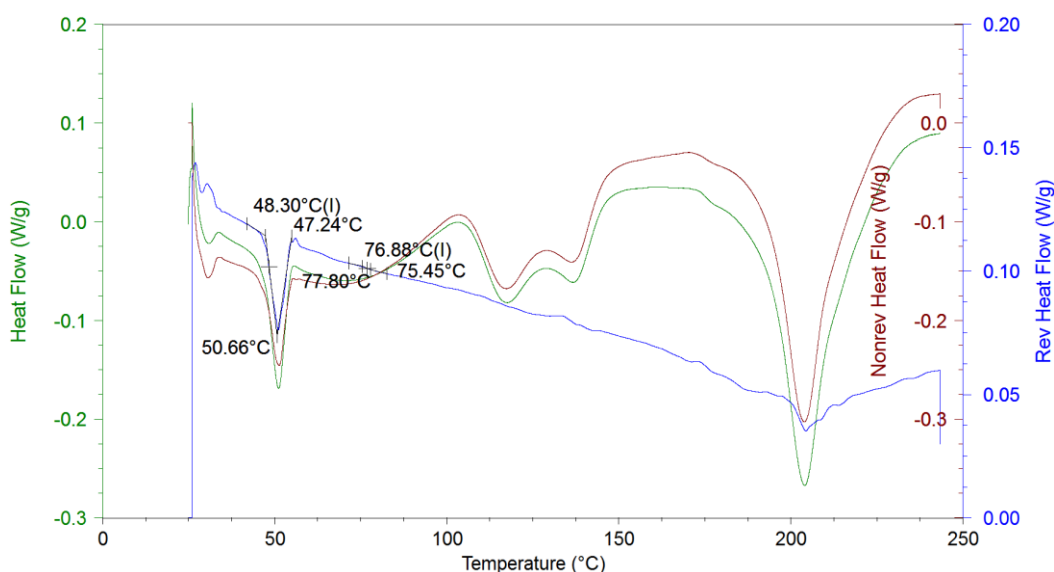


Figure 4.29 MTDSC trace of a minitabket coated with Surelease and Opadry II 50:50 blend

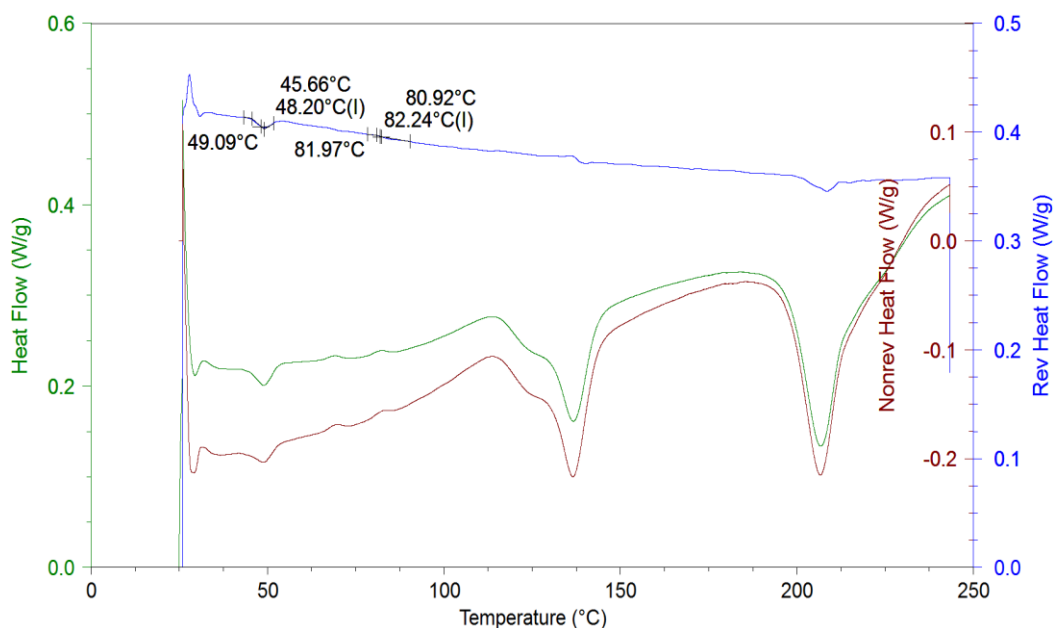


Figure 4.30 MTDSC trace of a minitabket coated with Surelease and Opadry II 70:30 blend

was considerably more residual core left on the film. This is probably due to PVA films having higher adhesion than HPMC and results in large endotherms on the MTDSC trace, leading to the melting endotherm of the crystalline part of PVA to be obscured.

However the glass transition of PVA can be observed and for the 50:50 blend of Surelease:Opadry II is 48.43°C ($\pm 0.82^\circ\text{C}$ sd; n=3), as shown in Fig. 4.29 This is in agreement with the values for the Opadry II coated minitabkets analysed with MTDSC, and indicates the possibility of MTDSC detecting phase separation of the two polymers. There is not a T_g present around 89°C to correspond with Surelease, however there is one at 77.98°C ($\pm 1.03^\circ\text{C}$ sd; n=3). Again this appears to be an intermediate glass transition similar to that present in the Surelease and Opadry I blends.

This intermediate transition is also present in the 70:30 and 90:10 Surelease:Opadry II blends, increasing to 82.09°C ($\pm 0.76^\circ\text{C}$ sd; n=3) and 83.02°C (± 0.30 sd; n=3) respectively, which is expected as the ratio of Surelease:Opadry II increases the T_g would be expected to increase towards that of Surelease.

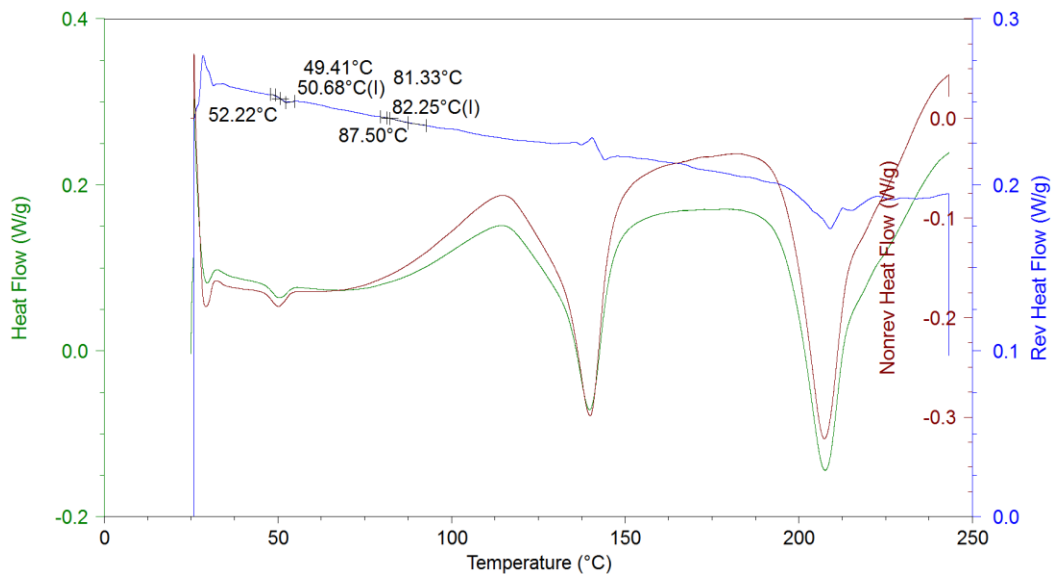


Figure 4.31 MTDSC trace of a minitabket coated with Surelease and Opadry II 90:10 blend

The glass transition of Opadry II remained around the value associated with unblended Opadry II (shown in Fig. 4.30 and 4.31) which is of note as there is no Surelease transition recorded. This may be explained by the strong glass forming properties of Surelease making the transition harder to observe, and in fact the glass transition of the intermediate value is weaker than that observed for Opadry II.

This leads to the same conclusions as with the Surelease:Opadry I film coated minitabkets, with MTDSC indicating partially miscibility of Surelease:Opadry II blends, due to the presence of an T_g at a value for the individual polymers and an intermediate T_g .

4.4.2.3.2 Localised Thermomechanical Analysis

The L-TMA results of Surelease:Opadry II blends produced similar results to the MTDSC, with a glass transition seen for Opadry II and an intermediate value associated with Surelease and Opadry II. However with L-TMA the melting endotherm for the crystalline part of PVA is observed as there is no interference from the tablet core.

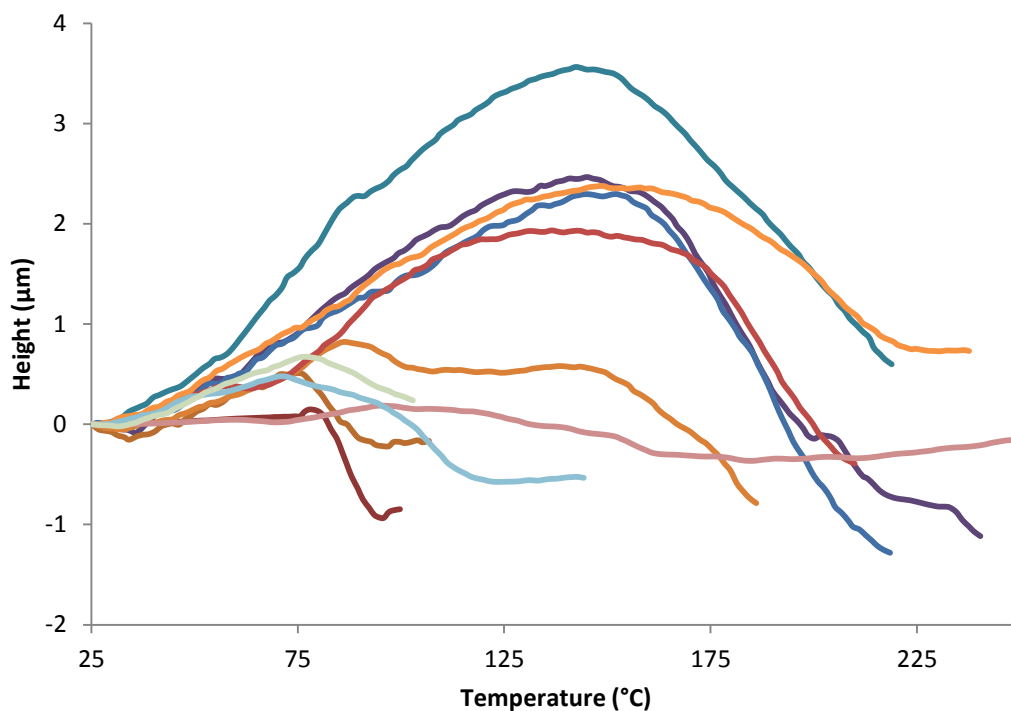


Figure 4.32 L-TMA of minitablets coated with a 50:50 Surelease:Opadry II blend

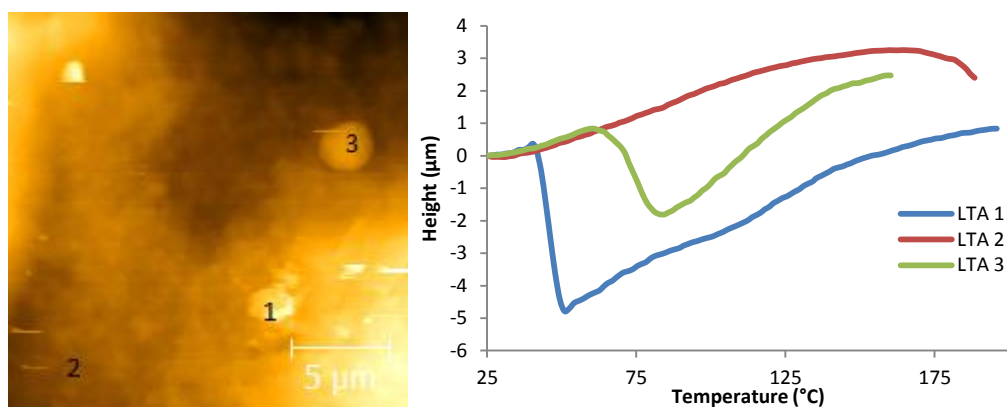


Figure 4.33 AFM contact image (left) and L-TMA results (right) for 50:50 Surelease:Opadry II blend

Additionally as with the L-TMA of Surelease:Opadry I individual traces tend to produce these results rather than all being seen in one trace as observed in MTDSC.

Results for the 50:50 blend of Surelease:Opadry are shown in fig 4.32, showing the glass transition of Opadry II to be 41.64°C (± 3.96 sd; $n=3$), and the melting point of the crystalline part as 159.90°C ($\pm 12.15^{\circ}\text{C}$ sd; $n=20$). Again the high standard deviation of this result is from the broad nature of this endotherm proving hard to determine.

Fig. 4.33 shows a contact AFM image of Surelease:Opadry II 50:50 blend with

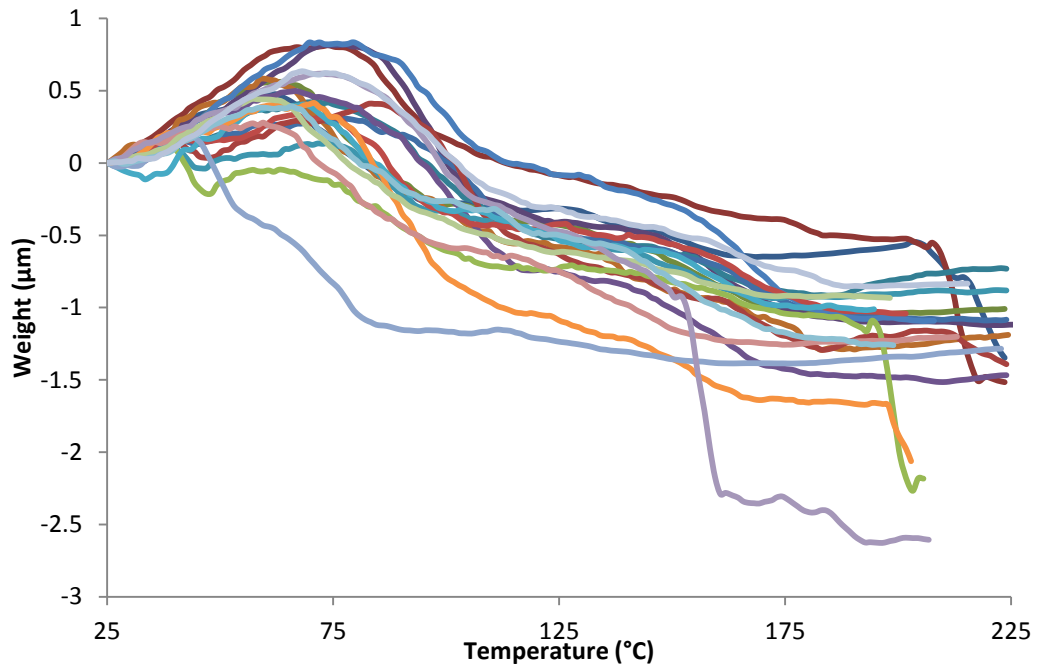


Figure 4.34 L-TMA of minitablets coated with a 70:30 Surelease:Opadry II blend

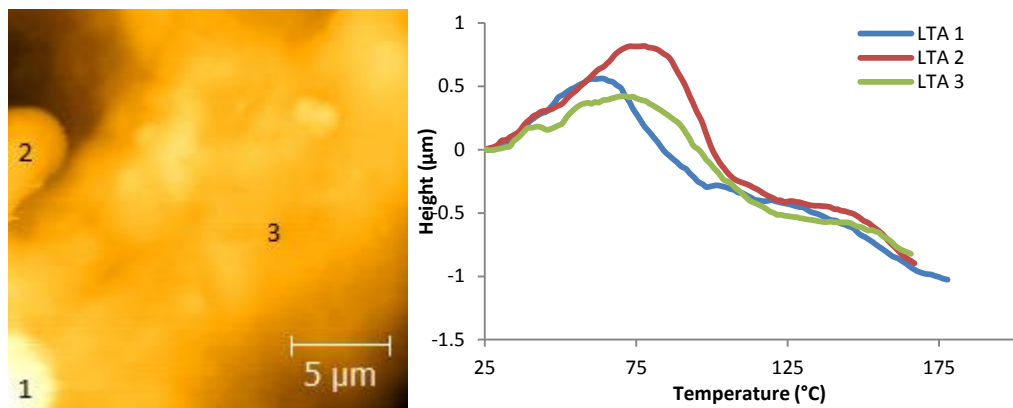


Figure 4.35 AFM contact image (left) and L-TMA results (right) for 70:30 Surelease:Opadry II blend

associated L-TMA results. The L-TMA show the different transitions observed in the sample, and although the image shows three different structures producing the differing L-TMA results this was not consistent across all images.

Also in these L-TMA results are transitions below the melting point of PVA at 119.22°C ($\pm 7.54^{\circ}\text{C}$ sd n=6). As mentioned in Chapter 3 there have been reports before (Park *et al.*, 2005) describing another polymorph of PVA produced when forming films, and this may be the case here. Unfortunately this transition cannot be observed in the MTDSC results for the film coated minitablets as an endotherm for

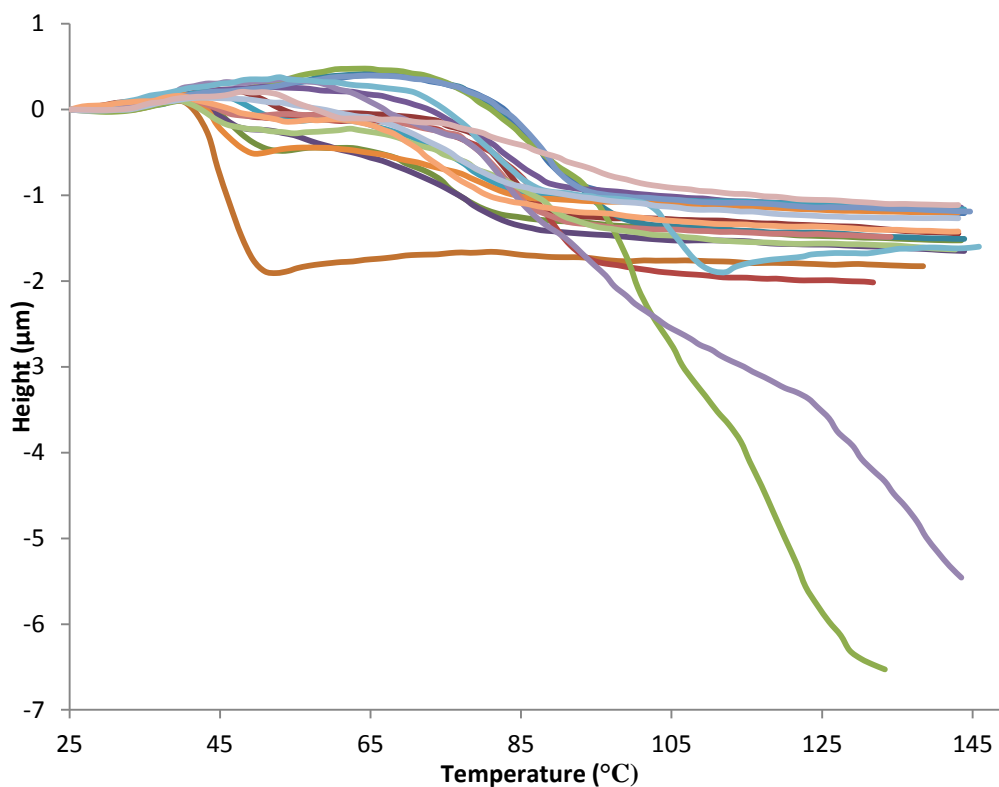


Figure 4.36 L-TMA of minitablets coated with a 90:10 Surelease:Opadry II blend

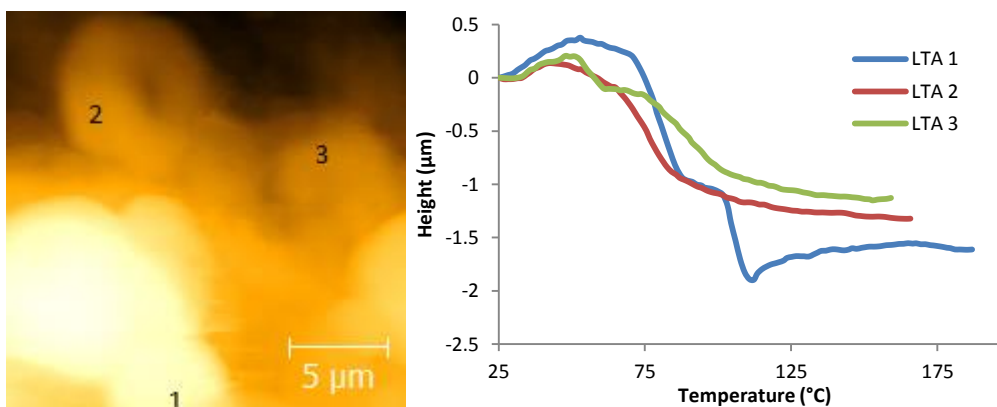


Figure 4.37 AFM contact image (left) and L-TMA results (right) for 90:10 Surelease:Opadry II blend

the tablet core obscures the region associated with this transition. It may however be possible to observe this transition in the MTDSC of Surelease and Opadry II, and it will be interesting to see if this is present or whether it is only produced during the process conditions of film coating.

As with the MTDSC results the glass transition for Opadry II stays around that observed for Opadry II coated minitablets, and the intermediate glass transition increases from 71.39°C ($\pm 6.52^{\circ}\text{C}$ sd; $n=20$) for the 50:50 blend to 73.54°C ($\pm 5.79^{\circ}\text{C}$

sd; n =20) and 74.29°C ($\pm 4.89^\circ\text{C}$ sd; n=14). Also of note is the number of transitions associated with the crystalline part of PVA, which decreases in the 70:30 and 90:10 blend, with none being observed above around 120°C in the 90:10 blend (Fig 4.36). This could be due to the increasing levels of Surelease in the blend not permitting the formation of crystalline areas.

These results as with those for Surelease and Opadry I blends analysed with MTDSC and L-TMA indicate phase miscibility. Again however it will be of interest to note the phase behaviour when analysed by heated tip tapping mode AFM to determine if similar results are produced.

4.4.2.3.3 Heated Tip Tapping Mode AFM

Interpretation of the images in heated tip tapping mode was difficult for Surelease:Opadry II blends, which is likely to be due to the glass transition temperatures of Surelease and Opadry II being relatively close together. As seen in

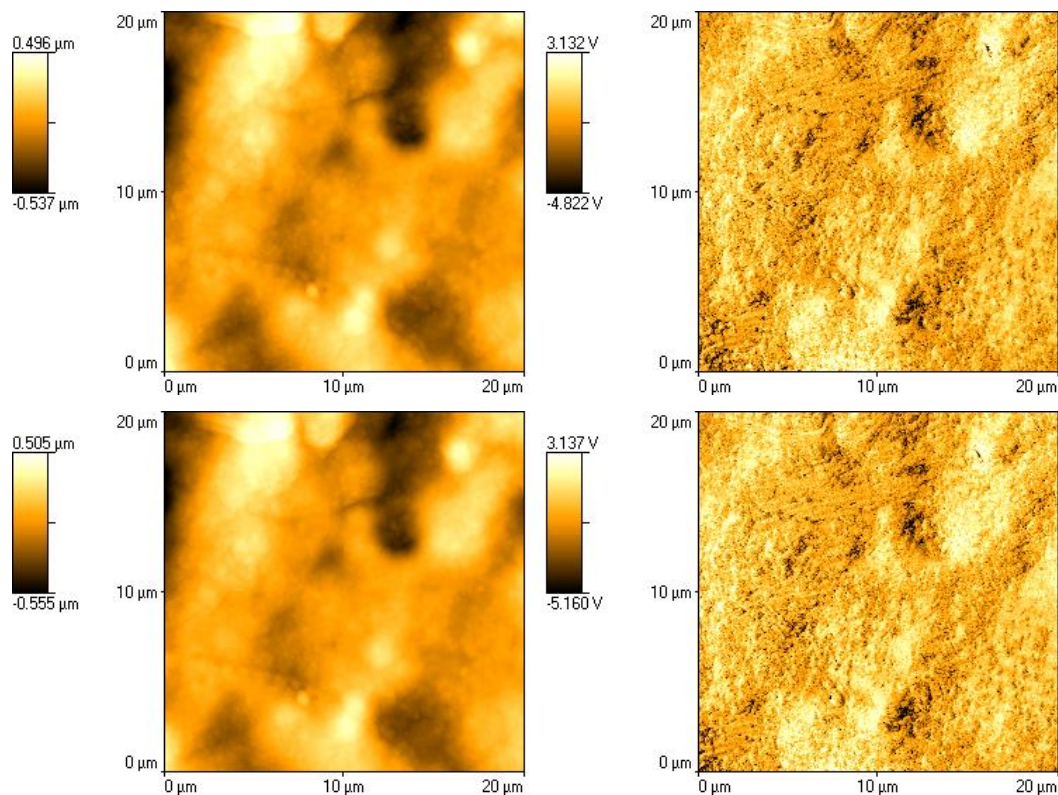


Figure 4.38 Heated Tip Tapping Mode images of a 50:50 blend of Surelease:Opadry II coated minitab (topography – left, phase image – right): From top to bottom 25°C and 30°C (continues overleaf)

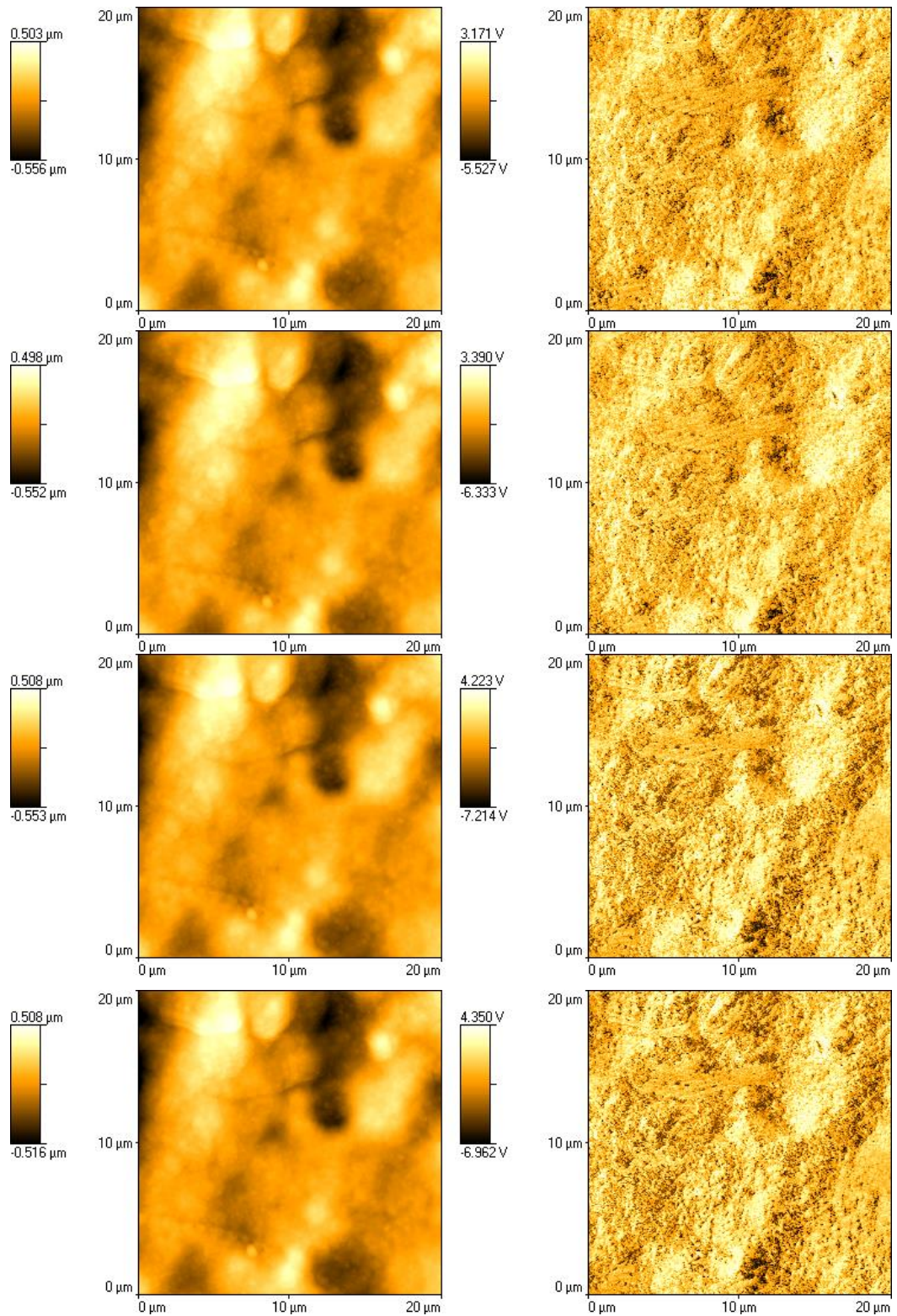


Figure 4.38 Heated Tip Tapping Mode images of a 50:50 blend of Surelease:Opadry II coated minitab (topography – left, phase image – right): From top to bottom 40°C, 50°C, 60°C and 70°C
(continues overleaf)

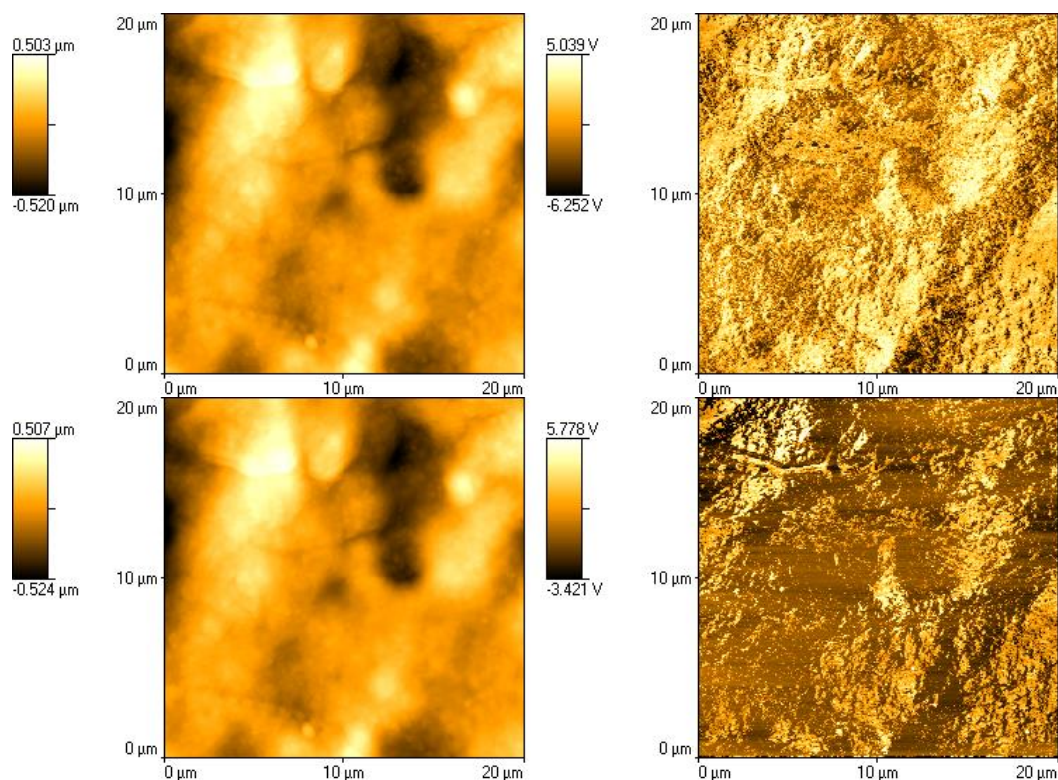


Figure 4.38 Heated Tip Tapping Mode images of a 50:50 blend of Surelease:Opadry II coated minitab (topography – left, phase image – right): From top to bottom 80°C and 90°C

the Surelease heated tip tapping mode images the Surelease started to soften at a lower temperature than its glass transition, meaning in the Surelease:Opadry II blend the softening of the glassy part of the Opadry II is obscured by the Surelease glass transition.

This points to a potential limitation of the technique, but this is a limitation common with other thermal analysis techniques when thermal transitions overlap and interfere with each other.

There is information to be gathered from the series of images in Fig. 4.38 however. At 90°C the Surelease appears to have softened but there still appears to be some relatively hard areas on the image. These light areas are likely to represent areas of crystalline PVA in Opadry II, with areas appearing large enough to be detected by L-TMA, and there were a number of L-TMA traces of Surelease:Opadry II blends showing one transition associated with crystalline melting of Opadry II.

4.4.2.4 FTIR of Film Coated Minitablets

To further the understanding of the interactions between EC and HPMC, FTIR spectroscopy was performed on the coated minitables. As discussed in FTIR spectroscopy has the advantage of being able to perform in-situ analysis of materials due to the principle requirement of satisfactory measurement of samples is a good contact with the ATR crystal. Additionally as ATR-FTIR is a reflectance measurement minimum sample preparation is necessary with no requirement for solvent casting, grinding or pressing, as is the case in transmission experiments. However as it produces spectra of the whole surface in contact with the ATR crystal, no spatially resolved information is produced.

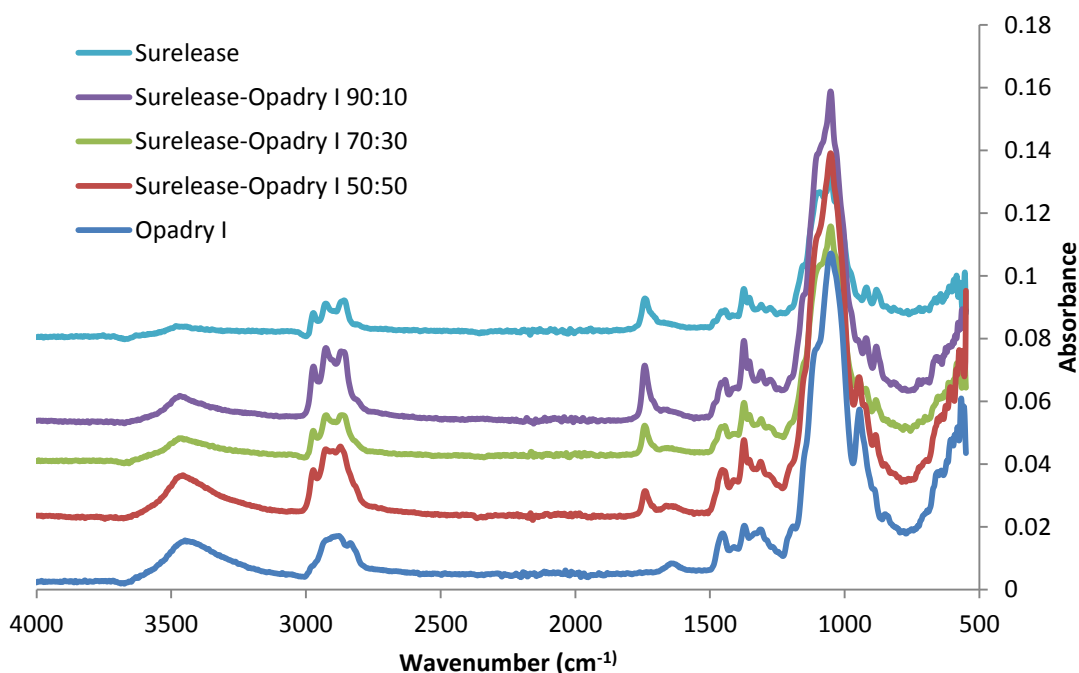


Figure 4.39 FTIR Spectra of minitables coated with Surelease, Opadry I and their blends

Fig. 4.39 shows FTIR spectra of minitables coated with Surelease, Opadry I and Surelease-Opadry I 50:50, 70:30 and 90:10 blends which shows no major shifts or additional peaks in the blends. The main type of interaction that is likely to be present in the blends is hydrogen bonding between hydroxyl groups which are present in both the polymers (Robeson, 2007). Stretching of hydrogen bonded hydroxyl groups occur between 3200-3600 cm⁻¹, and are usually present as a broad peak (Meaurio *et al.*, 1997). There is a peak observable in this range for the

Surelease and Opadry I and their blends with no discernible shift or additional in values between the blends. The intensity of the peak diminishes with increasing Surelease content, which is likely to be due to a decrease in bonding present between HPMC molecules owing to the decrease in Opadry I content.

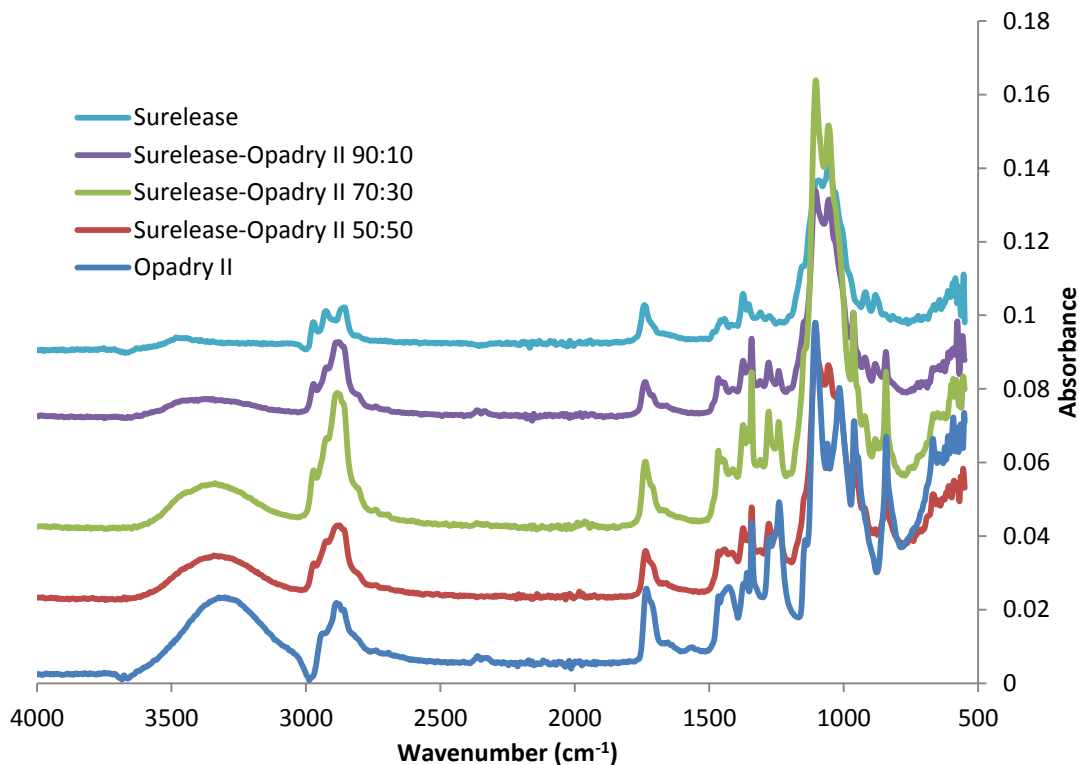


Figure 4.40 FTIR Spectra of minitables coated with Surelease, Opadry II and their blends

The spectra of Surelease, Opadry II and the blends of Surelease-Opadry II 50:50, 70:30 and 90:10 are shown in Fig 4.40 displaying no additional peaks of the blends. However the hydrogen bond peak present in the Opadry II spectra at 3320cm^{-1} does appear to shift towards the Surelease peak measured at 3470cm^{-1} with considerable flattening of the peak occurring too between the 50:50 and 90:10 blend. However on closer inspection of the Spectra for the 90:10 Surelease-Opadry II blend, shown in Fig 4.41, there appears to be two peaks present in the $3200\text{-}3600\text{cm}^{-1}$ range with one peak around 3470cm^{-1} and the other 3325cm^{-1} . The presence of two peaks is likely to give rise to the appearance of the peak becoming flatter with the close proximity of the peaks associated with Surelease and Opadry II not being possible to differentiate

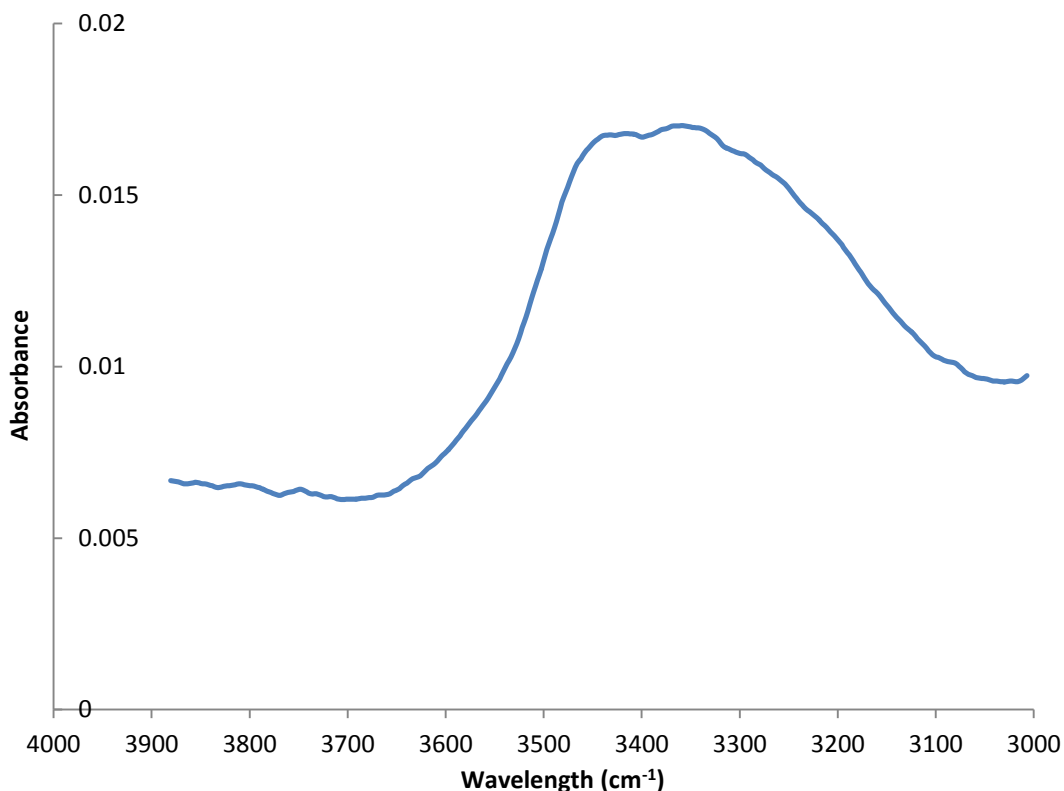


Figure 4.41 FTIR spectra of Surelease-Opadry II 50:50 blend from 3000cm⁻¹ to 3900cm⁻¹

by the FTIR. The magnitude of the Opadry II peak compared to that of Surelease is also likely to hinder the observation of two distinct peaks, with the Opadry II response masking that of the more modest peak of Surelease. Therefore there is unlikely to be significant interaction occurring between Surelease and Opadry II.

4.4.3 Analysis of Cast Free Films

4.4.3.1 Analysis of Surelease and Opadry I Cast Films

Cast films of the polymer blend were analysed in the same manner as the minitables, with MTDSC and L-TMA employed with the aim to determine the film blend morphology. As discussed above the different process conditions involved in producing cast free films compared to film coated minitables produced different surface morphologies in films of the individual polymers. Therefore it would be expected that differences will also be observed between cast free films and film coated minitables with polymer blends.

4.4.3.1.1 Localised Thermomechanical Analysis

Results for Surelease-Opadry I 50:50 blend are shown in Fig. 4.42 and although there still appears to be a T_g mix present at 152.33°C ($\pm 5.12^\circ\text{C}$ sd; $n=15$) on the L-

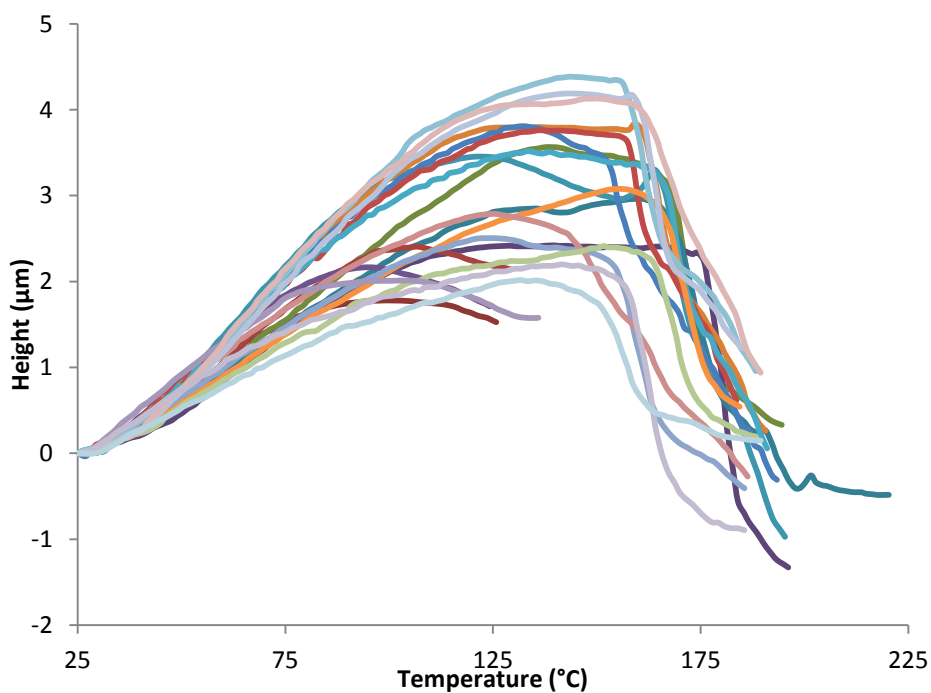


Figure 4.42 L-TMA of cast films of a 50:50 Surelease:Opadry blend

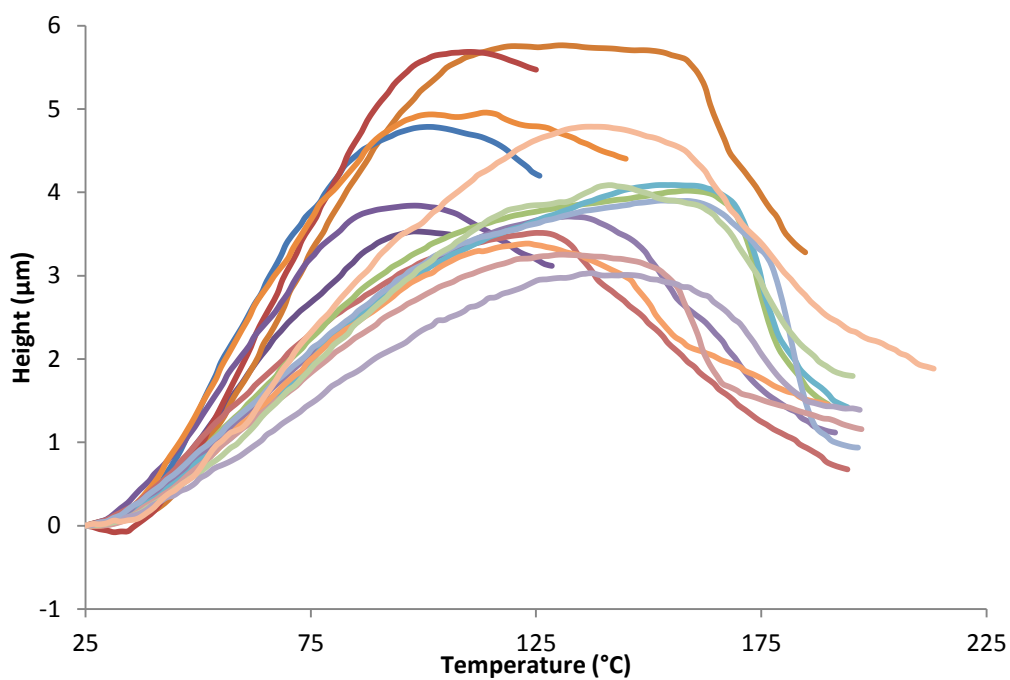


Figure 4.43 L-TMA of cast films of a 70:30 Surelease:Opadry blend

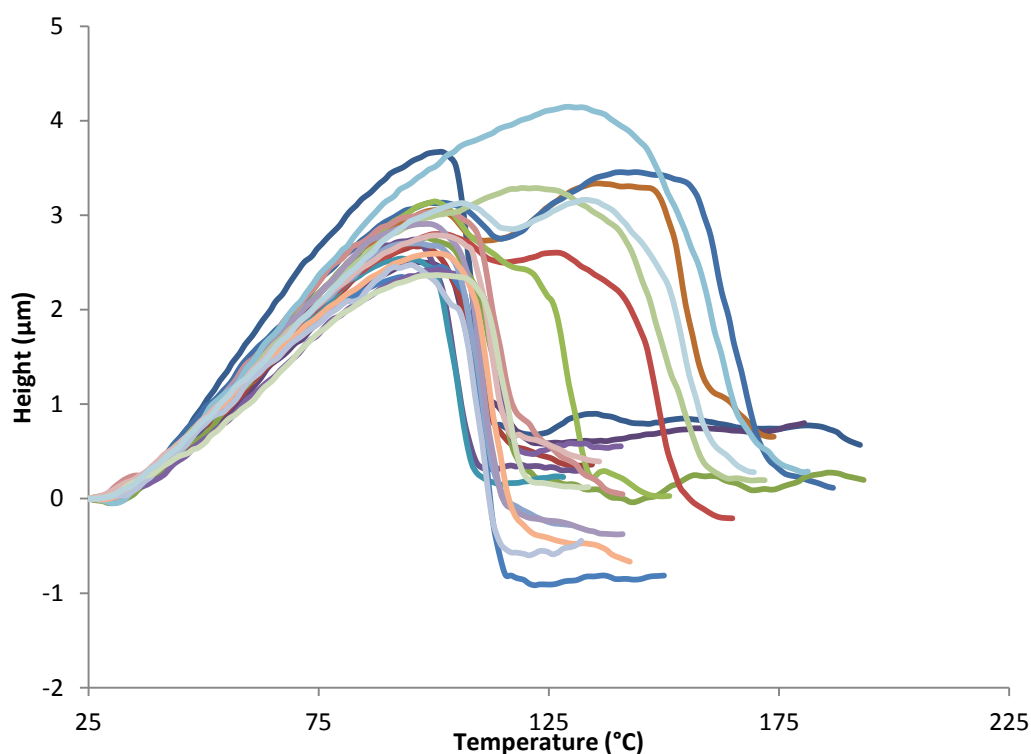


Figure 4.44 L-TMA of cast films of a 90:10 Surelease:Opadry blend

TMA results, there are also more transitions associated with just Surelease or Opadry I. When minitables coated with the 50:50 blend of Surelease and Opadry I were analysed by L-TMA out of 30 L-TMA experiments 3 transitions were associated with Opadry I, but in the cast film there were 8 transitions.

This result is also true for the 70:30 blend and 90:10 blend (shown in Fig. 4.43 and 4.44, with this most noticeable on the 90:10 blend, with a clear separation observed between the two polymer transitions.

4.4.3.1.2 Modulated Temperature DSC

MTDSC results showed similar information with the individual polymers more prominent on the MTDSC trace than in the film coated minitables. The films however are inherently easier to analyse on MTDSC as there was a greater weight of film present in the pan, with a better contact on the base and no residual tablet core present. This allows for easier detection of the subtle glass transitions such as those associated with strong glass formers or small levels of polymer, as present in these samples.

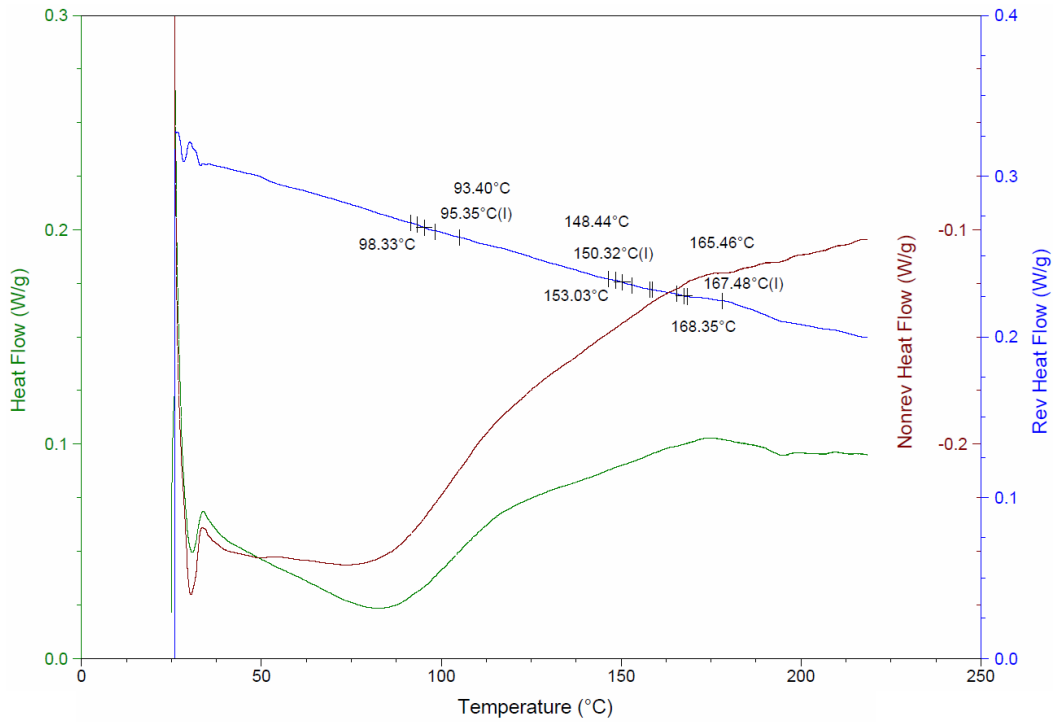


Figure 4.45 MTDSC trace of cast films of a Surelease and Opadry 50:50 blend

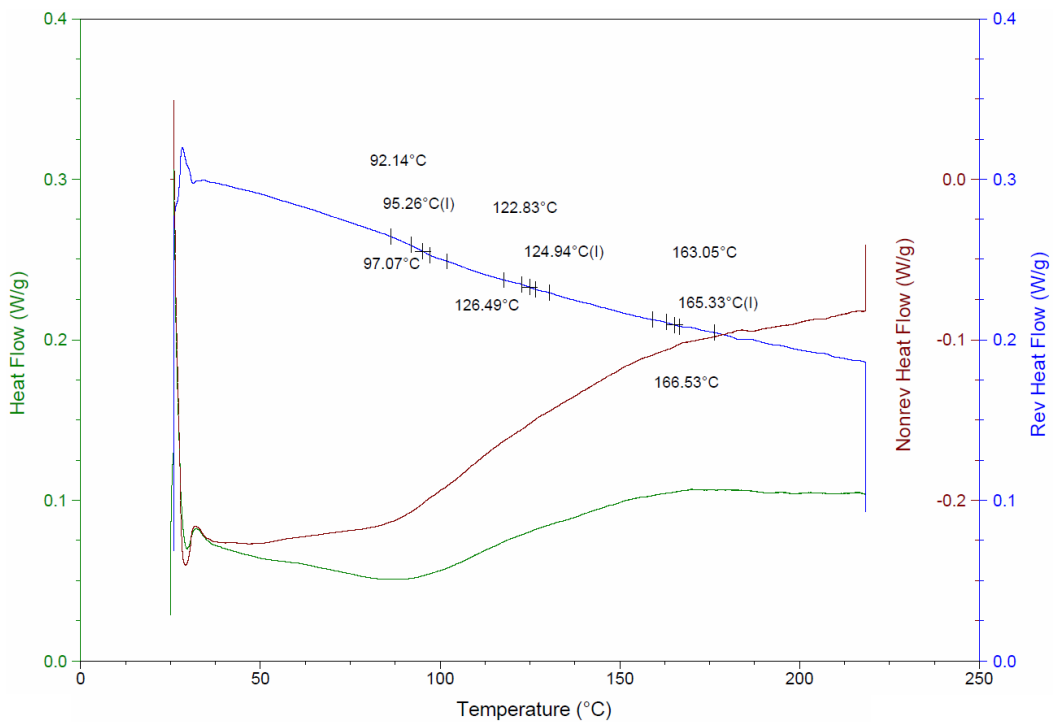


Figure 4.46 MTDSC trace of cast films of a Surelease and Opadry 70:30 blend

Similar transitions were observed for the cast films as were seen with the film coated minitables, with the two discrete transitions observed for Surelease and Opadry I, plus an intermediate transition temperature. The biggest discontinuation from the peeled films was the larger residual water endotherm in the nonreversing heat flow.

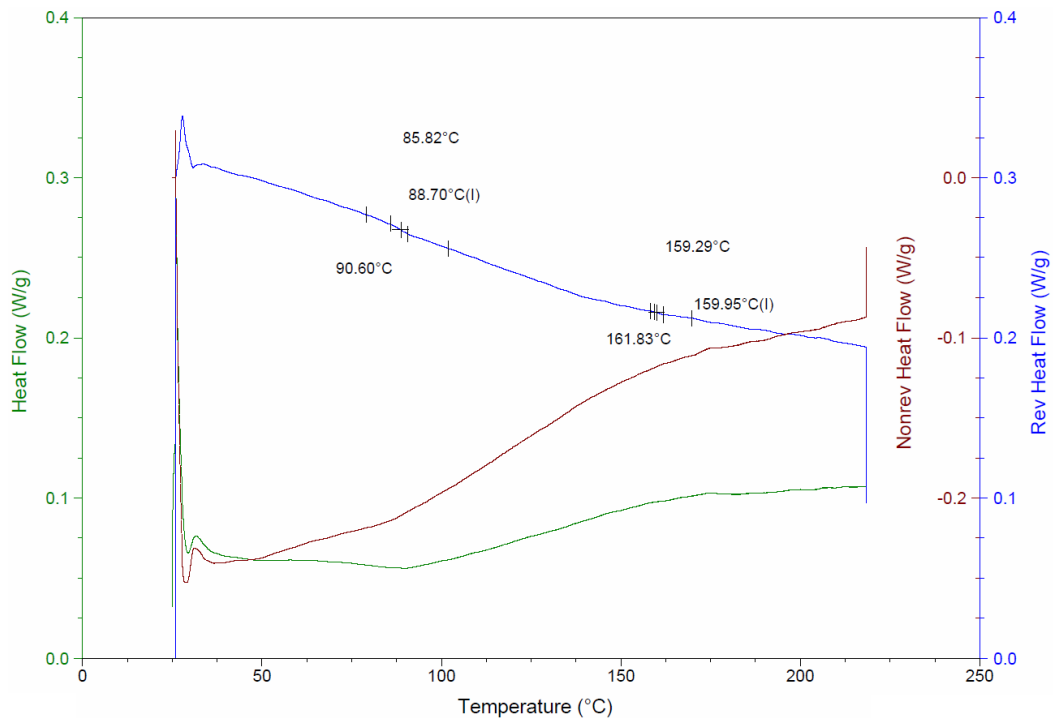


Figure 4.47 MTDSC trace of cast films of a Surelease and Opadry 90:10 blend

This is a result of the method of film preparation as cast films tend to have increased levels of residual water, which as water acts as a plasticiser can artificially lower the glass transition temperature.

Additionally there is no interference from the minitables core with the films being peeled from the relatively inert Petri dish compared to the minitables core, therefore making transitions around 130°C easier to discern.

These results highlight an advantage of thermal probe methods as opposed to MTDSC, with MTDSC detecting broadly the same transitions as seen with the peeled films from coated minitables. However the results observed with L-TMA show a difference in the distribution of the transitions with more observed for Surelease and Opadry I. Especially with such subtle glass transitions this information is difficult to discern from MTDSC data.

4.4.3.1.3 Heated Tip Tapping Mode AFM

The figure below shows heated tip tapping mode performed on a cast film of 50:50 Surelease:Opadry I. Even from the image at room temperature the phase image shows a marked difference to that of the film coated minitabilet with the same blend. Larger domains are seen for Surelease, and once the tip is heated with each subsequent image displaying a better contrast between the two films.

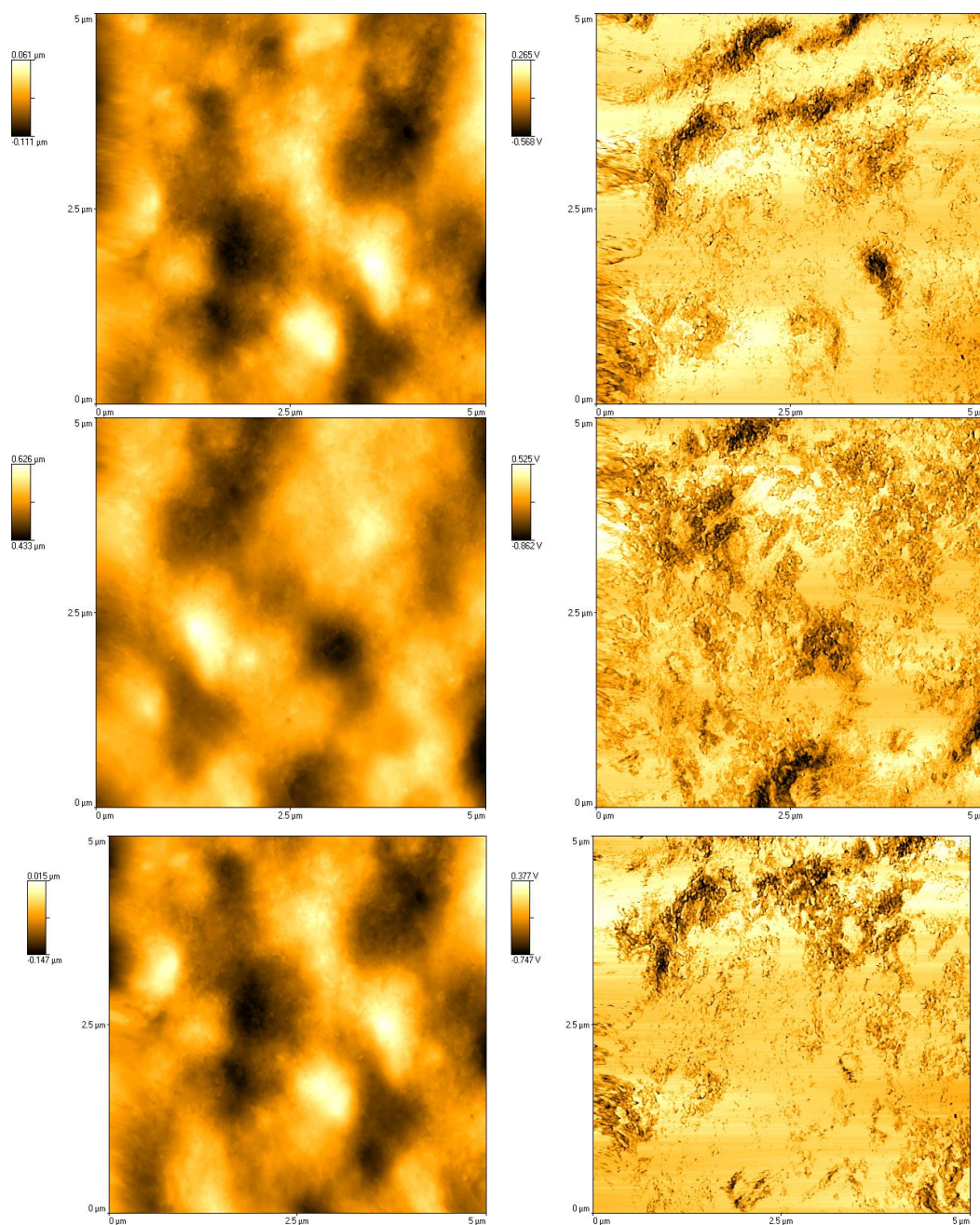


Figure 4.48 Heated Tip Tapping Mode images of a 50:50 blend of Surelease:Opadry I cast film (topography – left, phase – right): From top to bottom 25°C, 70°C and 80°C (continues overleaf)

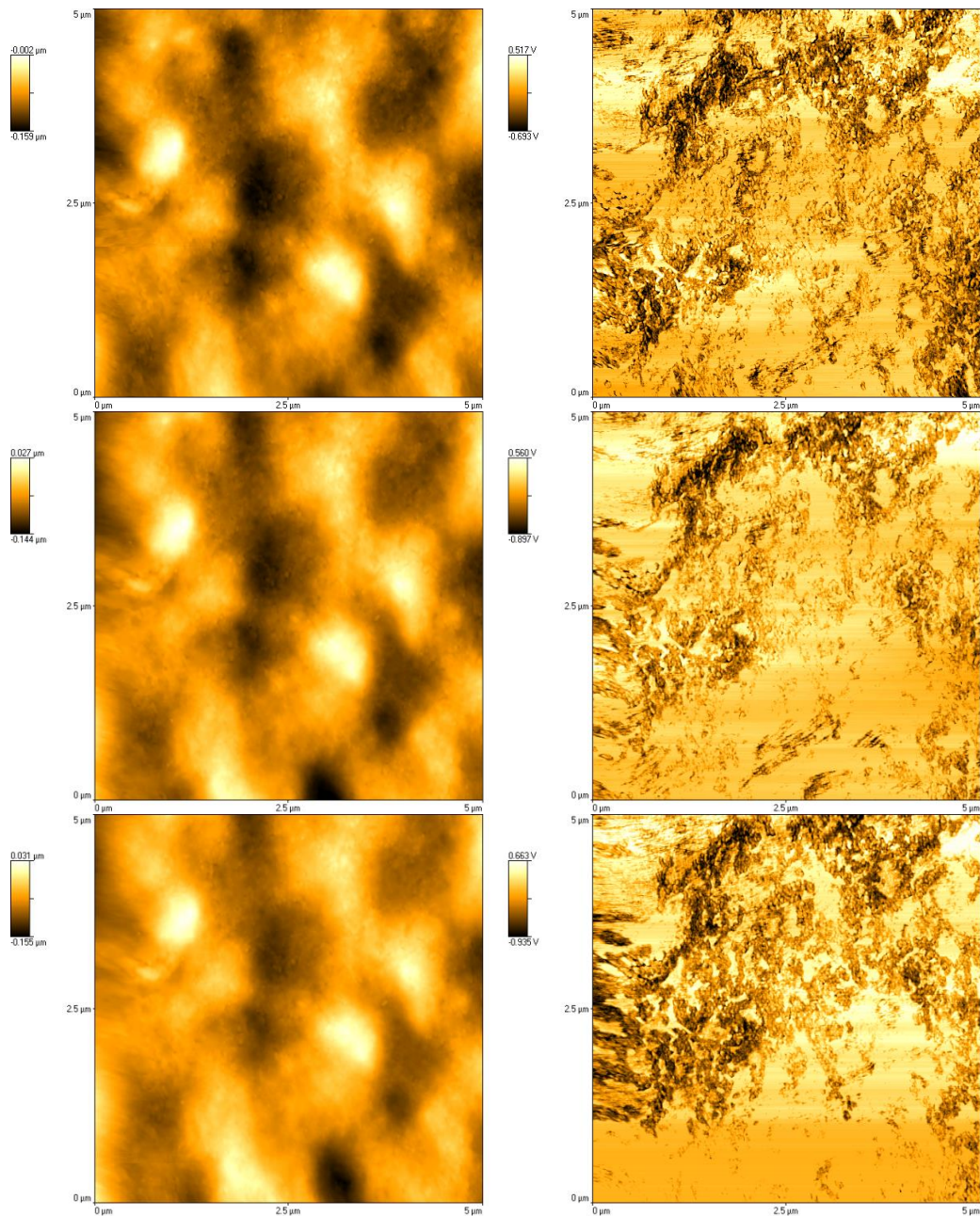


Figure 4.48 Heated Tip Tapping Mode images of a 50:50 blend of Surelease:Opadry I cast film (topography – left, phase image – right): From top to bottom, 90°C, 100°C and 110°C (continues overleaf)

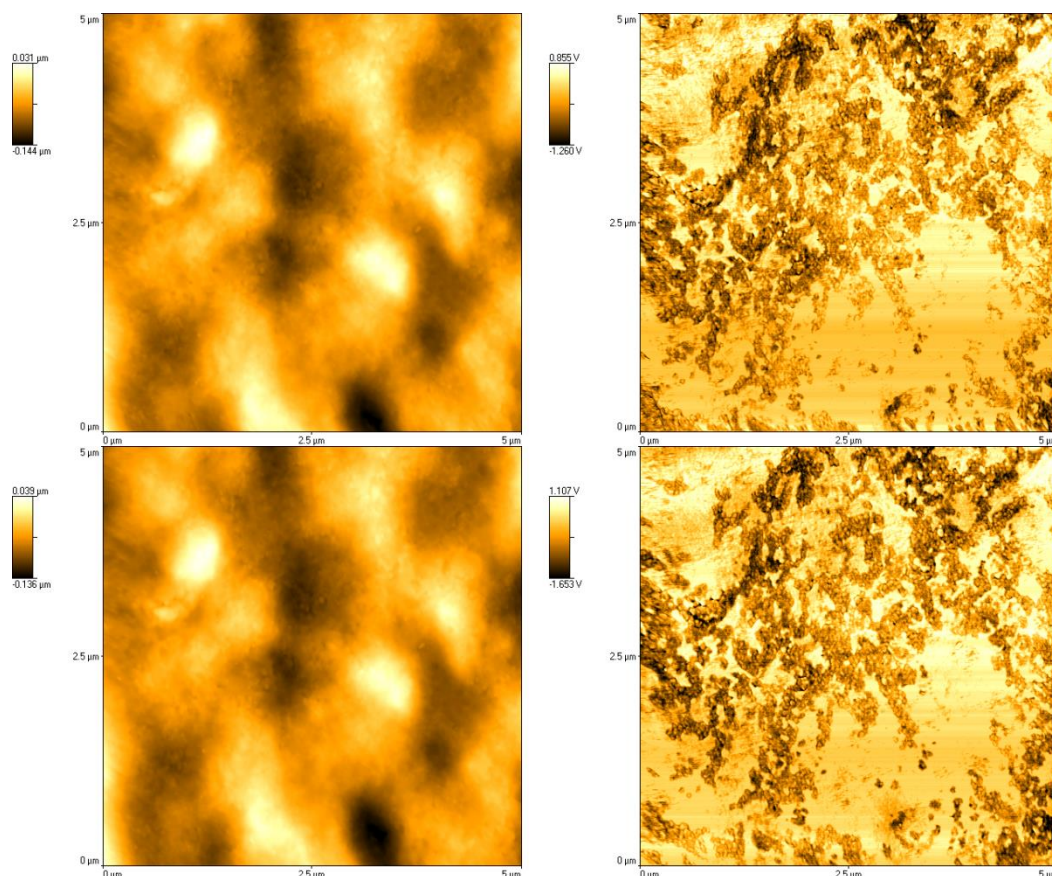


Figure 4.48 Heated Tip Tapping Mode images of a 50:50 blend of Surelease:Opadry I cast film (topography – left, phase image – right): From top to bottom 120°C and 130°C

The most likely explanation for this is the respective drying times of the two preparation methods. When spray coating films the drying times are considerably shorter than when casting films. The cast films tend to take around 12 hours to dry, whereas when spray coating the drying time is completed in minutes. As phase separation is based on nucleation and growth or spinodal decomposition the growth of phases is a time dependent process, therefore the longer the drying time the greater the domain sizes should be.

Drying rate is determined predominantly by the rate of heat transfer from the air to the solvent due to the thin nature of polymer film coats. This leads to the drying rate being determined by the latent heat of vaporisation of the solvent, the surface area of the substrate and the velocity of the drying air.

During spray coating the latent heat of vaporisation will remain the same but the surface area will increase due to the nature of the substrate being coated compared to

a flat Petri dish. Also the velocity of the drying air is substantially increased as in the oven the air velocity is negligible; however in the spray coater the process air flow into the coater was 12m/s.

Late phase separation, i.e. in an immobile film, as opposed to phase separation in solution, progresses via the following equation proposed by Siggia (1979):

$$r \approx \frac{0.1\sigma\Delta\rho}{\eta} t \quad (4.2)$$

where r is the radius of the droplets, σ the interfacial tension, $\Delta\rho$ is the density difference between the two phases, η is the zero-shear viscosity and t is time. A linear growth in droplet radius tends to exist leading to increasing radius of the droplets with increased time.

The intermediate T_g seen in the polymer blends therefore is likely to have appeared in the MTDSC and L-TMA results due to limitations in the area of scrutiny of the two techniques as opposed to any miscibility between the two components of the blend. The heated tip tapping mode experiments for both the film coated minitables and cast free films indicate domains that are likely to be at the limit of detection for both techniques but due to the unique method in which heated tip tapping mode operates these nanophases could be resolved.

4.4.3.2 Analysis of Surelease and Opadry II Cast Films

4.4.3.2.1 Modulated Temperature DSC

Similar to the results for cast films of Surelease:Opadry I blends the MTDSC data produced easier to interpret data due to the nature of the samples, with results shown in Fig. 4.49 to 4.51. A clear glass transition was present for Opadry II observed at 51.3°C ($\pm 0.3^\circ\text{C}$ sd; n=3), 50.7°C ($\pm 1.3^\circ\text{C}$ sd; n=3) and 50.5°C ($\pm 1.6^\circ\text{C}$ sd; n=3) for the 50:50, 70:30 and 90:10 blends respectively.

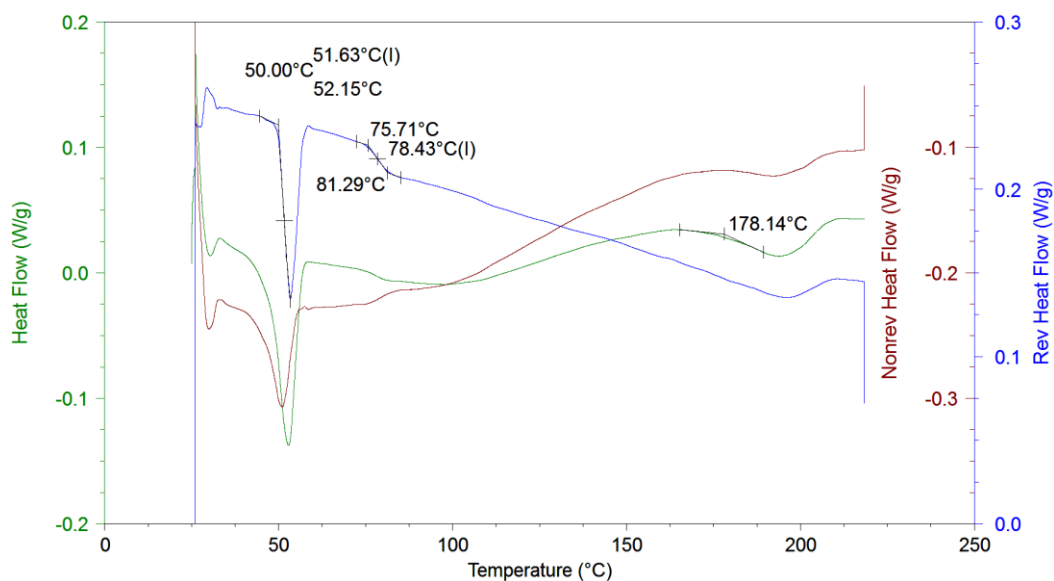


Figure 4.49 MTDSC trace of cast films of a Surelease and Opadry II 50:50 blend

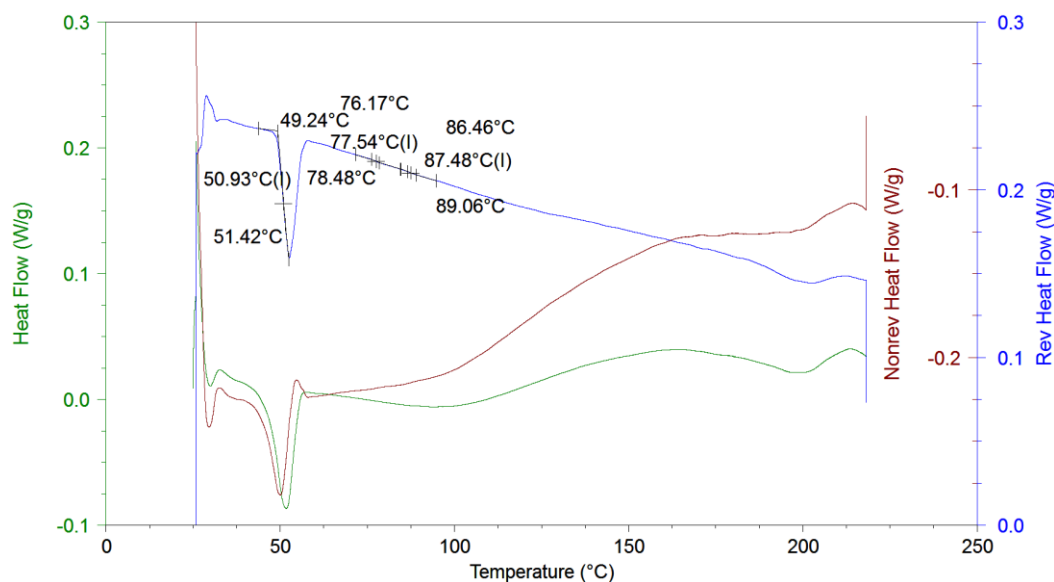


Figure 4.50 MTDSC trace of cast films of a Surelease and Opadry II 70:30 blend

There was also an intermediate temperature observed at 77.03 °C ($\pm 1.03^\circ\text{C}$ sd; $n=3$), 77.72°C ($\pm 1.22^\circ\text{C}$ sd; $n=3$) and 77.83°C ($\pm 2.86^\circ\text{C}$ sd; $n=3$) again for the 50:50, 70:30 and 90:10 blend. Although there is a modest increase in the glass transitions temperature the closeness of the result and the relatively large standard deviation prevents any firm conclusions.

The expected melting point for Opadry II was also observed, and as with the T_g this diminished in size with increasing Surelease content in the blend.

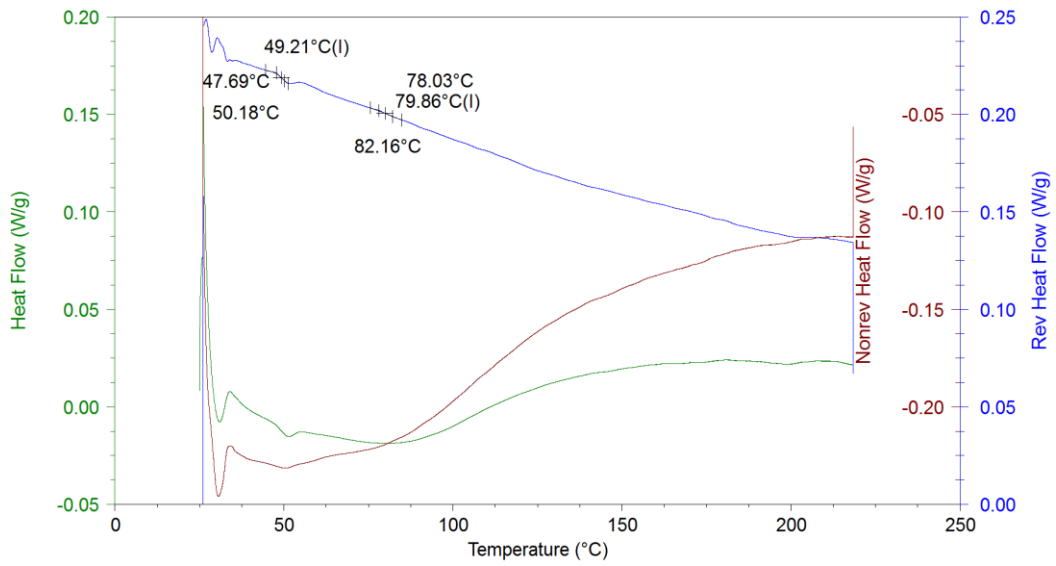


Figure 4.51 MTDSC trace of cast films of a Surelease and Opadry II 90:10 blend

4.4.3.2 Localised Thermomechanical Analysis

Fig. 4.52 shows results from analysis of Surelease:Opadry II 50:50 cast film, showing similarity to the MTDSC results with a transition observed at 78.78°C (± 2.98 sd $n=18$) and also transitions associated with amorphous and crystalline PVA.

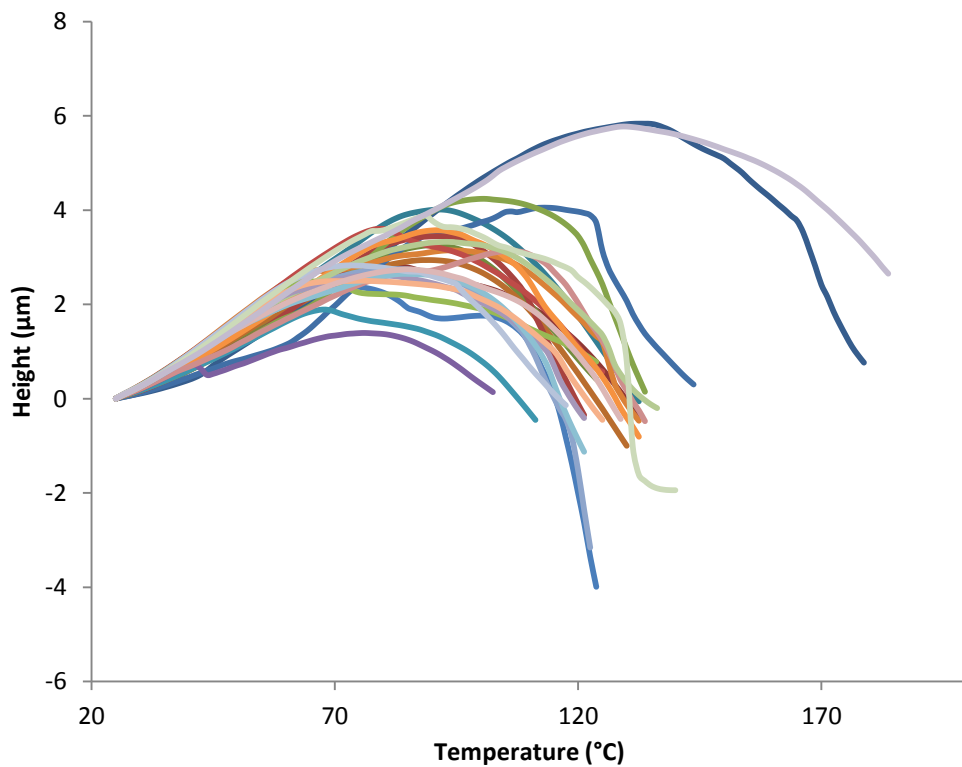


Figure 4.52 L-TMA of cast films of a 50:50 Surelease:Opadry II blend

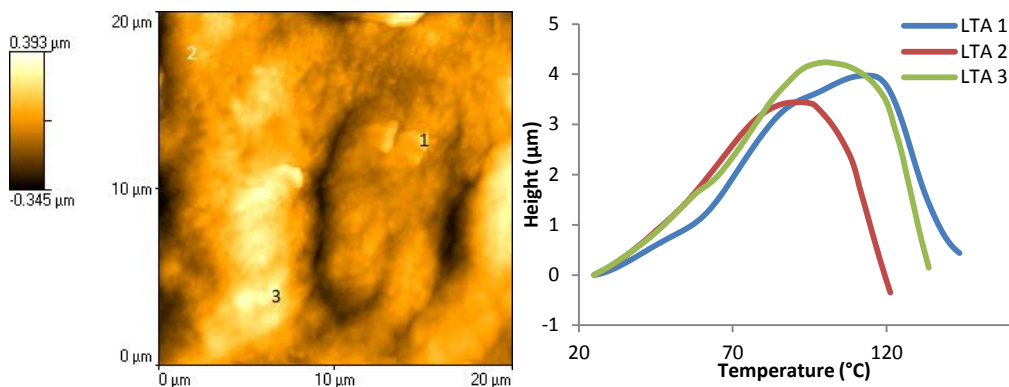


Figure 4.53 AFM contact image (left) and L-TMA results (right) for 50:50 Surelease:Opadry II blend

Also at 89.12°C ($\pm 2.31^\circ\text{C}$ sd; n=9) there were a number of transitions associated with Surelease which as with the Surelease:Opadry I blends is more than observed with film coated minitabets. This again indicates that phase separation is occurring to a higher degree in cast films than in spray coated minitabets.

As with the film coated minitabets the intermediate transition increases with increasing Surelease content with the 70:30 blend producing an average intermediate temperature of 81.73°C ($\pm 1.79^\circ\text{C}$ sd; n=16), and the 90:10 blend 83.49°C ($\pm 1.13^\circ\text{C}$ sd; n=15).

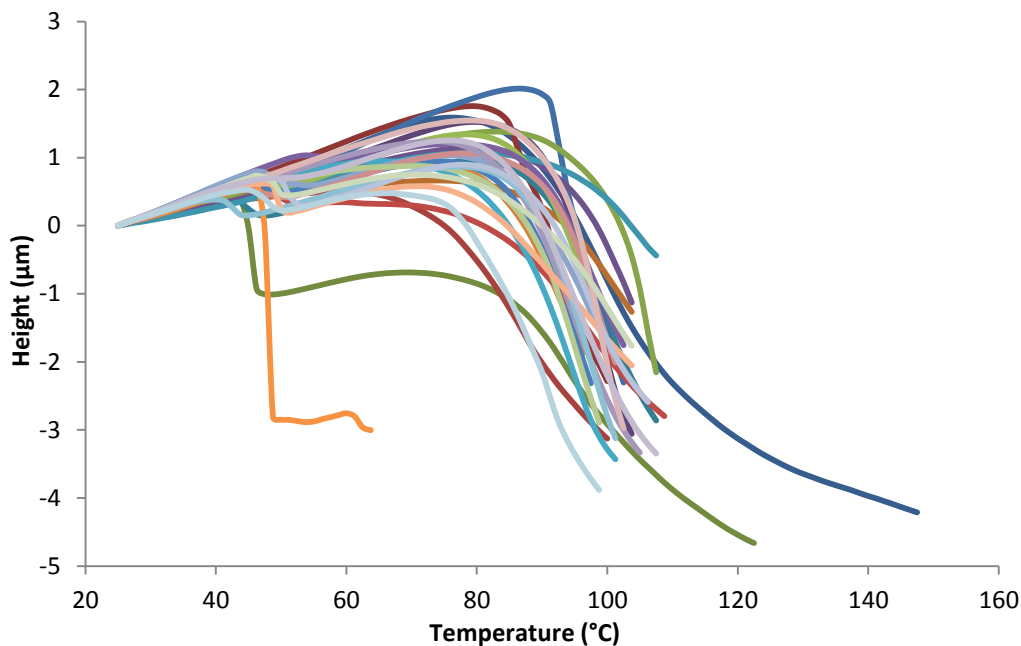


Figure 4.54 L-TMA of cast films of a 70:30 Surelease:Opadry II blend

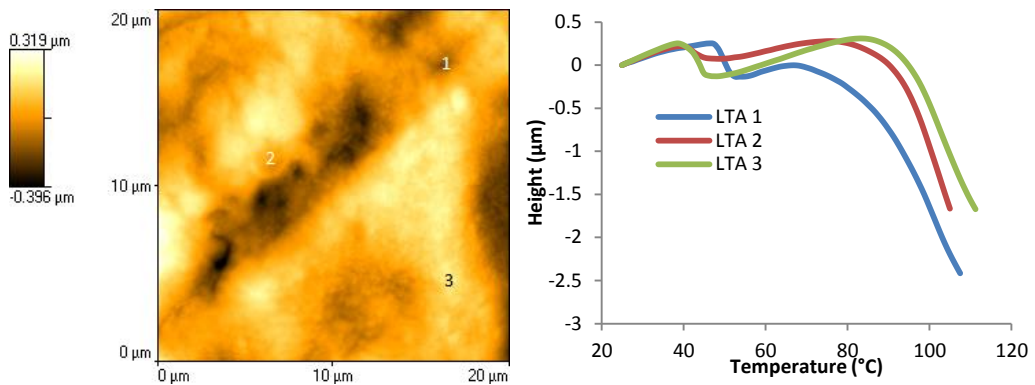


Figure 4.55 AFM contact image (left) and L-TMA results (right) for 70:30 Surelease:Opadry II blend

Due to the inherent spread of L-TMA results and the proximity of the intermediate transition between the blends phase, it is difficult to be certain regarding phase miscibility, however the trend suggests the intermediate transition is increasing.

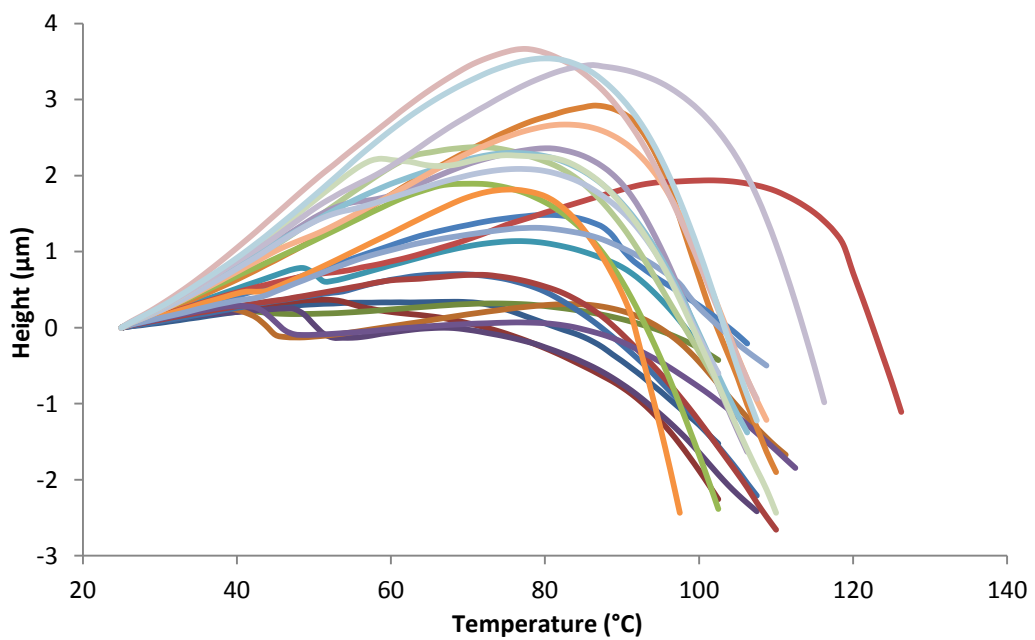


Figure 4.56 L-TMA of cast films of a 90:10 Surelease:Opadry II blend

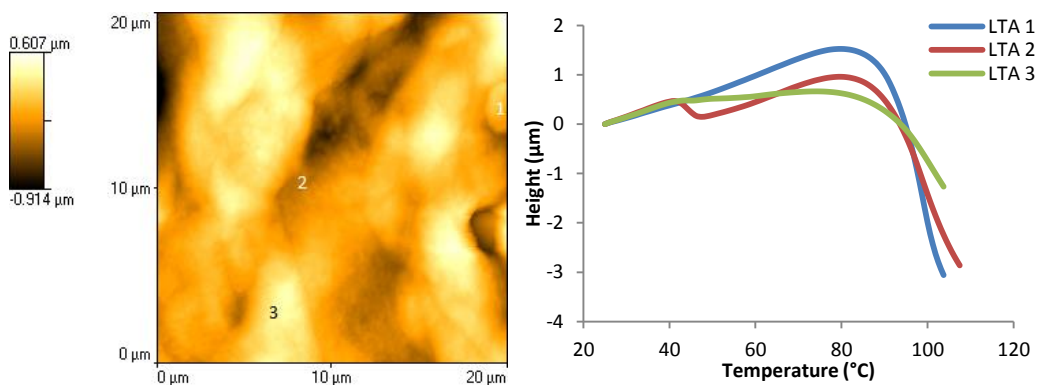


Figure 4.57 AFM contact image (left) and L-TMA results (right) for 70:30 Surelease:Opadry II blend

Also observed on the Surelease:Opadry II 50:50 blend are transitions associated with a different polymorph of PVA at 126.47°C ($\pm 9.74^\circ\text{C}$ sd; n=5), indicates that the polymorph is not unique to spray coating. Therefore the appearance of this polymorph is not affected by the method of film preparation and is therefore likely to be due to the presence of plasticisers.

4.5 Conclusions

This chapter has displayed several reasons for the in-situ analysis of pharmaceutical systems with respect to polymer film coats. From the AFM contact images the cast film morphology appeared to be different than the spray coated films indicating there may be differences in the phase behaviour of the two systems. This was backed up by the thermal analysis measurements which indicated phase separation in both systems; however this phase separation appears to be more complete in the cast films due to the longer drying times involved in preparing these films.

The large variations observed in the morphology of the films resulting in differences in the thermal properties of the films leads to the conclusion that cast films do not provide the most accurate method of analysing polymer films. Also this was only a thermal and surface morphology study; there may also be variations in the bulk properties of the different films, which could have a large bearing on the controlled release properties of the films.

The use of heated tip tapping mode AFM as a novel analytical technique was also demonstrated. This proved a useful tool in detecting the presence of nanophases in the film coated minitablets, and allowed information to be gathered regarding phase distribution between two systems of similar mechanical properties that ambient tapping mode may not have been able to detect. The advantage of using this technique over MTDSC and L-TMA was also highlighted, as it could have been concluded from MTDSC data that the materials were partially miscible. Also, apart from the presence of the residual tablet core, MTDSC for both cast and film coated tablets were comparable, however the L-TMA and heated tip tapping mode showed different surface morphologies.

The chapter has also contributed to the discussion of how pore formers behave in-situ to alter the controlled release properties of film coated solid dosage forms, with the presence of the pore formers in nanophases. The presence of these nanophases in the film coated minitablets showed the importance of the use of more than one analytical technique when analysing pharmaceutical samples to provide the most accurate conclusions.

CHAPTER 5

5. Characterisation of Cured Film Coated Minitablets

5.1 Introduction

There is considerable interest in understanding the phase distribution of polymer blends when incorporated into film coats, with determination of this phase behaviour potentially aiding the understanding of how drug molecules are released from barrier membrane systems. Chapter 4 presented evidence for the existence of nanophases when Surelease was blended with either Opadry I or Opadry II and spray coated onto minitables. However many substrates coated with an aqueous dispersion for modified release often require a curing step after the film coating process to produce a fully coalesced film with the necessary controlled release properties.

This extra requirement is due to the colloidal structure of the aqueous dispersion which, as the film dries, does not allow the polymer molecules to fully coalesce into a continuous film. Thermal post treatment is therefore used to achieve full coalescence. The coated substrate is held at a temperature above the minimum film forming temperature, either by keeping the substrates within the fluidised bed or by placing in an oven. These elevated temperatures increase molecular mobility allowing interpenetration of the polymer chains and full coalescence to be achieved. If curing does not take place then physical aging of the film can occur, where further coalescence of the film occurs during storage of the substrate, which can alter the drug release profile over the age of the substrate.

The effect of curing is generally to retard drug release through the formation of a continuous film; it is therefore an important step in sustained release coatings. However Bodmeier and Paeratakul (1994) found that the curing could enhance or retard release depending on the physicochemical properties of the drug, plasticiser

concentration and the curing conditions. For example chlorpheniramine maleate has a low affinity for ethylcellulose and curing slowed drug release. Ibuprofen on the other hand has a higher affinity to ethylcellulose and the researchers found ibuprofen crystals on the film surface, which were ascribed to the drug diffusing through the film, and in this case curing actually increased drug release.

Other authors (Bhattacharjya *et al.*, 2008) have indicated that the glass transition of polymers tends to increase with curing, as plasticisers and water tend to be driven off resulting in an increase in the glass transition of the final film. This increase in glass transition was also associated with decrease in the tensile strength of the polymer films analysed.

Therefore as curing can have a drastic effect on the final morphology and function of the final film coat, the characterisation of film coat to determine the influence of curing on the final morphology of the film is of great interest.

5.2 Research Objectives

A curing step is likely to lead to alterations in the film morphology due to the further coalescence and interpenetration of the polymer network. The previous chapter of this thesis detected the presence of nanophases in film coated minitablets prepared by spray coating through the use of the novel heated tapping mode technique, where a nanothermal probe was held at an elevated temperature whilst scanning in tapping mode. Any changes in the film morphology should be observable through the use of heated tip tapping mode AFM, and if nanophases are present in the film the expectation would be for these phases to grow and coalesce upon curing.

Previous studies have describe an increase in the glass transition temperature of polymer films after curing (Bhattacharjya *et al.*, 2008), therefore it is expected that this will occur here and be shown through an increase in transitions observed in L-TMA.

5.3 Materials and Methods

Surelease (Ethylcellulose), Opadry I (HPMC) and Opadry II (PVA) were all gifts from Colorcon (Dartford, UK). Coating solutions of Surelease and Opadry I and Surelease and Opadry II were prepared by dispersing either Opadry I or Opadry II in water, and once fully dispersed Surelease aqueous dispersion was added. A Blend of 50:50 by polymer weight were prepared and coated onto minitables, as described in the previous chapter.

Minitables were placed in open petri dishes and cured in an oven at 60°C for 24 hours. Sample were removed at 6, 12 and 24 hours and placed in airtight containers until analysis.

Contact images were obtained using AN2-200 nano-TA probes (Anasys instruments) mounted onto a Caliber AFM (Veeco), using a scan rate of 1.0 Hz, with a scan area of either 5µm or 20µm. L-TMA experiments were carried out with a nano-TA2 box (Anasys Instruments) using heating rate of 25°C sec⁻¹. Heated tip tapping mode images used a scan rate of 1.0Hz and a set point ratio between 0.3-0.5. The cantilever was tuned to determine the resonant frequency of the probe after each increase in probe tip temperature due to the possibility of a decrease in resonant frequency with increasing temperature. A minimum of three images were acquired for each minitabled or section of cast film and in addition three different minitables or sections of cast films were analysed. Grain analysis was performed in SPM labs, and the method is detailed in Chapter 4.

5.4 Results

5.4.1 Analysis of Individual Polymers

Fig. 5.1 shows L-TMA results for the individual polymer systems coated onto minitables showing the transition temperatures for Opadry I (161.6°C), Opadry II (48.8°C) and Surelease (85.0°C). L-TMA results from Chapter 4 of minitables

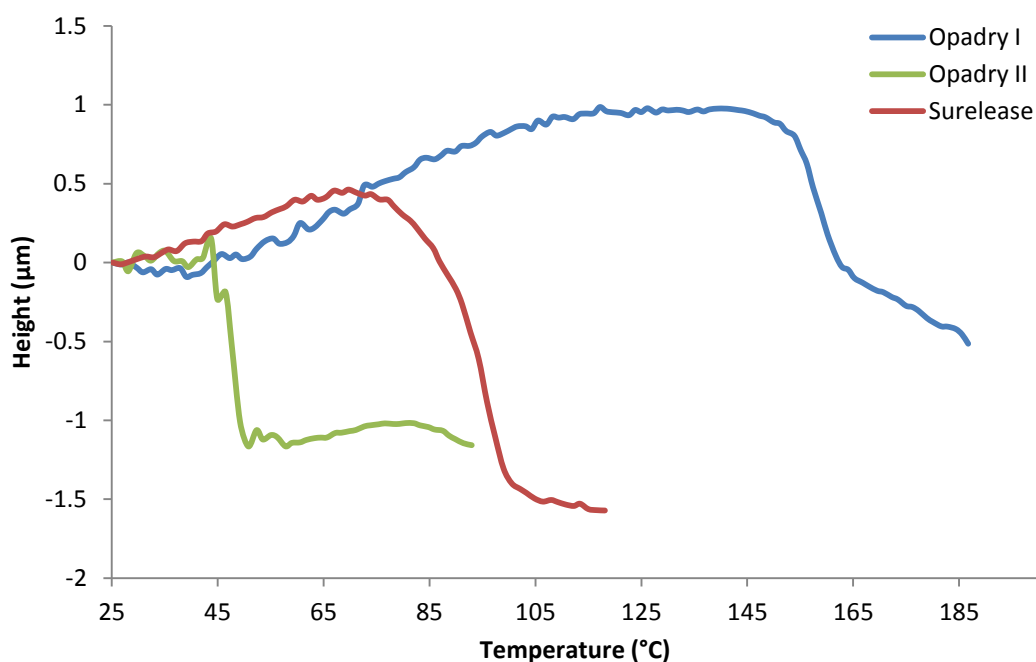


Figure 5.1 L-TMA of minitabets film coated with Opadry I, Opadry II and Surelease

coated with polymer blends showed intermediate transition temperatures to be observed, between the values of the respective polymers. Heated tip tapping mode was performed on the samples indicating the presence of nanophases in the film coat, and these intermediate values were ascribed to being present due to the domain size being at the limit of detection of MTDSC and L-TMA.

As described above curing tends to alter the morphology of film coats through further coalescence and the removal of water and plasticisers it will be of interest if there are any alterations in the L-TMA responses once the minitabets have been cured.

5.4.2 Surelease

5.4.2.1 Heated Tip Tapping Mode AFM

AFM images performed in tapping mode on Surelease coated minitabets cured for 6 hours are shown in Fig. 5.1 with Fig. 5.2 showing tapping mode performed with the tip held at 80°C. The topography image is similar to topography images acquired of uncured minitabets coated with Surelease (see Chapter 4), however the small

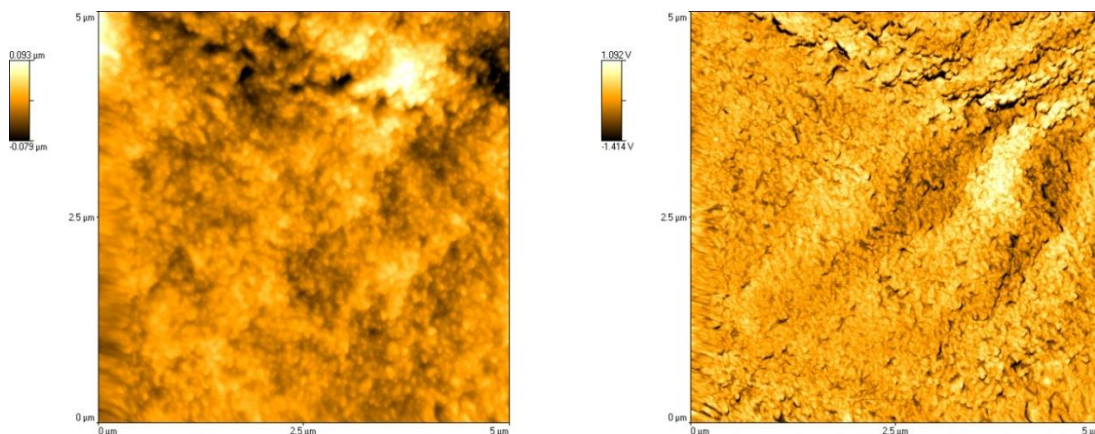


Figure 5.2 Tapping mode image of Surelease minitables cured for 6 hours showing topography (left) and phase (right)

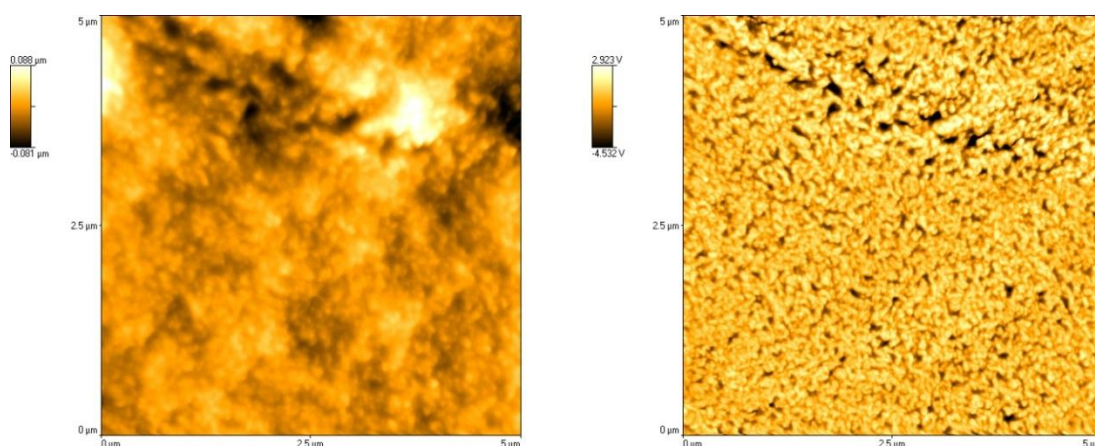


Figure 5.3 Heated tip tapping mode image with the probe held at 80°C of Surelease minitables cured for 6 hours showing topography (left) and phase (right)

spherical structures attributed to pseudolatex particles are less prominent and well defined than in the uncured minitables.

The phase image in Fig. 5.2 also displays differences to the uncured minitables, with a slightly more homogenous appearance, however once the probe tip was raised to 80°C the variation between the uncured minitables is more apparent. Once uncured minitables were raised to this temperature there were areas of the film surface that had softened and other areas that remained relatively firm however the phase image in Fig. 5.3 shows a far more homogenous surface.

This trend continues on the minitables cured for 12 and 24 hours with the results displayed in Figs. 5.4 through 5.7. The topography images appear “smoother” the

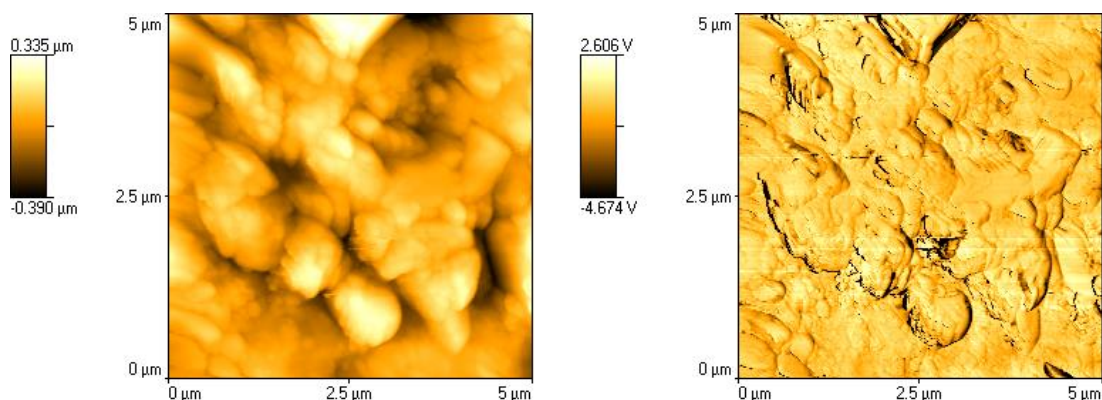


Figure 5.4 Tapping mode image of Surelease minitables cured for 12 hours showing topography (left) and phase (right)

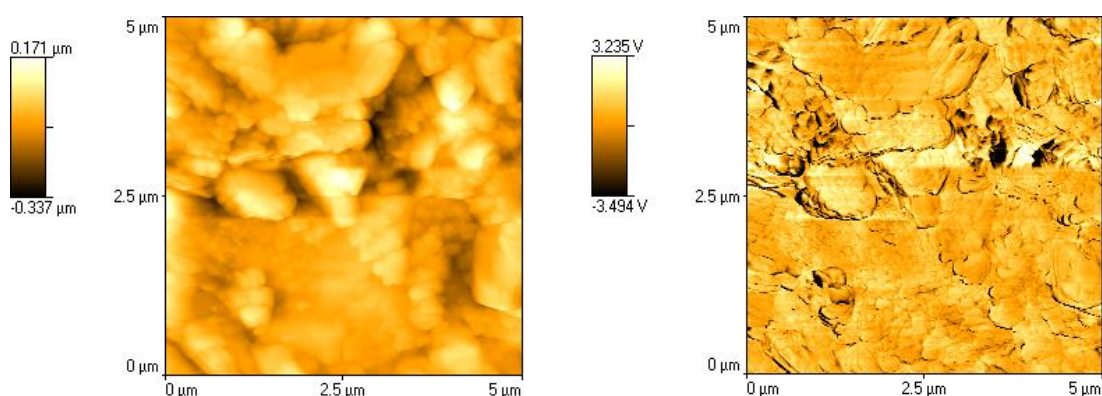


Figure 5.5 Heated tip tapping mode image with the probe held at 80°C of Surelease minitables cured for 12 hours showing topography (left) and phase (right)

longer the minitables are cured for, with the spherical structures becoming less well defined. Similarly the phase images give a more continuous appearance, which is particularly apparent in the phase image of Fig. 5.6. This image at room temperature

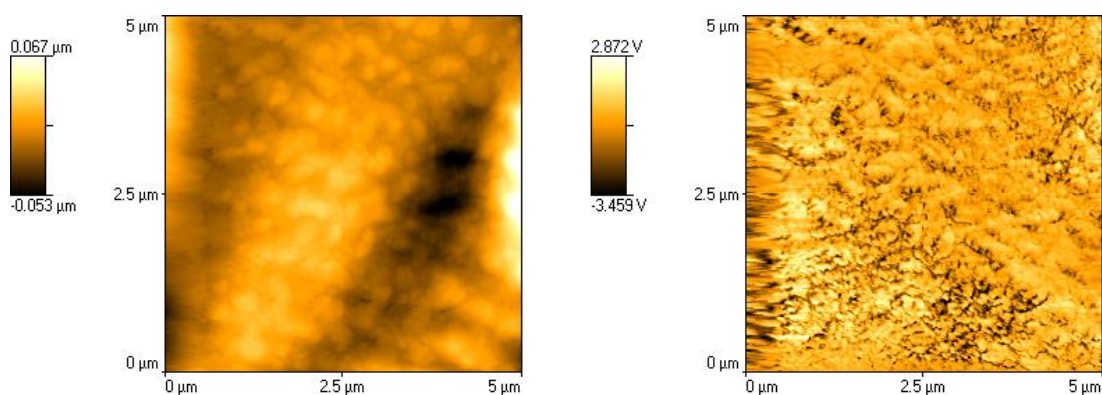


Figure 5.6 Tapping mode image of Surelease minitables cured for 24 hours showing topography (left) and phase (right)

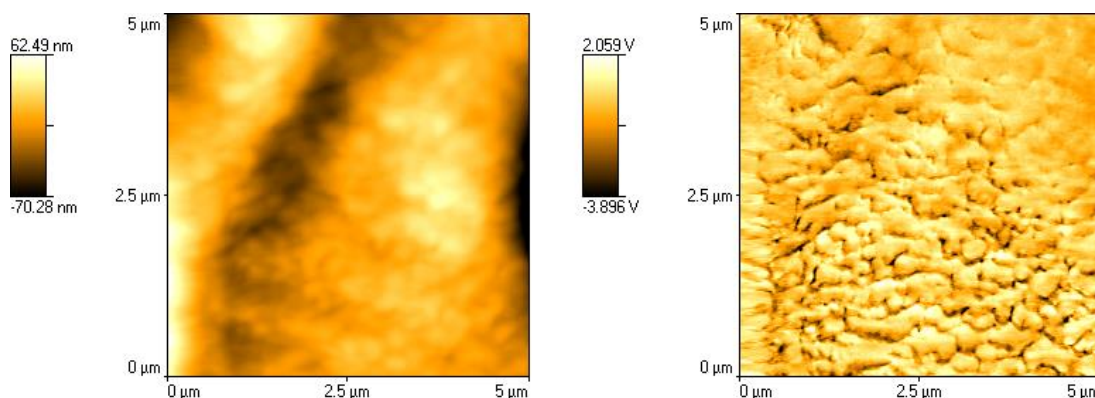


Figure 5.7 Heated tip tapping mode image with the probe held at 80°C of Surelease minitablets cured for 24 hours showing topography (left) and phase (right)

shows little of the detail observed in the uncured minitablet taken at the same temperature and once the probe tip temperature is raised to 80°C the minitablet surface still retains a broadly homogeneous appearance. This indicates further coalescence of the film occurs on curing of the Surelease films resulting in a more continuous film structure.

5.4.2.2 Contact Mode Images and L-TMA Analysis

The differences in surface morphology observed in both topography and phase images in heated tip tapping mode showed evidence of further coalescence of the polymer films. As discussed above films that undergo curing tend to have seen an increase in the glass transition temperature, and it is of interest if this occurs on curing of film coated minitablets.

L-TMA images were acquired in contact mode and can be seen in Fig. 5.8. The transition temperature observed for the film was 89.5°C ($\pm 2.8^\circ\text{C}$ sd; n=20), which agrees well with the values obtained for uncured minitablets both in regards of the temperature the transition was observed at, and the standard deviation observed.

Heated tip tapping mode showed subtle differences after curing for 6 hours, which may translate into limited changes in transition temperatures when the same minitablets are analysed by L-TMA. It will be of interest if changes in the distribution of L-TMA profiles is observed once the minitablets are cured for a greater length of time.

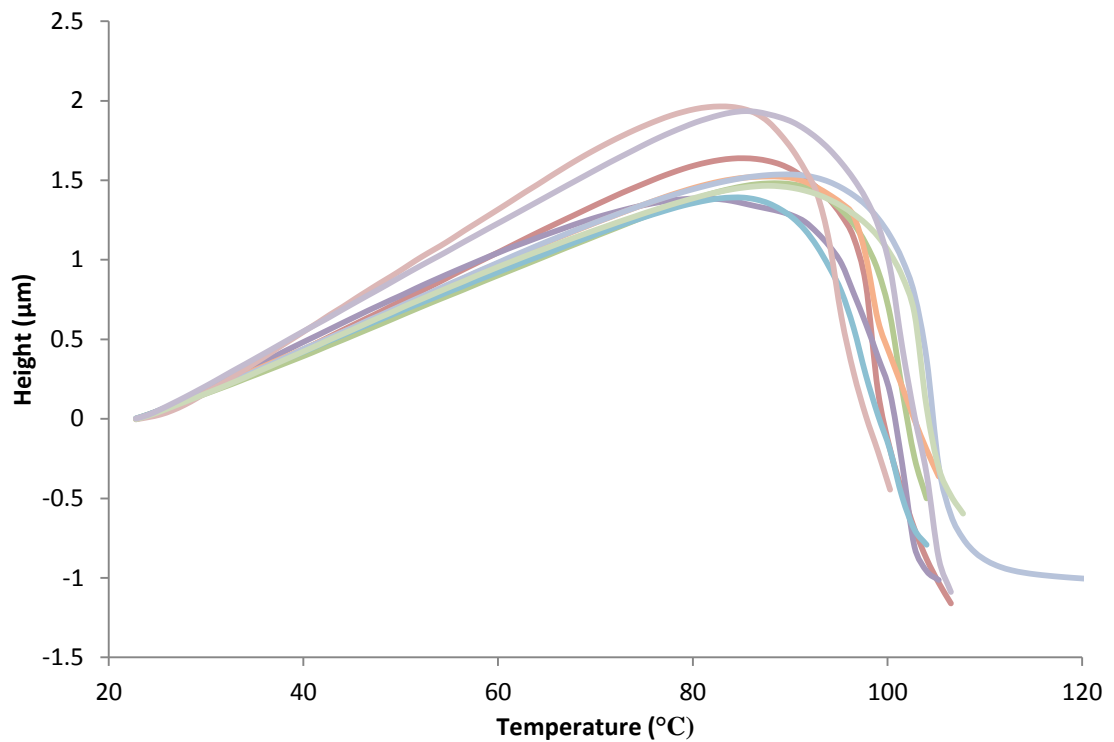


Figure 5.8 L-TMA of Surelease coated minitabets cured for 6 hours

Contact images were acquired and L-TMA experiments performed at specific locations which can be seen in Fig. 5.9 and 5.10 with the droplet structures observed on uncured minitabets still present. The lines seen in parts of the image are due to low frequency vibrations in the environment affecting the AFM rather than any structure on the minitabets surface.

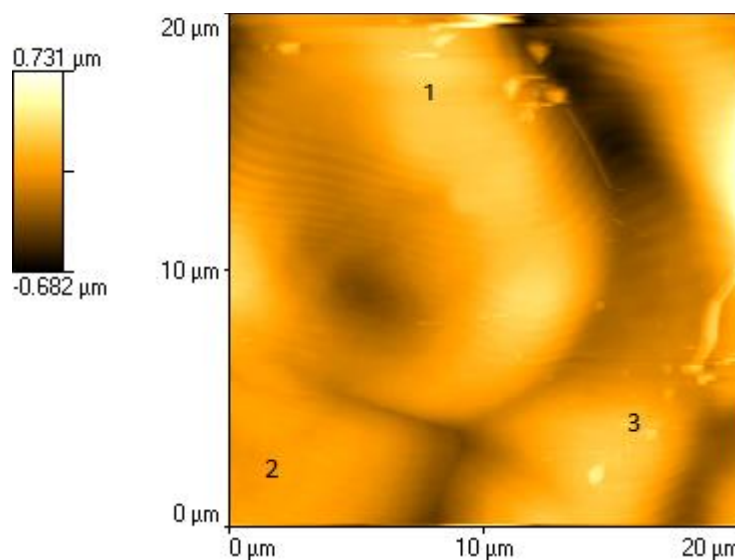


Figure 5.9 Contact AFM image of Surelease coated minitabets cured for 6 hours, numbers denote locations of L-TMA

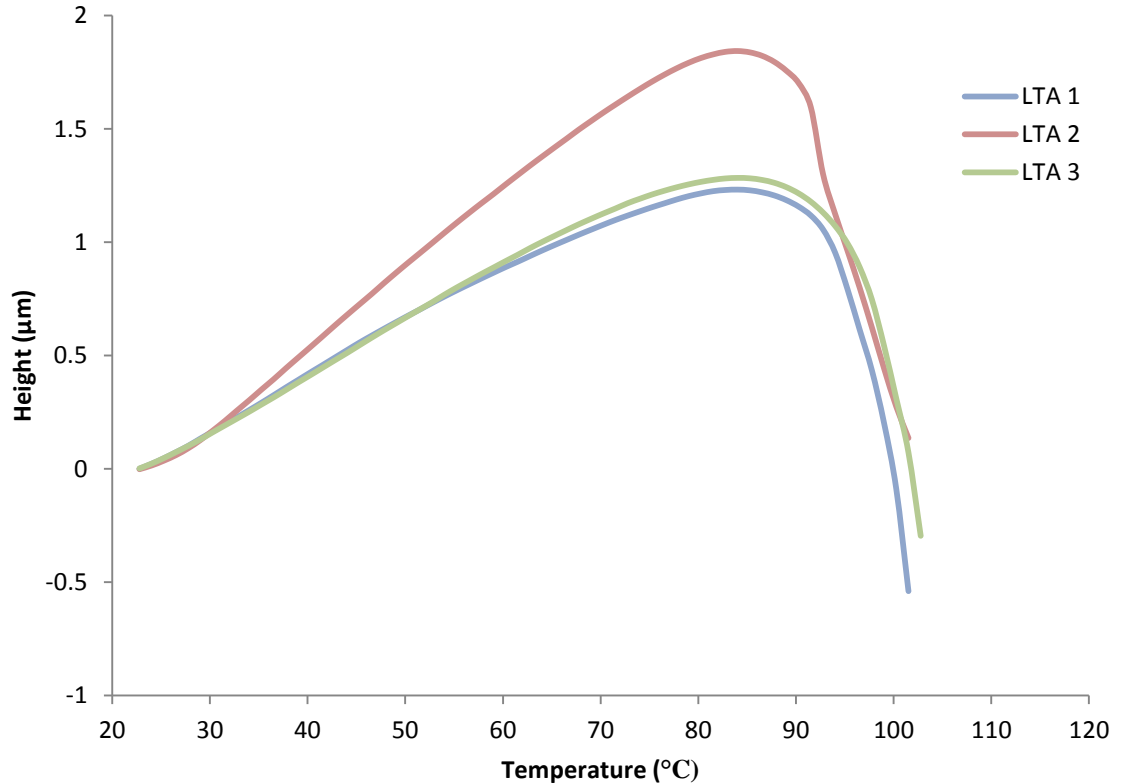


Figure 5.10 L-TMA of Surelease coated minitabets cured for 6 at locations specified in Fig 5.9

L-TMA performed at locations indicated in Fig. 5.9 are shown in Fig. 5.10, showing the consistency observed in the Surelease transitions for coated minitabets cured for 6 hours.

However once the minitabets were cured for 12 hours there were differences observed in the L-TMA responses. This is unsurprising as the changes to tapping mode phase images seen above would indicate there are changes occurring in the film. The transition temperature is still around 90°C, therefore similar to that observed for uncured minitabets and those cured for 6 hours, however at 91.9°C (± 7.2 sd; n=20), the standard deviation is somewhat greater than seen for these other minitabets. Also from inspection of the graph it appears that the increase in standard deviation is due to an increased number of transition temperatures in excess of 90°C with a number over 100°C. As discussed above increases in the glass transition of polymers is often observed on curing and this appears to be the case here; however it will be of note if this trend continues on increased cure time.

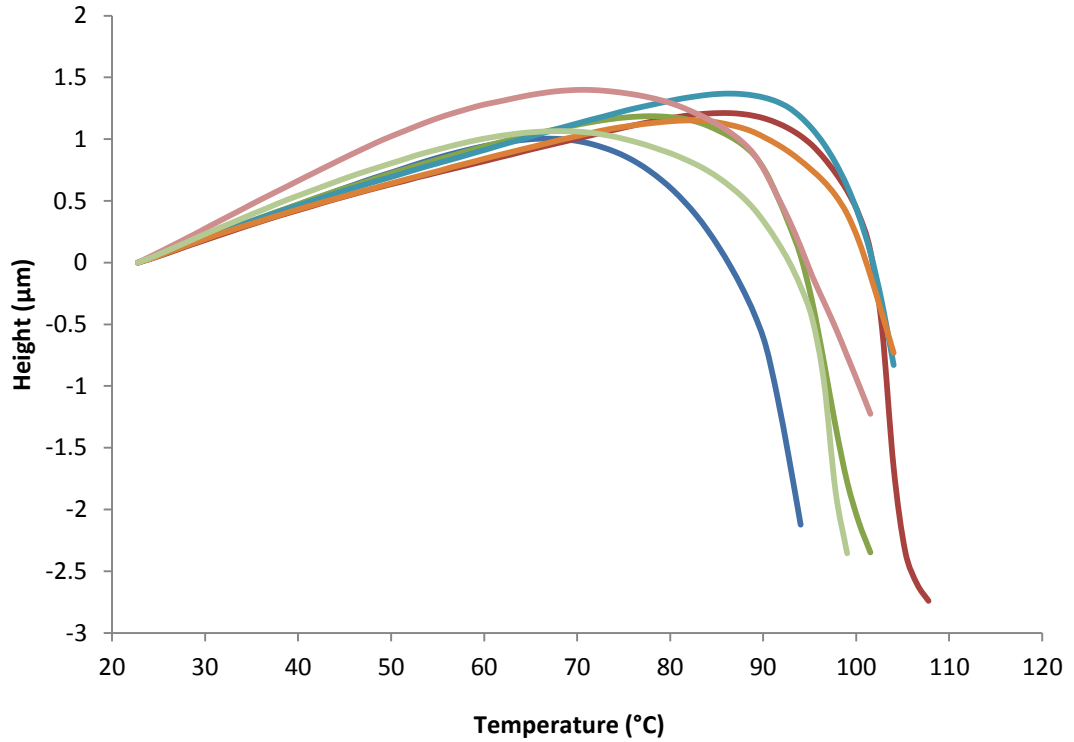


Figure 5.11 L-TMA of Surelease coated minitables cured for 12 hours

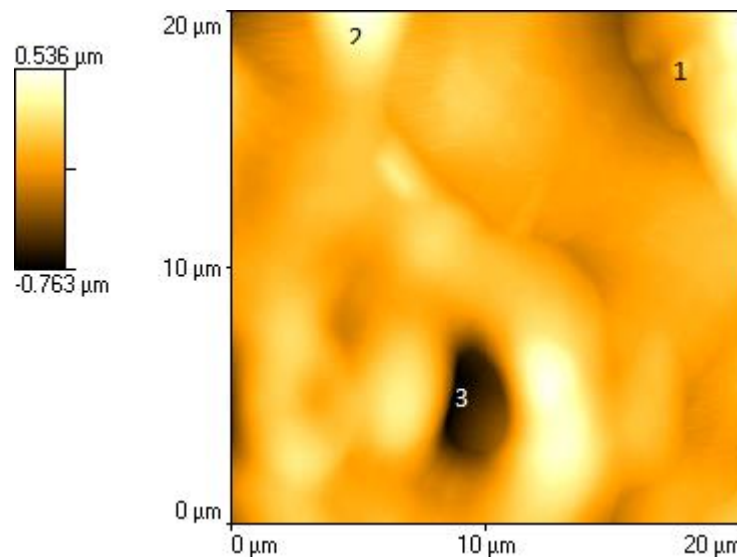


Figure 5.12 Contact AFM image of Surelease coated minitables and cured for 12 hours, numbers denote locations of L-TMA

This can be seen in Fig. 5.11, where the L-TMA traces can be seen to be over a greater temperature range than those seen for either uncured Surelease coated minitables or those cured for 6 hours.

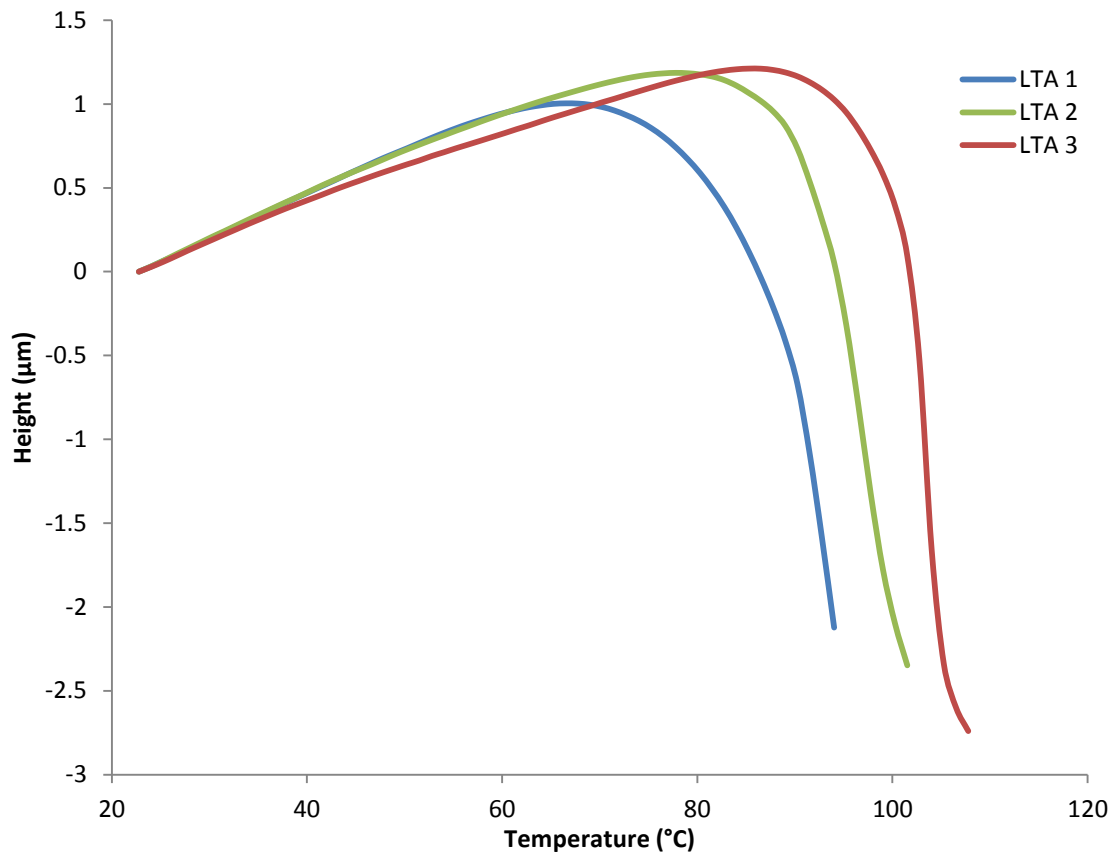


Figure 5.13 L-TMA of Surelease coated minitabets cured for 12 hours at locations specified in Fig. 5.12

The trends seen in Fig. 5.11 are also displayed when sites are chosen from contact images, and this data is shown in Fig. 5.12 and 5.13. The contact image in Fig. 5.12 reveals a “smoother” surface than seen for uncured or 6 hour cured coated minitabets consistent with the tapping mode images.

The L-TMA traces in Fig. 5.11 also support this, however the higher transition observed at location 3 could also be attributed to the probe location being in an indentation on the surface. However other images and L-TMA results combined with those seen in Fig. 5.11 show the increase in variation of the transition temperatures.

Once the minitabets were cured for 24 hours this variation becomes even more obvious with the L-TMA traces in Fig. 5.14 showing a wider range of transition

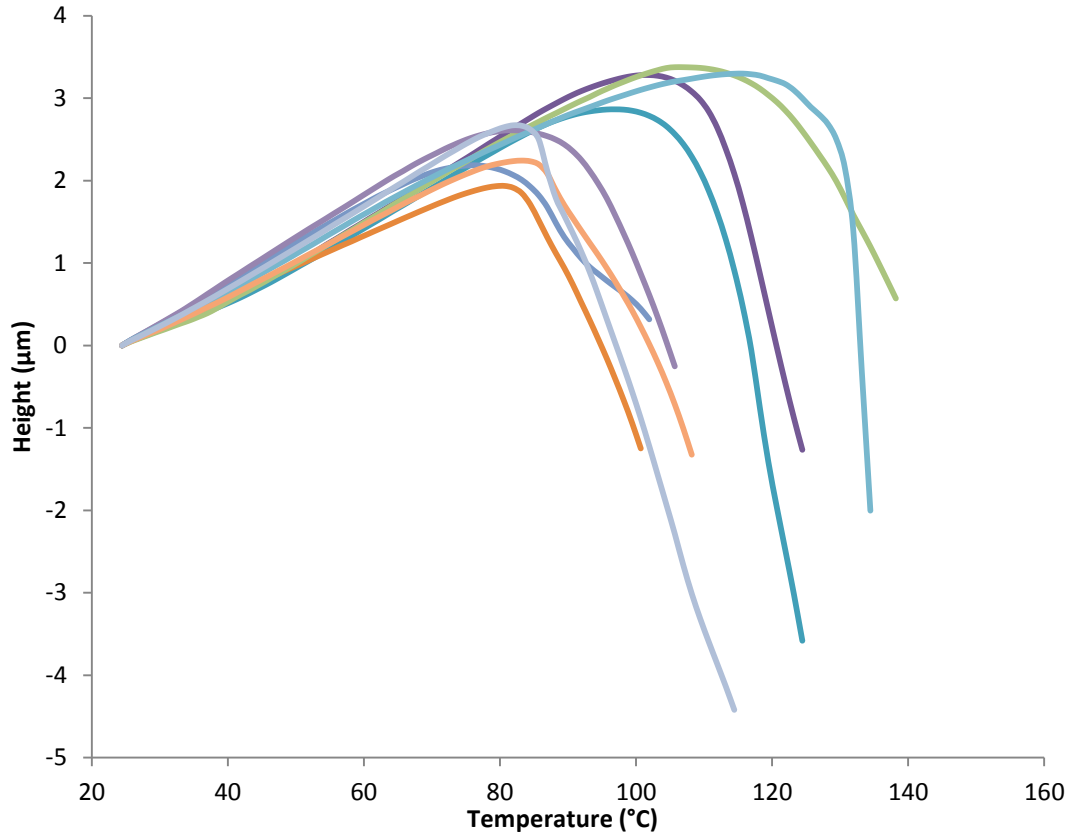


Figure 5.14 L-TMA of Surelease coated minitables cured for 24 hours, showing transitions associated with Surelease circa 90°C and EC circa 130°C

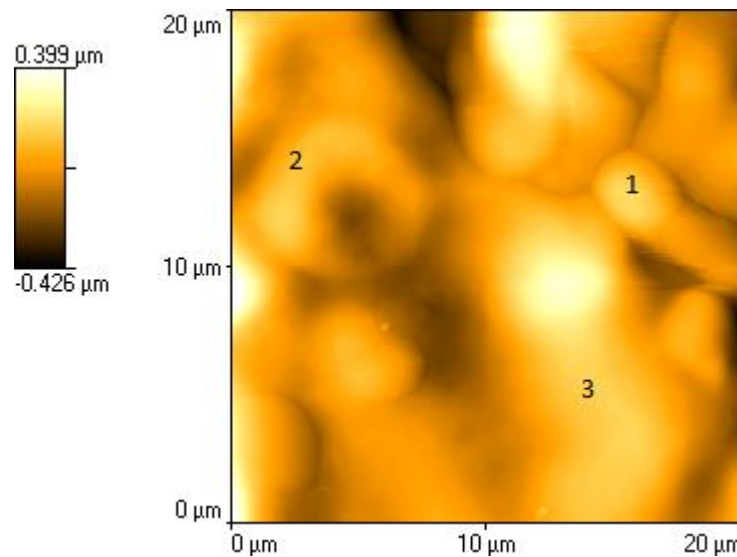


Figure 5.15 Contact AFM image of Surelease coated minitables and cured for 24 hours, numbers denote locations of L-TMA

temperatures observed. There are a number of transition temperatures observed in excess of 100°C, with a number approaching 130°C, which is in the region of the

glass transition temperature observed for ethylcellulose with no plasticisers added.

The average transition temperature observed for the minitables cured for 24 hours was recorded as 92.2°C (± 14.8), therefore showing an increase in both the transition observed and the variation compared to the minitables cured for 6 hours and 12 hours.

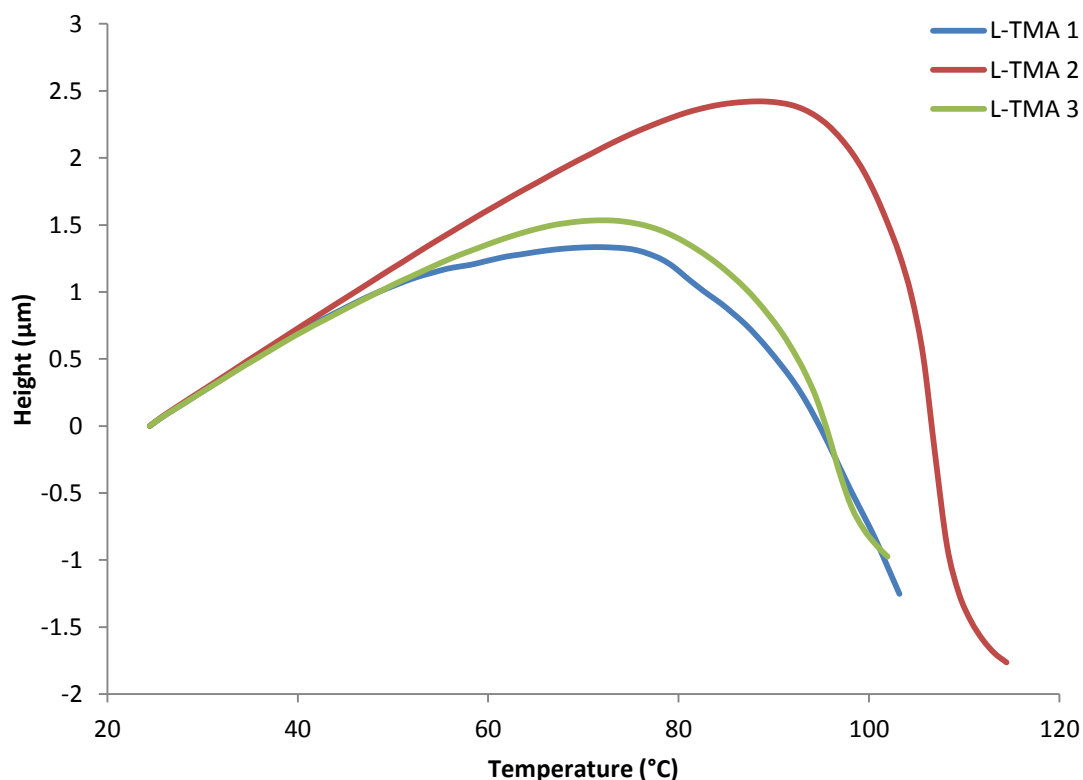


Figure 5.16 L-TMA of Surelease coated minitables cured for 24 hours at locations specified in Fig. 5.15

Fig. 5.15 and 5.16 show a contact AFM image and L-TMA performed at locations described in the contact image. The image as with other cured minitables shows a “smoother” appearance than those of uncured tablets, whilst still retaining the “droplet” structures seen in these minitables.

The L-TMA traces from Fig. 5.16 show the increase in variation of the Surelease transitions with two seen around 90°C and the third over 100°C. As with other contact images there was little correlation between the topography of the sample and the nature of the transition observed.

5.4.3 Surelease and Opadry I 50:50 blend

5.4.3.1 Heated Tip Tapping Mode Imaging

Fig. 5.17 and 5.18 show tapping mode and heated tip tapping mode images of Surelease and Opadry I 50:50 cured for 6 hours. The topography image on the left of the figures shows a similar result to those observed with the cured Surelease coated minitables, with the spherical structures becoming less well defined and a “smoother” appearance of the film being observed.

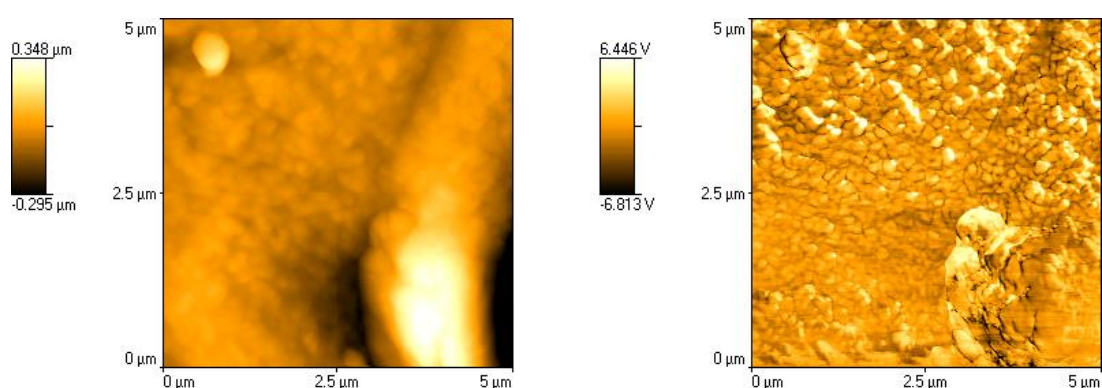


Figure 5.17 Tapping mode image of minitables coated with a Surelease and Opadry I 50:50 blend cured for 6 hours showing topography (left) and phase (right)

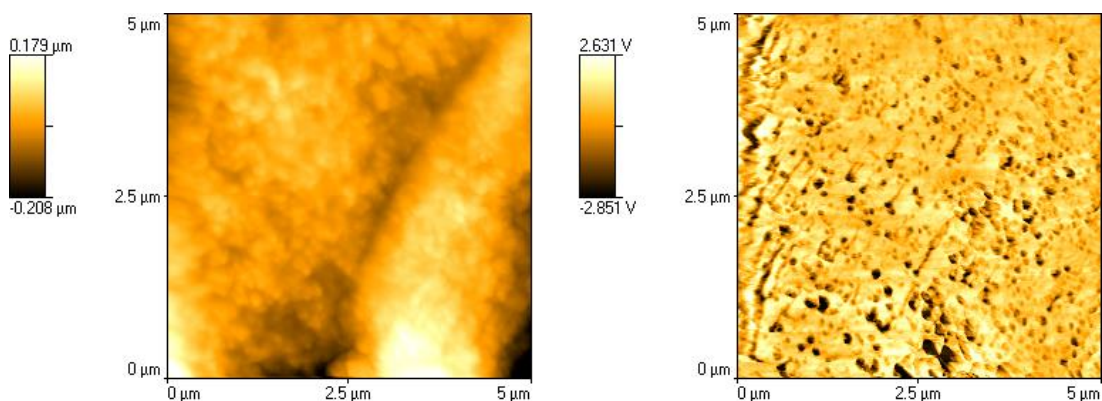


Figure 5.18 Heated tip tapping mode image with the probe held at 100oC of minitables coated with a Surelease and Opadry I 50:50 blend cured for 6 hours showing topography (left) and phase (right)

Although not apparent from the phase images at room temperature, once heated tip tapping mode is performed on the minitables the domain size of Surelease increased in size, with grain analysis indicating the domain size to be 57nm, which is considerably larger than the 20nm observed for uncured minitables.

As the curing time is increased to 12 hours the Surelease domains can be seen in the phase image more clearly at both room temperature, and are particularly prominent when the probe tip is at 100°C.

Grain analysis of the Surelease domains indicates the average domain size is 52nm, which is comparable to the domain size observed in the minitablets cured for 6 hours. It would be expected that the domain size would continue to grow with increased curing time, so it will be of interest if the domain size increases in the minitablets cured for 24 hours.

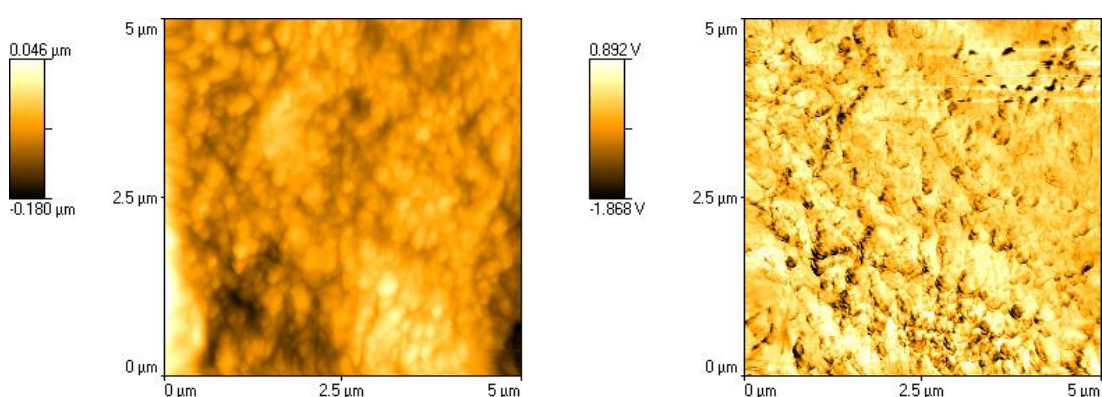


Figure 5.19 Tapping mode image of minitablets coated with a Surelease and Opadry I 50:50 blend cured for 12 hours showing topography (left) and phase (right)

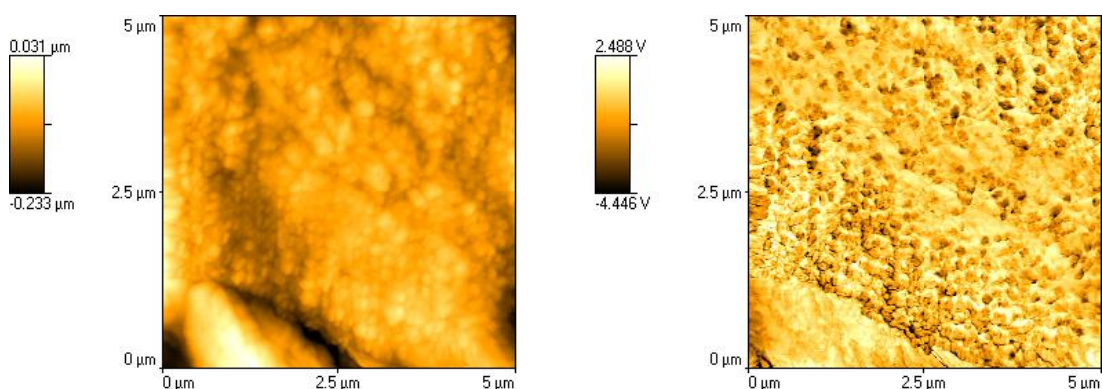


Figure 5.20 Heated tip tapping mode image with the probe held at 100°C of minitablets coated with a Surelease and Opadry I 50:50 blend cured for 12 hours showing topography (left) and phase (right)

The topography images follow the general trend of other images in this chapter with the spherical structures losing definition compared to uncured minitablets. This trend

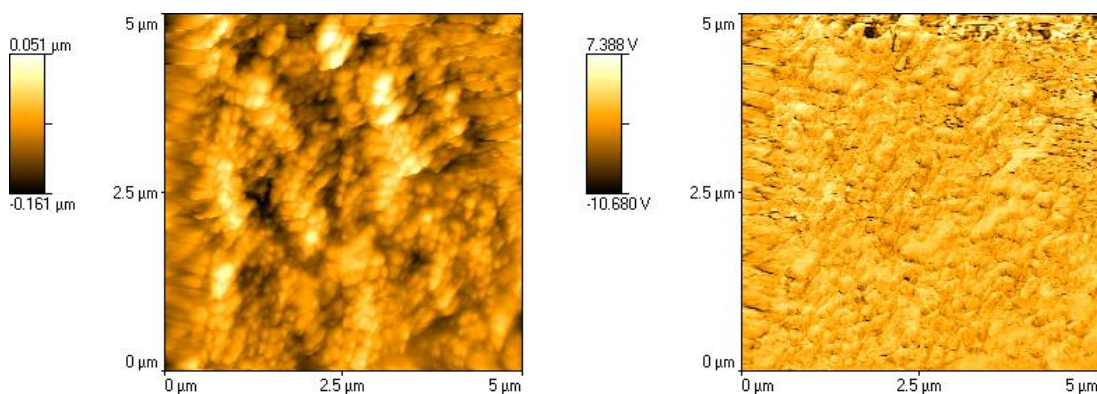


Figure 5.21 Tapping mode image of minitablests coated with a Surelease and Opadry I 50:50 blend cured for 24 hours showing topography (left) and phase (right)

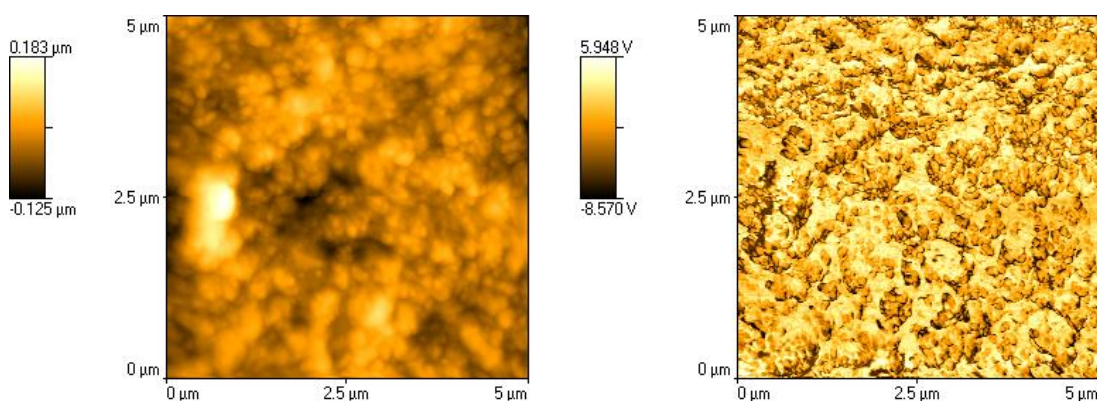


Figure 5.22 Heated tip tapping mode image with the probe held at 100°C of minitablests coated with a Surelease and Opadry I 50:50 blend cured for 24 hours showing topography (left) and phase (right)

continues in Fig. 5.21 and 5.22, where images for minitablests cured for 24 hours are displayed.

The phase images for minitablests cured for 24 hours also appear to follow this trend however the average domain size for Surelease domains is 55nm, similar to that observed for the minitablests cured for 6 and 12 hours. Although the grain analysis does not indicate an increase in the domain size of Surelease in the minitablests cured for 24 hours visual inspection of the phase image in Fig. 5.22 indicates that the domains of Surelease are becoming more substantial. The measured domain size of 55nm is therefore likely to be due to limitations in the software being able to accurately determine the grain size. The significance of the increase in domain size will be discussed further in the discussion.

5.4.3.2 Contact mode images and L-TMA

It would be expected that this further coalescence is likely to alter the distribution of L-TMA results with larger areas of Surelease rich areas present resulting in additional transitions observed for this polymer. Additionally if the further coalescence results in more Surelease rich areas then a corresponding increase in Opadry I transition would also be expected to be observed.

L-TMA performed on 50:50 blends of Surelease and Opadry I cured for 6 hours are shown in Fig. 5.23, with the intermediate glass transition observed in uncured minitablets present at 137.7°C ($\pm 5.5^{\circ}\text{C}$ sd; $n=20$). Additionally there are also transitions observed for Surelease at around 90°C (purple trace) and 160°C and for Opadry I (red trace). As tapping mode images showed an increase in domain size for Surelease then the observation of transitions for individual polymers would be expected.

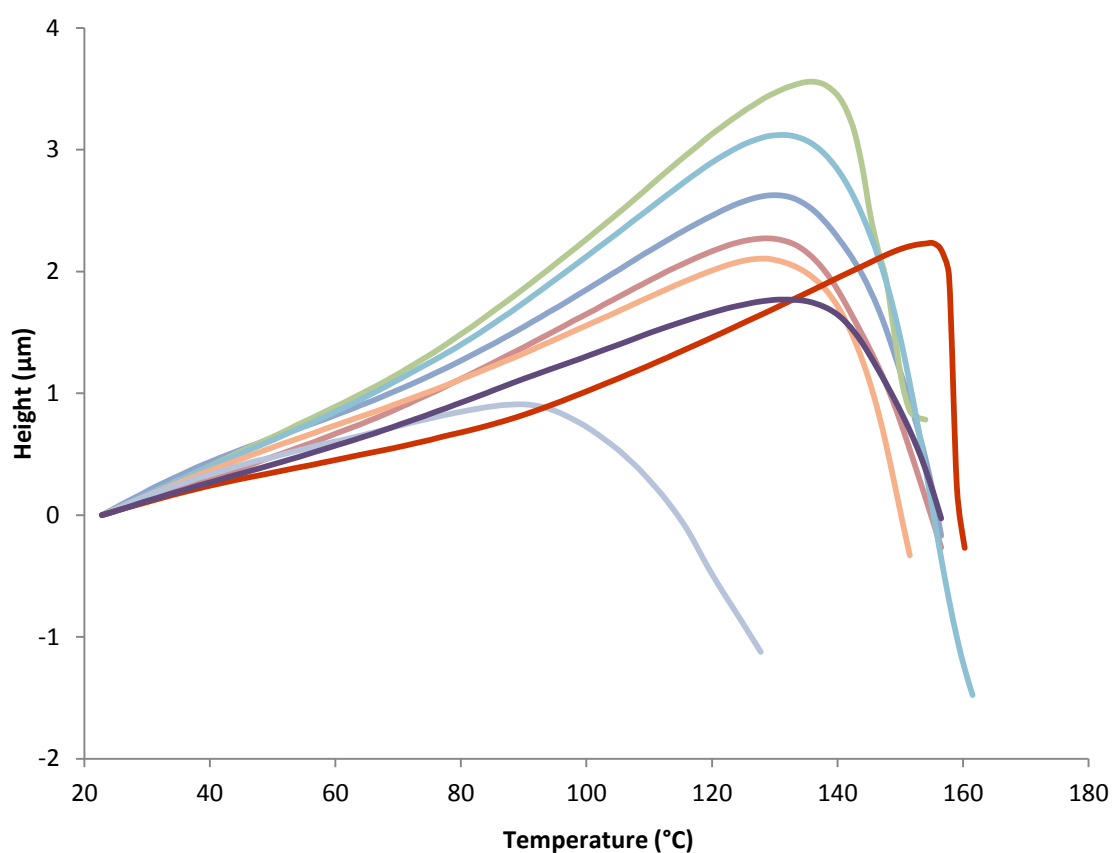


Figure 5.23 L-TMA of minitablets coated with a Surelease and Opadry I 50:50 blend cured for 6 hours

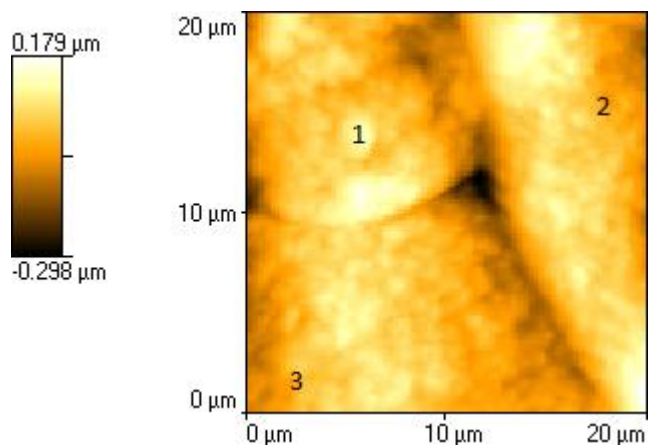


Figure 5.24 Contact AFM image of minitablets coated with a Surelease and Opadry I 50:50 blend and cured for 6 hours, numbers denote locations of L-TMA

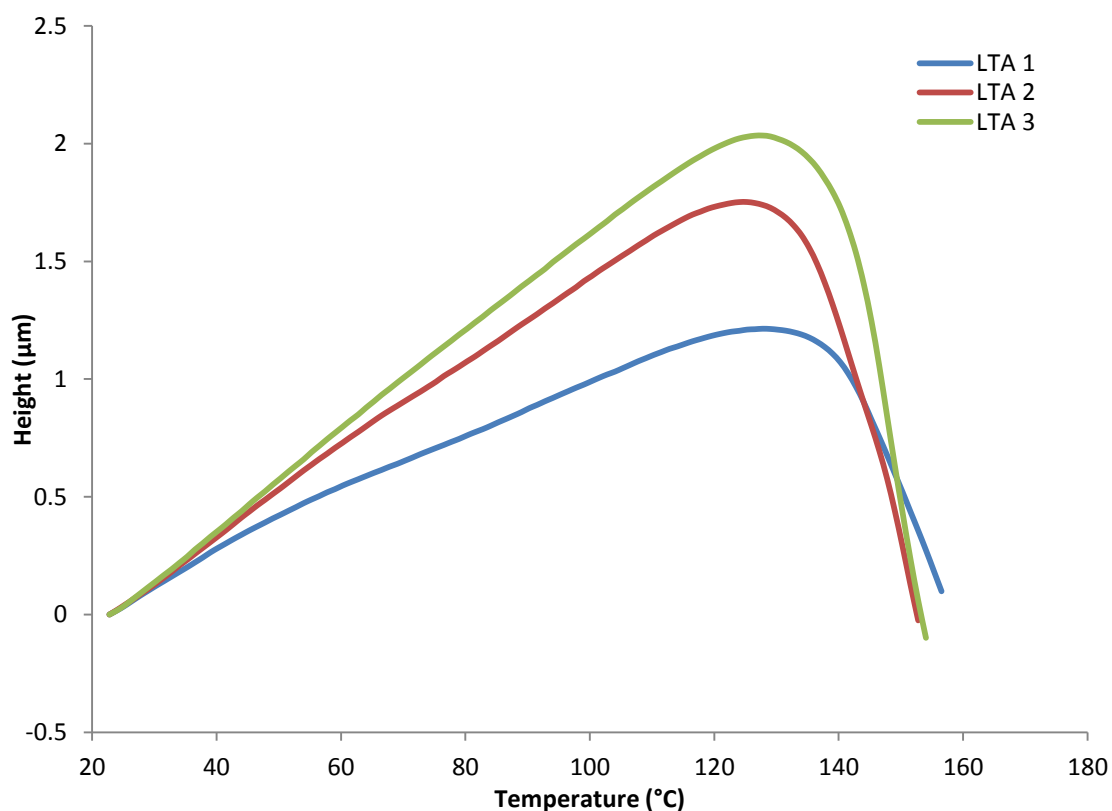


Figure 5.25 L-TMA of minitablets coated with a Surelease and Opadry I 50:50 blend and cured for 6 hours at locations specified in Fig. 5.24

Fig. 5.24 and 5.25 show contact images and L-TMA of 50:50 blends of Surelease and Opadry I cured for 6 hours. As with other results from previous chapters the L-TMA results show little resemblance to the topographic image with all traces producing similar results despite the differences in topology where the L-TMA was performed.

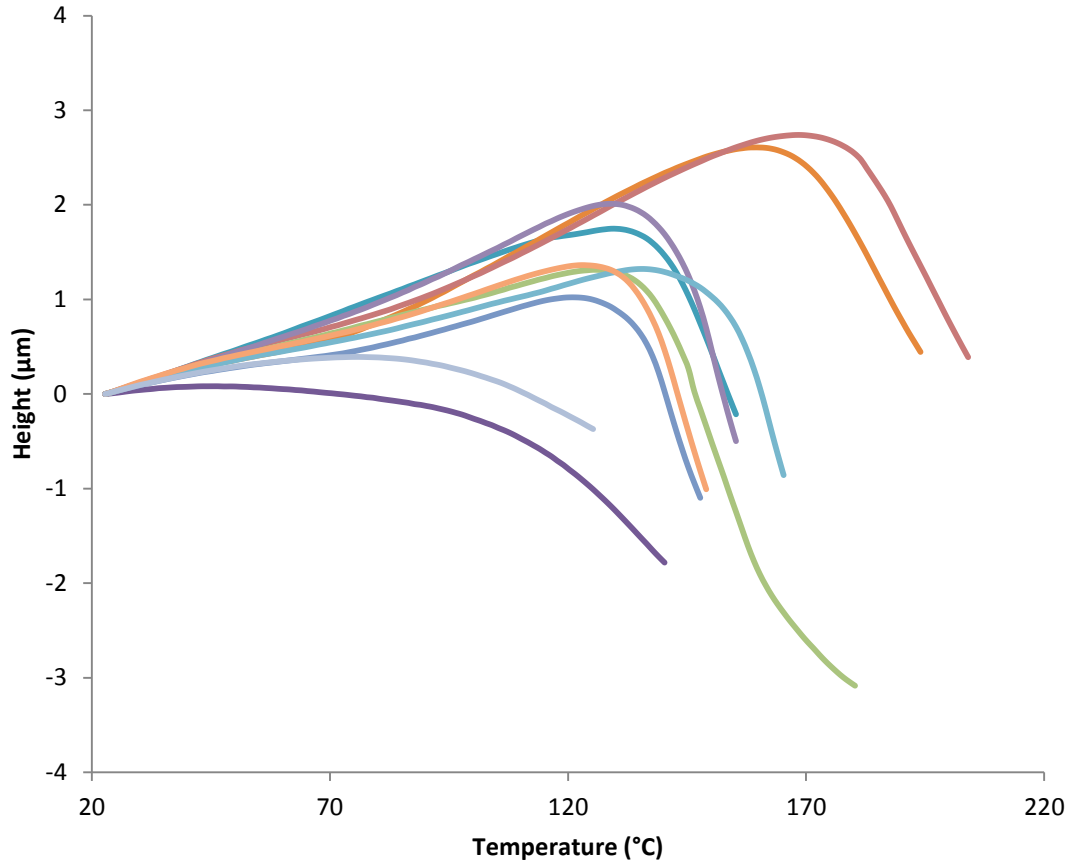


Figure 5.26 L-TMA of minitablets coated with a Surelease and Opadry I 50:50 blend cured for 12 hours

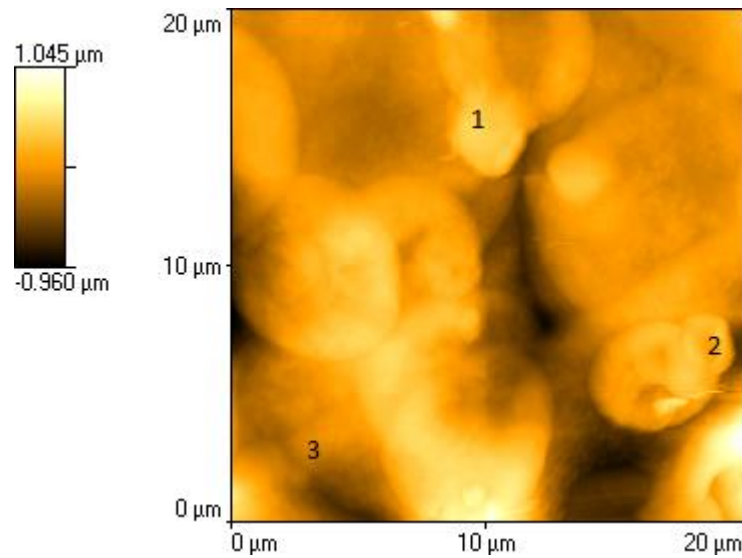


Figure 5.27 Contact AFM image of minitablets coated with a Surelease and Opadry I 50:50 blend and cured for 6 hours, numbers denote locations of L-TMA

After the minitablets had been cured for 12 hours the phase separation observed in the tapping mode images becomes more apparent. An intermediate glass transition is

observed at 140°C ($\pm 6.7^\circ\text{C}$ sd; n=16), however in Fig. 5.26 there are a greater number of transitions associated with either Surelease or Opadry I. This corresponds to the increase in domain size compared to minitables observed in tapping mode AFM of uncured minitables coated with a 50:50 blend of Surelease and Opadry I. The contact AFM image in Fig. 5.27 shows a similar appearance to other coated minitables in that a generally “smoother” appearance is observed.

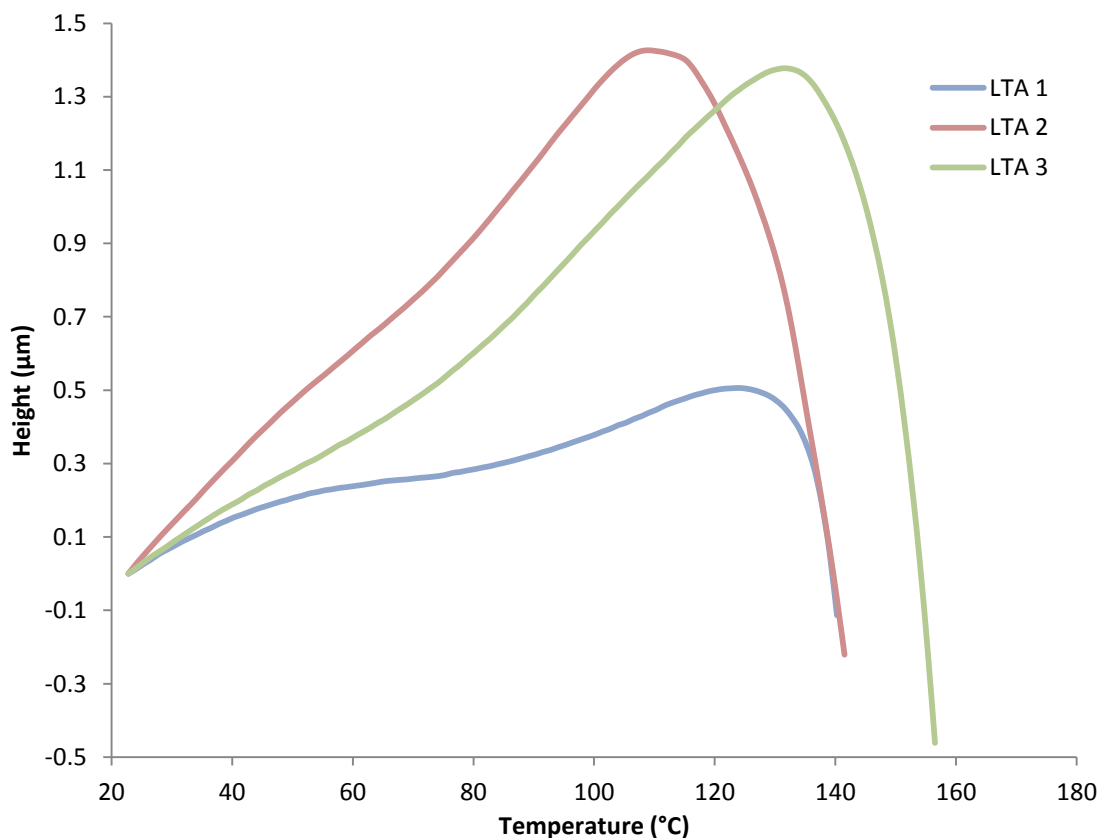


Figure 5.28 L-TMA of minitables coated with a Surelease and Opadry I 50:50 blend and cured for 6 hours at locations specified in Fig. 5.27

Fig. 5.28 shows L-TMA results performed at locations specified in Fig. 5.27, and consistent with other topography images of the polymer blends L-TMA on topographic features did not provide information on the morphology of the blend. Transitions in Fig. 5.28 show the intermediate transition around 140°C and a higher transition associated with a region of Opadry I.

L-TMA performed on minitables coated with 50:50 blends of Surelease and Opadry I and cured for 24 hours a number of L-TMA traces are present around 90°C and

160°C representing Surelease and Opadry I respectively.

There is still an intermediate glass transition present at 139.7°C ($\pm 6.49^\circ\text{C}$ sd; n=16), which is consistent with the intermediate value observed for minitablets cured for 6 and 12 hours. As discussed above the intermediate transition is somewhat lower than the transition observed for uncured minitablets and this observation will be considered further in the discussion.

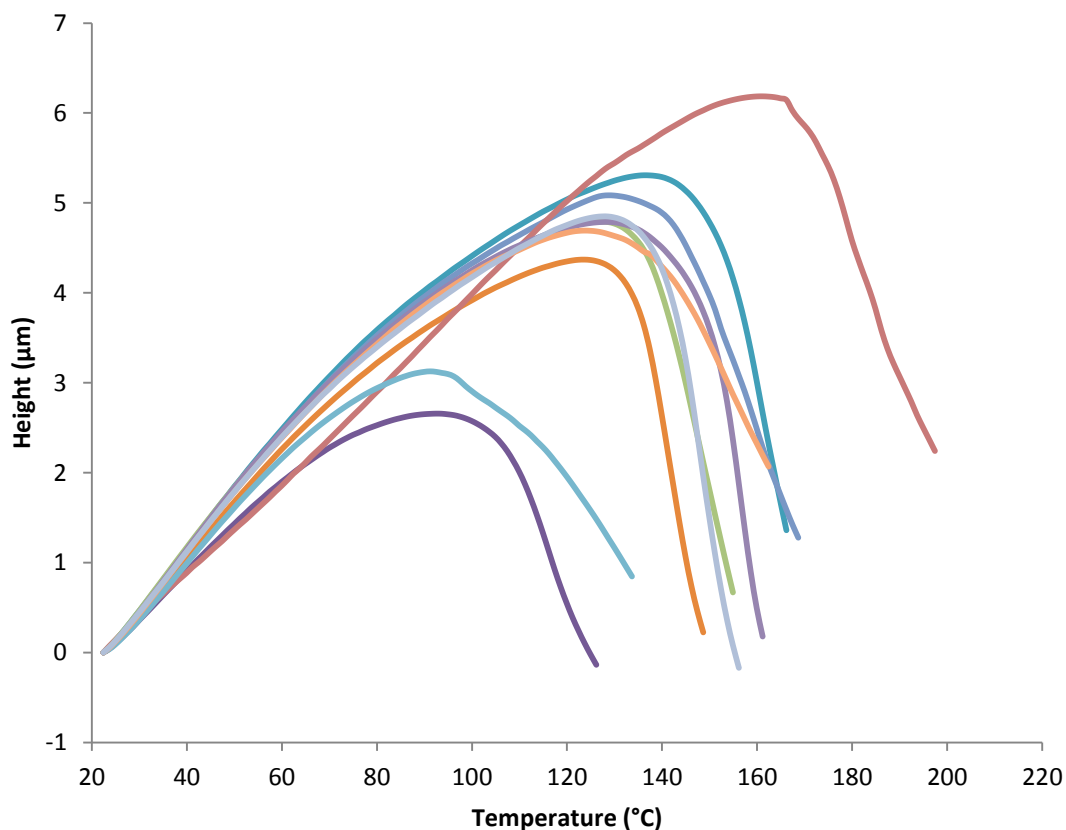


Figure 5.29 L-TMA of minitablets coated with a Surelease and Opadry I 50:50 blend cured for 24 hours

Figs. 5.30 and 5.31 show an AFM image acquired in contact mode with L-TMA performed at specific locations. The L-TMA show the increased occurrence of transitions associated with either Surelease or Opadry I; in this case being two L-TMA traces indicating the presence of Opadry I. As with other topography images the location of the L-TMA did not bear any significance to areas of topographic interest.

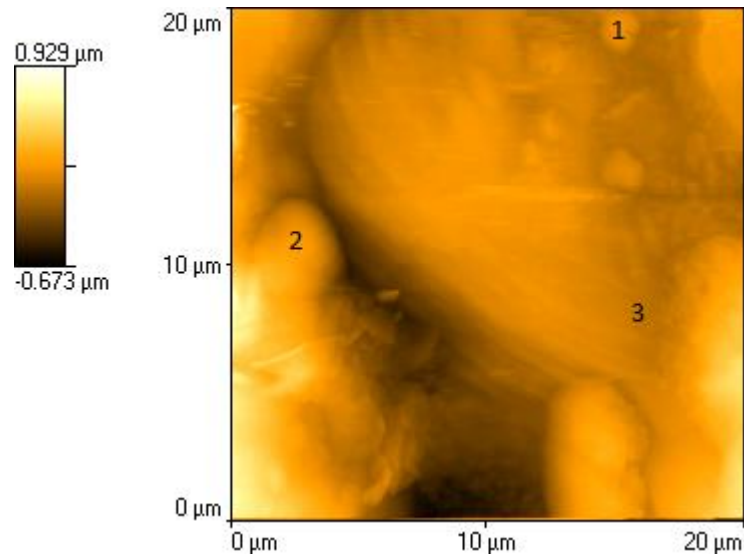


Figure 5.30 Contact AFM image of minitabets coated with a Surelease and Opadry I 50:50 blend and cured for 24 hours, numbers denote locations of L-TMA

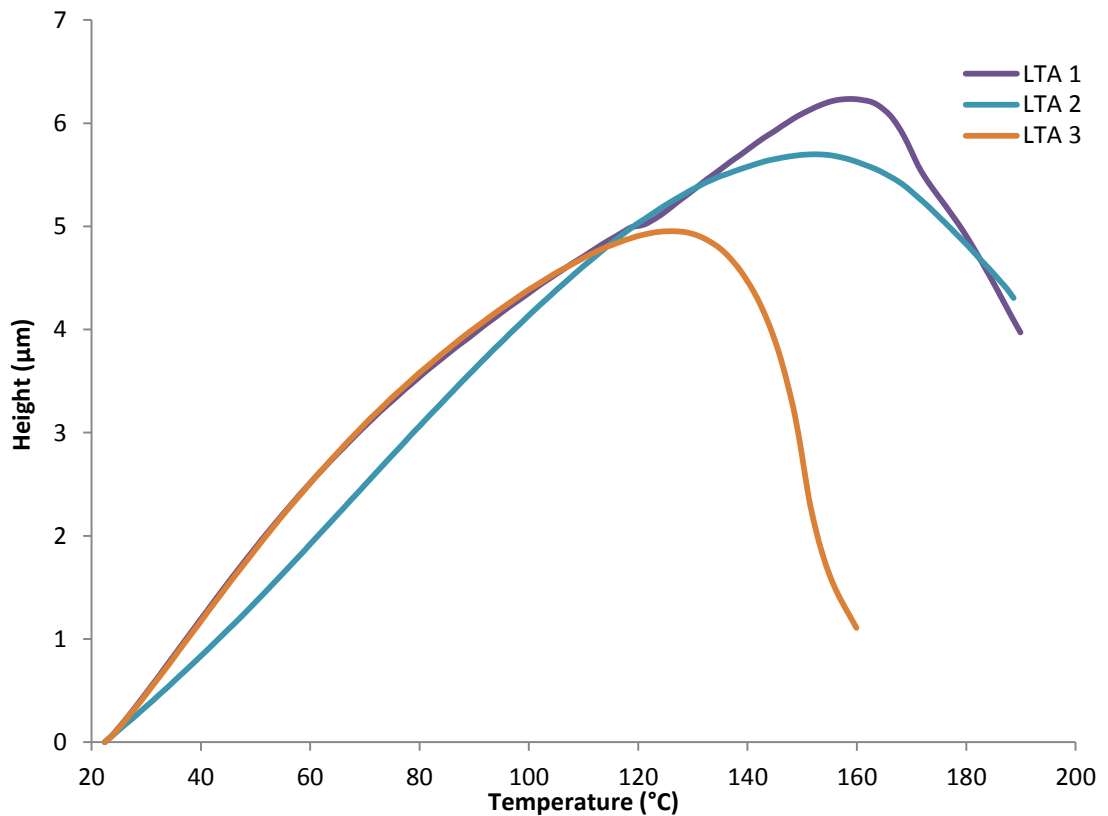


Figure 5.31 L-TMA of minitabets coated with a Surelease and Opadry I 50:50 blend and cured for 24 hours at locations specified in Fig. 30

The L-TMA combined with the heated tapping mode results indicate the further coalescence of the Surelease resulting in larger domains of Surelease rich areas of

the polymer films, with this increase resulting in a greater number of L-TMA results from attributed to either Surelease or Opadry I.

5.4.4 Surelease and Opadry II 50:50 Blend

5.4.4.1 Heated Tip Tapping Mode

Tapping mode images of minitables coated with a 50:50 blend of Surelease and Opadry II which were cured for 6 hours are shown in Fig. 5.32 and 5.33. The topography image at room temperature is similar to the topographic image of uncured minitables; however as with the other cured minitables of Surelease based films the phase image shows a more homogeneous film.

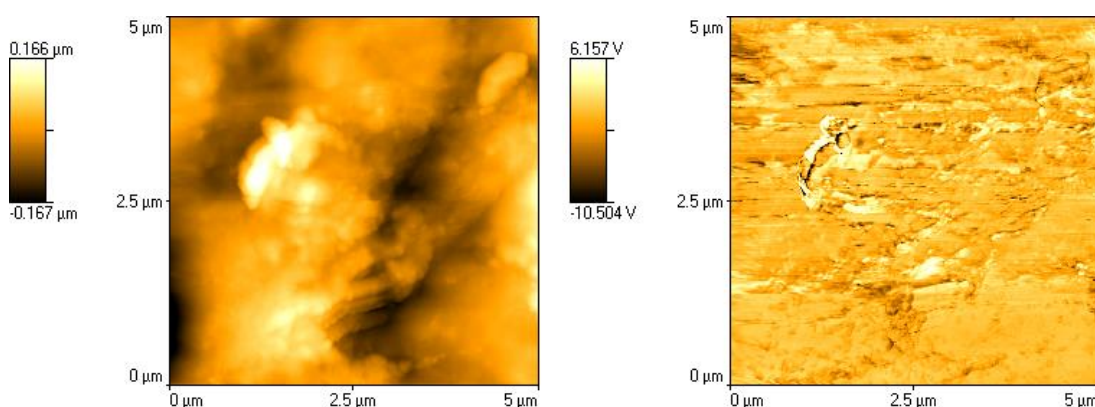


Figure 5.32 Tapping mode image of minitables coated with a Surelease and Opadry II 50:50 blend cured for 6 hours showing topography (left) and phase (right)

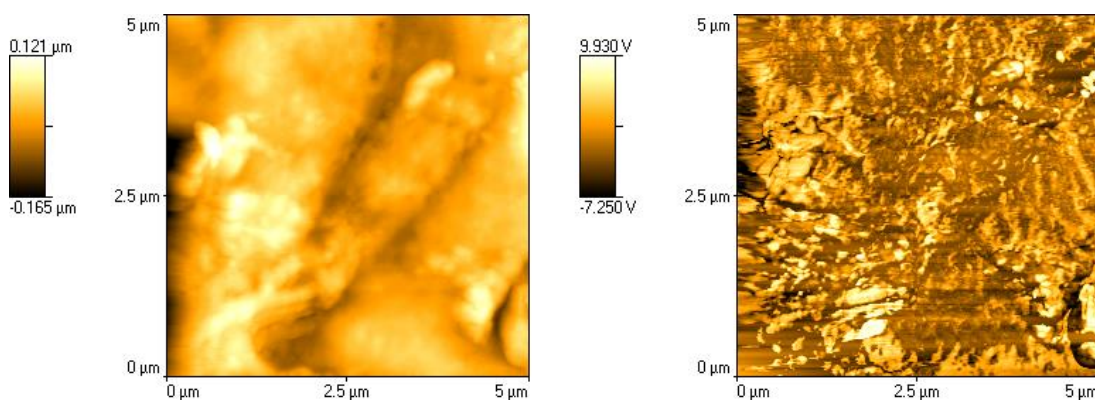


Figure 5.33 Heated tip tapping mode image with the probe held at 70°C of minitables coated with a Surelease and Opadry II 50:50 blend cured for 6 hours showing topography (left) and phase (right)

Heated tip tapping mode imaging was performed at 70°C, therefore aiming to soften PVA whilst keeping the ethylcellulose portion of the film relatively stiff, with the results for minitables cured for 6 hours shown in Fig. 5.33. Larger domains of Surelease can be observed in the phase image compared to uncured minitables indicating the further coalescence of the ethylcellulose on curing.

This trend continues with minitables cured for 12 and 24 hours which are shown in Figs. 5.34 through 5.37. Inspection of the heated tip tapping mode phase images indicates the further coalescence of the ethylcellulose film.

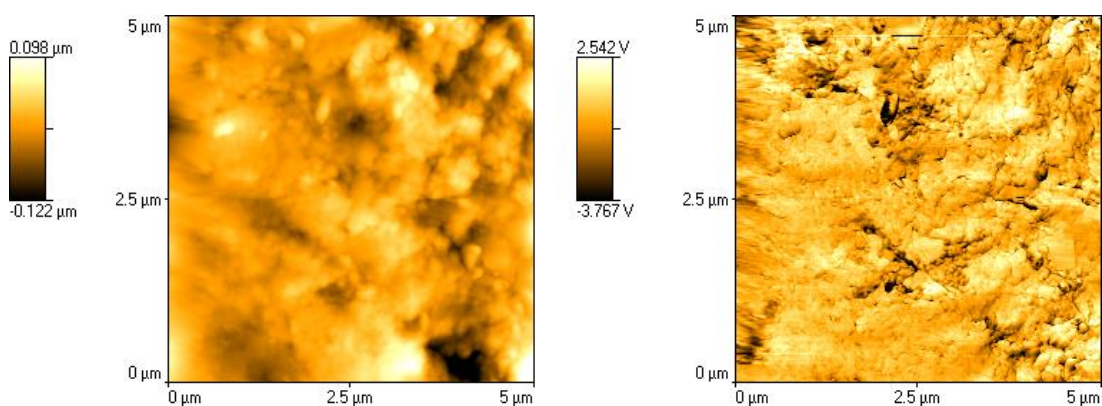


Figure 5.34 Tapping mode image of minitables coated with a Surelease and Opadry II 50:50 blend cured for 12 hours showing topography (left) and phase (right)

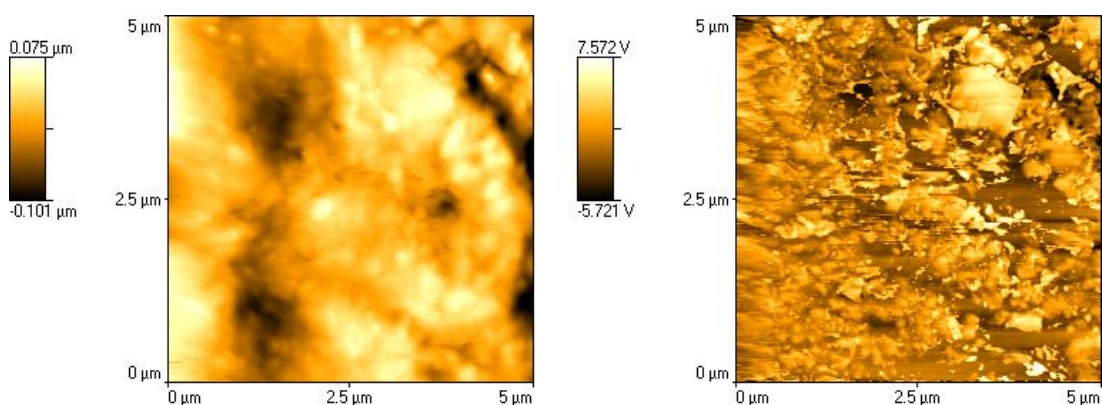


Figure 5.35 Heated tip tapping mode image with the probe held at 70°C of minitables coated with a Surelease and Opadry II 50:50 blend cured for 12 hours showing topography (left) and phase (right)

Of particular note is the heated tip tapping mode phase image of minitables cured for 24 hours. The further coalescence of Surelease has produced larger domains than those observed in uncured minitables with numerous domains in excess of $1\mu\text{m}^2$.

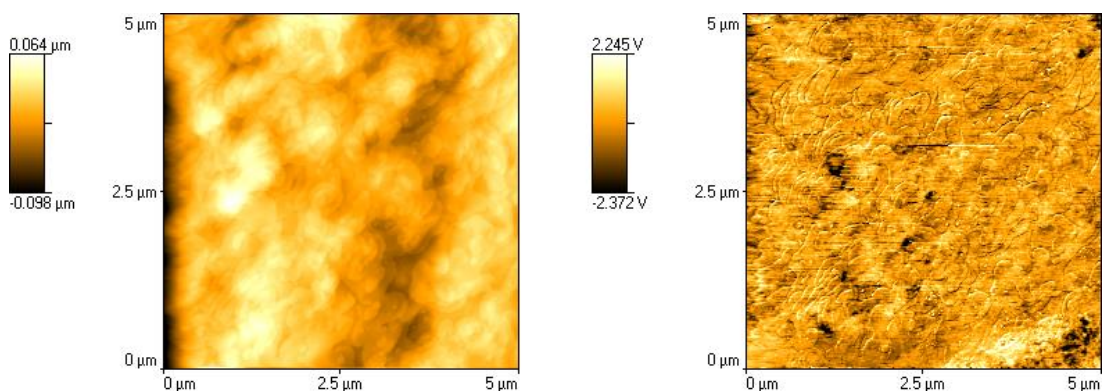


Figure 5.36 Tapping mode image of minitablests coated with a Surelease and Opadry II 50:50 blend cured for 24 hours showing topography (left) and phase (right)

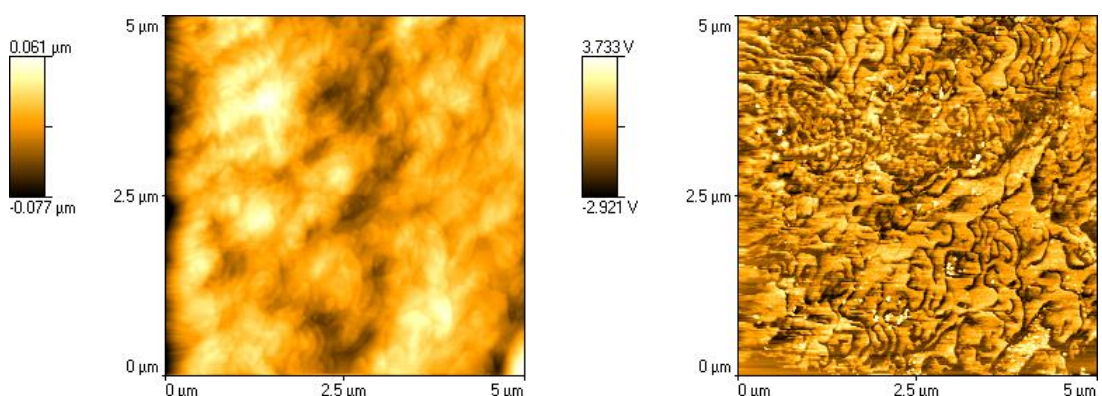


Figure 5.37 Heated tip tapping mode image with the probe held at 70°C of minitablests coated with a Surelease and Opadry II 50:50 blend cured for 24 hours showing topography (left) and phase (right)

The further coalescence of the Surelease in film also resulted in changed to the morphology of the Opadry II portion of the blend, with domains of Opadry II appearing as thin strips in the image analogous to blends undergoing spinodal decomposition.

With this change in morphology it will be of note to see if the L-TMA results correspond to this change in morphology, as the number of transitions associated with Opadry II should decrease and those for Surelease to increase.

5.4.4.2 Contact Mode Images and L-TMA

L-TMA results for Surelease and Opadry II 50:50 coated minitablests cured for 6 hours are shown in Fig. 5.38. The transition temperatures appear consistent with the

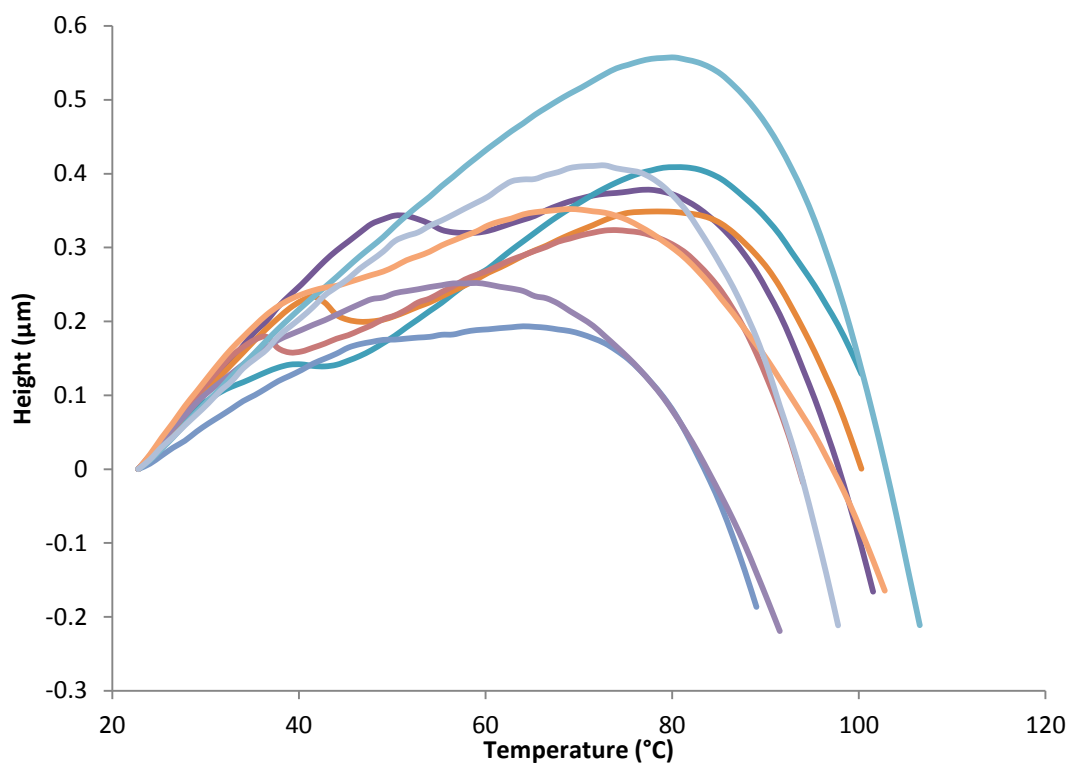


Figure 5.38 L-TMA of minitabets coated with a Surelease and Opadry II 50:50 blend cured for 6 hours

uncured minitabets with the transition for Opadry II appearing at 45.6°C ($\pm 3.3^{\circ}\text{C}$ sd; $n=5$), Surelease at 88.1°C ($\pm 1.9^{\circ}\text{C}$ sd; $n=10$) and the intermediate temperature observed at 79.8°C ($\pm 1.9^{\circ}\text{C}$ sd; $n=10$).

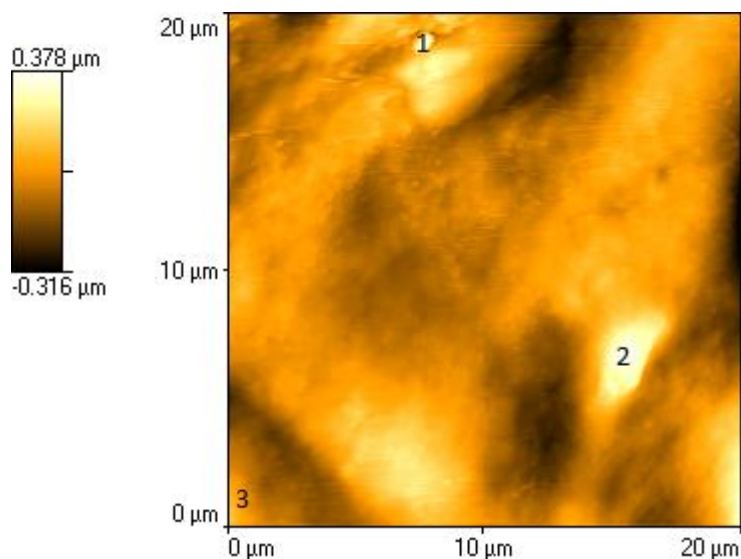


Figure 5.39 Contact AFM image of minitabets coated with a Surelease and Opadry II 50:50 blend and cured for 6 hours, numbers denote locations of L-TMA

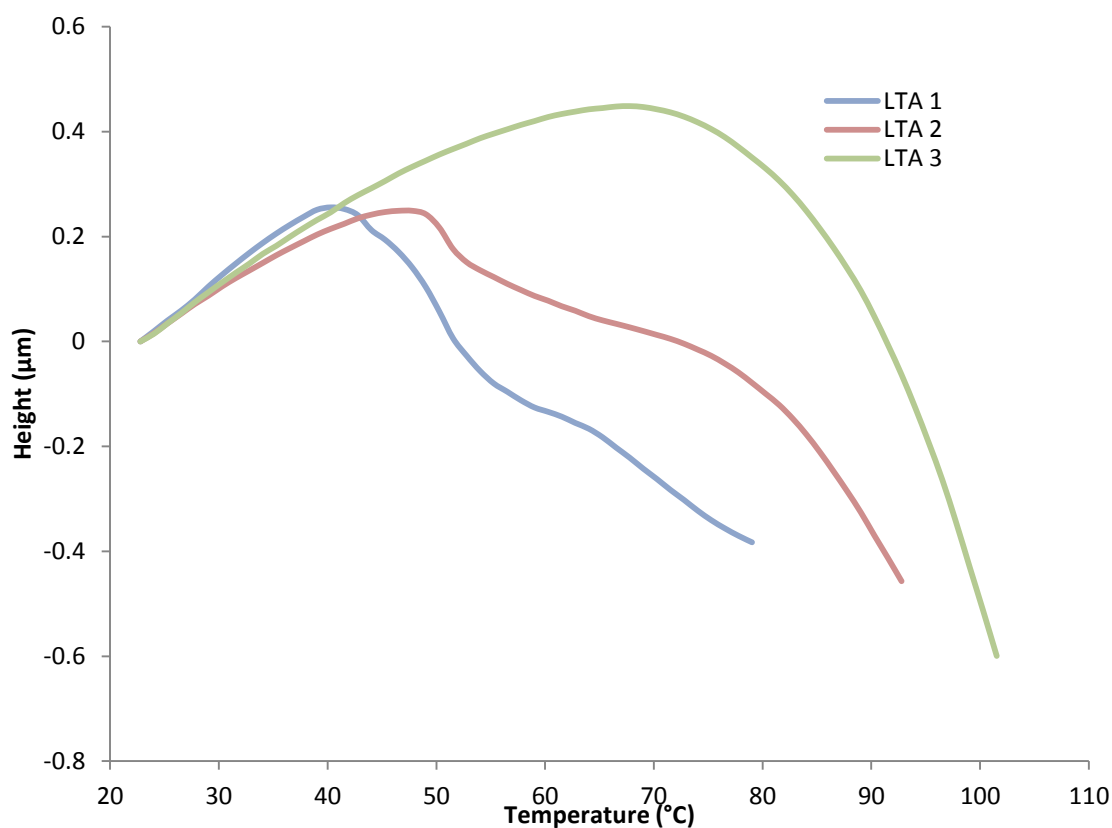


Figure 5.40 L-TMA of minitabets coated with a Surelease and Opadry II 50:50 blend and cured for 6 hours, at locations specified in Fig. 5.39

Contact images and L-TMA results performed at specified locations are shown in Fig. 5.39 and 5.40. The two lighter regions produce L-TMA results indicating the presence of Opadry II with the darker region in the image showing an intermediate transition. However, this was not consistent across all the images produced, therefore as with other contact images of polymer blends with L-TMA performed it was not possible to identify areas of polymer from sample topology.

Once minitabets had been cured for 12 hours the transition temperatures for the intermediate transition and for Surelease were recorded as 78.7°C ($\pm 4.9^\circ\text{C}$ sd; n=20) and 90.5°C ($\pm 2.9^\circ\text{C}$ sd; n=5), However the glass transition for Opadry II showed a decrease to 42.2°C ($\pm 4.9^\circ\text{C}$ sd; n=5).

Fig. 5.42 shows a contact mode image with locations for L-TMA indicated. The image is similar to minitabets cured for 6 hours, however as with Fig. 5.39 it is not possible to ascertain information regarding the locations of the polymers from the topographic information. This is shown in Fig. 5.42 and 5.43 with the light area

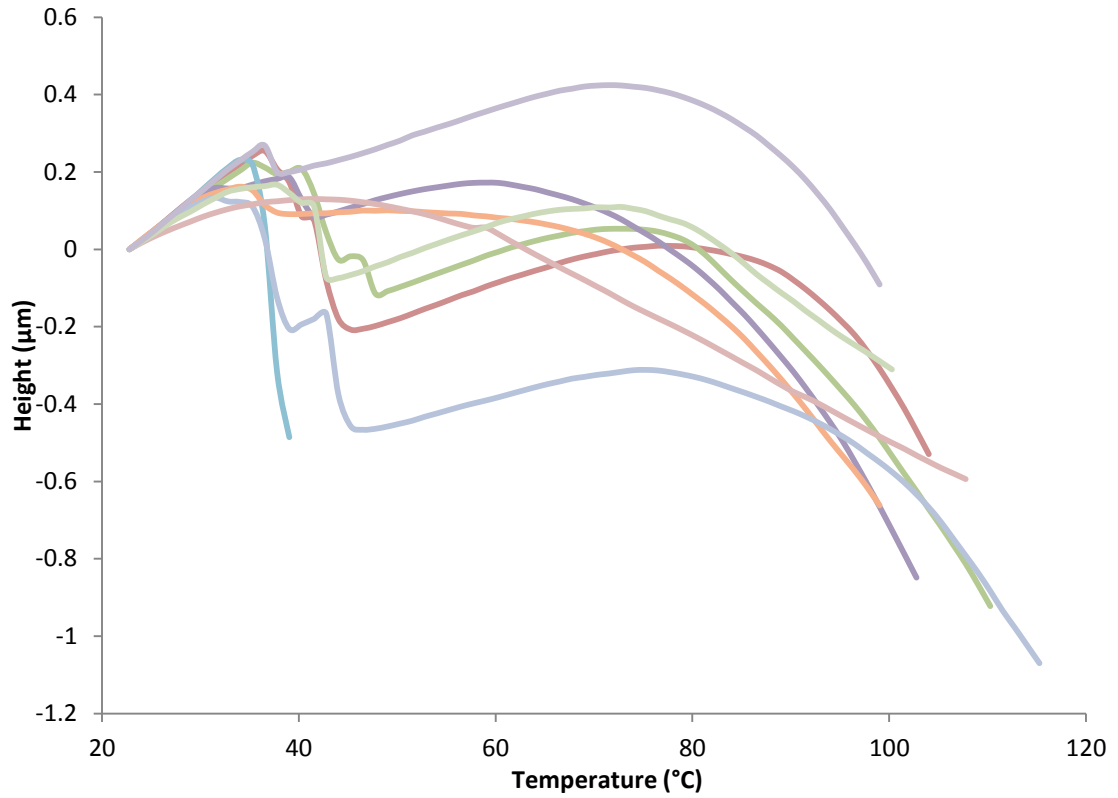


Figure 5.41 L-TMA of minitabets coated with a Surelease and Opadry II 50:50 blend cured for 12 hours

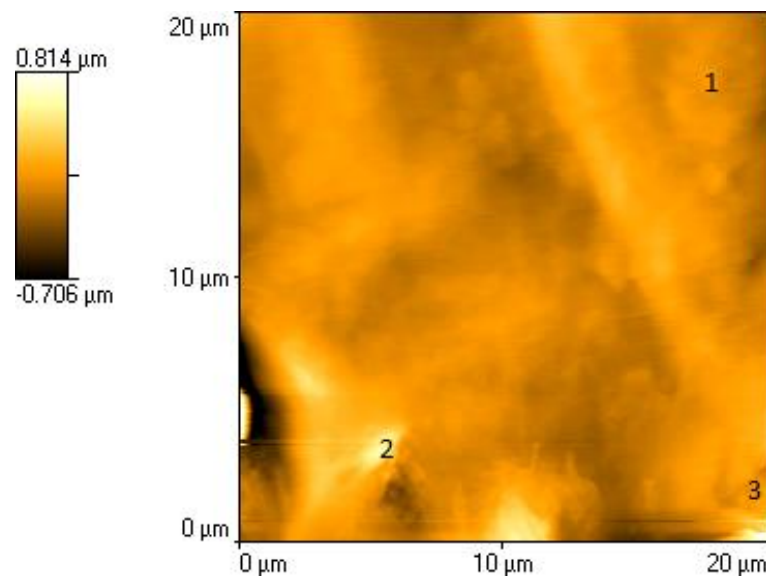


Figure 5.42 Contact AFM image of minitabets coated with a Surelease and Opadry II 50:50 blend and cured for 12 hours, numbers denote locations of L-TMA

showing an intermediate transition temperature, and darker areas showing transitions associated with both Opadry II and Surelease.

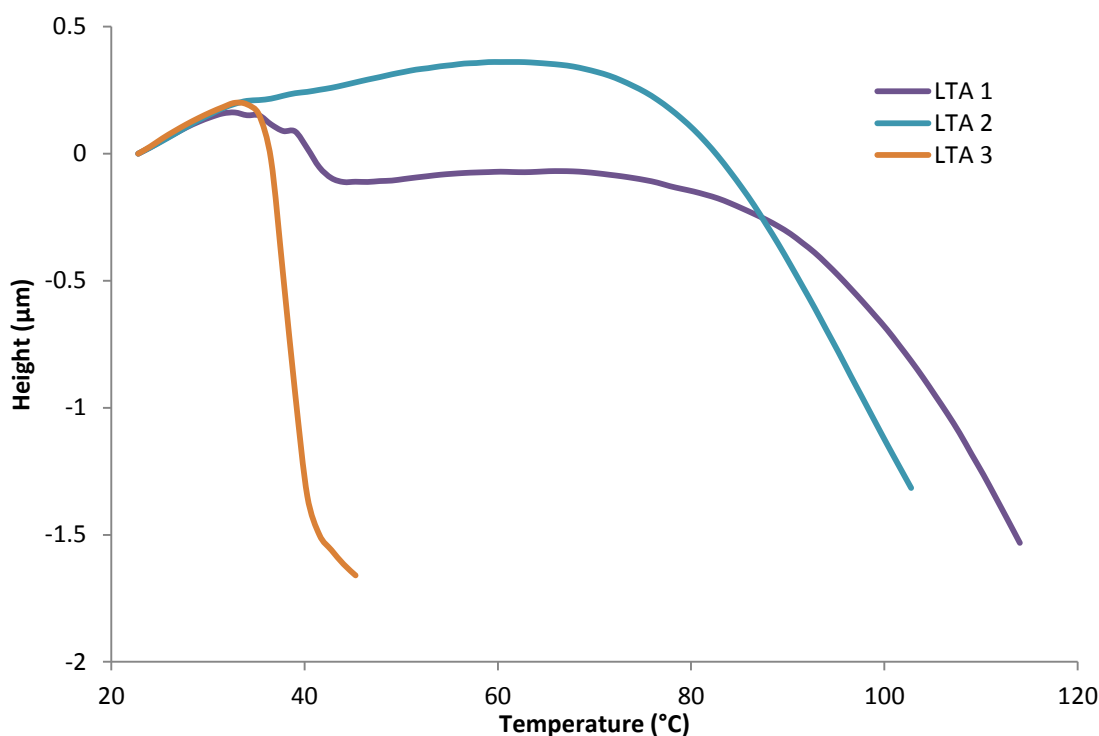


Figure 5.43 L-TMA of minitables coated with a Surelease and Opadry II 50:50 blend and cured for 12 hours, at locations specified in Fig. 5.41

As with the minitables cured for 12 hours the transition temperature of the intermediate transition and Surelease remained relatively constant at $78.4 (\pm 2.8^{\circ}\text{C sd}; n=10)$ and $88.7 (\pm 2.5^{\circ}\text{C sd}; n=10)$. The transition for Opadry II was recorded as $36.1 (\pm 3.3^{\circ}\text{C sd}; n=2)$, which continues the trend observed in minitables cured for 6 hours, and is shown in Fig. 5.44.

The likely cause of the low number of transitions observed is due to the further coalescence of the Surelease the Opadry II domains became smaller, which can be seen in Fig. 5.37. The relatively large Surelease domains resulted in many of the Opadry II domains being in the sub 100nm range making detection through L-TMA difficult.

Additionally a decrease in the number of transitions attributed to the crystalline component was observed, which again is likely to be due to the increased domain size of Surelease leading either to smaller regions of crystalline areas or the inhibition of growth of the crystalline phase.

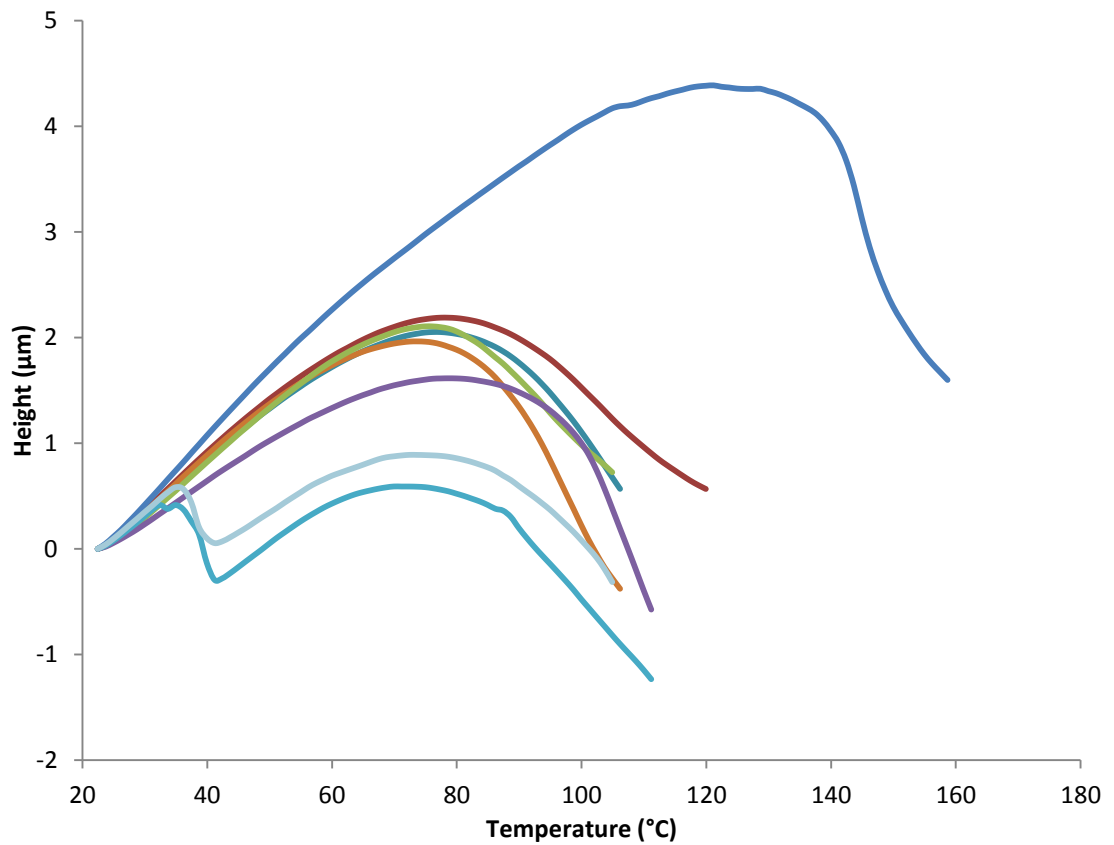


Figure 5.44 L-TMA of minitabets coated with a Surelease and Opadry II 50:50 blend cured for 24 hours

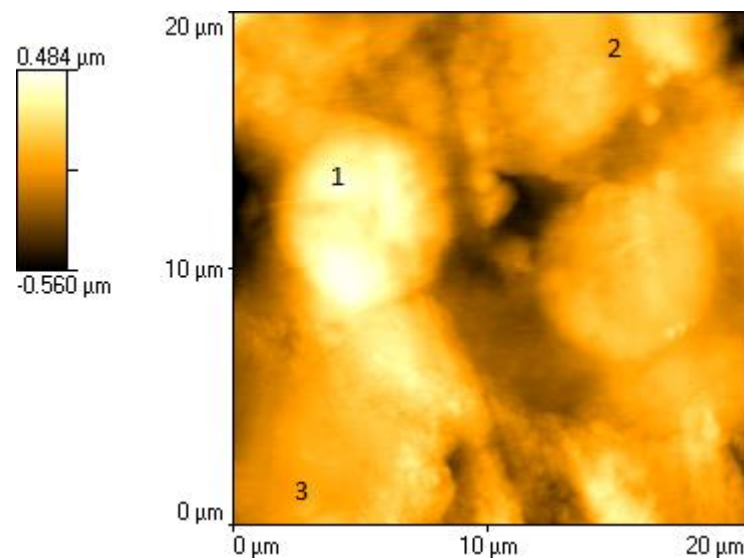


Figure 5.45 Contact AFM image of minitabets coated with a Surelease and Opadry II 50:50 blend and cured for 24 hours, numbers denote locations of L-TMA

The contact mode AFM image and corresponding L-TMA shown in Fig. 5.45 and 5.46 again does not show information on the distribution of phases, with intermediate transitions observed in both light structures and darker areas.

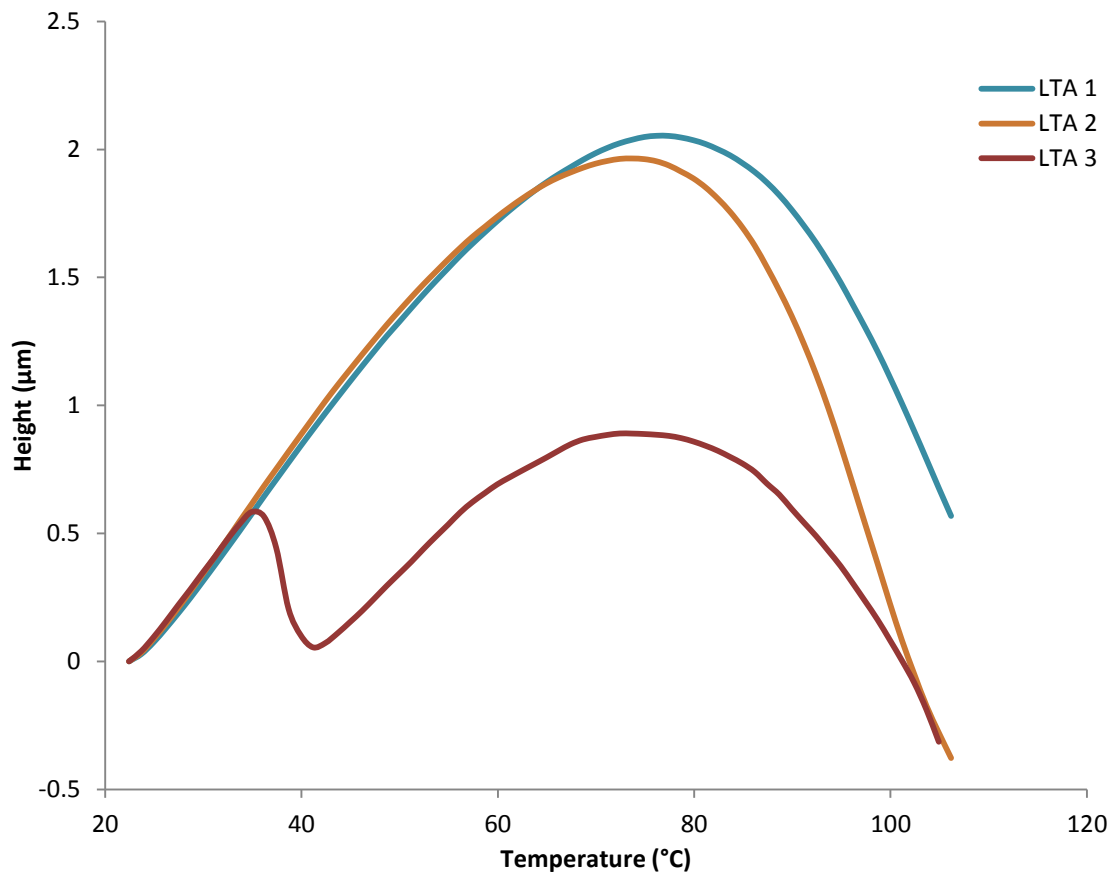


Figure 5.46 L-TMA of minitabets coated with a Surelease and Opadry II 50:50 blend and cured for 24 hours, at locations specified in Fig. 5.44

5.5 Discussion

Variations in the morphology of the film coated minitabets can be explained by film forming theories related to the formation of polymer films from aqueous latexes. As discussed in Chapter 1 water is driven off from a pseudolatex causing the dispersion to become more concentrated resulting in the pseudolatex particles coming closer together eventually deforming and trapping water between the particles. Further water is driven off and the particles start to coalesce and eventually polymer chains interdiffuse to produce a homogeneous mix. Of note is that the polymer chains must be mobile for interdiffusion to occur, therefore the film coat must be at a temperature approaching its T_g to allow for sufficient mobility of the polymer chains.

Once the film coating process was complete for the uncured minitabets they were dried in the MCD-2 coater for 10 minutes and then stored in desiccators until

analysed. This was unlikely to produce fully coalesced films therefore leading to changes in film morphology once the minitablets were cured. This would explain why the phase images appear to show a more continuous phase of Surelease in all the minitablets, both blends and those coated with a single polymer.

When analysing minitablets coated with Surelease that had not been cured using heated tip tapping mode AFM the onset of dark areas in the image indicating the softening on the polymer was attributed to the polydispersity of the polymer resulting in a wide range of transition temperatures. However the results in this chapter with heated tip tapping mode images displaying a more homogenous surface at elevated temperatures indicates a different conclusion should be drawn.

A possible explanation for appearance of softening at a lower temperature is when the polymer film forms and begins to coalesce the stabilising surfactant can be exuded into pockets, particularly at the film-substrate interface and pertinent to this study the film-air interface (Steward *et al.*, 2000). The ammonium oleate surfactant used in Surelease has melting point around 70°C (Tamamushi, 1972) which if present in small domains on the sample surface could lead to areas of the surface appearing to soften around 20°C lower than the glass transition for Surelease. Along with other additives that are produced in the Surelease film such as glycerine and various fatty acids (Colorcon 2006b), which are either liquid at room temperature or have relatively low melting points, this could lead to Surelease films appear to soften at considerably lower temperatures. As with the drying of minitablets coated with polymer blends these domains may be relatively small and not be detected during L-TMA measurements. In addition the close proximity of the transition temperatures will make it hard to observe in heated tip tapping mode AFM.

The appearance of larger domains when the films are cured helps support the conclusions of nanophases being present from Chapter 4. This is due to phase separated polymer system being thermodynamically stable as can be seen in the Flory-Huggins equation:

$$\Delta G_m = kT(N_1 \ln v_1 + N_2 \ln v_2 + \chi_1 N_1 v_2) \quad (5.1)$$

Where 1 and 2 represent the two polymers, ΔG_m is the Gibbs free energy of mixing, k is the Boltzmann constant, T is absolute temperature, N_x is the number of molecules of the polymers, v_x is the volume fraction of the polymers and χ_1 is the Flory-Huggins interaction parameter. As discussed in Chapter 1 the first two terms of equation 5.1 are entropic and for large molecular weight molecules such as polymers this value will be low leading to a low entropic value for the system. A negative ΔG_m is required for spontaneous mixing of the two polymers which is favoured by a large and positive entropy value, which is not possible with large molecular weight polymers.

Therefore a phase separated polymer system that is thermodynamically stable will progress to reduce the interfacial area between the two polymers and thus the interfacial energy in the system to remain stable. By definition this is due to an increase in the surface area which will result in a decrease in the Gibbs free energy:

$$\Delta G = \gamma \Delta A \quad (5.2)$$

where γ represents interfacial tension and ΔA the change in surface area. It has been thoroughly reported in the literature that the interfacial tension of polymer blends reduces with increased temperature (Dee *et al.*, 1992, Spiros *et al.*, 1988) and can be described by the Cahn-Hilliard power law:

$$\gamma \sim \left(1 - \frac{T}{T_c}\right)^\mu \quad (5.3)$$

where T_c is the critical temperature where surface tension disappears and μ is the critical exponent. It can be seen in eq. 5.3 that with increasing temperature the interfacial tension will decrease.

As stated above previous research has indicated that the glass transition of polymers tends to increase with curing (Bhattacharjya *et al.*, 2008, Felton *et al.*, 2001) as plasticisers and water tend to be driven off resulting in an increase in the glass transition of the final film. This occurred in the Surelease coated minitables with a gradual increase in the average transition temperature observed as the curing time

increased. This increase was coupled with a rise in the standard deviation in transition temperature observed resulting in the increase not being statistically significant, however the general trend was an increase in the transition temperature.

However in the polymer blends a decrease in the intermediate glass transition temperatures was observed for the Surelease and Opadry I 50:50 blend. This result was not expected due to the results from previous studies and the L-TMA results for Surelease also observing an increase in the transition temperature.

A possible explanation for this is due to the increase in domain size of Surelease in the film coated minitables the alteration in the phase distribution could lead to a change in the intermediate transition temperature observed. Therefore when L-TMA is performed on the minitables surface there may be a larger proportion of Surelease under the probe tip leading to a lower transition temperature observed, analogous to the reduction in the intermediate transition observed when the ratio of Surelease is increased in the polymer blend.

As with the Surelease and Opadry I blend alterations in the L-TMA profiles were observed for Surelease and Opadry II blends, however these changes were different between the two polymer blend systems. The Surelease and Opadry I system exhibited a higher number of transitions for the individual polymers and a decrease in the intermediate transition temperature observed. In the Surelease and Opadry II blend, however, the number of transitions associated with the individual polymers did not increase and the intermediate transition temperature remained constant with increased curing time. These differences in alterations to the L-TMA responses could be due to differences observed in the heated tip tapping mode experiments. On curing the Surelease rich domains in the Surelease and Opadry I blend tended to be present as spherical droplets which grew in size, however the Surelease and Opadry II phase separation produced differing surface morphology. This is likely to lead to the different variations of L-TMA results present for the two systems.

5.6 Conclusions

The results in this chapter indicate the further coalescence of Surelease resulting in observable changes in the surface morphology of the film coated minitablets through the use of heated tip tapping mode AFM. An increase in the domain size of Surelease was observed in the both the blends of Surelease and Opadry I and Surelease and Opadry II indicating the further coalescence of Surelease into a homogenous film.

L-TMA was able to detect alterations in the glass transition temperatures of the polymer systems from alterations in phase distribution due to further coalescence of the polymers. Although there was an increase in the domains of Surelease observed in heated tip tapping mode, this was not sufficient to eliminate the intermediate transition observed in L-TMA profiles of the polymer blends.

The 50:50 blend used in this study is a composition that would not be used in film coating for controlled release, and was used in this study as a model system to determine the feasibility of the techniques used to analyse them. Therefore it would be of interested to analyse blends with a higher Surelease content that are commonly used for controlled release coatings. Additionally once a curing step has been completed any changes to the phase distribution on aging would be valuable to ascertain as the curing step should reduce the effects of physical aging.

The use of heated tip tapping mode AFM to characterise film coated dosage forms could potentially be employed to assess the performance of prolonged release formulations through the measurement of the degree to which the film has been cured. There would be limitations as the process would have be validated to ensure the alteration of surface characteristics observed in the AFM images related to a change in film behaviour in-vivo. However it could be a useful tool complementary to dissolution testing.

CHAPTER 6

6. Analysis of Pigments Incorporated into Polymer Films

6.1 Introduction

Pigments are frequently used in polymer film coats for numerous reasons, including improvement of the appearance of the final dosage form, easing of product identification for healthcare professionals and patients, and enhancement of drug stability for photolytic compounds and counterfeiting.

The numerous excipients required in a solid dosage form can culminate in a mottled tablet core, which an opaque pigment can disguise, and along with the glossy finish of a polymer film coat can improve the final appearance of the solid dosage form. The opaque nature of pigments can also provide increased stability for photolytic compounds which, similar to mottled tablet core, a translucent film coat could not provide.

The formulation of many solid dosage forms results in a white finish, which can lead to confusion with patients, especially in elderly and visually impaired populations which a distinctly marked tablet can help avoid. Distinctly marked solid dosage forms can also help reduce counterfeiting; with, for example, Colorcon employing pearlescent coatings to help distinguish legitimate tablets from counterfeited examples. There are several innovative attempts to reduce counterfeiting including applying a pigmented film coat, the printing of a holographic logo onto the tablet and then a final film coat being applied (Yoder *et al.*, 2007). Another approach is to apply two coats of distinct colours and the use of a laser to etch the top layer and expose the underlying film to provide a two tone appearance (Yoder *et al.*, 2010).

Commonly used pigments include aluminium lakes of water soluble dyes, where by a dye is chemically bonded to aluminium hydroxide producing a water insoluble

pigment. Iron oxides are also commonly used including Fe_3O_4 (black), Fe_2O_3 (red) and $\text{Fe}_2\text{O}_3 \cdot \text{H}_2\text{O}$ (yellow). Titanium dioxide produces extremely white films, and is therefore often used as an opacifier. It can also be mixed with aluminium lakes or iron oxides to produce pastel shades (Nyamweya *et al.*, 2008).

The content of pigments in the film coat can vary greatly with the range in a typical Methocel formulation being between 50-200% (Dow 2002); with the amount of pigment added to a film dependent on the final shade required. There is a maximum concentration of pigment that can be incorporated into the polymer film, known as the critical pigment volume concentration (CPVC), which is defined as the minimum amount of polymer needed to completely surround the pigment particles in the dry film. Once the CPVC is reached properties of the film such as permeability, gloss or mechanical strength alter substantially (Gibson *et al.*, 1988).

The distribution of pigments in polymers films is a key concern in solid dosage form development as consistency of colour over the surface and between each unit can easily be detected by the patient and the manufacturer. Colour uniformity tests have historically been carried out using a tristimulus colorimeter and the “CIE ($L^* a^* b$) Formula”, which is standard method for the representation of colour in computer software (Bogdansky 1975, Chan *et al.*, 2001), and recently there has been interest in the use of spectroscopy (Madamba *et al.*, 2007). To the authors knowledge there has not been any work analysing pharmaceutical film coats with pigments added by AFM or thermal probe methods. AFM could provide a useful tool in this area, as surface roughness, which has an effect on gloss, can be determined by AFM, and the distribution of pigments on the surface of the film coat can also be determined.

It would be expected that AFM imaging should be able to determine areas of pigment, especially in tapping mode as the difference in stiffness between the polymer and the iron oxide should be considerable. L-TMA should also be able to distinguish between areas of polymer and pigment once an image has been acquired. In addition the pigments can cause restriction of polymer chain movement therefore an increase of the glass transition temperature of the polymer films would be expected to occur.

6.2 Materials and Methods

Iron (III) oxide (99%) (Sigma Aldrich) was used as a model pigment and was incorporated into coating solutions of Opadry I or Opadry II. The polymer was distributed in distilled water according to the manufacturer's guidelines, and once the polymer was fully dispersed 10% w/w by polymer weight of pigment was added and mixed using a magnetic stirrer for 30 minutes prior to coating.

Cast films were prepared from the film coating solutions by pouring 15ml into Petri dishes of 9cm diameter, which were then placed in an oven and held at 45°C overnight for 12 hours. The dried films were then placed in a desiccator until analysed.

Bi-convex minitables were prepared on a Riva Piccola rotary tablet press and were also gifts from Colorcon. 20g batches of minitables were coated in a Caleva Mini Coater Drier-2 (Caleva Sturminster Newton, Dorset). Process conditions are listed in table 1, with a weight gain of 2% achieved for both Opadry I and II coated minitables.

Parameter	Opadry I + Fe ₂ O ₃	Opadry II + Fe ₂ O ₃
Air Inlet Temperature (°C)	40	45
Process Air Flow (m/s)	12	12
Atomising Air Pressure (bar)	0.7	0.7
Flow Rate (ml/hr)	23	23
Process time (min)	45	45

Table 6.1 Process conditions for film coating of minitables

All MTDSC measurements were carried out using a Q2000 DSC (TA instruments, Newcastle, USA) and L-TMA experiments were carried out with a nano-TA2 box (Anasys Instruments) using AN2-200 nano-TA probes (Anasys instruments) mounted onto a Caliber AFM (Veeco) AFM head. Statistical analysis was performed in a separate spread sheet using the student t-test.

Grain analysis was performed in the AFM software to determine the percentage of the film attributed to the pigment particles, with the edge of the pigment particles being determined by marking a threshold of a certain parameter in the image. In the case of the phase images a certain voltage was set as the threshold with values above and below this voltage attributed to the polymer or the pigment. A detailed method is provided in Chapter 3.

In addition to L-TMA being performed in contact mode, experiments were also conducted in Tapping Mode AFM. Any features therefore observed in the phase image but not seen in the topography can be analysed directly without the need for withdrawing the tip and changing modes, which may cause significant displacement of the tip relative to the sample.

The procedure to perform L-TMA in tapping mode compared to contact mode is slightly different as when undertaking L-TMA in contact mode the probe has to be in contact with the sample to allow for data to be collected. As tapping mode is an intermittent contact mode if the feedback is simply disengaged the resultant L-TMA trace will not show the correct probe response. Therefore after the image is acquired in tapping mode and the probe positioned in the desired location the probe has to come into contact with the sample. As mentioned above changing the mode of the AFM is not practical as the probe has to be withdrawn and there is considerable movement of the probe tip relative to the sample when changing the mode. It is therefore more accurate to force the probe into contact whilst still in tapping mode. This is achieved by lowering the set point to roughly one tenth of the value for imaging, causing the probe to effectively not leave contact during oscillation. Before lowering the set point the probe can be moved to any location in the image, in identical fashion to when the probe is in contact mode, and before the thermal ramp is applied to the probe feedback is disengaged. In addition once the thermal ramp is then commenced the set point has to be raised; which is to avoid the probe driving too far into the sample once softening occurs due to the high set point used.

The main difference observed in L-TMA obtained in tapping mode is at the beginning of the L-TMA, where a sharp dip can be observed in the y -axis. This is the probe “jumping” into contact. This precludes using the technique to analyse samples

with a transition temperature below around 50°C as any transitions occurring below this temperature cannot be used with any confidence. Furthermore any transitions occurring in this range may be masked by the “jump to contact”. In this study this would preclude the use of L-TMA in tapping mode when analysing Opadry II samples, thus limiting the technique to the samples it can be used to analyse.

6.3 Results

6.3.1 Iron Oxide

6.3.1.2 Modulated Temperature DSC of Iron Oxide Powder

Initially iron oxide was analysed in powder form to ascertain if there were any thermal transitions observable in the temperature range of the polymers used in the study. Iron oxide has a melting point in excess of 1500°C so it was not expected to undergo any form of thermal transition up to 250°C. This indeed was the case for MTDSC as seen in Fig. 6.1, with no observable transitions occurring below 250°C. As the polymers thermal transitions are below this temperature and the nanothermal probes have a maximum operating temperature around 250°C then there is no reason to test the iron powder at these elevated temperatures.

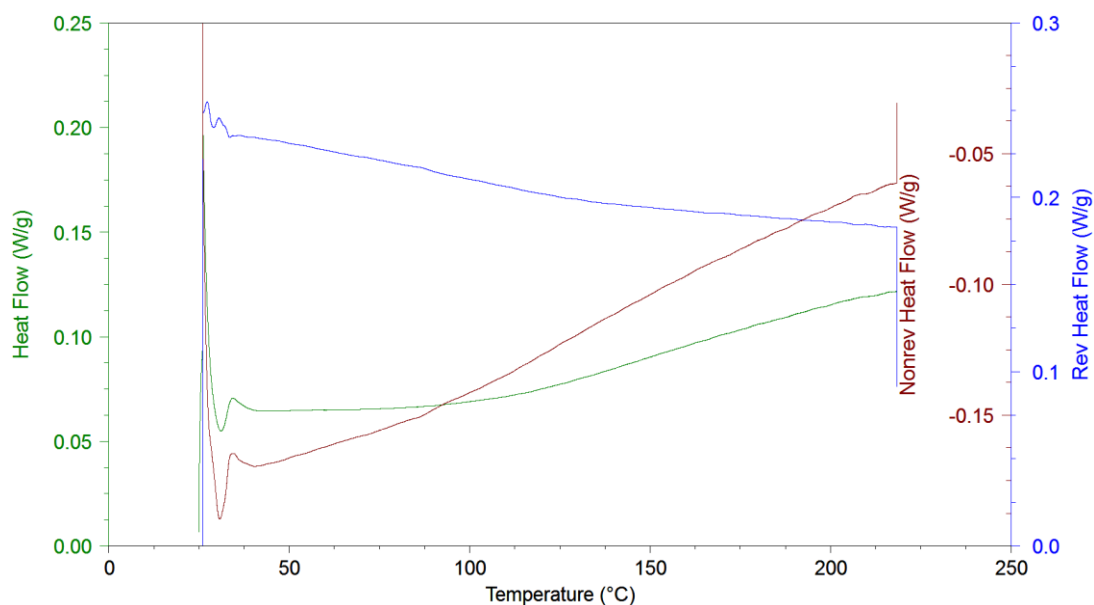


Figure 6.1 MTDSC trace of iron oxide powder

6.3.1.2 L-TMA of Iron Oxide Powder

The iron oxide powder was also analysed using L-TMA with the same results expected. Although imaging powders on AFM is notoriously difficult due to the probe tip dragging the sample across the image as L-TMA only has to make contact with the sample it is easier to achieve.

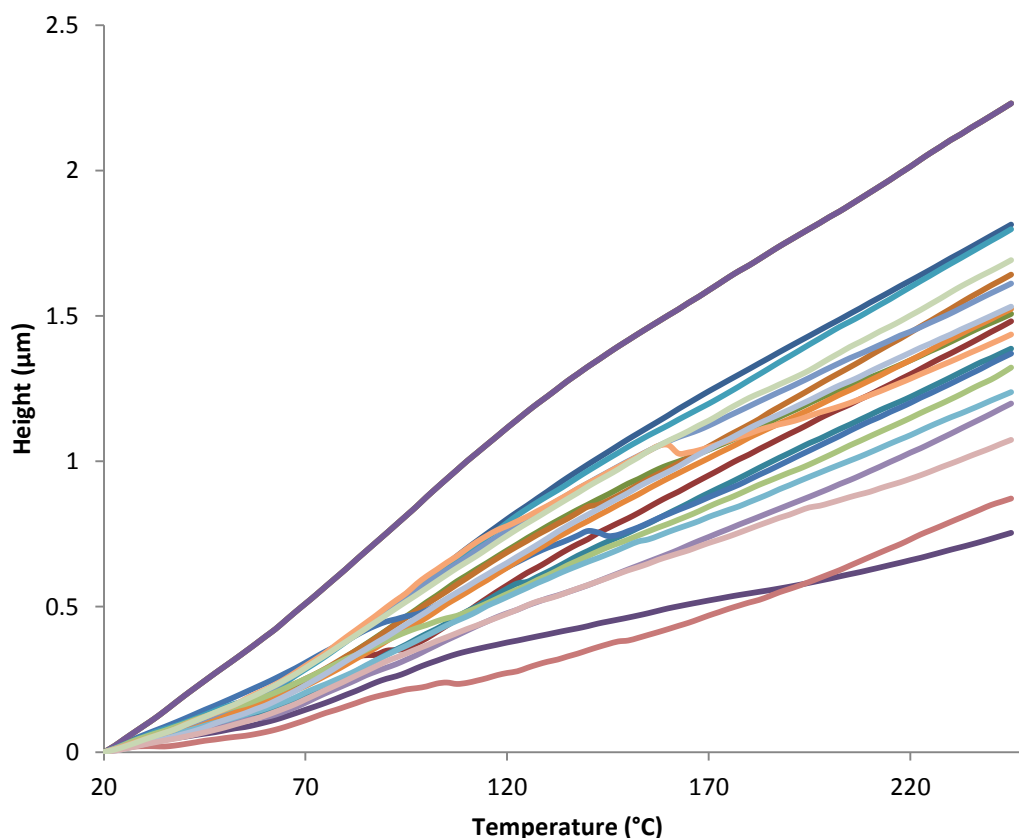


Figure 6.2 Iron oxide Powder analysed by L-TMA

The results were as expected with thermal expansion observed up to 250°C before the temperature ramp was terminated. As none of the transitions for the polymers are observed above 250°C, then there is no reason to run the experiment beyond this value. Some slight discontinuation was observed on some of the traces, but is likely to be due to movement of the iron oxide particles through thermal expansion as the movement of the probe was a fraction of micron, therefore not sufficient to constitute a thermal transition.

Imaging of the iron oxide powder was attempted in tapping mode AFM in an attempt to ascertain the pigment particle shape. However even with the lower forces involved compared to contact mode AFM the tip movement resulted in dragging particles across the image, leading to poor images that could not be analysed.

6.3.2 Cast Films

Cast films were initially analysed by contact mode AFM, tapping mode AFM and L-TMA. Aside from issues with cast film not representing the in-situ behaviour of polymer films other issues such as sedimentation can occur when adding other excipients or drug compounds to cast films. Due to the drying times involved when the coating solution is poured into the petri dish there is sufficient time for these compounds to begin to sediment (Felton *et al.*, 2008). As there has been no work in analysing film coats with added pigments to pharmaceutical films by AFM there is no information on whether pigments will sediment or remain distributed in the films. Tiarks *et al.* (2003) was successful in the use of AFM in determining titanium dioxide distribution in dried paint films, with the results showing the ability to observe the pigment on the film surface.

6.3.2.1 Opadry I with 10% w/w Iron Oxide

6.3.2.1.1 Modulated Temperature DSC

MTDSC results for cast Opadry I films with 10% w/w iron oxide are shown in Fig. 6.3. The average transitions observed was 175.4°C ($\pm 1.4^\circ\text{C}$ sd; n=3), which as recorded in Chapter 3 is higher than the glass transition temperature observed for Opadry I films, which was seen at 166.3°C.

Okhamafe and York (1984) described the increase in glass transition of HPMC films after addition of talc and titanium dioxide attributing the increase to the restriction in the polymer chains mobility. As the concentration of the pigment increases this will result in a reduction in free volume reducing mobility and therefore increasing the

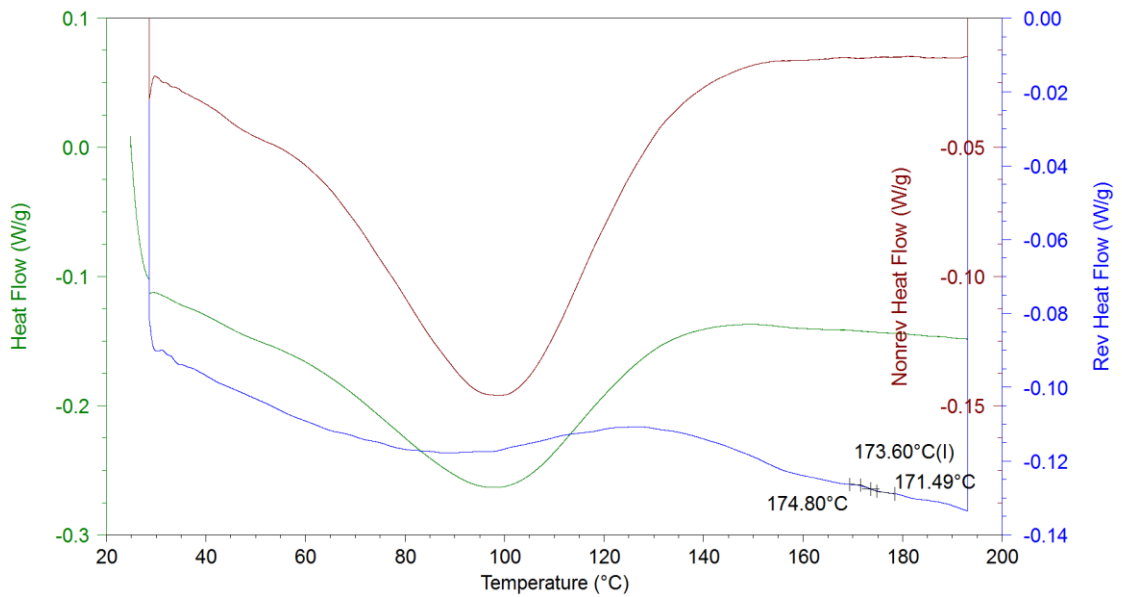


Figure 6.3 MTDSC of Opadry I cast film with 10% w/w iron oxide

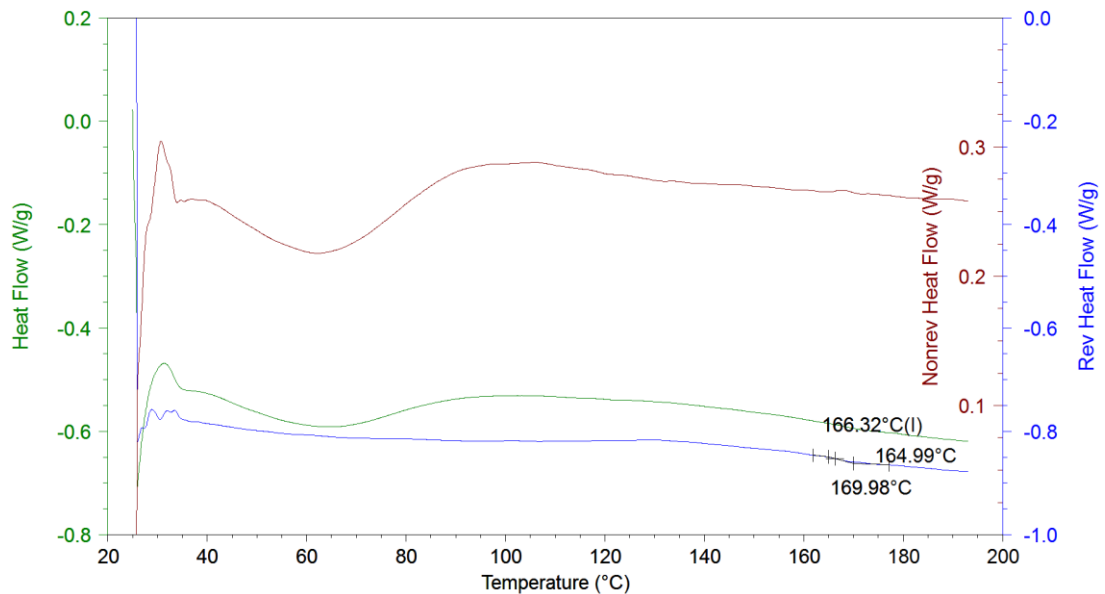


Figure 6.4 MTDSC of Opadry I cast films

glass transition. This appears to be the situation in this sample with the glass transition increasing compared to films with no added pigment.

6.3.2.1.2 Contact Mode AFM and L-TMA

The graph in Fig. 6.5 shows L-TMA results for cast Opadry I films with 10% w/w iron oxide added, and shows the usual thermal expansion followed by probe indentation into the sample surface. The average transition temperature is 177.4°C (\pm

2.5°C sd; n=10), which is significantly higher than that observed for Opadry I films with no additional pigments ($p < 0.001$), with a typical trace for these films shown in Fig 6.6.

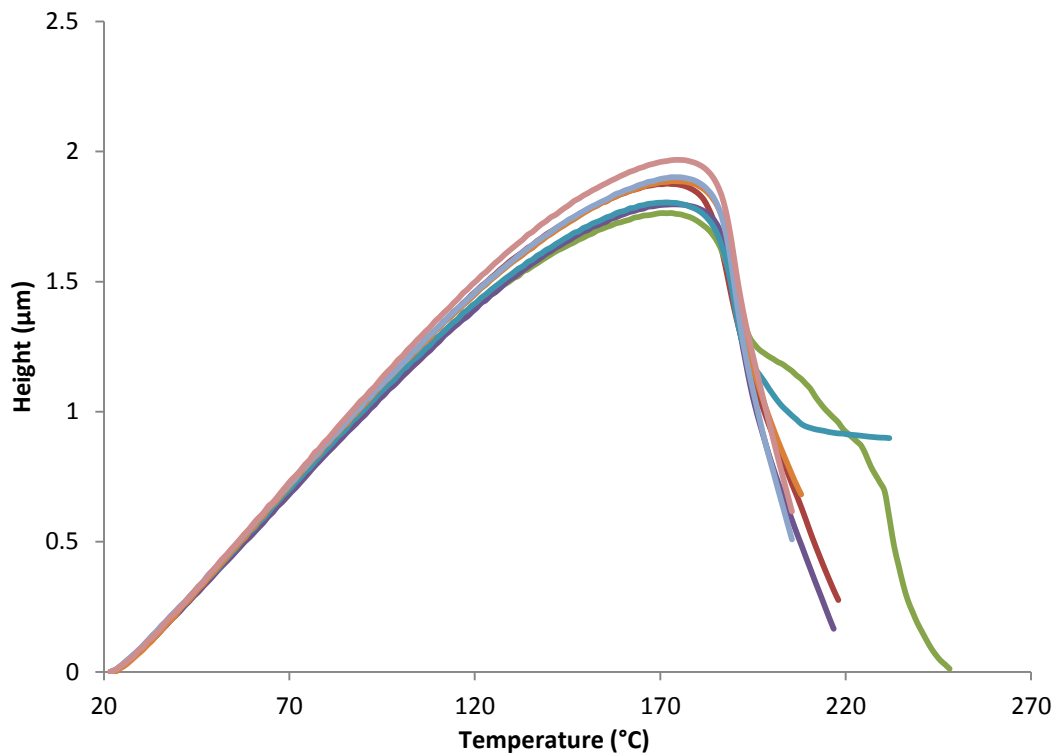


Figure 6.5 L-TMA of Opadry I with 10% w/w iron oxide cast films

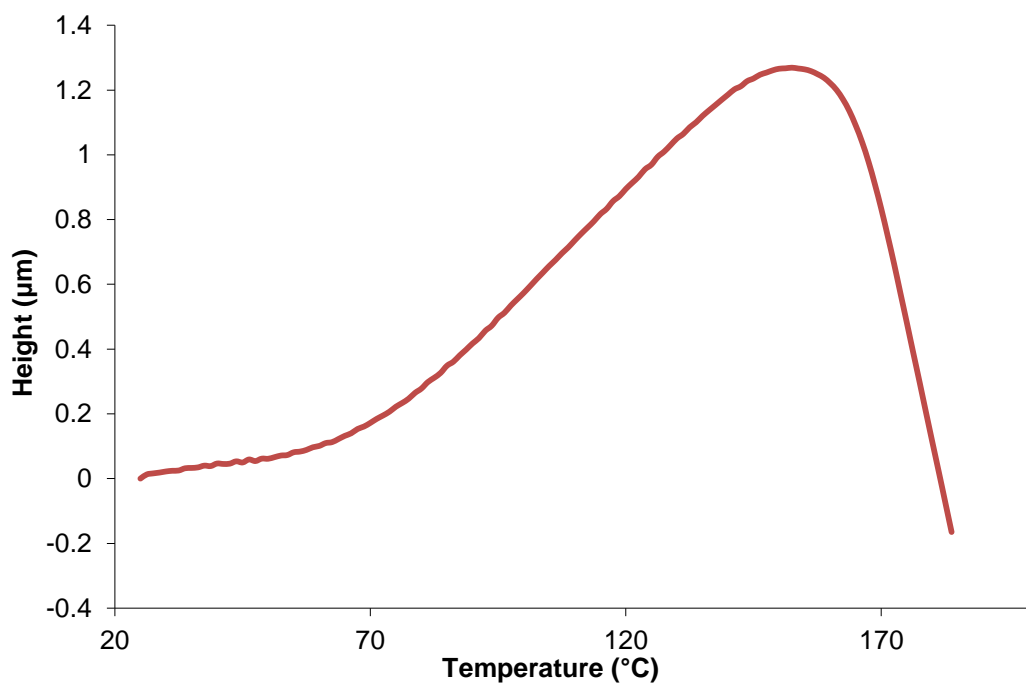


Figure 6.6 L-TMA trace of Opadry I cast film

Fig. 6.7 shows a contact AFM image of a cast film of Opadry I with 10% w/w iron

oxide added, with what appears to be areas of iron oxide represented by the lighter areas on the AFM image. This morphology is considerably different to the films of Opadry I with no pigment added so is likely that these lighter areas correspond with areas of iron oxide.

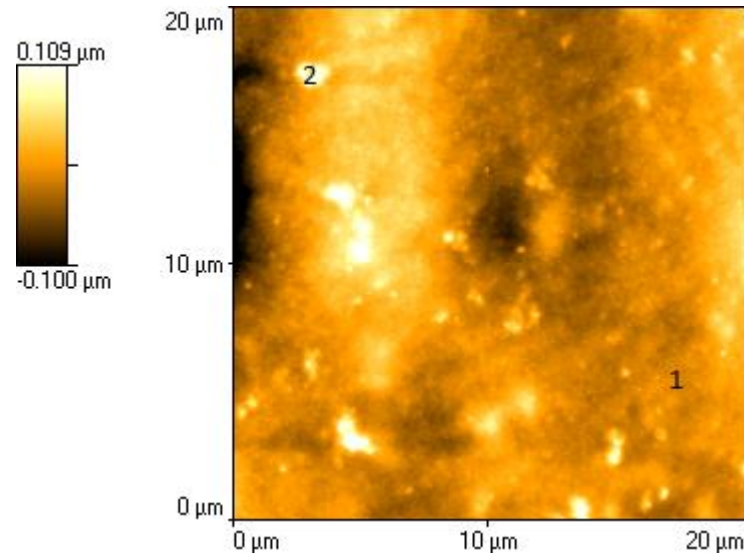


Figure 6.7 AFM image in contact mode of Opadry I with 10% w/w iron oxide, area 1 represents an area of suspected Opadry I and area 2 suspected iron oxide

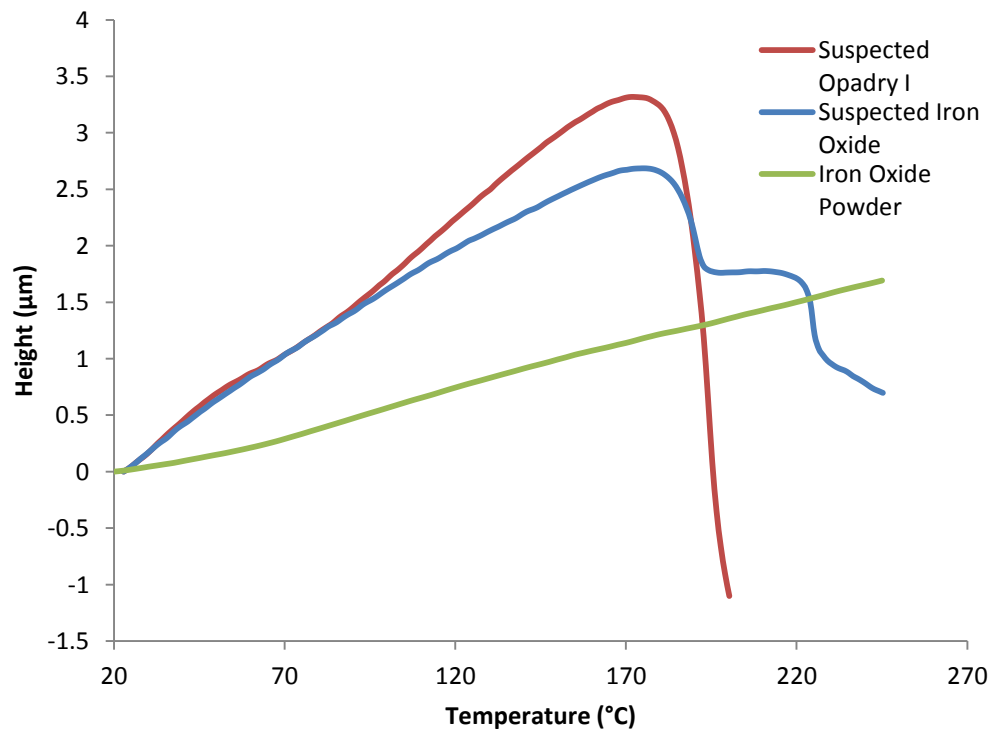


Figure 6.8 L-TMA of Cast Opadry I films with 10% w/w iron oxide
L-TMA was performed at two locations on the film surface, shown in Fig. 6.8, which

also has the L-TMA of iron oxide powder included for reference. The first L-TMA performed was in a region believed to be Opadry I, producing an L-TMA result similar to that of Opadry I films with no pigment, albeit with a higher glass transition noted earlier. The second area analysed by L-TMA would be expected to show a similar trace to that of the iron oxide powder, however the result showed a thermal transition in the same region as the region of suspected Opadry I.

This unexpected result could arise from melting of the polymer underneath the area of iron oxide or from a thin layer of polymer film being present over the pigment particle and will be discussed in more depth in the discussion.

6.3.2.1.3 Tapping Mode AFM and L-TMA

Images of the cast films of Opadry I with 10% w/w iron oxide were imaged in tapping mode AFM and shown in Fig. 6.9. The topography images display a similar morphology to that of images acquired in contact mode with lighter areas appearing to correspond to iron oxide. The phase image displayed on the right of Fig. 6.9

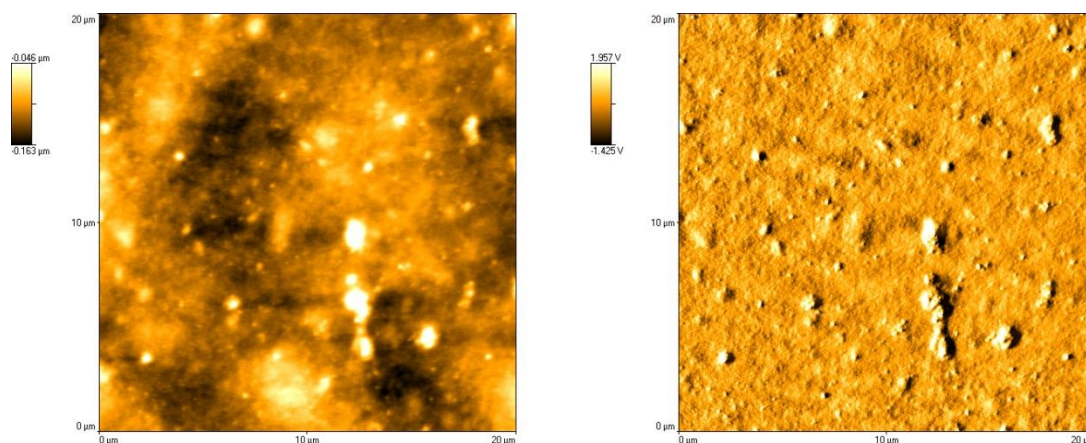


Figure 6.9 Tapping mode AFM images of Opadry I with 10% w/w iron oxide, showing topography (left) and phase (right)

shows a broadly homogenous surface where Opadry I is suspected, however where the areas of suspected iron oxide are seen on the topography image these too appear as light specks on the phase image indicating they do represent areas of iron oxide.

Grain analysis performed on the image indicated that 4.7% of the surface was made up of iron oxide, meaning half the quantity of iron oxide that would be expected is observed on the surface. This is possibly due to sedimentation of the iron in oxide during drying leading to less observed iron oxide on the surface; however there was sufficient iron oxide to perform L-TMA experiments.

Also of note is that AFM images indicate there are areas of pigment that appear in clusters and previous authors have reported iron oxide pigments aggregating together (Gibson *et al.*, 1988).

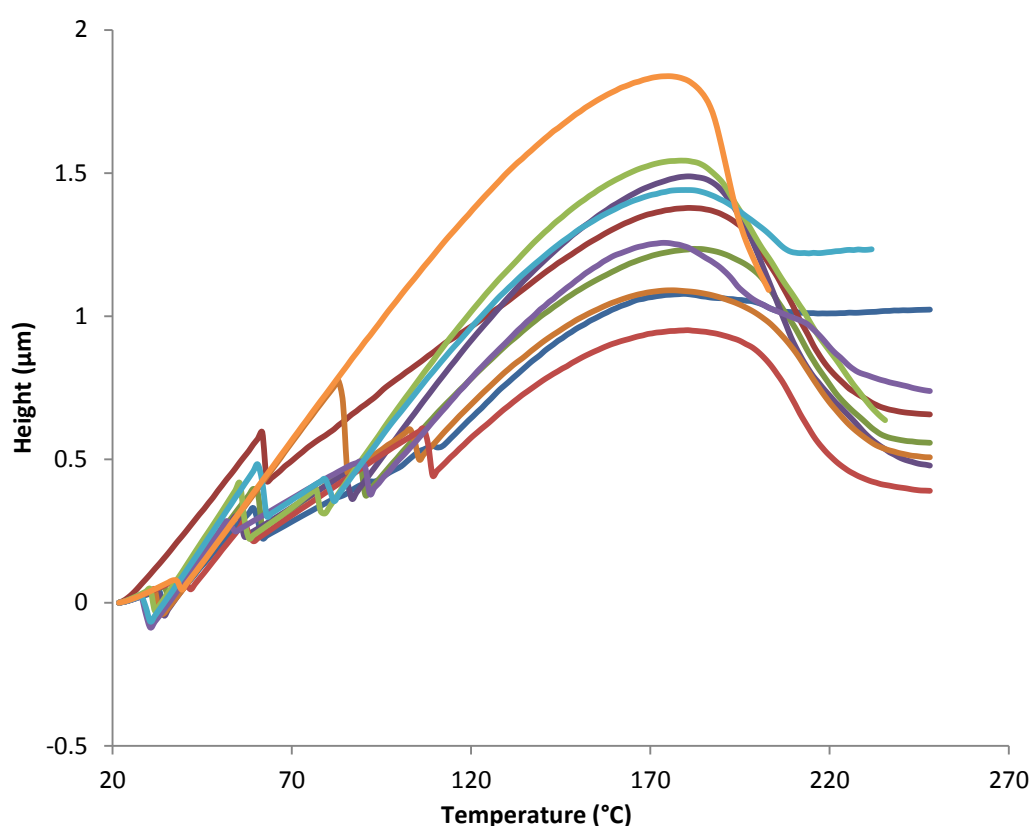


Figure 6.10 L-TMA results of Opadry I with 10% w/w iron oxide performed in tapping mode

The results in Fig. 6.10 show L-TMA performed in tapping mode, with the “jump to contact” observed at the beginning of the L-TMA trace. This temperature can be relatively high, which would preclude the use of L-TMA in tapping mode to be used to analysis samples of temperatures under approximately 120°C. The jump to contact however does not appear to affect the resulting L-TMA result, with L-TMA traces that contain the jump to contact at high values appearing to have transitions within

the expected range. The L-TMA traces show good correlation to L-TMA acquired in contact mode for Opadry I with 10% w/w iron oxide, although the average transition temperature was higher at 179.6°C (± 4.12 sd; n=10), this was not significantly higher ($p > 0.05$).

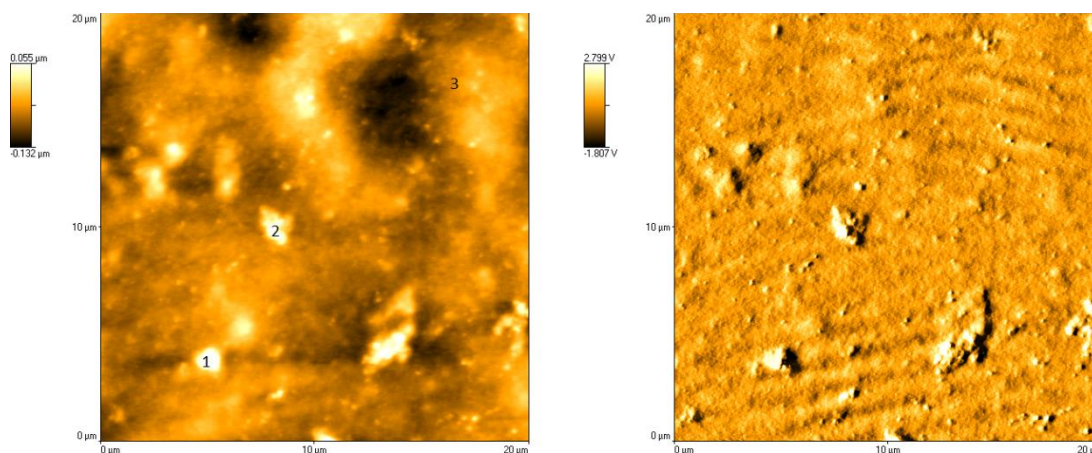


Figure 6.11 Tapping mode AFM images of Opadry I with 10% w/w iron oxide, showing topography (left) and phase (right) with numbers denoting locations of L-TMA

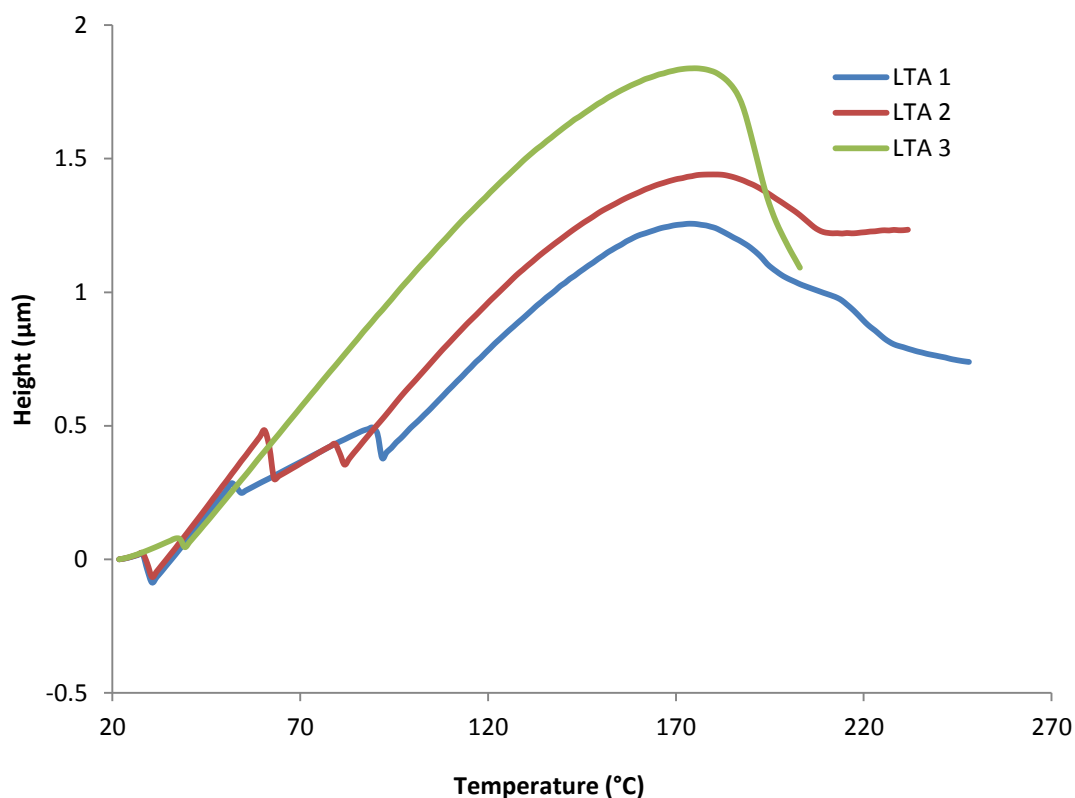


Figure 6.12 L-TMA of Cast Opadry I films with 10% w/w iron oxide performed in tapping mode

Fig. 6.11 shows a tapping mode image of Opadry I with 10% w/w iron oxide,

showing the same morphology as previous results, however after this image was acquired L-TMA was performed on areas of interest. In the same manner as for the images acquired in contact mode areas of suspected Opadry I and iron oxide were tested.

The first two L-TMA results were performed on areas of suspected iron oxide producing L-TMA traces showing a similar response to that of the L-TMA acquired in contact mode, with the probe indenting after a thermal transition and then the probe either stopping moving downwards into the sample or slowing. The final L-TMA was performed on an area likely to represent Opadry I and showed a thermal transition consistent with Opadry I.

6.3.2.2 Opadry II and 10% w/w Iron Oxide

6.3.2.2.1 Modulated Temperature DSC

Fig. 6.13 shows an MTDSC trace for cast Opadry II films without 10% iron oxide added, which as reported in Chapter 3 was 47.8°C. The average transition for Opadry II films with 10% iron oxide added was measured to be 50.0°C ($\pm 0.1^\circ\text{C}$ sd; $n=3$), which as for the Opadry I films with iron oxide was significantly higher ($p<0.05$) than for films without iron oxide.

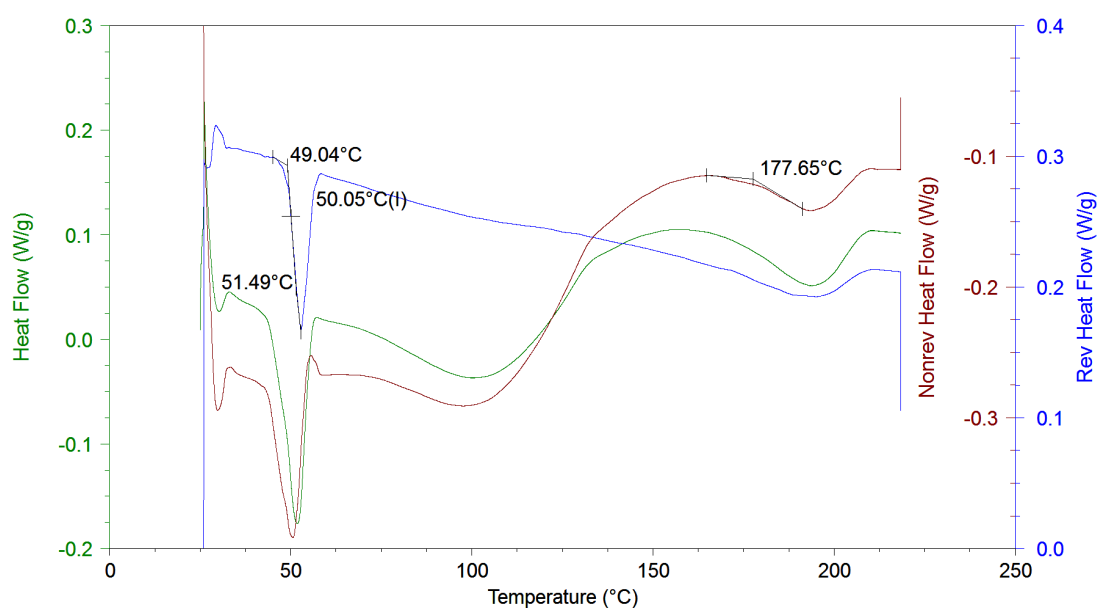


Figure 6.13 MTDSC of Opadry II cast films

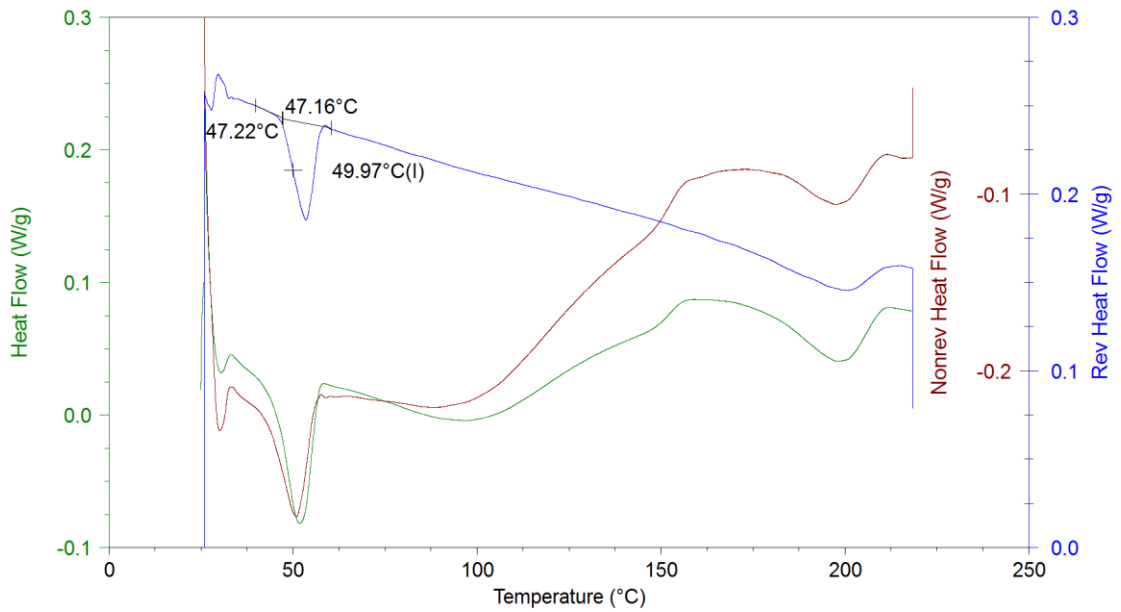


Figure 6.14 MTDSC of Opadry II cast film with 10% w/w iron oxide

6.3.2.2.2 Tapping Mode AFM

Images were acquired in tapping mode AFM for Opadry II with 10% iron oxide with the results shown in Fig. 6.15. Dark areas are noticeable in topography image, which were not present in the topography images acquired for Opadry II films in contact mode AFM.

In the right hand image of Fig. 6.15 representing the phase image these dark areas correspond to light areas indicating areas of higher stiffness than the surrounding

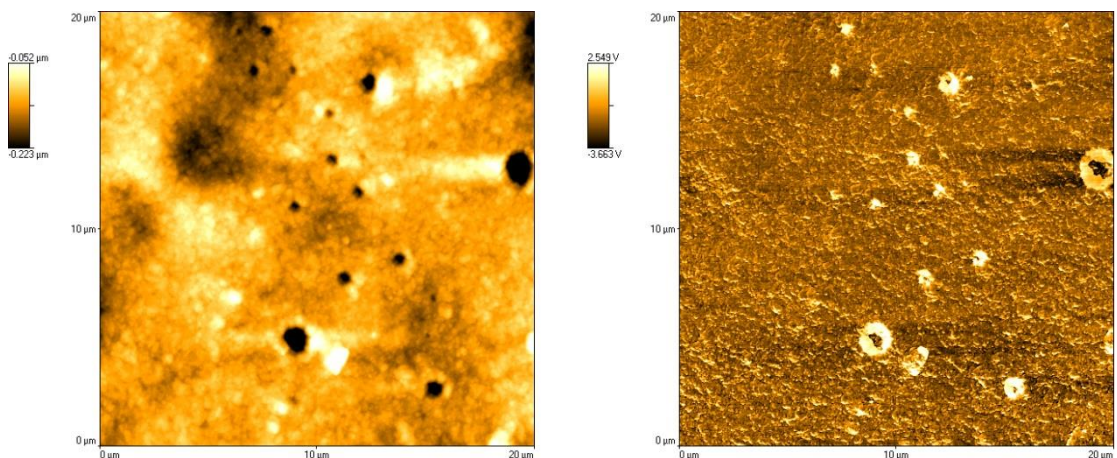


Figure 6.15 Cast films of Opadry II in tapping mode showing topography (left) and phase (right)

polymer. Although these areas correspond to areas on the topographic image as the whole area is the same shade it is unlikely to be caused by topographic effects. However as these areas do appear to represent areas of iron oxide it would indicate that the iron oxide could be undergoing sedimentation in the film. This is further supported by grain analysis which showed 3.6% of the surface represented areas of iron oxide.

Unfortunately due to the “jump to contact” observed when performing L-TMA in tapping mode it was not possible to perform L-TMA on these samples as the glass transition for Opadry II would not be able to be ascertained. This highlights a limitation of this technique, however it would still be possible to obtain an image in tapping mode, switch to contact mode and perform an L-TMA, although it would be more time consuming due to the extra images needed. Also in this sample the contact image can be used to observe where likely areas of iron oxide are due the occurrence of structures in the topography of the sample.

6.3.2.2.3 Contact Mode AFM and L-TMA

L-TMA however could be performed in contact mode, with the results shown below. Fig. 6.16 shows an L-TMA trace for an Opadry II film with no pigment added showing the transition temperature of the film to be in the region of 48°C.

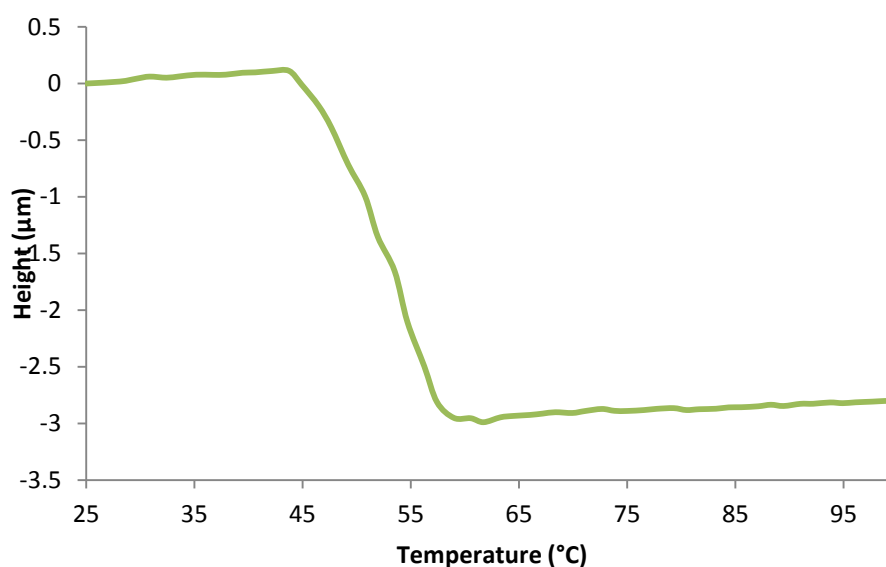


Figure 6.16 L-TMA of Opadry II cast films

The results can be seen in Fig 6.17 for Opadry II films with 10% iron oxide added. The average transition temperature for PVA seen in these results is 59.3°C ($\pm 5.2^\circ\text{C}$); which as for the Opadry I films with 10% w/w iron oxide is significantly higher ($p < 0.05$) than for Opadry II films without iron oxide. However there does appear to be two groups of transitions, and once the data was analysed in spatially resolved manner it is evident that the differences in transition temperature result from different areas of the analysed film. One transition occurs at 51.6°C ($\pm 3.4^\circ\text{C}$ sd; $n=10$) and another on separate L-TMA traces at 63.1°C ($\pm 1.6^\circ\text{C}$ sd; $n= 10$).

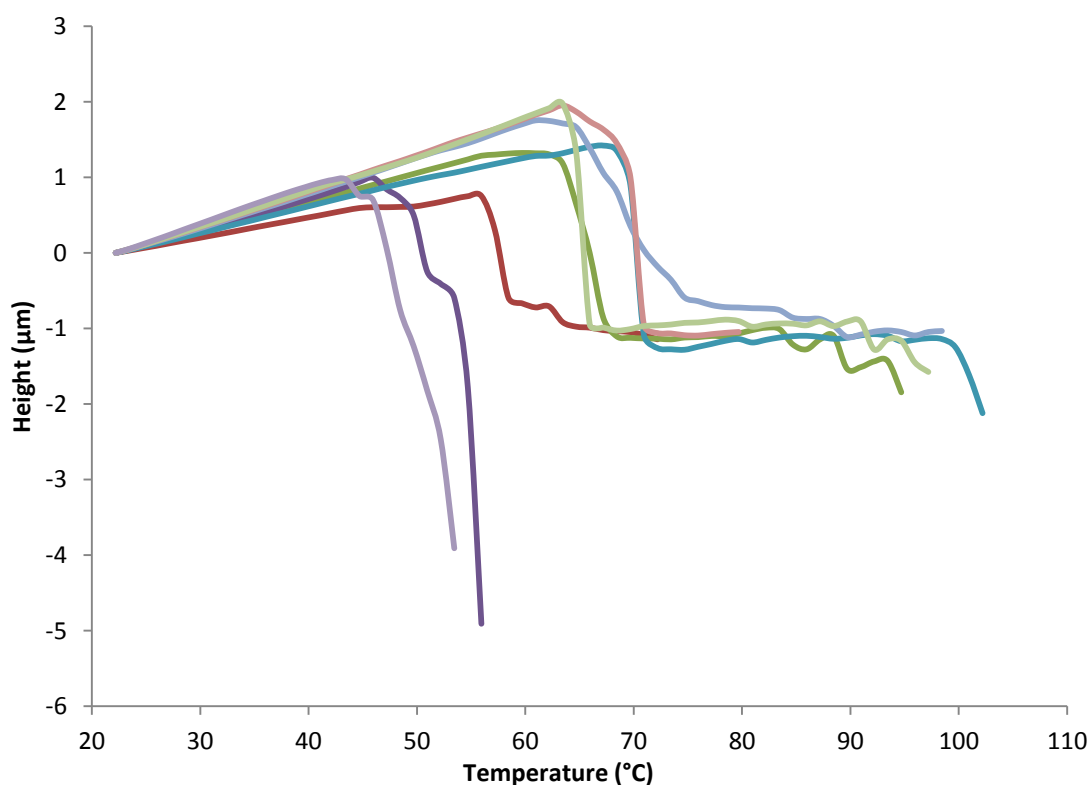


Figure 6.17 L-TMA of Cast films of Opadry II with 10% w/w iron oxide

This can be seen in Fig. 6.18, with the figure shows a contact image of Opadry II with 10% w/w iron oxide, and a similar topography image as seen previously in tapping mode is observed, with dark circles present in the image. Two locations for L-TMA were chosen, one in an area of suspected Opadry II and one for suspected iron oxide.

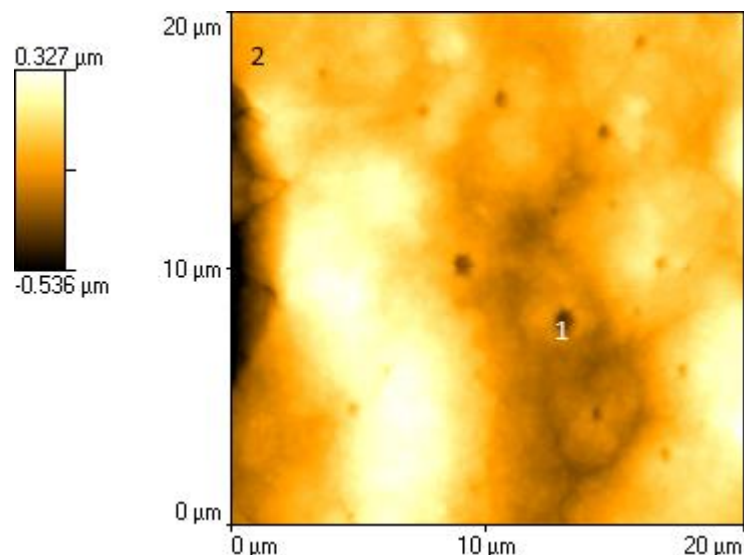


Figure 6.18 Contact AFM image of Opadry II with 10% w/w iron oxide, with area 1 representing suspected iron oxide and area 2 suspected Opadry II

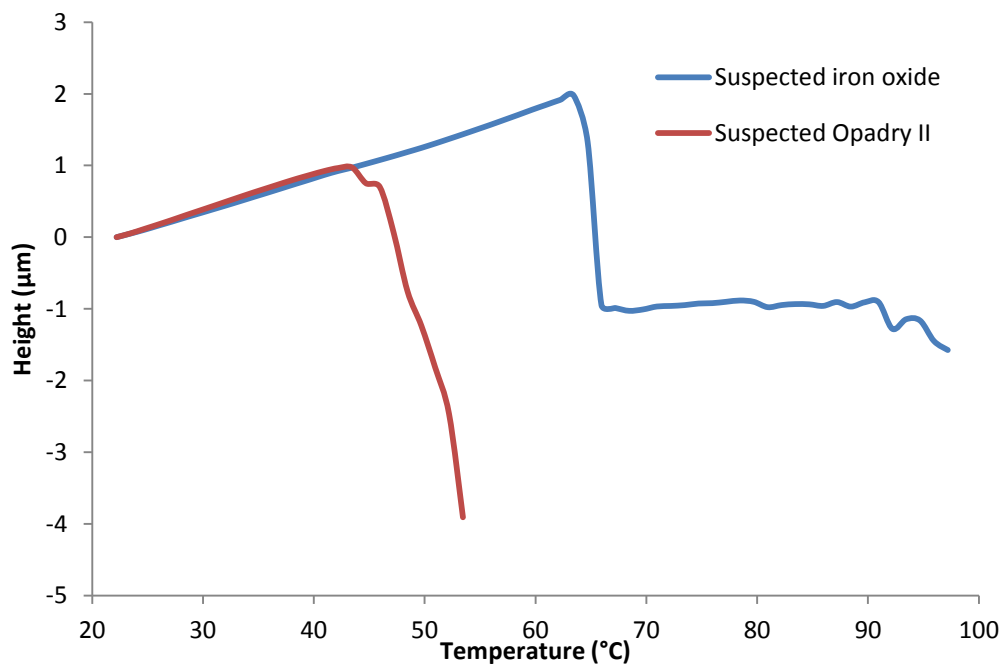


Figure 6.19 L-TMA of cast films of Opadry II with 10% iron oxide performed on a suspected area of iron oxide and Opadry II

Fig. 6.19 shows the L-TMA results performed on the areas selected in Fig. 6.18 and as with the result for Opadry I with 10% iron oxide w/w the L-TMA results are markedly different. However instead of a transition temperature being observed at the same temperature and then the indentation slowing or stopping, the transition temperature was raised significantly higher ($p < 0.05$) than that for areas of suspected Opadry II.

This is an interesting result as it is unlikely that Opadry II and iron oxide will mix and produce a molecularly dispersed system with a single transition, especially with the massive melting point of iron oxide compared to the glass transition of Opadry II. As stated above this is likely to be due to polymer underneath the area of iron oxide undergoing a thermal transition or from a thin layer of polymer film being present over the pigment particle and will be considered further in the discussion.

By determining the higher glass transition observed is due to iron oxide particles, the lower transitions observed in Fig. 6.16 are likely to be attributable to Opadry II. The average glass transition of 51.6°C, as with MTDSC data, is not significantly higher ($p > 0.05$) than the glass transition observed for films of solely Opadry II.

6.3.2.3 Minitablets

6.3.2.3.1 Opadry I and 10% w/w Iron Oxide

Fig. 6.20 shows an AFM image of a film coated minitabilet coated with an Opadry I solution with 10% w/w iron oxide. The topographic image has structures consistent with Opadry I coated minitablets, however there are also similar areas to the cast films analysed above in this chapter that contained 10% iron oxide. Lighter areas in the top half of the image are comparable to the areas of iron oxide seen on the cast films, and this is reflected in the phase image with lighter areas seen also. The

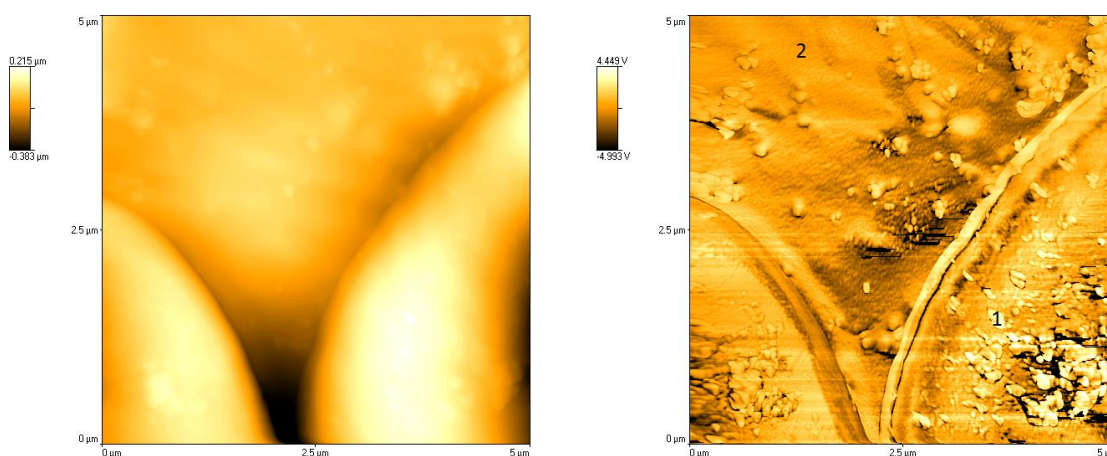


Figure 6.20 Tapping mode image of Film coated minitablets of Opadry I with 10% w/w iron oxide showing topography (left) and phase image (right)

“droplet” in the bottom right of the topographic image appears similar in nature to the rest of the image, however the phase image shows the presence of a number of suspected iron oxide particles. As mentioned previously in the chapter pigment particles can aggregate together and this appears to be true in this instance.

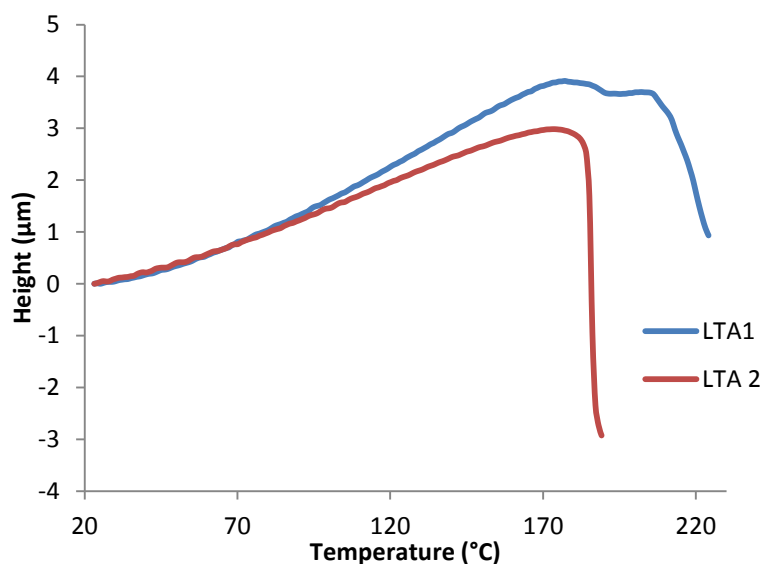


Fig 6.21 L-TMA of minitablets film coated with Opadry I and 10% iron oxide. With L-TMA performed on an area of suspected iron oxide and L-TMA 2 on an area of suspected Opadry I.

The L-TMA performed on these areas, displayed in Fig. 6.21 shows the suspected Opadry I to undergo a transition at the elevated temperature associated with the Opadry I films with the iron oxide added. L-TMA performed on an area of suspected iron oxide reveals similar behaviour to the cast films of Opadry I and iron oxide with the probe penetrating a small amount initially at the glass transition of Opadry I, then halting and indenting further.

6.3.2.3.2 Opadry II and 10% w/w Iron Oxide

Tapping mode images of Opadry II with 10% iron oxide are shown in Fig. 6.22, with a number of iron oxide particles identified in the topography and phase image of the sample. As for the Opadry II cast films L-TMA is hard to perform on Opadry II samples due to the “jumping” into contact of the probe obscuring the glass transition of Opadry II.

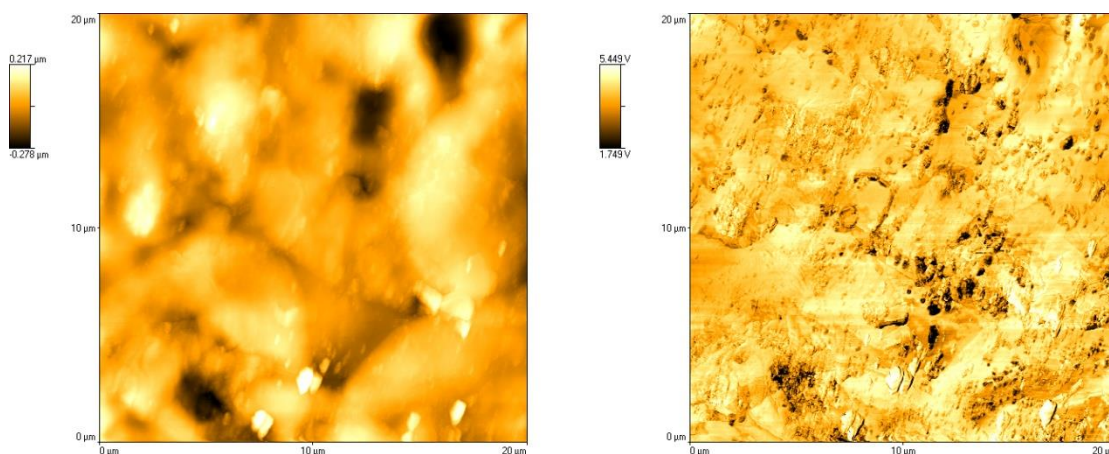


Figure 6.22 Tapping mode image of film coated minitables of Opadry II with 10% w/w iron oxide showing topography (left) and phase image (right)

L-TMA could be performed in contact mode, and the results are shown in Fig. 6.23 and 6.24. The topography image in contact mode displays areas likely to correspond to iron oxide pigments, and L-TMA was performed at these locations in addition to areas considered to be Opadry II.

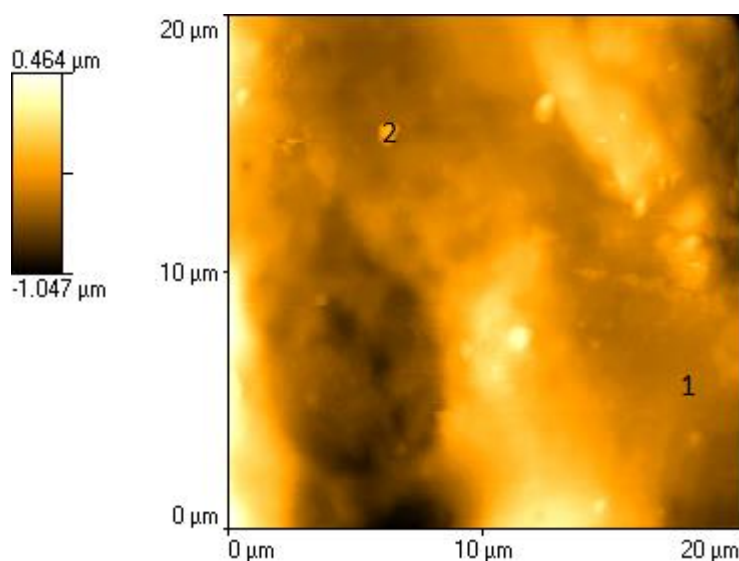


Figure 6.23 Contact AFM image of film coated Opadry II minitables with 10% iron oxide

The L-TMA traces display a similar pattern to the cast Opadry II and iron oxide films with the areas of suspected iron oxide showing a higher transition compared to the L-TMA of Opadry II. The transition temperature of Opadry II remained at the same temperature observed for Opadry II coated minitables without added iron oxide consistent with earlier MTDSC and L-TMA results.

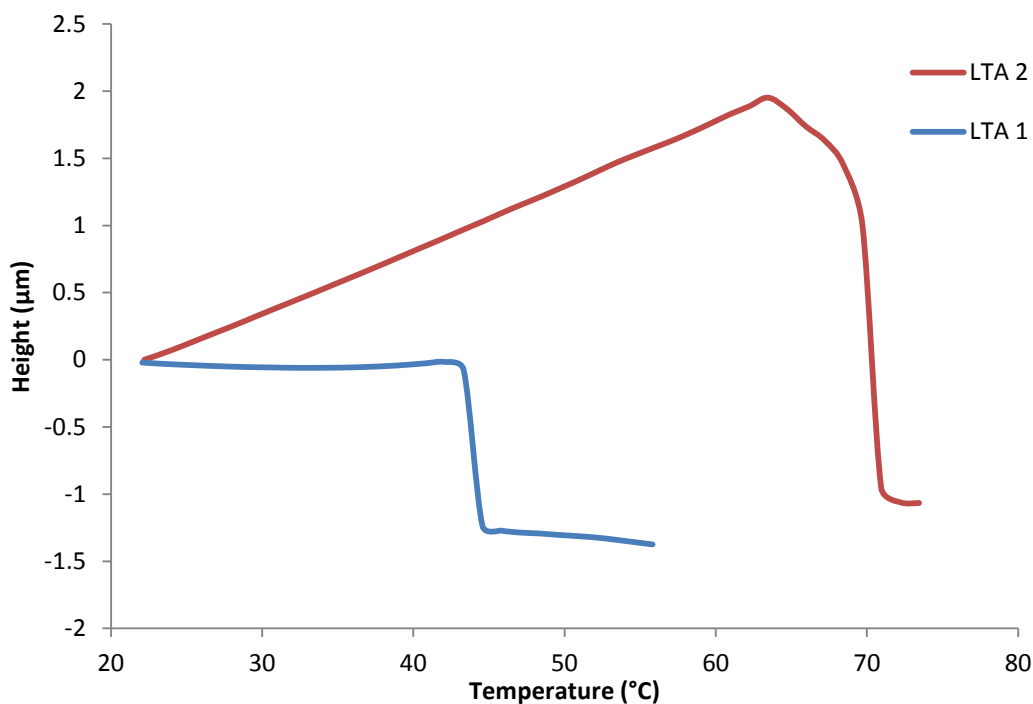


Figure 6.24 L-TMA of minitables film coated with Opadry II and 10% iron oxide. With L-TMA performed on an area of suspected Opadry II and L-TMA 2 on an area of suspected iron oxide

6.3.3 Use of AFM for the Measurement of Gloss

The roughness of a polymer film coat is directly related to the gloss of the film coat, with Rowe (1985) describing a decrease in gloss associated with an increase in the surface roughness. AFM topology images can be analysed for sample roughness and some initial measurements were taken to investigate whether it was possible to determine changes in gloss associated with surface roughness.

The roughness of the sample can be determined using the arithmetic mean of the deviations in height from the images mean height value, which is calculated by the following equation.

$$R_a = \frac{1}{N} \sum_{i=1}^N |Z_i - \bar{Z}| \quad (6.1)$$

With R_a representing the average roughness, N the number of points analysed, Z_i the individual height of each point analysed and \bar{Z} the mean height of the sample. This formula is a function of the AFM software and can be performed within the image analysis software after the image has been gathered.

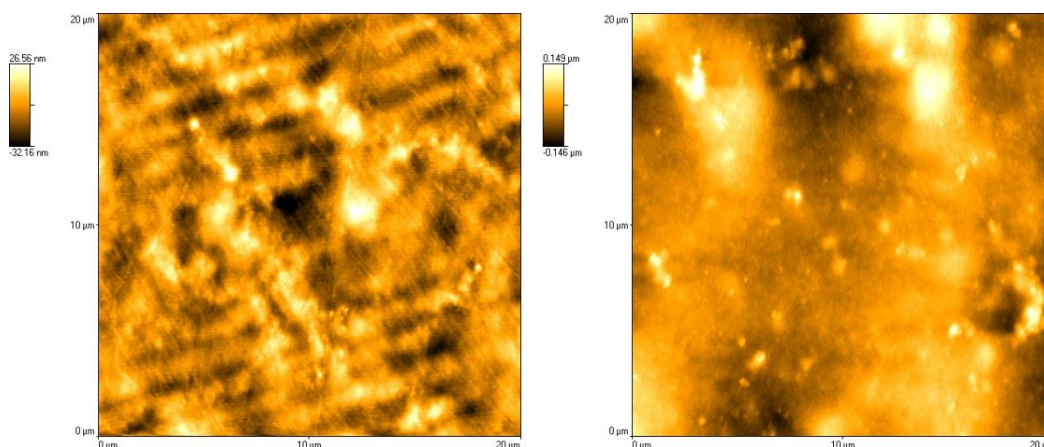


Figure 6.25 AFM contact images of Opadry I with 10% w/v of the underside (left) and top (right) of the film

Cast films once peeled from petri dishes were visually inspected and the underside of the film appeared to have a higher gloss than the top. A section of cast film was mounted onto the AFM and $20\mu\text{m}^2$ images were acquired in contact mode on the top side of cast films, with a fresh sample cut and attached with the underside of the film facing the AFM probe. Initial inspection of the images in Fig. 6.25 indicate the underside of the film of the is likely to be less rough as the height scale to the left of the image is measured in nm opposed to μm as seen in the top of the film. R_a was determined to be 36.2nm ($\pm 0.01\text{nm}$ sd; $n=4$) for the top side of the film and 10.3nm ($\pm 0.002\text{nm}$ sd; $n=4$), showing a significant difference ($p < 0.05$) in the roughness between the underside and the top of the film.

Although other methods can be used to accurately determine gloss, the measurements in AFM result from the intrinsic nature of topographic AFM images measuring the sample height, therefore surface roughness can be determined concurrently with AFM imaging without the need for separate measurements.

6.4 Discussion

MTDSC and L-TMA analysis of the thermal properties of the polymer films with iron oxide added indicated that the glass transition temperature of both Opadry I and Opadry II increased significantly to that observed in the films without iron oxide added. The increase in glass transition temperature after the addition of the pigment

particle is of significance as it can result in changes to the mechanical properties of the polymer film; therefore increasing the risk of a brittle coat being produced. The increase in glass transition is likely to result from the restriction of polymer chain movement from a reduction in the free volume of the system. Additionally the glass transition temperature of the polymer is an important factor in the coating process with an increase in process air temperature required to form the film if the glass transition of the polymer is increased. Increases in the glass transition of the film however can be remedied by the addition of further plasticiser to the coating system to compensate for the increase in T_g .

The interesting results of altered L-TMA responses observed in areas of suspected iron oxide in Opadry I and II films in worth considering in more detail. At the beginning of the chapter it was hypothesised that iron oxide could potentially be identified using tapping mode AFM and L-TMA results would be a means of verifying this. It was predicted that the L-TMA would produce traces with no response due to the high melting point of iron oxide compared to the polymers studied, however when L-TMA was performed on areas suspected of being iron oxide either showed a raised transition temperature or an altered L-TMA profile.

The explanation for this is likely to lie with iron oxide, which is a good conductor of heat, with thermal conductivity in the region of an order of magnitude greater than that for PVA and HPMC. Therefore if the probe is placed on an area of iron oxide it will conduct heat through the particle into the polymer matrix beneath thereby raising the temperature of the polymer film. The amount of heat conducted through the iron oxide particle will eventually be sufficient to raise the temperature of the polymer film underneath to its glass transition temperature resulting in softening of polymer. Once the polymer softens the force applied to the iron oxide particle by the AFM cantilever will drive the particle into the softened polymer underneath resulting in deflection of the cantilever which is subsequently observed on the L-TMA trace.

The diagram in Fig. 6.26 depicts this behaviour, which would explain the raised transition temperature observed in Opadry II and iron oxide cast films as there will be a time lag in the heat conducting through the area of iron oxide into the Opadry II

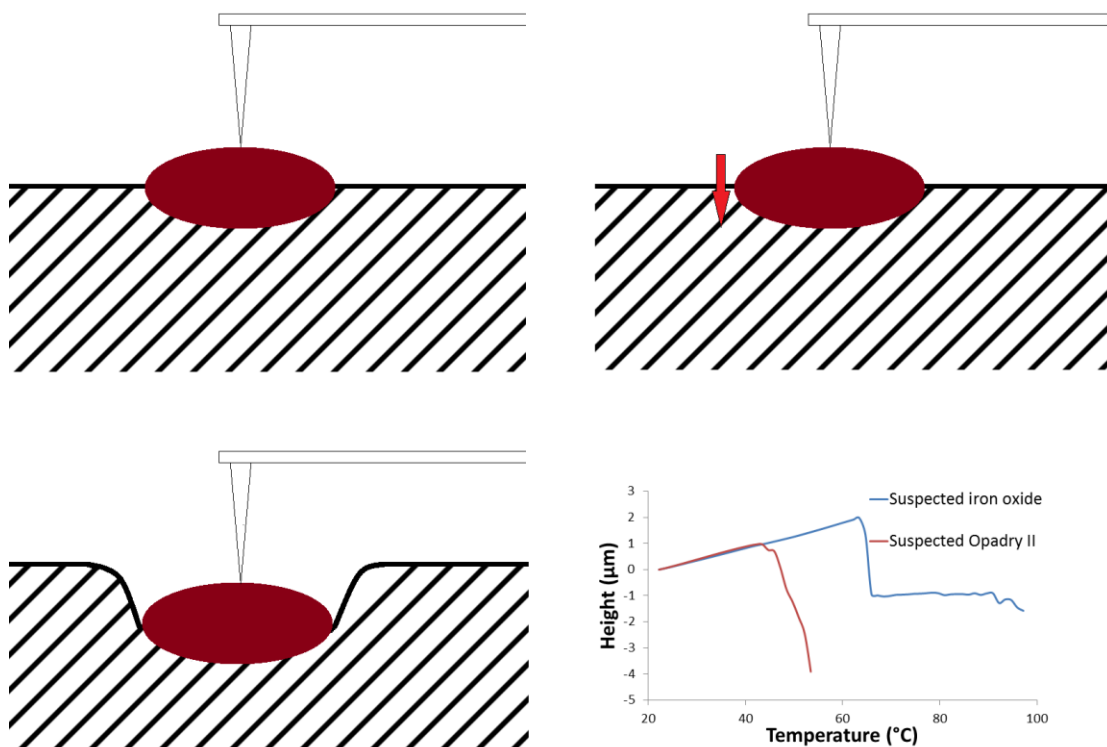


Figure 6.26 Diagram depicting likely positioning of iron oxide to produce the L-TMA in the bottom right (see text for full explanation)

underneath, by which time the probe temperature will be raised giving the appearance of a higher transition temperature.

This can be related to Newton's Law of cooling, which is also applicable to heating, as is the case here. The law states the rate of heat loss of a body is proportional to the difference in temperatures between the body and its surroundings, and is given by the following equation:

$$\frac{\Delta Q}{\Delta T} = hA(T - T_1) \quad (6.2)$$

where $\frac{\Delta Q}{\Delta T}$ is the heat flow rate (J sec^{-1}), A the area for heat flow (m^2), $T - T_1$ the temperature difference between the probe and sample (K), and the constant h the heat flow coefficient given as:

$$h = \left(\rho c \lambda / L \right)^{\frac{1}{2}} \quad (6.3)$$

where ρ is the density (kg m^{-3}), v the velocity (m sec^{-1}), c the specific heat capacity ($\text{J Kg}^{-1} \text{K}^{-1}$), λ the thermal conductivity ($\text{W}/(\text{m K})$) and L the length between the probe and the sample. From these equations it can be seen that the rate of heating of an object is not only dependent on the temperature difference between the two bodies, but is also inversely proportional to the distance between the two, as shown by the heat flow coefficient. Therefore the further under the surface the pigment particle is the slower the rate of heat flow to it, and the higher the transition observed.

Due to the semiquantitative nature of L-TMA the area for heat flow is not known due to the size of the probe and the area in contact with the sample being unknown. In addition the size of the pigment particle not being known, thus precluding the equations from being able to predict the rise in transition temperature. However Newton's law of cooling does provide a model for understanding the process of the raised transitions observed when performing L-TMA on suspected iron oxide particles.

The L-TMA profile where the transition temperature of the polymer appears the same but the probe indentation then appears to stop or slow is likely to be due to the iron oxide particle being underneath the film surface with a thin polymer layer on top. Even though the pigment particle is not on the film surface the presence just under the surface will still influence the stiffness of the sample if the layer is sufficiently thin. However this thin layer is composed of just the film forming polymer it will soften at the same temperature as that of suspected areas of polymer. Once the probe has penetrated through the polymer layer and encounters the iron oxide particle the probe will come to a rest which is what is observed in Fig 6.27. As with the iron oxide located on the sample surface the iron oxide particle will conduct heat through into the sample below its location and once the temperature is raised to

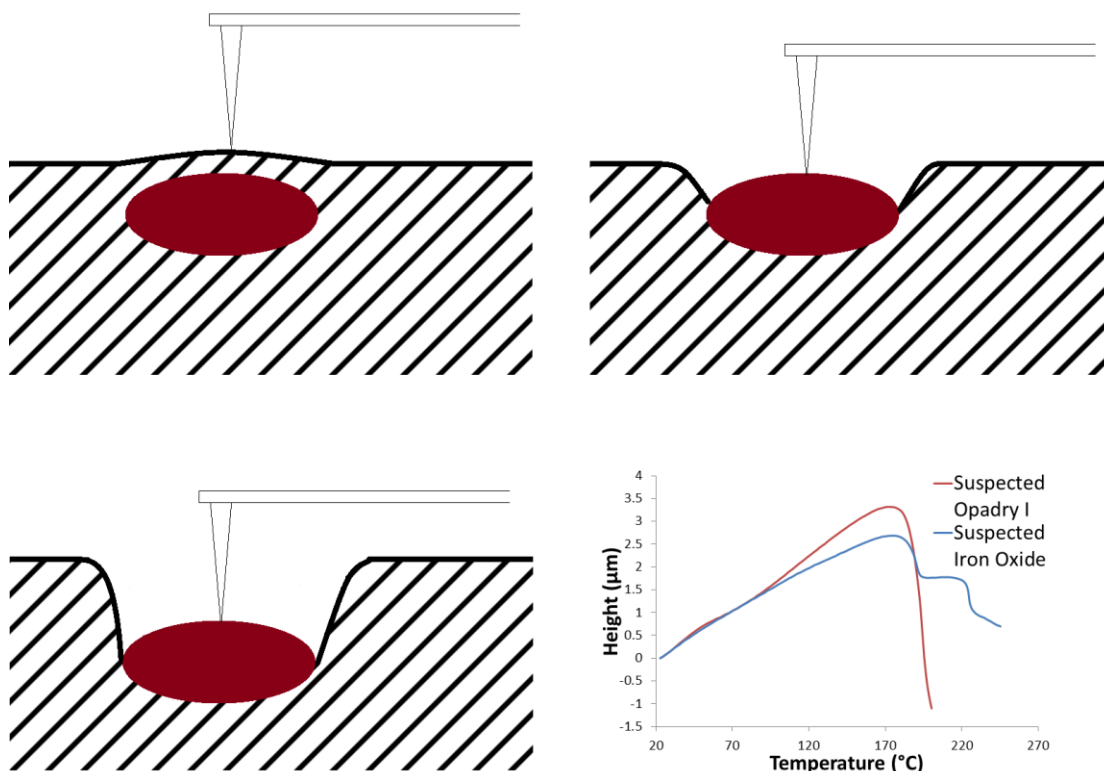


Fig 6.27 Diagram depicting likely positioning of iron oxide to produce the L-TMA in the bottom right (see text for full explanation)

the sample glass transition it will soften and the probe will continue penetrating the sample. This again will be at a raised temperature as the probe will already be above the glass transition of the polymer and there will be a time lag as heat conducts through the iron oxide.

6.5 Conclusions

AFM combined with nanothermal analysis has been shown to identify the location of pigments particles in polymer films prepared both through casting and spray coating. Iron oxide particles could be identified with AFM in contact mode, through comparison with films composed of only the polymer however in tapping mode the location of the pigments particle could be ascertained with greater certainty.

Thermal Analysis of the films showed that the glass transition temperature of Opadry I and Opadry II both increased significantly on addition of iron oxide to the film.

This was attributable to a decrease in molecular mobility of the polymer and is of significance as it can have a bearing on the mechanical properties of the final film coat.

The use of AFM combined with L-TMA it was revealed through alterations in the L-TMA profile that some of the iron particles observed in the AFM image were below a thin layer of polymer resulting in marked differences in the L-TMA profiles.

The novel use of L-TMA whilst in tapping mode lead to a decrease in the time required to perform the L-TMA measurements, as the need to remove the probe from the sample surface and change mode was removed. However this technique is limited by the presence of the probe “jumping” into contact at the beginning of the L-TMA precluding its use for samples with transitions observable below around 50°C.

Additionally AFM was shown to be able to provide information on the gloss of the film coated minitables, and although other techniques are available to measure gloss, as the surface roughness can be extracted from information already present in the AFM image without the need for additional measurements this is advantageous.

Also the difference between films prepared by casting and spray drying has been further highlighted. There were considerable differences between the location and distribution of the pigments between the two methods of preparation providing further evidence for the need of the in-situ analysis of pharmaceuticals.

CHAPTER 7

7. Conclusions

7.1 Final Conclusions

This project has been concerned with the in-situ analysis of polymer films either prepared as film coated minitables or cast free films. The use of a variety of thermal analysis techniques combined with AFM were employed to aid the understanding of the in-situ behaviour of film coats. Work focused on the characterisation of the preformulated coating systems Surelease (ethylcellulose), Opadry I (hydroxypropyl methylcellulose) and Opadry II (polyvinyl alcohol). Blends of Surelease and Opadry I, and Surelease and Opadry II were also analysed alongside Opadry I and Opadry II with pigments added to the coating solution. The complex behaviour of the systems especially regarding the polymer blends necessitated the use of a multi-instrumental and multi-technique approach gain a complete understanding of the sample morphology.

Initial results of film coated minitables and cast free films revealed glass transitions for all three polymers; however only subtle glass transitions were observed using MTDSC for Surelease and Opadry I due to the strong glass forming nature of ethylcellulose and HPMC. Additionally the glass transition for Opadry II showed considerable enthalpic relaxation which was attributed to the semicrystalline nature of PVA leading to increased relaxation times present in semicrystalline polymers. AFM imaging in contact mode also indicated differences in film morphology between cast free films and film coated minitables. Little topographic information of interest was seen for cast films; however film coated minitables displayed circular structures on the film surface attributed to the drying of atomised droplets of the film coating solution on the surface. FTIR spectra was also obtained for the individual polymers to detect the behaviour of hydrogen bonding in the individual systems,

with the aim to compare these results with the minitablets coated with the polymer blends.

Also data was presented to add to the debate of whether L-TMA measures the glass transition temperature or a softening point. An increase in the transition temperature was observed during L-TMA experiments when the heating rate of the L-TMA experiment was raised, indicative of measurement of the glass transition. However other research has found no increase in T_g when increasing the heating rate, and only one material was tested in this study; therefore the L-TMA response may be specific to the sample and further work is required.

L-TMA and MTDSC of Opadry II films also detected a transition not associated with either the glass transition or the expected crystalline melting temperature of the PVA. This extra transition was ascribed to a different polymorph of PVA being formed in the film, with previous research attributing it to the presence of plasticisers in the film.

Thermal Analysis using MTDSC and L-TMA was performed on minitablets coated with polymer blends of Surelease and Opadry I and Surelease and Opadry II in ratios of 50:50, 70:30 and 90:10. The results from these experiments indicated miscibility of the polymers through the presence of an intermediate glass transition temperature at an intermediate temperature between the two polymers. Further investigation of the film coated minitablets with the novel heated tip tapping mode AFM showed the presence of nano-phases with an average domain sizes substantially below 100nm which is at the limit of detection to be resolved using MTDSC and L-TMA. This lead to the conclusion that the systems were indeed phase separated.

Comparisons with free films were made using the same techniques with MTDSC and L-TMA suggesting an increase in domain size compared to film coated minitablets with an increase in thermal transitions observed for the individual polymers. However heated tip tapping mode again resolved the separate polymer phases and showed an increase in Surelease domain size, which was attributed to the longer drying times associated with film casting leading to growth of the domains of the individual polymers.

The use of heated tip tapping mode has highlighted the importance for the use of a number of analytical techniques when analysing pharmaceutical samples as the conclusions drawn for MTDSC and L-TMA would have been for a miscible or partially miscible system between Surelease and Opadry I or II. However heated tip tapping mode AFM was able to identify the presence of nanophases in film coated minitablets resulting in a different conclusion to be drawn.

Minitablets coated with Surelease and blends of Surelease and Opadry I, and Surelease and Opadry II were cured for up to 24 hours and were subsequently analysed using contact mode AFM combined with L-TMA and heated tip tapping mode AFM. A growth in the domain size observed for Surelease in tapping mode AFM was observed for both Surelease and Opadry I and Surelease and Opadry II blends. The increase in Surelease domain sizes was due to the Surelease undergoing further coalescence due to the elevated temperatures of the oven producing a more homogeneous film.

As with previous results in the study little information could be gained from images acquired in contact mode AFM. Alterations in the L-TMA results of the polymer blends were noted; however the two polymer blend systems exhibited different alterations. The Surelease and Opadry I blend displayed more transitions associated with the individual polymers, and a change in the value of the intermediate transition. The Surelease and Opadry II blend however showed no decrease in the intermediate transition temperature, and no increase in the number of transitions associated with Opadry II. This was attributed to the differences observed in the phase images of the cured minitablets with the Surelease and Opadry I blend showing growth of spherical droplets and Surelease and Opadry II showing a more coherent Surelease phase. This Surelease phase was likely to result in there being fewer transitions observed for the crystalline and amorphous portions of Opadry II due to the decreased domain size of Opadry II.

AFM combined with nanothermal analysis was also employed to determine the distribution of pigment particles in film coated minitablets and cast free films. MTDSC results for Opadry I and Opadry II films with iron oxide incorporated into them showed significant increases in the glass transition temperature observed for

the films. This increase in glass transition has been observed previously and is likely to be due to the pigment particles restricting mobility of the polymer chains through a reduction in the free volume of the system. The location of pigment particles in contact mode AFM could be inferred through contact mode AFM images through comparison with images of films not containing any pigment. However tapping mode AFM was able to provide greater confidence in the location of pigment particles through phase imaging of the films. Phase images provided clear location of the pigment particles through light areas being present on the phase image compared to the darker areas of pigment. L-TMA and MTDSC performed on the iron oxide powder produced no thermal transitions in the range associated with the polymers; however L-TMA performed on areas of pigment identified in phase imaging and contact mode images did undergo transitions. The conclusion drawn was that pigment particles could be covered with a thin layer of polymer film or be located on the sample surface, and once heat had conducted through the pigment the film underneath would soften giving the appearance of the pigment softening.

In Chapter 5 and Chapter 6 L-TMA was performed with the AFM in tapping mode as opposed to the conventional contact mode, which allowed for areas of interest to be analysed directly without the need to withdraw the tip and change mode. This allowed for more accurate and less time consuming measurements of areas of interest such as the location of pigment particles compared to having to change to contact mode. The disadvantage with this technique however is the probe may “jump to contact” once the film starts to undergo thermal expansion causing inaccurate results to be obtained below around 50°C.

The results from the thesis have shown the importance of the in-situ analysis of pharmaceuticals as the considerable differences in the film morphology between the film coated minitables and cast free films could have led to different conclusions being drawn. The results also highlighted that it is often necessary to use a number of analytical techniques to gain a full insight into the behaviour of complex systems as again differing conclusions could have been drawn if not all the techniques were employed during the study.

7.2 Suggestions for Further Work

7.2.1 Scanning Thermal Microscopy

The inability of MTDSC and L-TMA to resolve nano-phases present in the film coated minitables in this study necessitated the use of the novel heated tip tapping mode to be able to differentiate between the two phases. Although the limitations of scanning thermal microscopy (SThM) have been outlined in the literature (Harding 2006, Royall *et al.*, 2001a), in this instance it may be of use as SThM could provide a similar option to heated tip tapping mode in being able to resolve structures that cannot be observed in standard analytical techniques.

As with nano-TA probes the probes used in SThM have progressed from the Wollaston probes used when MTA was first introduced. The GLA style probes (see Fig 1. below) are analogous to nano-TA probes, however they do not have the same resolution, having a tip radius circa 100nm as opposed to the 30nm of nano-TA probes (Anasys instruments, 2012). This does however provide a far improved resolution compared to the 1 μ m of Wollaston probes.

The SThM field has undergone further development in recent years with various models employed to reduce the topographic effects on the thermal conductivity image. Of note is the use of a neural net algorithm to allow the computer to “learn” what effect the topography has on the thermal image and to “smooth” out the thermal image (Brown *et al.*, 2008).

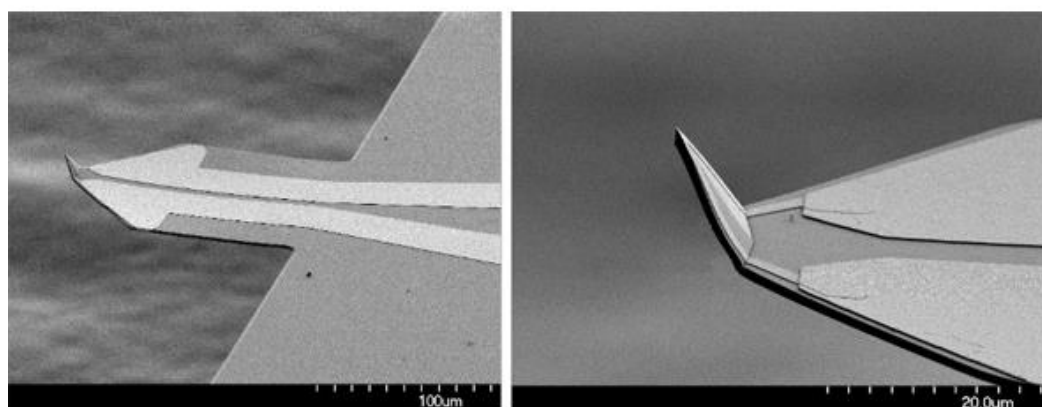


Figure 7.1 GLA style probes used in SThM showing the different in tip compared to NanoTA probes

Similar to heated tip tapping mode the images provided cannot on their own identify the different polymers, however when L-TMA and MTDSC are used to provide the expected transition temperatures, this should allow identification of the polymers under investigation.

SThM could also be used to determine the location of pigments in film coats. The thermal conductivity of pigments, especially metallic pigments such as titanium dioxide, the iron oxides and aluminium lakes are higher than for organic polymers. This difference will result in heat being conducted from the tip at a quicker rate when the probe tip is above a pigment particle compared to when it is over the polymer matrix. This should provide a clear contrast between the pigment and the polymer matrix in the thermal conductivity image, allowing identification of the location of pigment particles within the film coat.

The disadvantage of using the GLA style probes for SThM is that they cannot be used to perform L-TMA, therefore L-TMA cannot then be performed on the same area of the sample surface without replacing the probe with a NanoTA or Wollaston probe. Wollaston probes can also be used to perform SThM and carry out subsequent L-TMA experiments, and although the resolution of the probes is lower than GLA style probes the size of the pigment particles is such that Wollaston probes should still be able to capture them in an image.

7.2.2 Dissolution Testing

Along with the poor understanding of the distribution of pore formers in polymer film coats, so too is their behaviour in-situ. It could be of interest therefore to perform dissolution testing on the film, but stop the testing prior to rupturing of the tablet film coat. If the tablet is then dried and imaged under the AFM any changes in the film coat composition can be observed.

It would be expected that the nano phases present of Opadry I and Opadry II may either leach out of the film allowing the drug to diffuse through the resulting pores or the pore former may hydrate and remain in the Surelease matrix, with the drug migrating through the hydrated Opadry I or Opadry II.

The before and after dissolution images should provide a good indication of what is occurring in the film coat in-situ. If the Opadry leaches out the film coat, there should be changes in the morphology of the film, which should be visible on both topographic and phase images. Even if the pore former hydrates and remains in the film it would still be sensible to expect changes in film morphology.

A potential downside of analysing the films in this manner is the same area of the film will not be analysed before and after dissolution. To overcome this issue the minitabulet could be analysed in a liquid cell, with the minitabulet being left in the cell for sufficient time to allow for Leeching out or hydration of the pore former. This method however is likely to preclude the use of heated tip methods to analyse the film and will not provide a standardised dissolution method.

If the dissolution testing is undertaken according to pharmacopeial standards then this will provide a more accurate approximation of the in-situ behaviour of the pore former. In addition although the same area of the film coat will not be analysed each coat in this study tended to possess broadly similar features, therefore allowing for comparison between different areas of the film.

7.3 Concluding Remarks

The importance of in-situ analysis of pharmaceutical systems for the development of accurate models of pharmaceutical systems is of paramount importance to the pharmaceutical industry. Especially with the move towards continuous processing rather than batch processing leading to a drive for process analytical technology (PAT) to be able to measure dosage forms either in-line or on-line the importance to industry to be able to analyse samples in-situ is of great value. Although AFM combined with nanothermal analysis cannot be used to measure in-line or for fast moving activities such as film coating there is scope for its use in characterisation during product development or in testing of a final product in-situ.

The thesis has outlined arguments for the in-situ analysis of pharmaceuticals complimentary to the standard laboratory techniques traditionally employed.

Chapters 4 and 6 showed the differences observed between film coated minitablets and free films prepared by film casting into Petri dishes, with the phase distribution of polymer blends and the distribution of pigments within a polymer matrix markedly different between the two methods of preparation. The increased drying times required for cast films allowed for increased phase separation to occur in the polymer blends and the sedimentation of pigment particles to occur in films cast with pigments added to the coating solution.

Heated tip tapping mode has been shown to be a useful tool in the determination of phase behaviour of two materials with similar viscoelastic properties with the increased temperature enhancing the contrast between the two polymers in the AFM phase image. The technique is also potentially of more use than the previously developed heated tip pulsed force mode due to the more widespread implementation of tapping mode AFM compared with pulsed force mode. Most AFM instruments are equipped with an intermittent contact mode analogous to tapping mode AFM; however pulsed force mode AFM requires the purchasing of extra modules and expertise to perform this technique. There are limitations to heated tip tapping mode, most notably if two of the components in the system have a similar transition temperature

Another novel technique for pharmaceutical analysis is the use of L-TMA whilst in tapping mode, thus allowing for L-TMA to be performed without removal of the tip from the sample surface and switching to contact mode. By retaining the tip in feedback with the sample time will be saved as removal of the tip and the changing of mode will require a further image to be acquired in contact mode to ensure the probe is in the same location when performing L-TMA. In addition the accuracy of the location of the L-TMA will be increased, especially if the area of interest being analysed is only visible in the phase image.

Overall the project has shown that the in-situ analysis of pharmaceutical film coats is required due to the considerable differences in film morphology observed between film coated minitablets and cast free films. This was particularly evident in minitablets coated with polymer blends but also observed with films of single polymers and films with additional pigments. AFM combined with nanothermal

analysis was shown to be able to analyse film morphology with the novel technique of heated tip tapping mode and L-TMA performed in tapping mode AFM able to provide additional information that could not be acquired using other techniques.

References

Abuchowski, A., McCoy, J. R., Palczuk, N. C., Vanes, T. & Davis, F. F. 1977a. Effect of covalent attachment of polyethylene-glycol on immunogenicity and circulating life of bovine liver catalase. *Journal of Biological Chemistry*, 252, 3582-3586.

Abuchowski, A., Vanes, T., Palczuk, N. C. & Davis, F. F. 1977b. Alteration of immunological properties of bovine serum-albumin by covalent attachment of polyethylene-glycol. *Journal of Biological Chemistry*, 252, 3578-3581.

Almeida, E., BalmayorE, M. & Santos, T. 2002. Some relevant aspects of the use of FTIR associated techniques in the study of surfaces and coatings. *Progress in Organic Coatings*, 44, 233-242.

Amighi, K., Moes, A.J. 1995. Evaluation of thermal and film-forming properties of acrylic aqueous polymer dispersion blends – application to formulation of sustained-release film-coated theophylline pellets. *Drug Development and Industrial Pharmacy*. 21, 2355-69.

Anasys Instruments, 2012. Accessed 16th June, 2012, at <http://www.anasysinstruments.com/probes.php?fi=products>.

Ancykowski, B., Gotsmann, B., Fuchs, H., Cleveland, J. P. & Elings, V. B. 1999. How to measure energy dissipation in dynamic mode atomic force microscopy. *Applied Surface Science*, 140, 376-382.

Angell, C. A. 1995. Formation of glasses from liquids and biopolymers. *Science*, 267, 1924-1935. "A Practical Guide to SPM". Veeco, Santa Barbara. 2005.

Atkins, P., de Paula, J. 2005. Thermodynamics: The first law. In Atkins, P., de Paula, J. Editors. *Elements of Physical Chemistry*. 4th ed. Oxford: Oxford University Press.

Atkinson, J.R., Hay, J.N., Jenkins, M.J. 2002 Enthalpic relaxation in semi-crystalline PEEK. *Polymer*. 43, 731-735.

Avalle, P., Pygall, S.R., Gower, N., Midwinter, A. 2011. The use of in situ near infrared spectroscopy to provide mechanistic insights into gel layer development in HPMC hydrophilic matrices. *European Journal of Pharmaceutical Sciences*. 43, 400–408.

Aulton, M.E., Twitchell, A.M. 2002. Film Coat Quality. In: Cole C, Hogan J, Aulton M, editors. *Pharmaceutical Coating Technology*. London: Taylor & Francis.

Bhattacharjya, S. & Wurster, D. E. 2008. Investigation of the drug release and surface morphological properties of film-coated pellets, and physical, thermal and mechanical properties of free films as a function of various curing conditions. *AAPS Pharmaceutical Science and Technology*. 9, 449-457.

Binnig, G., Quate, C.F., Gerber, C. 1986. Atomic Force Microscope. *Physical Review Letters*. 56, 930-3.

Binnig, G. K. 1987. Atomic-Force Microscopy. *Physica Scripta*, T19, 53-54.

Bisharat, L., Barker, S., Narbad, A., Fuell, Craig. D. 2011. The potential of aqueous-based amylose-zein film coatings for oral colon-specific drug delivery. *AAPS Pharmaceutical Science and Technology*. 13 (S2).

Blackley, D.C. Colloidal destabilization of lattices: Destabilization by physical influences. In: Blackley, D.C. ed. *Polymer Lattices: Science and Technology: Volume 1: Fundamental Principles*. 2nd ed. London: Chapman & Hall; 1997.

Bodmeier, R., Paeratakul, O. 1989. Evaluation of drug-containing polymer-films prepared from aqueous latexes. *Pharmaceutical Research*. 6, 725-30.

Bodmeier, R., Paeratakul, O. 1993. Dry and wet strengths of polymeric films prepared from aqueous colloidal polymer dispersion, Eudragit RS30D. *International Journal of Pharmaceutics*, 96, 129-138.

Bodmeier, R., Paeratakul, O. 1994. The effect of curing on drug-release and morphological properties of ethylcellulose pseudolatex coated beads. *Drug Development and Industrial Pharmacy*. 20, 1517-33.

Bohlmann, G.M. 2005. General characteristics, processability, industrial applications and market evolution of biodegradable polymers. In: Bastioli, C. Editor. Handbook of Biodegradable Polymers. Shrewsbury. Smithers Rapra Publishing.

Borde, B., Bizot, H., Vigier, G. & Buleon, A. 2002. Calorimetric analysis of the structural relaxation in partially hydrated amorphous polysaccharides. I. Glass transition and fragility. *Carbohydrate Polymers*, 48, 83-96.

Bozzola, J. J., Russell, L. D. 1998. The Scanning Electron Microscope. In: Bozzola, J. J., Russel, L. D. Editors. Electron microscopy: Principles and techniques for biologists. 2nd ed. London, Jones and Bartlett Publishers.

Bouissou, C., Rouse, J. J., Price, R. & Van Der Walle, C. F. 2006. The Influence of Surfactant on PLGA Microsphere Glass Transition and Water Sorption: Remodeling the Surface Morphology to Attenuate the Burst Release. *Pharmaceutical Research*, 23, 1295-1305.

British National Formulary. September 2011. 62nd ed. London. BMJ Group and Pharmaceutical Press.

Broekmaat, J., Brinkman, A., Blank, D. H. A. and Rijnders, G. 2008. High temperature surface imaging using atomic force microscopy. *Applied Physics Letters*, 92, 043102.

Brown, M.E., Gallagher, P.K. eds., 2008. Handbook of Thermal Analysis and Calorimetry, Volume 5: Recent advances and techniques. Oxford: Elsevier

Bushan, B., Marti, O. Scanning probe microscopy – principle of operation, instrumentation, and probes. In: Bushan, B. Editor. Springer Handbook of

Nanotechnology. 3rd ed. 2010. New York. Springer.

Caleva. 2013. Laboratory Coater for Tablets and Pellets Accessed 12th May, 2013, at <http://www.caleva.com/downloads/Laboratory%20Coater%20for%20Tablets%20and%20Pellets.pdf>).

Cerea, M., Zheng, W.J., Young, C.R., McGinity, J.W. 2004. A novel powder coating process for attaining taste masking and moisture protective films applied to tablets. *International Journal of Pharmaceutics*. 279, 127-39.

Chevalier, Y., Pichot, C., Graillat, C., Joanicot, M., Wong, K., Maquet, J. 1992. Film formation with latex particles. *Colloid and Polymer Science*. 270, 806-821.

Chourasia, M.K., Jain, S.K. 2004. Pharmaceutical approaches to colon targeted drug delivery systems. *Journal of Pharmacy and Pharmaceutical Sciences*. 6, 33-66.

Cleveland, J. P., Anczykowski, B., Schmid, A. E. & Elings, V. B. 1998. Energy dissipation in tapping-mode Atomic Force Microscopy. *Applied Physics Letters*, 72, 2613-2615.

Coleman, N. J. & Craig, D. Q. M. 1996. Modulated Temperature Differential Scanning Calorimetry: A novel approach to pharmaceutical thermal analysis. *International Journal of Pharmaceutics*, 135, 13-29.

Colombo, P., Bettini, R., Santi, P., Deascentiis, A. & Peppas, N. A. 1996. Analysis of the swelling and release mechanisms from drug delivery systems with emphasis on drug solubility and water transport. *Journal of Controlled Release*, 39, 231-237.

Colorcon. 2006a. Surelease: Aqueous ethylcellulose dispersion. Product information sheet formula No: E-7-19020. Accessed 21st December 2008, at http://www.colorcon.com/literature/marketing/mr/Extended%20Release/Surelease%20AE/English/prod_info_19020.pdf.

Colorcon. 2006b. Surelease: Aqueous ethylcellulose dispersion, Product information

sheet formula No: E-7-19040. Accessed 21st August, 2012, at http://www.colorcon.com/literature/marketing/mr/Extended%20Release/Surelease/English/prod_info_19040.pdf.

Craig, D. Q. M., Royall, P. G. 1998. The use of Modulated Temperature DSC for the study of pharmaceutical systems: potential uses and limitations. *Pharmaceutical Research*, 15, 1152-1153.

Craig, D.Q.M., Royall, P.G., Kett, V.L., Hopton, M.L. 1999. The relevance of the amorphous state to pharmaceutical dosage forms: glassy drugs and freeze dried systems. *International Journal of Pharmaceutics*. 179, 179-207.

Craig, D.Q.M., Kett, V. L., Andrews, A. S. & Royall, P. G. 2002. Pharmaceutical applications of Micro-Thermal Analysis. *Journal of Pharmaceutical Sciences*, 91, 1201-1213.

Craig, D.Q.M., Reading, M. 2007. Principles of Differential Scanning Calorimetry. In: Craig, D.Q.M., Reading, M. eds. *Thermal Analysis of Pharmaceuticals*. London: CRC Press.

Craig, D.Q.M. 2008. The Application of Thermal Analysis to Pharmaceutical Dosage Forms. In: Augsburger LL ed. *Pharmaceutical Dosage Forms: Tablets. Volume 1: Unit Operations and Mechanical Properties*. 3rd ed. London: Informa Healthcare.

Dansereau R, Brock M, Redmanfurey N. The solubilization of drug and excipient into a hydroxypropyl methylcellulose (HPMC)-based film coating as a function for the coating parameters in a 24" Accela-cota®. *Drug Development and Industrial Pharmacy*. 1993;19(7):793-808.122.

Dee, G. T., Sauer, B.B. 1992. The molecular weight and temperature dependence of polymer surface tension: Comparison of experiment with interface gradient theory. *Journal of Colloid and Interface Science*. 152, 85-103.

Dow. 2002. METHOCEL Cellulose Ethers in Aqueous Systems for Tablet Coating. (Accessed May 16th, 2013, at http://msdssearch.dow.com/PublishedLiteratureDOWCOM/dh_004a/0901b8038004ab56.pdf?filepath=/198-00755.pdf&fromPage=GetDoc).

Dow. 2005a. Ethocel: Ethylcellulose Polymers Technical Handbook. (Accessed May 19th, 2013, at [http://www.dow.com/PublishedLiterature/dh004f/0901b8038004fb7c.pdf?filepath=ethocel/pdfs/no reg/192-00818.pdf&fromPage=GetDoc](http://www.dow.com/PublishedLiterature/dh004f/0901b8038004fb7c.pdf?filepath=ethocel/pdfs/no%20reg/192-00818.pdf&fromPage=GetDoc)).

Dow. 2005b. Methocel cellulose ethers. Accessed February 24th 2012 at http://www.dow.com/PublishedLiterature/dh_0050/0901b80380050865.pdf?filepath=amerchol/pdfs/noreg/324-00180.pdf&fromPage=GetDoc.

Dow. 2008. Dow excipients (Accessed May 16th, 2013, at <http://www.dow.com/dowexcipients/applications/films.htm>).

Ebube, N. K. & Jones, A. B. 2004. Sustained release of acetaminophen from a heterogeneous mixture of two hydrophilic non-ionic cellulose ether polymers. *International Journal of Pharmaceutics*, 272, 19-27.

Edwardson, J. M. & Henderson, R. M. 2004. Atomic Force Microscopy and drug discovery. *Drug Discovery Today*, 15, 64-71.

Electronic Medicines Compendium - Asacol SPC. 2013 (Accessed May 18th, 2013, at <http://emc.medicines.org.uk>).

Electronic Medicines Compendium - Colpermin SPC. 2010 (Accessed May 18th, 2013, at <http://emc.medicines.org.uk>).

Evonik. 2008. EUDRAGIT[®] Acrylic Polymers for Solid Oral Dosage Forms. (Accessed December 17th, 2008, at <http://www.pharma-polymere.de/NR/rdonlyres/3D19A053-7628-41B1-BC52-123763B75566/0/080620FinalProduktbrosch>

%C3%BCre.pdf).

FDA. 2004. Guidance for Industry PAT — A Framework for Innovative Pharmaceutical Development, Manufacturing, and Quality Assurance.

Felton, L.A., Shah, N.H., Zhang, G., Infeld, M.H., Malick, A.W., McGinity, J.W. 1996. Physicalmechanical properties of film-coated soft gelatin capsules. *International Journal of Pharmaceutics*. 127, 203-11.

Felton, L.A., McGinity, J.W. 1997. Influence of plasticizers on the adhesive properties of an acrylic resin copolymer to hydrophilic and hydrophobic tablet compacts. *International Journal of Pharmaceutics*. 154, 167-78.

Felton, L.A., McGinity, J.W. 1999. Adhesion of polymeric films to pharmaceutical solids. *European Journal of Pharmaceutics and Biopharmaceutics*. 47, 3-14.

Felton, L. A. & Baca, M. L. 2001. Influence of curing on the adhesive and thermomechanical properties of an applied acrylic polymer. *Pharmaceutical Development and Technology*. 6, 53-59.

Felton, L.A. 2004. Film Coating of Oral Solid Dosage Forms. In: Swarbrick, S. ed. *Encyclopedia of Pharmaceutical Technology*. 2nd ed. New York: Marcel Dekker.

Felton L. A., O'Donnell P. B., and McGinity J. W. 2008. Mechanical properties of polymeric films prepared from aqueous dispersions. In: McGinity J. W., Felton L. A., editors. *Aqueous Polymeric Coatings for Pharmaceutical Dosage Forms*, Informa Healthcare, New York.

Felton, L.A., 2007. Characterization of coating systems. *AAPS Pharmaceutical Science and Technology*. 8, E1-E9.

Fitzgerald, A.J., Cole, B.E., Taday, P.F. 2005. Nondestructive analysis of tablet coating thicknesses using terahertz pulsed imaging. *Journal of Pharmaceutical Sciences*. 94, 177-83.

Flory P.J. Thermodynamics of Polymer Solutions. In: Flory, P.J. ed. Principles of Polymer Chemistry. London: Cornell University Press; 1966.

Friend, D.R. 2005. New oral delivery systems for treatment of inflammatory bowel disease. *Advanced Drug Delivery Reviews*. 2005. 57, 247-65.

Frohoff-Hulsmann, M.A., Schmitz, A., Lippold, B.C. 1999a. Aqueous ethyl cellulose dispersions containing plasticizers of different water solubility and hydroxypropyl methylcellulose as coating material for diffusion pellets I. Drug release rates from coated pellets. *International Journal of Pharmaceutics*. 177, 69-82.

Frohoff-Hulsmann, M.A., Schmitz, A., Lippold, B.C. 1999b. Aqueous ethyl cellulose dispersions containing plasticizers of different water solubility and hydroxypropyl methylcellulose as coating material for diffusion pellets II. Properties of sprayed films. *European Journal of Pharmaceutics and Biopharmaceutics*. 48, 67-75.

Garcia, R. & Perez, R. 2002. Dynamic Atomic Force Microscopy methods. *Surface Science Reports*, 47, 197-301.

Gill, P. S., Sauerbrunn, S. R. & Reading, M. 1993. Modulated Differential Scanning Calorimetry. *Journal of Thermal Analysis*, 40, 931-939.

Gendrin, C., Roggo, Y., Collet, C. 2008. Pharmaceutical applications of vibrational chemical imaging and chemometrics: A review. *Journal of Pharmaceutical and Biomedical Analysis*. 48, 533-53.

Georget, D.M.R., Barker, S.A., Belton, P.S. 2008. A study on maize proteins as a potential new tablet excipient. *European Journal of Pharmaceutics and Biopharmaceutics*. 69.

Gandhi, R., Kaul, C.L., Panchagnula, R. 1999. Extrusion and spheronization in the

development of oral controlled-release dosage forms. *Pharmaceutical Science & Technology Today*. 1999. 2, 160-70.

Goldstein, J., Newbury, D. Joy, D., Lyman, C., Echlin, P., Lifshin, E., Sawyer, L., Michael, J. 2003. New York: Springer Science.

Guo, H.X., Heinamaki, J., Yliruusi, J. 2008. Stable aqueous film coating dispersion of zein. *Journal of Colloid and Interface Science*. 322, 478-84.

Grosse, P. & Offermann, V. 1995. Quantitative infrared-spectroscopy of thin solid and liquid-films under attenuated total-reflection conditions. *Vibrational Spectroscopy*, 8, 121-133.

Grossel, P., Raphael, O., Depasse, F., Duvaut, T. & Trannoy, N. 2007. Multifrequential AC modeling of the SThM probe behavior. *International Journal of Thermal Sciences*, 46, 980-988.

Hahn, K., Ley, G., Schuller, H., Oberthur, R. 1986. On particle coalescence in latex films. *Colloid and Polymer Science*. 264, 1092-6.

Hahn, K., Ley, G., Oberthur, R. 1988. On particle coalescence in latex films (II). *Colloid and Polymer Science*. 266, 631-9.

Hale A. 2002. Themosets. In: Cheng S. Z. D., editor. Handbook of Thermal Analysis and Calorimetry. Volume 3: Applications to Polymers and Plastics. Elsevier Science B.V., Amsterdam.

Hall, D.B., Underhill, P., Torkelson, J.M. 1998. Spin coating of thin and ultrathin polymer films. *Polymer engineering and Science*. 38, 2039-2045

Hancock, B. C. & Zograf, G. 1997. Characteristics and significance of the amorphous state in pharmaceutical systems. *Journal of Pharmaceutical Sciences*, 86, 1-12.

Harding, L., 2006. Microthermal analysis of pharmaceutical materials. Ph. D. University of East Anglia.

Harding, L., King, W. P., Dai, X., Craig, D. Q. M. & Reading, M. 2007. Nanoscale characterisation and imaging of partially amorphous materials using local thermomechanical analysis and heated tip AFM. *Pharmaceutical Research*, 24, 2048-2054.

Harding, L., Wood, J., Reading, M., Craig, D.Q.M. 2007. Two- and three-dimensional imaging of multicomponent systems using scanning thermal microscopy and localized thermomechanical analysis. *Analytical Chemistry*. 79, 129-39.

Hind, A. R., Bhargava, S. K. & McKinnon, A. 2001. At the solid/liquid interface: FTIR/ATR - the tool of choice. *Advances in Colloid and Interface Science*, 93, 91-114.

Ho, L., Muller, F., Romer, M., Gordon, K.C., Heinamaki, J., Kleinebudde, P. 2007. Analysis of tablet film coating quality using terahertz pulsed imaging. *Journal of Pharmacy and Pharmacology*. 59, A1-A20.

Ho, L., Mueller, R., Gordon, K.C., Kleinebudde, P., Pepper, M., Rades, T. 2008. Applications of terahertz pulsed imaging to sustained-release tablet film coating quality assessment and dissolution performance. *Journal of Controlled Release*. 127, 79-87.

Hofmann, S., Foo, C., Rossetti, F., Textor, M., Vunjak-Novakovic, G., Kaplan, D.L. 2006. Silk fibroin as an organic polymer for controlled drug delivery. *Journal of Controlled Release*. 11, 219-27.

Hogan, J.E. 2002. Coating of tablets and multiparticulates. In: Aulton, M.E., ed. *Pharmaceutics: The science of dosage form design*. 2nd ed. London: Churchill Livingstone.

Holscher, H., Schwarz, U. D. & Wiesendanger, R. 1999. Calculation of the frequency shift in dynamic force microscopy. *Applied Surface Science*, 140, 344-351.

Ishida, M., Abe, K., Hashizume, M., Kawamura, M. 2008. A novel approach to sustained pseudoephedrine release: Differentially coated mini-tablets in HPMC capsules. *International Journal of Pharmaceutics*. 2008. 359, 46-52.

Jones, D.M. 2008. Coating Process and Equipment. In: Augsburg, L.L. ed. *Pharmaceutical Dosage Forms: Tablets. Volume 1: Unit Operations and Mechanical Properties*. 3rd ed. London: Informa Healthcare.

Jones, S. A., Martin, G. P., Royall, P. G. & Brown, M. B. 2005. Biocompatible polymer blends: Effects of physical processing on the molecular interaction of poly(vinyl alcohol) and poly(vinyl pyrrolidone). *Journal of Applied Polymer Science*, 98, 2290-2299.

Kendall, K. & Tabor, D. 1971. Ultrasonic study of area of contact between stationary and sliding surfaces. *Proceedings of the Royal Society of London Series a-Mathematical and Physical Sciences*, 323, 321-&.

Kirsch, J.D., Drennen, J.K. 1995. Determination of film-coated tablet parameters by nearinfrared spectroscopy. *Journal of Pharmaceutical and Biomedical Analysis*. 13, 1273-81.

Kirsch, J.D., Drennen, J.K. 1996. Near-infrared spectroscopic monitoring of the film coating process. *Pharmaceutical Research*. 13, 234-7.

Lafferty, S.V., Newton, J.M., Podczek, F. 2002. Dynamic mechanical thermal analysis studies of polymer films prepared from aqueous dispersion. *International Journal of Pharmaceutics*, 235, 107-111.

Lai, H. L., Pitt, K. & Craig, D. Q. M. 2010. Characterisation of the thermal properties of ethylcellulose using differential scanning and quasi-isothermal calorimetric approaches. *International Journal of Pharmaceutics*, 386, 178-184.

Lecomte, F., Siepmann, J., Walther, M., MacRae, R.J., Bodmeier, R. 2004a. Polymer blends used for the aqueous coating of solid dosage forms: importance of the type of plasticizer. *Journal of Controlled Release*. 99, 1-13.

Lecomte, F., Siepmann, J., Walther, M., MacRae, R.J., Bodmeier, R. 2004b. Polymer blends used for the coating of multiparticulates: Comparison of aqueous and organic coating techniques. *Pharmaceutical Research*. 21, 882-90.

Lehmann, K., 1994. Coating of multiparticulates using polymeric solutions: Formulation and process considerations. In: Ghebre-Sellassie, I, ed. *Multiparticulate Oral Drug Delivery*. New York: Marcel Dekker.

Lennartz, P., Mielck, J.B. 1998. Minitabletting: improving the compactability of paracetamol powder mixtures. *International Journal of Pharmaceutics*. 1998. 173, 75-85.

Lewin, M, Vinyl Fibers. 2007. In: Lewin, M. Editor. *Handbook of Fiber Chemistry*. Boca Raton FL: CRC Press.

Li, C. L., Martini, L. G., Ford, J. L. & Roberts, M. 2005. The use of hypromellose in oral drug delivery. *Journal of Pharmacy and Pharmacology*, 57, 533-546.

Lieb, S., Szeimies, R.M., Lee, G. 2002. Self-adhesive thin films for topical delivery of 5-aminolevulinic acid. *European Journal of Pharmaceutics and Biopharmaceutics*. 2002. 53, 99-106.

Lippold, B.H., Sutter, B.K., Lippold, B.C. 1989. Parameters controlling drug release from pellets coated with aqueous ethyl cellulose dispersion. *International Journal of Pharmaceutics*. 54, 15-25.

Lippold, B.C., Monells-Pages, R. 2001. Control and stability of drug release from diffusion pellets coated with the aqueous quaternary polymethacrylate dispersion Eudragit RS40D. *Pharmazie*. 56, 477-483.

Lopes, C.M., Lobo, J.M.S., Pinto, J.F., Costa, P. 2006. Compressed mini-tablets as a biphasic delivery system. *International Journal of Pharmaceutics*. 2006. 323, 93-100.

Macdonald, B.F., Prebble, K.A. 1993. Some applications of near-infrared reflectance analysis in the pharmaceutical industry. *Journal of Pharmaceutical and Biomedical Analysis*. 11, 1077-85.

Magonov, S. N., Elings, V. & Whangbo, M. H. 1997. Phase imaging and stiffness in tapping-mode atomic force microscopy. *Surface Science*, 375, L385-L391.

Marcilla A, Beltrán M. Mechanism of Plasticizers Action. In: Wypych G ed. Handbook of Plasticizers Chemtec Publishing; 2004.

Mark H.F. 2004. In Mark H. F., editor, Encyclopaedia of Polymer Science and Technology. Volume 3, 3rd ed. John Wiley & Sons. New Jersey.

McGoverin, C.M., Rades, T., Gordon, K.C. 2008. Recent Pharmaceutical Applications of Raman and Terahertz Spectroscopies. *Journal of Pharmaceutical Sciences*. 97, 4598-621.

McPhillips, H., Craig, D. Q. M., Royall, P. G. & Hill, V. L. 1999. Characterisation of the glass transition of HPMC using Modulated Temperature Differential Scanning Calorimetry. *International Journal of Pharmaceutics*, 180, 83-90.

Mehta, A.M. 2008. Processing and equipment considerations for aqueous coatings. In: McGinity J. W., Felton L. A., editors. Aqueous Polymeric Coatings for Pharmaceutical Dosage Forms, Informa Healthcare, New York.

Meaurio, E., Cesteros, L. C. & Katime, I. 1997. FTIR study of hydrogen bonding of blends of poly(mono n-alkyl itaconates) with poly(N,N-dimethylacrylamide) and poly(ethyloxazoline). *Macromolecules*, 30, 4567-4573.

Meulendijks, G.H.W.M., De Hann, J.W., Vos, A.H.J.A., Vad de Ven, L.M., Buck, H.M. 1989. Carbon-13 cross-polarization magic-angle-spinning NMR study on the chain packing in anhydrous and hydrated DL- and L-dipalmitoyl-phosphatidylcholine. *Journal of Physical Chemistry*. 93, 3806-3809.

Miller, D.A, McGinity, J.W. 2008. Aqueous Polymeric Film Coating. In: Augsburger LL ed. *Pharmaceutical Dosage Forms: Tablets. Volume 1: Unit Operations and Mechanical Properties*. 3rd ed. London: Informa Healthcare.

Madamba, M.C., Mullett, W.M., Debnath, S., Kwong, E. 2007. Characterization of Tablet Film Coatings Using a Laser-Induced Breakdown Spectroscopic Technique. *AAPS Pharmaceutical Science and Technology*. 8, 184-190.

Moon, I., Androsch, R., Chen, W. & Wunderlich, B. 2000. The principles of Micro-Thermal Analysis and its application to the study of macromolecules. *Journal of Thermal Analysis and Calorimetry*, 59, 187-203.

Mowery, M.D., Sing, R., Kirsch, J., Razaghi, A., Bechard, S., Reed, R.A. 2002. Rapid at-line analysis of coating thickness and uniformity on tablets using laser induced breakdown spectroscopy. *Journal of Pharmaceutical and Biomedical Analysis*. 28, 935-43.

Mucha, M. & Pawlak, A. 2005. Thermal analysis of chitosan and its blends. *Thermochimica Acta*, 427, 69-76.

Nelson, B. A. & King, W. P. 2007. Measuring material softening with nanoscale spatial resolution using heated silicon probes. *The Review of scientific instruments*, 78, 023702-1-023702-8.

Newman, A., Engers, D., Bates, S., Ivanisevic, I., Kelly, R.C., Zograf, G. 2008. Characterization of amorphous API: Polymer mixtures using x-ray powder diffraction. *Journal of Pharmaceutical Sciences*. 97, 4840-4856.

Nyamweya N. N., Hoag S. W. 2008 Influence of Coloring agents on the properties of polymeric coating systems. In: McGinity J. W., Felton L. A., editors. *Aqueous Polymeric Coatings for Pharmaceutical Dosage Forms*, Informa Healthcare, New York.

Obara, S., McGinity, J.W. 1994. Properties of Free Films Prepared from Aqueous Polymers by a Spraying Technique. *Pharmaceutical Research*. 11, 1562-1567.

Offermann, V., Grosse, P., Feuerbacher, M. & Dittmar, G. 1995. Experimental aspects of attenuated total reflectance spectroscopy in the infrared. *Vibrational Spectroscopy*, 8, 135-140.

Okhamafe, A.O., York, P. 1987. Interaction phenomena in pharmaceutical film coatings and testing methods. *International Journal of Pharmaceutics*. 39, 1-21.

Okhamafe, A. O. & York, P. 1988. Studies of interaction phenomena in aqueous-based film coatings containing soluble additives using thermal-analysis techniques. *Journal of Pharmaceutical Sciences*, 77, 438-443.

Okutgen, E., Hogan J.E., Aulton M.E. 1995. Quantitative estimation of internal stress development in aqueous HPMC tablet film coats, *International Journal of Pharmaceutics*. 119, 193–202.

Ougizawa, T., Inoue, T. Miscibility and Interfacial Behaviour in Polymer-Polymer Mixtures. In: Shonaike GO, Simon GP. *Polymer Blends and alloys*. New York: Marcel Dekker; 1999.

Ozturk, A.G., Ozturk, S.S., Palsson, B.O., Wheatley, T.A., Dressman, J.B. 1990. Mechanism of release from pellets coated with an ethylcellulose-based film. *Journal of Controlled Release*. 14, 203-13.

Ozawa, T. 2000. Thermal analysis - review and prospect. *Thermochimica Acta*, 355, 35-42.

- Park, J. S., Park, J. W. & Ruckenstein, E. 2001. A dynamic mechanical and thermal analysis of unplasticized and plasticized poly(vinyl alcohol)/ methylcellulose blends. *Journal of Applied Polymer Science*, 80, 1825-1834.
- Peh, K.K., Wong, C.F. 1999. Polymeric films as vehicle for buccal delivery: Swelling, mechanical, and bioadhesive properties. *Journal of Pharmacy and Pharmaceutical Sciences*. 2, 53-61.
- Podczeczek, F., Almeida, S.M. 2002. Determination of the mechanical properties of pellets and film coated pellets using Dynamic Mechanical Analysis (DMA). *European Journal of Pharmaceutical Sciences*. 16, 209-214.
- Pollock, H. M. & Hammiche, A. 2001. Micro-Thermal Analysis: techniques and applications. *Journal of Physics D-Applied Physics*, 34, R23-R53.
- Porter, S.C. 1989. Controlled-release film coatings based on ethylcellulose. *Drug Development and Industrial Pharmacy*. 15, 1495-521.
- Puttipipatkachorn S., Nunthanid J., Yamamoto K., and Peck G. E. 2001. Drug physical state and drug-polymer interaction on drug release from chitosan matrix films. *Journal of Controlled Release*. 75.
- Price, D. M. 1995. Temperature Calibration of Differential Scanning Calorimeters. *Journal of Thermal Analysis*, 45, 1285-1296.
- Price, D. M., Reading, M., Hammiche, A. & Pollock, H. M. 1999a. Micro-thermal analysis: scanning thermal microscopy and localised thermal analysis. *International Journal of Pharmaceutics*, 192, 85-96.
- Price, D. M., Reading, M. & Lever, T. J. 1999b. Applications of Micro-Thermal Analysis. *Journal of Thermal Analysis and Calorimetry*, 56, 673-679.
- Qi, S., Avalle, P., Saklatvala, R., Craig, D.Q.M. 2008 An investigation into the effects of thermal history on the crystallisation behaviour of amorphous paracetamol.

European Journal of Pharmaceutics and Biopharmaceutics. 69, 364-371.

Qi, S., Craig, D.Q.M. 2010 Detection of phase separation in hot melt extruded solid dispersion formulations: Global vs. localised characterisation. *American Pharmaceutical Review*. September 2010.

Rajabi-Siahboomi, A.R., Farrell, T.P. 2008. The applications of formulated systems for the aqueous film coating of pharmaceutical oral solid dosage forms. In: McGinity J. W., Felton L. A., editors. *Aqueous Polymeric Coatings for Pharmaceutical Dosage Forms*, Informa Healthcare, New York.

Reading, M., Price, D. M., Grandy, D. B., Smith, R. M., Bozec, L., Conroy, M., Hammiche, A. & Pollock, H. M. 2001. Micro-Thermal Analysis of polymers: Current capabilities and future prospects. *Macromolecular Symposia*, 167, 45-62.

Reed, S. J. B., 2005. *Electron Probe Analysis and Scanning Electron Microscopy in Geology*. 2nd Edition. Cambridge: Cambridge University Press.

Rege, P.R., Ong, K., Rajabi-Siahboomi, A.R. 2006. Hypromellose as a pore-former in aqueous ethylcellulose dispersion: stability and film properties. *AAPS Pharmaceutical Science and Technology*. 8, S1.

Repka, M.A., Gerding, T.G., Repka, S.L., McGinity, J.W. 1999. Influence of plasticizers and drugs on the physical-mechanical properties of hydroxypropyl cellulose films prepared by hot melt extrusion. *Drug Development and Industrial Pharmacy*. 1999. 25, 625-33.

Rho, J.Y., Ashman, R.B., Turner, C.H. 1994. Young's modulus of trabecular and cortical bone material: Ultrasonic and microtensile measurements. *Journal of Biomechanics*. 26, 111-119.

Robeson, L.M. 2007. *Fundamentals of polymer blends*. In: Robeson, L.M. Editor. *Polymer blends: A comprehensive review*. München: Hanser.

Romero-Torres, S., Perez-Ramos, J.D., Morris, K.R., Grant, E.R. 2006. Raman Spectroscopy for tablet coating thickness quantification and coating characterization in the presence of strong fluorescent interference. *Journal of Pharmaceutical and Biomedical Analysis*. 41, 811-9.

Rowe, R.C. 1977. Adhesion of film coatings to tablet surfaces – effect of some direct compression excipients and lubricants. *Journal of Pharmacy and Pharmacology*. 29, 723-6.

Rowe, R.C., Forse, S.F. 1983. Pitting – A defect on film-coated pellets. *International Journal of Pharmaceutics*. 17, 347-9.

Rowe, R.C., 1985. Gloss measurement on film coated tablets. *Journal of Pharmacy and Pharmacology*. 37, 761-765.

Rowe, R.C. 1986. The effect of the molecular-weight of ethyl cellulose on the drug release properties of mixed films of ethyl cellulose and hydroxypropyl methylcellulose. *International Journal of Pharmaceutics*. 29, 37-41.

Rowe, R.C. 1996. Predicting film thickness on film coated tablets. *International Journal of Pharmaceutics*. 133, 253-256.

Rowe, R.C. 1997. Defects in Aqueous Film-Coated Tablets. In McGinity, J.W. editor. *Aqueous Polymeric Coatings for Pharmaceutical Dosage Forms*. 2nd ed. New York: Marcel Dekker.

Royall, P. G., Craig, D. Q. M. & Doherty, C. 1999a. Characterisation of moisture uptake effects on the glass transitional behaviour of an amorphous drug using Modulated Temperature DSC. *International Journal of Pharmaceutics*, 192, 39-46.

Royall, P. G., Craig, D. Q. M., Price, D. M., Reading, M. Lever, T. J. 1999b. An Investigation into the Use of Micro-thermal Analysis for the Solid State Characterisation of an HPMC Tablet Formulation. *International Journal of*

Pharmaceutics, 192.

Royall, P. G., Craig, D. Q. M. & Grandy, D. B. 2001a. The use of Micro-Thermal Analysis as a means of in situ characterisation of a pharmaceutical tablet coat. *Thermochimica Acta*, 380, 165-173.

Royall, P. G., Kett, V. L., Andrews, C. S. & Craig, D. Q. M. 2001b. Identification of crystalline and amorphous regions in low molecular weight materials using microthermal analysis. *Journal of Physical Chemistry B*, 105, 7021-7026.

Rugar, D. & Hansma, P. 1990. Atomic Force Microscopy. *Physics Today*, 43, 23-30.

Sakellariou, P., Rowe, R. C. & White, E. F. T. 1985. The thermomechanical properties and glass-transition temperatures of some cellulose derivatives used in film coating. *International Journal of Pharmaceutics*, 27, 267-277.

Sakellariou, P., Rowe, R. C. & White, E. F. T. 1986. Polymer-Polymer Interaction in Blends of Ethyl Cellulose with Both Cellulose Derivatives and Polyethylene Glycol-6000. *International Journal of Pharmaceutics*, 34, 93-103.

Sakellariou, P., Rowe, R.C. 1995a. Interactions in Cellulose Derivative Films for Controlled Oral Drug Delivery. *Progress in Polymer Science*. 20, 889-942.

Sakellariou, P., Rowe, R.C. 1995b. The morphology of blends of ethylcellulose with hydroxypropyl methylcellulose as used in film coating. *International Journal of Pharmaceutics*. 125, 289-96.

Sanders, G. H. W., Roberts, C. J., Danesh, A., Murray, A. J., Price, D. M., Davies, M. C., Tendler, S. J. B. & Wilkins, M. J. 2000. Discrimination of polymorphic forms of a drug product by localized thermal analysis. *Journal of Microscopy-Oxford*, 198, 77-81.

Siepe, S., Lueckel, B., Kramer, A., Ries, A., Gurny, R. 2008. Assessment of tailor-made HPMC based matrix minitablets comprising a weakly basic drug compound. *Drug Development and Industrial Pharmacy*. 34, 46-52.

Siepmann, F., Hoffmann, A., Leclercq, B., Carlin, B. & Siepmann, J. 2007. How to adjust desired drug release patterns from ethylcellulose-coated dosage forms. *Journal of Controlled Release*, 119, 182-189.

Siepmann, F., Siepmann, J., Walther, M., MacRae, R.J., Bodmeier, R. 2008. Polymer blends for controlled release coatings. *Journal of Controlled Release*. 125, 1-15.

Siggia, E.D., 1979. Late stages of spinodal decomposition in binary mixtures. *Physics Review A*. 20, 595-605.

Sigma-Aldrich. 2011. Poly (ethylene glycol) Materials Safety Data Sheet. Accessed 12th March 2011 at <http://www.sigmaaldrich.com/MSDS>.

Sperling, L.H. 2006. Concentrated solutions, phase separation behaviour and diffusion. In: Sperling, L.H. ed. *Introduction to Physical Polymer Science*. 4th ed. New Jersey: John Wiley & Sons.

Spiros, H.A., Gancarz, I, Koberstein, J.T. 1988. Interfacial Tension of Immiscible Polymer Blends: Temperature and Molecular Weight Dependence. *Macromolecules*. 21, 2980-2987.

Steward, P.A., Hearn, J., Wilkinson, M.C. 2000. An overview of polymer latex film formation and properties. *Advances in Colloid and Interface Science*. 86, 195-267.

Sudhamani, S. R., Prasada, M. S. & Udaya Sankar, K. 2003. DSC and FTIR studies on Gellan and Polyvinyl alcohol (PVA) blend films. *Food Hydrocolloids*, 17. 245–250.

Tamamushi, B. 1973 Flow properties of smectic liquid crystals. *Biorheology*, 10. 239-247.

Temple-Boyer, P., Mazonq, L., Doucet, J.B., Conedera, V., Torbiero, B., Launay, J. 2010. Theoretical studies of the spin coating process for the deposition of polymer-

based maxwellian liquids. *Microelectronic Engineering*. 87, 163-166.

Thornton, J. 200. Scanning Probe Microscopy Training Notebook. Veeco; Santa Barbara

Veronese, F. M. & Pasut, G. 2005. PEGylation, successful approach to drug delivery. *Drug Discovery Today*, 10, 1451-1458.

Vervaeet, C., Baert, L., Remon, J.P. 1995. Extrusion-spheronisation – A literature review. *International Journal of Pharmaceutics*. 116, 131-46.

Vesey, C.F. 2002. Physical properties and stability of Opaglos 2, a pigmentable, high gloss film coating system. *AAPS Pharmaceutical Science and Technology*. 4, S1.

Watson, D.G. 2003. Infrared spectrophotometry. In: *Pharmaceutical Analysis: A textbook for Pharmacy students and pharmaceutical scientists*. London: Churchill Livingstone.

Whangbo, M. H., Bar, G. & Brandsch, R. 1998. Qualitative relationships describing height and phase images of tapping mode Atomic Force Microscopy. An application to micro-contact-printed patterned self-assembled monolayers. *Applied Physics a- Materials Science & Processing*, 66, S1267-S1270.

Wu, C.B., McGinity, J.W. 1999. Non-traditional plasticization of polymeric films. *International Journal of Pharmaceutics*. 177, 15-27.

Wu, C., McGinity, J.W. 2001. Influence of ibuprofen as a solid-state plasticizer in Eudragit RS 30 D on the physicochemical properties of coated beads. *AAPS Pharmaceutical Science and Technology*. 2001. 2, 35-43.

Yoder S. L., Korchok B. D., Kettinger F. R. 2007 Pharmaceutical Dosage Forms having watermark-type identification and authentication indicia. US Patent 20070026064.

Yoder S. L., Kettinger F. R. Dolbier M Method and arrangement for forming variable color pharmaceutical products. US Patent 20100303735.

Zeitler, J.A., Taday, P.F., Newnham, D.A., Pepper, M., Gordon, K.C., Rades, T. 2007a. Terahertz pulsed spectroscopy and imaging in the pharmaceutical setting - a review. *Journal of Pharmacy and Pharmacology*. 59, 209-23.

Zeitler, J.A., Shen, Y.C., Baker, C., Taday, P.F., Pepper, M., Rades, T. 2007b. Analysis of Coating structures and interfaces in solid oral dosage forms by three dimensional terahertz pulsed imaging. *Journal of Pharmaceutical Sciences*. 96, 330-40.